JSCSEN 78(8)1079–1268(2013)

ISSN 1820-7421(Online)

Journal of the Serbian Chemical Society

Electronic Version

VOLUME 78

No 8

BELGRADE 2013

Available on line at

www.shd.org.rs/JSCS/

Journal of the Serbian Chemical Society
JSCS-info@shd.org.rs • www.shd.org.rs/JSCS

J. Serb. Chem. Soc. Vol. 78, No. 9 (2013)

CONTENTS

Published by the Serbian Chemical Society
Karnegijeva 4/III, 11000 Belgrade, Serbia
Printed by the Faculty of Technology and Metallurgy
Karnegijeva 4, P.O. Box 35-03, 11120 Belgrade, Serbia

Journal of the Serbian Chemical Society
JSCS-info@shd.org.rs • www.shd.org.rs/JSCS
J. Serb. Chem. Soc. 78 (9) 1269–1289 (2013)
JSCS–4496
UDC 547.466.3+641.3:641.1:613:616.1:61614–002
Review

REVIEW

Polyunsaturated fatty acids in health and disease

DANIJELA RISTIĆ-MEDIĆ*, VESNA VUČIĆ, MARIJA TAKIĆ, IVANA KARADŽIĆ and MARIJA GLIBETIĆ

Centre of Research Excellence in Nutrition and Metabolism, Institute for Medical Research, University of Belgrade, Dr Subotića 4, 11000 Belgrade, Serbia

(Received 2 April, revised 15 April 2013)

Abstract: Polyunsaturated fatty acids (PUFAs) are necessary for overall health. Two PUFAs families, n-6 and n-3 fatty acids, are physiologically and metabolically distinct. The proportion of PUFAs in serum and erythrocyte phospholipids, which depends on endogenous metabolism controlled by genetic polymorphisms and dietary intake, is an important determinant of both health and disease. Both n-3 and n-6 PUFAs are processed to powerful promoters of eicosanoids synthesis at the cyclooxygenase and lipoxygenase level. Evidence from observational and intervention studies suggest that n-3 PUFAs are cardioprotective, perhaps through their anti-inflammatory, anti-arrhythmic, lipid-lowering and antihypertensive effects. In contrast, dietary n-6 PUFAs have pro-inflammatory effects. Low n-3 and elevated n-6 PUFAs levels were found in patients with cancer on different sites. The present review focuses on current knowledge related to PUFAs intake and status in health and disease, with reference to the Serbian population.

Keywords: n-3; n-6; PUFA; inflammation; cardiovascular disease; chronic diseases.

CONTENTS

* Corresponding author. E-mail: dristicmedic@gmail.com
doi: 10.2298/JSC130402040R

1. INTRODUCTION

Polyunsaturated fatty acids (PUFAs) play important roles in maintaining normal physiological conditions and, consequently, in human health. Two PUFAs families, n-6 and n-3 fatty acids (FA), are physiologically and metabolically distinct. Their precursors, linoleic acid (18:2n-6; LA) and α-linolenic acid (18:3n-3; ALA) are essential fatty acids (EFA), meaning that they cannot be synthesized in the human body and must be obtained from the diet. Thus, LA can be converted *via* γ-linolenic acid (18:3n-6) and dihomo-γ-linolenic acid (20:3n-6; DGLA) to arachidonic acid (20:4n-6; AA) (Fig. 1). Arachidonic acid plays important biological roles. It is released from phospholipids by phospholipase A2 and is the precursor of pro-inflammatory eicosanoids, which include prostaglandins of the two series (PGE2, PGD2), leukotrienes of the four series (LTA4, LTB4, LTC4, LTD4 and LTE4) and lipoxines.[1] Their production is catalyzed by cyclo-oxygenase, lipoxygenase and epoxygenase enzymes, respectively. By an analogous set of reactions catalyzed by the same enzymes, precursor of n-3 PUFAs, ALA, can be converted into eicosapentaenoic acid (20:5n-3; EPA), and further to docosapentaenoic acid (22:5n-3; DPAn-3) and docosahexaenoic acid (22:6n-3; DHA). This is achieved by insertion of additional double bonds into the acyl chain (*i.e.*, unsaturation) and by elongation of the acyl chain. EPA is a precursor of the other classes of eicosanoids, namely the three series of prostaglandins and the five series of leukotrienes. Eicosanoids derived from AA have opposing properties from those originating from EPA. Therefore, an increase in the dietary intake of LA changes the physiological state to a prothrombotic, proconstrictive, and pro-inflammatory one. Many of the chronic conditions, cardiovascular disease, diabetes, cancer, obesity, auto-immune diseases, rheumatoid arthritis, asthma and depression are associated with an increased production of thromboxane A2, leukotriene B4, IL-1, IL-6, tumour necrosis factor (TNF), and C-reactive protein.[2,3] All these factors are increased by increased n-6 PUFAs intake and decreased by increased n-3 PUFAs intake, either ALA or EPA and DHA. However, there is one exception. DGLA of the n-6 family can be further converted by inflammatory cells to 15-(*S*)-hydroxy-8,11,13-eicosatrienoic acid and PGE1. This is interesting because these compounds possess anti-inflammatory and anti-proliferative properties. PGE1 could also induce growth inhibition and

differentiation of cancer cells.[4] The mechanism of DGLA action has not yet been elucidated.

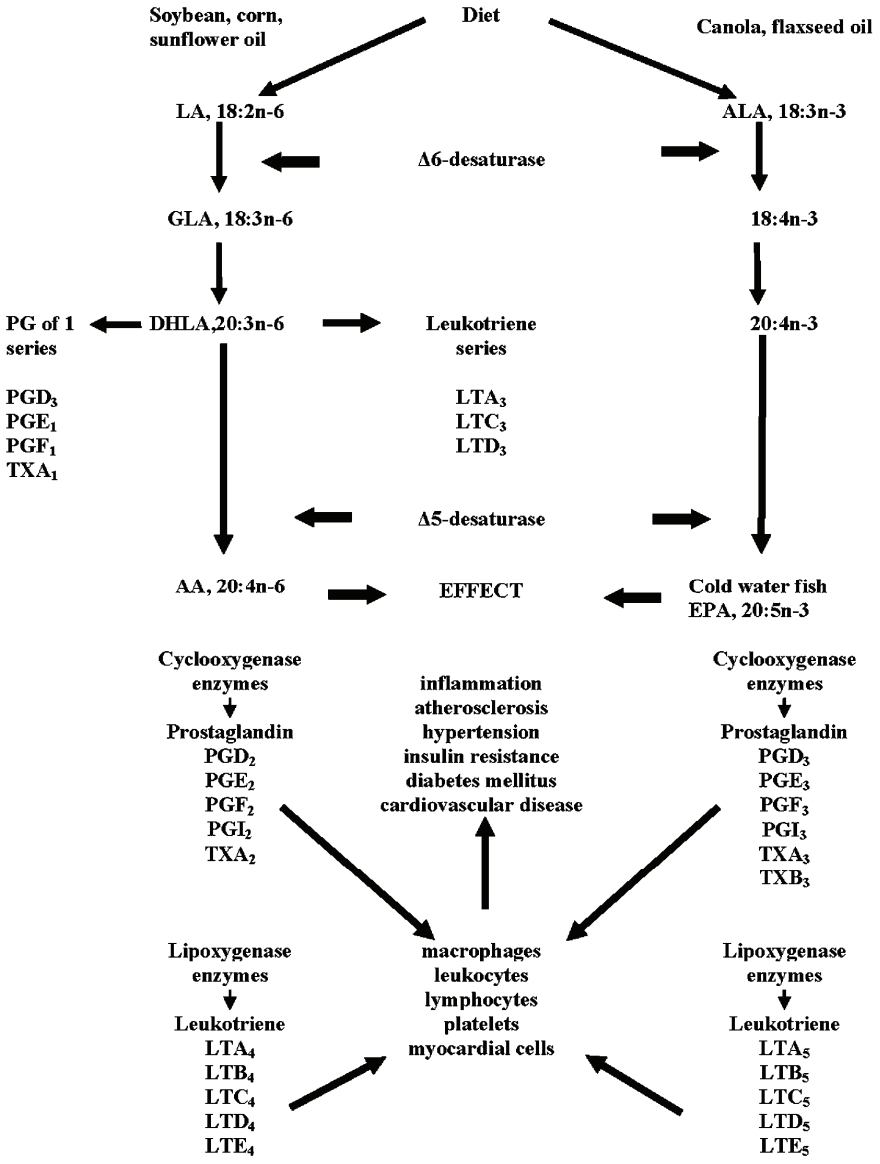

Fig. 1. Dietary sources, metabolism of n-3 and n-6 PUFAs and clinical outcomes.

It is well known that PUFAs favourably affect the blood lipid profile (Table I). LA is associated with a lower risk of atherosclerosis, cardiovascular heart disease (CHD) and type 2 diabetes.[5–8] Consumption of ALA has also been sug-

TABLE I. Potential beneficial effects of PUFA on physiological parameters[6,7,9,11]

Total PUFA	Diseases	Physiological parameters
ALA	Cancer/coronary heart disease	↓Serum total cholesterol
	Cardiovascular disease Myocardial infraction Cardiac arrhythmias Colon cancer Deficiency symptoms	↓Serum total cholesterol ↓Platelet aggregation, adhesion of monocytes to vessel walls, vascular dilatation, blood pressure, inflammatory processes, and immune reaction ↑Leukocyte function ↑Neural integrity n-3 deficiency in pre- and postnatal nutrition of infants affects: neural integrity, learning and visual abilities and depressed development of retinal function and visual acuity
EPA and DHA	CHD Fatal myocardial infraction Inflammatory diseases Bipolar disorder, cognitive decline, aggression, hostility, Anti-social behaviour Age-related maculopathy	↓Production of PGE2 metabolites ↓Thromboxane A2, a potent platelet aggregator and vasoconstrictor ↓Leukotriene B4 formation, an inducer of inflammation, and a powerful inducer of leukocyte chemotaxis and adherence ↑Thromboxane A3, a weak platelet aggregator and weak vasoconstrictor ↑Prostacyclin PGI3, leading to an overall ↑ in total prostacyclin by ↑ PGI3 without a ↓ PGI2, both PGI2 and PGI3 are active vasodilators and inhibitors of platelet aggregation ↑Leukotriene B5, a weak inducer of inflammation and a weak chemotactic agent ↓Serum triglycerides, VLDL-C ↓Platelet aggregation, adhesion of monocytes to vessel walls, vascular dilatation, blood pressure, inflammatory processes, and immune reaction ↑Rod photoreceptor, visual acuity, neural function (infants)
LA	CVD mortality Deficiency disease	↓Serum total cholesterol, LDL-C, HDL-C ↑Platelet aggregation, adhesion of monocytes to vessel walls, vascular dilatation, blood pressure, inflammatory processes, and immune reaction

gested to reduce the risk of CHD events.[9–12] Nevertheless, clinical benefits have not been confirmed in all studies, and further research on the association between ALA consumption and the incidence of CHD are required. The long chain n-3 PUFAs, EPA and DHA, consumption have demonstrated physiological benefits on blood pressure, heart rate, triglycerides, likely inflammation, endothelial function, and cardiac diastolic function.[13–16] Furthermore, consistent evidence for a decreased risk of fatal CHD and sudden cardiac death at consumption of > 250 mg day^{-1} of EPA plus DHA were also reported.[17] For primary prevention of car-

diac arrest, minimum intakes of 250 mg day^{-1} of marine EPA and DHA have been suggested.[14]

DHA also plays a major role in cognitive functions. Therefore, its intake is very important during pregnancy, in young children but also in the elderly. DHA is involved in normal development of the brain and retina during foetal development and the first 2 years of life.[18–20] In healthy children a positive associations between DHA levels in blood and improvements on tests of cognitive and visual function was found.[21] A study in human adults using positron emission tomography showed that a normal human brain consumes around 17.8 and 4.6 mg day^{-1} of AA and DHA, respectively, and that brain AA consumption is increased in Alzheimer disease patients.[22] In addition, some clinical evidence suggests that an AA/DHA ratio greater than 1/1 is associated with improved cognitive outcomes.[23] These findings suggest that recommendations for adequate intakes of DHA and other PUFAs in pregnant women, young children and elderly are urgently needed. The present review focuses on the current knowledge related to PUFAs intake and status in health and disease, with reference to the Serbian population.

2. PUFAs INTAKE AND STATUS

2.1. Dietary sources

LA is present in significant amounts in many vegetable oils, including corn, sunflower, grape seed and soybean oils, and in products made from these oils, such as margarines. ALA is found in green plant tissues, in some common vegetable oils, including soybean and rapeseed oils, in some nuts and in particular in linseeds and linseed oil.[24] Arachidonic acid is mostly present in meats and its intake is estimated at 50 to 500 mg day^{-1}. The richest sources of EPA, DPA and DHA are oily fish (tuna, salmon, mackerel, herring, and sardine). One oily fish meal can provide between 1.5 and 3.5 g EPA+DHA.[25] Consumption of 1 g fish oil capsule per day can provide about 300 mg of these fatty acids. In the absence of oily fish or fish oil consumption, the intake of n-3 PUFAs is likely to be 100 mg day^{-1}.[26] According to habitual dietary information in Serbia, low fat consumers have an intake of 5.4 % of daily energy intake (%*E*) and high fat consumers around 5.9 % *E* from PUFAs.[27]

2.2. n-6 to n-3 PUFAs ratio

The intake of LA in western countries has increased greatly in the last few decades, due to the introduction and marketing of cooking oils and margarines.[28] Typical intakes of both EFA exceed requirements. However, replacing lard with sunflower oil in the diet has resulted in a marked increase in the ratio of n-6 to n-3 PUFAs. This ratio is typically between 5 and 20 in most Western populations.[29] A lower n-6 to n-3 PUFAs ratio consumption has been recommended in order to

reduce the formation of pro-inflammatory eicosanoids from n-6 PUFAs and to increase the production of anti-inflammatory mediators from n-3 FA.[2,30] Additionally, it was suggested that lowering the n–6 FA intake would have the same health effects as increasing n-3 FA intake. Wall *et al.*[31] recently reviewed that reductions in the n-6 to n-3 FA ratio in the diet may lower the incidence of many chronic diseases that involve inflammatory processes; these include cardiovascular diseases, inflammatory bowel disease, cancer, rheumatoid arthritis and psychiatric and neurodegenerative illnesses. Thus, the specific n-6/n-3 ratio in the diet is of particular interest for maintaining overall health.

2.3. Recommendations for intake of PUFAs

In the light of new evidence for associations between low intakes of some PUFAs and increased risk of chronic disease that was mentioned above, optimal criteria for dietary recommendation aim to achieve optimal health and to reduce risk of developing chronic disease.[32] A World Health Organization report from 1994[33] did not suggest nutrient intake values for total PUFAs, but focused on the ratio of LA/ALA in the diet. Recent reports indicated that in healthy adults, the minimum intake levels for EFA should be 2.5 % LA plus 0.5 % ALA of daily energy intake to prevent deficiency symptoms.[32] Recommendations on the intake of PUFAs in healthy adults from Nutrition bodies and International Dietary Recommendations[32–40] are listed in Table II. An effective intake for the prevention of chronic diseases is higher, 6–11 % *E*, which is considered as the optimal range for the total intake of PUFAs.[2,32,40] Currently, there is no upper n-6 PUFAs value in the Eurodiet core report.[39] These different positions reflect the current worldwide debate on the relevance of an upper limit in dietary n-6 PUFA intake and highlight the need for further *in vivo* investigations. At the moment, the nutrition body supports the recommendation for n-6 PUFA intake above 5 %, and ideally about 10 % of total energy. However, balance in the n-6/n-3 ratio issue was debated in detail by Stanley *et al.*[41] and Harris,[42] who concluded that this ratio is not relevant for setting up recommendations. Based on both evidence and conceptual limitations, there is no compelling scientific rationale for the continued recommendation of a specific ratio of n-6 to n-3 PUFAs or LA to ALA.

2.4. PUFAs intake in relation to status biomarker

The proportion of PUFAs in serum and erythrocyte phospholipids, an important determinant of both health and disease, depends on the dietary intake and endogenous metabolism controlled by genetic polymorphisms. The FA composition of serum phospholipids is genetically controlled by the FADS1 and FADS2 gene cluster. Based on this genetic variation, individuals may require different amounts of dietary PUFAs to achieve comparable biological effects.[43] Nevertheless, the FA composition in serum lipids can be used not only as a biomarker of fat quality intake, but also as an indicator of disease risk.

TABLE II. Dietary recommendations for PUFAs intake; AI = adequate intake; *E*% = energy of fat; IOM = Dietary reference intakes of the American Institute of the Medicine's Food and Nutrition Board; AHA = American Health Association Science Advisory, Australia/NZ = Nutrient reference values for Australia and New Zealand; BNF = British nutrition foundation; FS = French food safety agency report; EDC = Eurodiet core report; LA = linoleic acid, LNA = α-linolenic acid, AA = arachidonic acid, DHA = docosahexaenoic acid, EPA = eicosapentaenoic acid; m = male, f = female

PUFA	FAO/WHO *E*%[33,34]	IOM[35]	AHA *E*%[7,37]	Australia/ NZ *E*%[38]	BNF *E*%[54]	EDC *E*%[39]	AI for adults g day^{-1}, *E*%[39]	AI for infants formula/diet of FA[39]	Recent report[32,40] *E*%
n-6 PUFA	4–10 5–8	5–10 *E*%	At least 5–10	4–10	–	4–8	–	–	Ranging 2–10
LA	2.5	m 17 g f 12 g	–	8–13 g	Min. 1	–	2; upper limit 3 4.44 g; 6.67 %	10	–
AA	0.5	–	–	–	–	–	–	0.5	–
n-3 PUFA	1–2	–	–	–	–	–	–	–	–
LNA	None/min <0.05	m 1.6 g f 1.1 g	–	0.8–1.3 g	0.6 g; 1.2 %	2 g	2.2 g; 1 %	1.5	Ranging 0.2–2
EPA	None %	–	Patient with CHD: 1 g/fish oil/d Without CHD: 500 mg/d TG↑ 3–4 g	–	–	200 mg	0.22 g, at least 0.1	upper limit < 0.1	90–650 mg/d
DHA	None %						0.22 g, at least 0.1	0.35	40–3000 mg/d
EPA +DHA	None %, / 0.25 g/d						0.65 g, 0.3%		for different age groups
Total PUFA (n-3 + n-6)	6–10	6–12	–	–	6–10	–	–	–	10–12 us upper level

PUFAs are important constituents of the phospholipids of all cell membranes. LA, ALA and their metabolic products, AA, EPA and DHA are crucial structural and functional components of cellular and intracellular membranes in the human body, but especially in brain, heart, retina, and testes. Phospholipids play an essential role in membrane structure and function. PUFAs of both the n-6 and n-3 series are incorporated into membrane phospholipids, and the AA/EPA ratio ranges between 1:1 and 5–10:1. The higher ratio stimulates the incorporation of EPA, because of the greater affinity of enzymes for EPA.[44] The length and degree of unsaturated FAs in membrane phospholipids are the main determinants of fluidity, transport systems, activity of membrane-bound enzymes, and susceptibility to lipid peroxidation.[45–47] In this context, an altered FA composition with reduced levels of PUFAs and increased contents of saturated FA (SFA), that consequently decrease the PUFA/SFA ratio in erythrocyte membranes, may be associated with lower membrane fluidity in patients with chronic diseases.[48,49] This is often found in elite athletes.[50–52]

It was previously established that erythrocytes reflect the general FA metabolism in other organs and tissues.[53,54] A poor n-3 PUFAs status is often related to a low consumption of cold-water fish, as the primary source of EPA and DHA, and then to income status, national and social eating habits. However, an inadequate EFA intake is not the only cause for a disturbance in the FA profile. EFA deficiency is also present in chronic inflammatory conditions,[55] increased oxidative stress related to PUFAs oxidation[56] and in elevated intracellular calcium concentration.[57] A number of studies showed that different pathologies, such as cancer, diabetes, coronary heart disease, pancreatitis, *etc*., could be associated to altered FA profiles of plasma or serum phospholipids.[58–61] Patients with renal failure, liver cirrhosis or diabetes mellitus often have plasma FA profiles similar to those with nutritional deficiency of EFA.[62–65] Considering limited storage of n-3 FA in adipose tissue in both patients and healthy people, a continued dietary supply with the optimal n-6/n-3 ratio of PUFAs has been suggested. A diet supplemented with n-3 PUFAs partially replace n-6 PUFAs in the majority of the membranes of cells (*e.g.*, erythrocytes, platelets, monocytes, lymphocytes and granulocytes, and endothelial neuronal, colon, and hepatic cells), suggesting that in spite of pathologies, diet could markedly change the FA profiles in patients.

In the Serbian population with type 2 diabetes[59] who also had abnormal lipid levels, the total n-3 PUFAs in plasma were lower, while the n-6/n-3 ratio was higher when compared to healthy subjects (Table III). EPA, DHA and total n-3 PUFAs in the erythrocyte phospholipids in these patients[59] were also low (Table IV). Patients with hyperlipidemia[60] had a significantly lower proportion of EPA and DHA than healthy subjects. Suboptimal levels of n-3 FA in erythrocytes have been found in obese subjects,[67] as well as a lower proportion of EPA, DHA and total n-3 FA, and a significantly higher n-6/n-3 ratio in insulin-resistant

obese women when compared to obese women with normal glucose tolerance (Table IV). A similar n-3 FA status in serum phospholipids and red blood cells was reported in well-nourished patients[62] undergoing haemodialysis. Proportions of DHA and n-3 PUFAs in serum phospholipids of patients with non-Hodgkin lymphoma,[61] as well as in patients with obstructive jaundice[66] were extremely low, which led to very high n-6/n-3 ratios of around 15 in both groups of patients, demonstrating a complete imbalance of FA in these patients. However, the n-6/n-3 ratio in healthy subjects in the Serbian population was also very high (11–12), suggesting the importance of changing dietary habits in Serbia.[50–52,61,62]

TABLE III. Plasma phospholipids fatty acids composition (mol %) with reference to the Serbian population; HLP, hyperlipidemic patients; DM, diabetes mellitus; HD, haemodialyses patients; NHL, patients with non-Hodgkin lymphoma

Serum	Healthy controls (n = 27)[62]	HLP (n = 41)[60]	DM 2, HLP (n = 29)[59]	Obstructive jaundice (n = 13)[66]	HD (n = 29)[62]	NHL (n = 47)[61]
LA	26.5±2.8	23.1±1.4	22.6±2.4	24.8±3.4	25.5±2.9	20.2±2.4
DGLA	2.4±0.7	3.0±0.4	3.0±0.8	2.6±1.0	2.0±0.5	3.9±1.0
AA	11.6±2.3	11.4±1.0	13.2±2.9	8.8±1.50	11.1±2.2	14.3±1.5
22:4 n-6	0.4±0.2	0.4±0.1	0.6±0.3	0.2±0.1	0.4±0.1	0.6±0.2
Σn-6	40.8±2.9	38.0±1.7	39.5±3.4	35.6±3.2	39.0±3.3	38.8±2.6
ALA	0.11±0.01[52]	0.10±0.02	–	–	–	–
EPA	0.4±0.1	0.3±0.05	0.4±0.3	0.35±0.07	0.3±0.1	0.2±0.1
DPAn-3	0.6±0.1	0.5±0.1	0.6±0.2	0.35±0.10	0.5±0.1	0.4±0.2
DHA	3.6±1.1	3.1±0.3	2.5±0.7	2.2±0.7	3.0±0.9	2.1±0.7
Σn-3	4.7±1.4	4.0±0.3	3.5±0.8	2.6±0.8	3.8±1.2	2.7±0.7
n-6/n-3	8.8±1.6	9.4±0.9	11.2±2.7	14.2±3.5	9.6±1.3	15.4±4.6

3. BIOLOGICAL EFFECTS AND METABOLIC FUNCTIONS OF n-6 AND n-3 PUFAs

An increasing body of evidence suggests that n–3 PUFAs supplementation may improve defects in insulin signaling and prevent alterations in glucose homeostasis and further development of diabetes type 2.[63,68] These effects are possibly mediated through the peroxisome proliferator-activated receptors (PPARs), which are up-regulated by long-chain PUFA and in turn are related to the gene expression involved in lipid oxidation and synthesis.[69] Other pleiotrophic effects of n–3 PUFAs may contribute to decreased condition of the metabolic syndrome, such as modulation of inflammation, platelet activation, endothelial function and blood pressure.[70]

In addition, a high proportion of n-3 PUFAs in red blood cell membranes is associated with a reduced risk of primary cardiac arrest. The American Heart Association recommended that individuals at high cardiovascular risk should consume 1 g daily of fish oil.[7,71] It was shown that n-3 PUFAs oral supplementation quickly and effectively raised the blood n-3 PUFAs levels.[72] However, some new data and meta analyses showed no effect of n-3 supplementation and

TABLE IV. Erythrocyte phospholipids fatty acids composition (mol %) with reference to the Serbian population; HLP, hyperlipidemic patients; DM, diabetes mellitus; NGT, normal glucose tolerance; IR, insulin resistance; HD, haemodialyses patients; NHL, patients with non-Hodgkin lymphoma; Er, erythrocyte

Er	Healthy controls (n = 27)[62]	HLP (n = 41)[60]	DM 2, HLP (n = 29)[59]	Obesity, HLP (n = 30)[66]	Obesity, HLP, NGT (n = 12)[66]	Obesity, HLP, IR (n = 18)[66]	HD (n = 29)[62]
LA	15.5±1.8	13.5±1.1	13.0±3.5	12.6±1.7	12.2±1.6	13.0±1.7	14.8±2.0
DGLA	1.2±0.4	1.5±0.2	1.7±0.6	1.8±0.4	1.7± 0.3	2.0±0.4	1.3±0.4
AA	16.2±2.0	16.5±1.5	11.3±3.8	16.7±1.9	17.3±1.7	16.3±2.0	15.3±1.8
22:4 n-6	3.5±1.2	3.6±0.5	2.4±1.1	3.8±0.7	3.8±0.7	3.8±0.7	3.5±0.9
Σn-6	36.5±2.4	35.2±2.2	28.4±6.5	35.1±3.0	35.0±2.4	35.0±3.4	34.9±3.5
ALA	0.11±0.09[52]	0.10±0.02	–	–	–	–	–
EPA	0.5±0.1	0.3±0.1	0.3±0.2	0.4±0.2	0.5±0.2	0.4±0.2	0.2±0.1
DPAn-3	1.3±0.5	1.6±0.3	0.9±0.5	1.7±0.4	1.8±0.4	1.5±0.3	1.1±0.4
DHA	5.3±1.1	3.8±0.6	2.2±1.1	4.3 ±1.2	5.2±1.3	3.8±1.9	4.3±0.8
Σn-3	6.9±1.3	5.9±0.6	3.3±1.6	6.5±1.7	7.6±1.7	5.7±1.2	6.0±0.9
n-6/n-3	5.4±1.1	6.0±0.7	8.6±4.8	5.7±0.7	4.9±1.4	6.4 ±1.4	5.9±0.9

health benefits. Considering these facts, further work is required to confirm the association between plasma PUFAs levels and clinical outcomes.

3.1. PUFAs and dyslipidemia

One of the most investigated health effect of n-3 PUFA is their capability to reduce serum triglyceride levels. Many different mechanisms seem to be involved in the hypotriglyceridemic effect of n-3 PUFAs in humans. First, it is assumed that the lipid-altering effects of n-3 PUFA could modify gene expression.[73,74] At the gene transcriptional level, they can act on liver X receptor, hepatocyte nuclear factor-4a, farnesol X receptor and PPAR-alpha and PPAR--gamma. They simultaneously down-regulate genes encoding proteins that stimulate lipid synthesis and up-regulate genes encoding proteins that stimulate fatty acid oxidation, both processes resulting in lower serum triglyceride levels.[75–77] EPA and/or DHA supplementation in animal studies reduced the substrate for triglyceride synthesis and increased peroxisomal, mitochondrial FA β-oxidation[78] and decreased concentrations of all blood lipids.[79] These FA activate expressions of genes involved in β-oxidation controlled by PPAR-α receptors. It was also reported that fish oil supplementation decreased the fractional catabolic rates of high density lipoprotein (HDL) and increased the ratio of HDL--2/HDL-3 cholesterol.[80] This was related to a decrease in the levels of plasma triglycerides, which stabilizes HDL particles as they become larger, retain more cholesterol and are less susceptible to catabolism by hepatic and renal clearance pathways.[81] At the level of low density lipoprotein (LDL) cholesterol and very low density lipoprotein (VLDL), peroxidation of PUFAs stimulates apoB degradation, reduces VLDL secretion, stimulates lipoprotein lipase activity mechanisms and increases postprandial clearance.[82,83]

The dosage of n-3 PUFA that lowers triglycerides differs among studies. Bays[84] found that 4 g of n-3 PUFAs per day, in the form of fish oil capsules, reduced serum triglyceride levels by 35 to 45 %. In a meta-analysis of 72 randomized control trials, Harris[78] reported a serum triglyceride reduction of 25––30 % at a dosage of 3–4 g day^{-1} of EPA + DHA. The effect of n-6 PUFAs enriched diets was also studied. A meta-analysis of 60 controlled trials reported that replacement of carbohydrates with PUFAs (largely n-6) had a beneficial effect on the total cholesterol/HDL-cholesterol ratio, and on the LDL concentration.[85] Replacing SFA by n-6 PUFAs also led to a substantial reduction in the total cholesterol and LDL-cholesterol, a reduction of the total cholesterol/HDL--cholesterol ratio and thus may reduce the risk of CHD.[86–88] A recently published paper[89] showed that the plasma cholesterol value was negatively correlated with serum levels of EPA.

3.2. PUFAs and obesity and diabetes

Although a favourable effect of n-3 PUFAs on development of diabetes mellitus was shown in several studies, the overall pooled data findings do not support any benefits of oily fish/seafood or EPA+DHA intake on diabetes and suggest that ALA may be associated with a modestly lower risk.[90] However, some evidence indicates that higher proportion of n-3 PUFAs in the diet may have anti-obesity effects and protection against metabolic syndrome through a number of metabolic effects.

It was proposed that n-6 PUFAs may be involved in the differentiation of preadipose cells to adipocytes.[91,92] To date, no firm conclusion could be drawn from available *in vitro* studies[93,94] on the role of AA in the differentiation of preadipose cells. Moreover, animal studies investigating the effect of a diet enriched in n-6 PUFAs on adipose tissue produced conflicting results.[91,94–96] More research is required to ascertain whether a balance of n-3 and n-6 in the diet contributes to excessive development of adipose tissue.

3.3. PUFAs and inflammation response

The possible mechanisms in PUFAs modulation of inflammatory response were investigated in a number of studies but the data were often inconsistent. Based on preclinical studies, the underlining mechanisms include transcriptional down-regulation of the production of pro-inflammatory cytokines,[97] cyclooxygenase-2 activity,[98] and vascular surface expression of endothelial leukocyte adhesion molecules.[99] These effects are a consequence of altered gene expression. Animal studies showed that n-3 PUFAs supplementation inhibited the production of pro-inflammatory cytokines IL-1 and TNF.[100] Similar observations were reported in studies in humans. In particular, studies of fish oil supplementation in patients with active inflammation diseases, such as rheumatoid arthritis and Crohn's disease,[100] supported a potentially beneficial anti-inflammatory effect of n-3 PUFAs. Dietary supplementation with n-3 PUFAs in healthy subjects was associated with reduced levels of IL-1, thromboxane 2 and prostaglandin E2,[101,102] but not of C-reactive protein.[103]

A potential protective effect of PUFAs supplementation on the progression of renal disease based on its action on inflammation in the renal fibrosis process, was suggested in studies on animal models.[104] The actions of PUFAs interfere directly with mesangial cell activation and proliferation and extra-cellular matrix protein synthesis, and they are involved in the regulation of pro-inflammatory cytokine production.[105,106] It is possible that PUFAs suppress the activity of the angiotensin-converting enzyme, reduce angiotensin II formation, enhance endothelium nitric oxide generation, and down-regulate the expression of the transforming growth factor-β (TGF-β).[107]

The anti-inflammatory effects of n-3 fatty acids from seafood may contribute to their protective actions towards atherosclerosis, plaque rupture and cardiovascular mortality. In inflammatory bowel diseases, some trials reported improved gut histology, duration of morning stiffness, global assessments of pain, decreased disease activity, use of corticosteroids and relapse.[108] However, the therapeutic dose of n-3 PUFA has not yet been established.[109] For instance, reduction of pro-inflammatory eicosanoids and cytokines could be achieved with an intake of 2–4 g day^{-1} of 84 % EPA+DHA ethyl esters.[110] In the inCHIANTI study,[111] the intake of 7 g day^{-1} PUFAs led to higher plasma levels of AA and n-3 PUFA (mainly DHA) and these FA profiles were independently associated with lower levels of serum pro-inflammatory markers. Thies *et al.*[112] reported that a dietary supplementation with moderate amounts of long-chain n-6 or n-3 PUFAs neither significantly affected inflammatory cell numbers nor neutrophil and monocyte responses.

3.4. PUFAs and oxidative stress

Both n-3 and n-6 PUFAs are highly susceptible to oxidation because of their multiple double bonds. This lipid peroxidation, leading to pro-inflammatory oxidised LDL and HDL, is highly suspected of contributing to the pathogenesis of atherosclerosis. Several studies showed that dietary supplementation of n-6 PUFAs increased the extent of LDL oxidation *in vitro* compared with a diet enriched in mono-unsaturated FA.[113] In contrast, markers related to LDL oxidation *in vitro* or malondialdehyde derived from LDL showed no correlation with n-6 PUFA intake in a group of healthy volunteers.[114] Furthermore, a double-blind controlled intervention in a cohort of healthy men showed that fish oil consumption combined with a high LA intake (21 g day^{-1}) did not raise the plasma level of oxidised LDL compared with the same fish oil consumption but combined with a low level of LA.[115] Parameters of oxidative stress were significantly improved after fish oil supplementation in an animal study.[79] EPA and DHA have beneficial effects in glomerular disease, which are attributed to their effect on the pro-oxidant and antioxidant status and EFA metabolism, as reviewed by Das.[107] However, recent evidence does not support the idea that n-3 PUFAs up-regulate oxidative stress. Further investigations would enable more definitive conclusions to be made.

3.5. PUFAs and blood pressure and mortality

As highlighted by a review of cross-sectional studies, an increase in the dietary intake of n-6 PUFAs is often associated with a decrease in blood pressure.[116] It was also reported that plasma levels of LA were inversely associated with systolic and diastolic blood pressures.[117] Combining the results from different studies in a meta-analysis, Morris *et al.*[118] found that at supraphysiological

doses of 5.6 g n-3 PUFAs in hypertensive subjects, systolic pressure was reduced by 3.4 and diastolic pressure by 2.0 mmHg. Possible mechanisms include modulation of the biosynthesis of eicosanoids: hydroxyeicosatetraenoates or epoxyeicosatrienoates.[119] A more recently published meta-analysis also supported the antihypertensive effects of n-3 PUFAs.[120] Similar findings were obtained in animal models and cell culture studies, which indicate that n-3 PUFAs supplementation can lower blood pressure and proteinuria, potentially by the vasorelaxation action of n-3 PUFAs with increased endothelium-derived releasing factor[107] and by having effects on TGF-β, renin, fibronectin and nitric oxide synthesis.[104]

Another meta-analysis of 25 case–control studies was performed by Harris *et al.*[121] in order to assess the association between the tissue contents of n-3 and n-6 PUFAs and CHD events. They found that content of LA in tissue was significantly decreased in patients with CHD events. Similar results were found in a study by Block *et al.*[122] on the relation between acute coronary syndrome and the fatty acid content of whole-blood cell membranes. The renal, cardiovascular and reduced mortality benefits of n-3 fatty acids are still areas of active investigation. Kutner *et al.*[123] in a prospective cohort study showed that dialysis patients with a high intake of fish live longer, with an approximately 50 % lower rate of mortality over 3 years. Regarding the role of n-3 PUFAs and CVD, a randomized clinical trial by Svensson *et al.*[124] found that compared with placebo groups, patients receiving n-3 PUFAs supplementation (1.7 g day^{-1}) had a protective effect on the rate of myocardial infarctions but led to no improvement in the primary end point of total cardiovascular events and death, with a follow-up of 2 years. The same authors reported that there was no change in heart rate variability in haemodialyzed patients during 8 weeks of n-3 PUFA supplementation at a dosage of 1.7 g day^{-1}.[125] A recently published controlled study by Kirkegaard *et al.*[126] showed an inverse association between the presence of arterial fibrillation and plasma DHA. This is very important because high risk of sudden cardiac death is often caused by arrhythmias. Finally, a new meta-analysis of 20 clinical studies[127] looking at the effects of n-3 PUFAs in patients at high risk for cardiovascular events showed that the supplements had no effect on hard clinical outcomes, including all-cause mortality, cardiac death, sudden death, myocard infarction or stroke. In the future, better-powered studies would need to be conducted to resolve the relationship between n-3 PUFAs status and the mortality risk.

3.6. PUFAs and haematological parameters

The effect of fish oil supplementation and n-3 PUFAs on red blood cell deformability and aggregation has also been investigated.[128,129] Findings from these studies suggest that n-3 PUFAs have antithrombotic, antiproliferative and anti-aggregatory platelet effects.[130] These FAs can influence gene regulation by down-regulating gene expression of platelet-derived growth factors and suppress the platelet activating factor, a potent platelet aggregator and leukocyte acti-

vator.[81,131] n-3 DPA can be metabolised by lipoxygenase in platelets, to form 11-hydroxy-7,9,13,16,19- and 14-hydroxy-7,10,12,16,19-DPA. It was also reported that n-3 DPA is effective (more than EPA and DHA) in the inhibition of aggregation in platelets obtained from rabbit blood.[132] The results from human studies are not conclusive, and further investigations are required to clarify the role of n-6 PUFAs in susceptibility to thrombosis.

3.7. PUFAs and cancer

Data from epidemiological studies suggest that diets rich in n-6 PUFAs may be associated with cancer risk. Studies on patients with cancer at different sites have shown a poor n-3 FA status due to suboptimal intakes and possible metabolic disturbances. Low proportions of n-3 PUFAs in plasma and/or erythrocytes phospholipids were found in pancreatic, lung and prostate cancer, and non-Hodgkin lymphoma.[61,133,134] All n-3 PUFAs were shown to be particularly depleted in advanced cancer patients, during chemotherapy and in cancer patients close to death. Additionally, low plasma n-3 fatty acids were associated with loss of skeletal muscle in these patients.[135]

Considering all these findings, supplementation with EPA and DHA in patients suffering from cancer was the objective in many trials. Long chain n-3 PUFA have inhibitory effects in tumour formation, probably through alteration of prostaglandins synthesis and inhibition of cell proliferation in colon and breast cancer.[136] A beneficial effect of n-3 supplementation throughout antineoplastic therapy was confirmed through weight, lean body mass and treatment outcomes. In patients with pancreatic cancer, fish oil supplementation may prevent cachexia.[137] In contrast, n-6 PUFAs have been associated with a greater capacity to induce tumour formation.[136] As mentioned above, Western diet contains disproportionally high n-6/n-3 PUFA ratios, which is thought to contribute to cancer. In favour of this assumption is the proportion of n-6 PUFA in cancer patients, which was found to be very high in patients with non-Hodgkin lymphoma.

The nature of the anti-tumour effects of EPA are not clearly understood, but one of the mechanisms is competitive inhibition of the use of AA for the production of eicosanoids. Eicosanoids derived from AA have been associated with both tumour promotion and progression. EPA is also a potent angiogenesis inhibitor, which suppresses the production of crucial angiogenic mediators, namely: vascular endothelial growth factor, platelet-derived growth factor, cyclo--oxygenase 2, nuclear factor kappa beta and nitric oxide.[138]

4. CONCLUSIONS

In conclusion, PUFAs have important roles in a wide range of physiological and pathologic processes. However, more conclusive relationships between PUFAs and metabolic pathways of insulin resistance, obesity, pancreatic and liver function, diabetic nephropathy, asthma clinical outcomes, mental health and

PUFAs supplementation in cachexia should be established. Future supplementation studies in larger, randomized control trials are required to reveal the full potential of PUFAs in the prevention and therapy of chronic diseases.

LIST OF ABBREVIATIONS

AA – arachidonic acid
ALA – α-linolenic acid
CHD – cardiovascular heart disease
DGLA – dihomo-γ-linolenic acid
DHA – docosahexaenoic acid
DPA – docosapentaenoic acid
EFA – essential fatty acids
EPA – eicosapentaenoic acid
FA – fatty acid
HDL – high density lipoprotein
LA – linoleic acid
LDL – low density lipoprotein
PPAR – proliferator-activated receptors
PUFA – polyunsaturated fatty acid
SFA – saturated fatty acid
TGF – transforming growth factor
TNF – tumour necrosis factor
VLDL – very low density lipoprotein
E% – percentage of energy

Acknowledgement. This work was supported by the Project III41030 financed by the Ministry of Education, Science and Technological Development of the Republic of Serbia.

И З В О Д

ПОЛИНЕЗАСИЋЕНЕ МАСНЕ КИСЕЛИНЕ У ЗДРАВЉУ И БОЛЕСТИ

ДАНИЈЕЛА РИСТИЋ-МЕДИЋ, ВЕСНА ВУЧИЋ, МАРИЈА ТАКИЋ, ИВАНА КАРАЦИЋ и МАРИЈА ГЛИБЕТИЋ

Центар изузетних вредности у области истраживања исхране и метаболизма, Институт за медицинска истраживања, Универзитет у Београду, Београд

Полинезасићене масне киселине (ПМК) су неопходне за нормално функционисање организма. Две ПМК фамилије, n-6 и n-3 масне киселине се физиолошки и метаболички разликују. Удео ПМК у фосфолипидима серума и еритроцита је важан показатељ здравља и болести, и зависи од ендогеног метаболизма, који је контролисан генетским полиморфизмом, и уноса хране. И n-6 и n-3 ПМК су прекурсори за синтезу еикозаноида на циклооксигеназном и липооксигеназном нивоу. Опсервационе и интервентне студије указују да n-3 ПМК имају кардиопротективни ефекат, делујући анти-инфламаторно, анти-аритмогено, хиполипидемично и антихипертензивно. Насупрот томе, сматра се да n-6 ПМК имају про-инфламаторно дејство. Низак ниво n-3 и повишен удео n-6 ПМК је показан код пацијената са различитим типовима малигнитета. У оквиру овог рада дат је преглед најновијих сазнања о дијетарном уносу и биомаркерима статуса ПМК у промоцији здравља и превенцији болести, са посебним осврtом на резултате у нашој популацији.

(Примљено 2. априла, ревидирано 15. априла 2013)

REFERENCES

1. J. Schwab, C. N. Serhan, *Curr. Opin. Pharmacol.* **6** (2006) 414
2. A. P. Simopoulos, *Exp. Biol. Med.* **233** (2008) 674
3. V. Wijendran, B. C. Hayes, *Annu. Rev. Nutr.* **24** (2004) 597
4. X. Wang, H. Lin, Y. Gu, *Lipids Health Dis.* **14** (2012) 25
5. F. M. Sacks, M. Katan, *Am. J. Med.* **13** (2002) S113
6. W. C. Willett, *J. Cardiovasc. Med.* **8** (2007) S42
7. W. S. Harris, D. Mozaffarian, E. Rimm, P. Kris-Etherton, L. L. Rudel, L. J. Appel, M. M. Engler, F. Sacks, *Circulation* **119** (2009) 902
8. A. M. Hodge, D. R. English, K. O'Dea, A. J. Sinclair, M. Makrides, R. A. Gibson, G. G. Giles, *Am. J. Clin. Nutr.* **86** (2007) 189
9. D. Ristic-Medic, G. Ristic, V. Tepsic, *Med. Pregl.* **60** (2007) S43 (in Serbian)
10. C. M. Albert, K. Oh, W. Whang, J. E. Manson, C. U. Chae, M. J. Stampfer, W. C. Willett, F. B. Hu, *Circulation* **112** (2005) 3232
11. D. Mozaffarian, *Ther. Health Med.* **11** (2005) 24
12. A. Sala-Vila, E. Ros, *Clin. Lipidol.* **6** (2011) 365
13. M. L. Burr, A. M. Fehily, J. F. Gilbert, S. Rogers, R. M. Holliday, P. M. Sweetnam, P. C. Elwood, N. M. Deadman, *Lancet* **2** (1989) 757
14. D. Mozaffarian, E. B. Rimm, *JAMA* **296** (2006) 1885
15. D. Ristić-Medić, G. Peruničić-Peković, Z. Rašić-Milutinović, *Nutr. Therapy Met.* **29** (2011) 178
16. M. Yokoyama, H. Origasa, M. Matsuzaki, Y. Matsuzawa, Y. Saito, Y. Ishikawa, S. Oikawa, J. Sasaki, H. Hishida, H. Itakura, T. Kita, A. Kitabatake, N. Nakaya, T. Sakata, K. Shimada, K. Shirato, *Lancet* **369** (2007) 1090
17. L. Tavazzi, A. P. Maggioni, R. S. Barlera, M. G. R. Franzos, D. Latini, G. L. Lucci, M. Nicolosi, M. Porcu, G. Tognoni, *Lancet* **372** (2008) 1223
18. I. Cetin, B. Koletzko, *Curr. Opin. Clin. Nutr. Metab. Care* **11** (2008) 297
19. T. Decsi, B. Koletzko, *Curr. Opin. Clin. Nutr. Metab. Care* **8** (2005) 161
20. I. B. Helland, L. Smith, B. Blomen, K. Saarem, O. D. Saugstad, C. A. Drevon, *Pediatrics* **122** (2008) 472
21. A. S. Ryan, J. D. Astwood, S. Gautier, C. N. Kuratko, E. B. Nelson, N. Salem, *Prostaglandins Leukot. Essent. Fatty Acids* **82** (2010) 305
22. S. I. Rapoport, *Prostaglandins Leukot. Essent. Fatty Acids* **79** (2008) 305
23. D. R. Hoffman, J. A Boettcher, D. A. Diersen-Schade, *Prostaglandins Leukot. Essent. Fatty Acids* **81** (2009) 151
24. V. Vučić, J. Tepšić, A. Arsić, T. Popović, J. Debeljak-Martačić, M. Glibetić, *Acta Aliment. Hung.* **41** (2012) 343
25. Department of Health, *Dietary Reference Values for Food Energy and Nutrients for the United Kingdom*, HMSO, London, 1991.
26. B. J. Meyer, N. J. Mann, J. L Lewis, G. C. Milligan, A. J. Sinclair, R. P. Howe, *Lipids* **38** (2003) 391
27. M. Nikolic, D. Ristic Medic, D. Stanic, M. Postic, A. Arsic, V. Niketic, *Eur. J. Nutr.* **47** (2008) 123
28. T. L. Blasbalg, J. R. Hibbeln, C. E. Ramsden, S. F. Majchrzak, R. R. Rawlings, *Am. J. Clin. Nutr.* **93** (2011) 950
29. G. C. Burdge, P. C. Calder, *Nutr. Res. Rev.* **19** (2006) 26
30. A. P. Simopoulos, A. Leaf, N. Salem Jr., *Ann. Nutr. Metab.* **43**(1999) 127
31. R. Wall, R. P. Ross, G. F. Fitzgerald, C. Stanton, *Nutr. Rev.* **68** (2010) 280

32. L. A. Smith, D. Mozaffarian, *Ann. Nutr. Metab.* **55** (2009) 44
33. FAO, *Fats and Oils in Human Nutrition*, Report of a Joint FAO/WHO Expert Consultation, FAO, Rome, 1994
34. H. Tunstall-Pedoe, *Preventing Chronic Diseases. A Vital Investment:* WHO Global Report, Geneva, 2006
35. Institute of Medicine, *Dietary Reference Intakes for Energy, Carbohydrate, Fiber, Fat, Fatty Acids, Cholesterol, Protein, and Amino Acids*, National Academies, Washington DC, 2005
36. ISSFAL 2004, *Report of the Sub-Committee on Recommendations for the Intake of Polyunsaturated Fatty Acids in Healthy Adults*, The Sixth International Society for the Study of Fatty Acids and Lipids. Brighton, 2004, http://www.issfal.org.uk/pdfs/ /PUFAIntakeReccomdFinalReport.pdf (accessed 13 April 2006)
37. R. J. Harper, J. A. Jacobson, *J. Am. Coll. Cardiol.* **51** (2008) 2375
38. National Health and Medical Research Council, *Nutrient Reference Values for Australia and New Zealand*, NHMRC, Canberra, 2003
39. Eurodiet: Eurodiet core report: European dietary guidelines, 2000. http://eurodiet.med.uoc.gr/eurodietcorereport.pdf (accessed 1 October 2008)
40. I. Elmadfa, M. Kornsteiner, *Ann. Nutr. Metab.* **59** (2009) 56
41. J. C. Stanley, R. L. Elsom, P. C. Calder, B. A. Griffin, W. S. Harris, S. A. Jebb, J. A. Lovegrove, C. S. Moore, R. A. Riemersma, T. A. Sanders, *Br. J. Nutr.* **98** (2007) 1305
42. W. S. Harris, *Curr. Atheroscler. Rep*. **8** (2006) 453
43. C. Glaser, J. Heinrich, B. Koletzko, *Metabolism* **59 (**2010) 993
44. J. Whelan, *J. Nutr.***126** (1996) S1086
45. C. D. Stubbs, A. D. Smith, *Biochim. Biophys. Acta* **779** (1984) 89
46. A. Spector, M. A. Yorek, *J. Lipid Res.* **26** (1985)1015
47. M. R. Clemens, M. Ruess, Z. Bursa, H. D. Waller, *Free Rad. Res. Commun.* **3** (1987) 265
48. D. E. Mills, M. Murphy, W. R. Galley, *Lipids* **30** (1995) 657
49. K. Komidori, T. Kamada, T. Yamashita, R. Harada, Y. Otsuji, S. Hashimoto, Y. Chuman, S. Otsuji, *Nephron* **40** (1985)185
50. J. Tepsic, V. Vucic, A. Arsic, S. Mazic, M. Djelic, M. Glibetic, *Eur. J. Sport Sci*. **51** (2011) 2044
51. J. Tepšić, V. Vučić, A. Arsić, V. Blaženčić-Mladenović, S. Mazić, M. Glibetić, *Eur. J. Appl. Physiol.* **107** (2009) 359
52. A. Arsić, V. Vučić, J. Tepšić, S. Mazić, M. Djelić, M. Glibetić, *Appl. Physiol. Nutr. Metab.* **37** (2012) 40
53. S. B. Shohet, D. G. Nathan, *Biochim. Biophys. Acta* **202** (1970) 202
54. E. Mulder E, L. M. Van Deenen, *Biochim, Biophys. Acta* **106** (1965) 348
55. L. W. Peck, *J. Am. Diet. Assoc.* **97** (1997) S150
56. M. Taccone-Gallucci, R. Lubrano, A. Clerico, C. Meloni, M. Morosetti, L. Meschini, E. Trapasso, M. A. Castello, C. U. Casciani, *ASAIO J.* **38** (1992) 855
57. J. C. Duncan, *Calcium, oxygen radicals and cellular damage*, Cambridge University Press, Cambridge, 1991
58. D. Ristić-Medić, V. Ristić, V. Tepšić, M. Ranić, G. Ristić, S. Vrbaški, I. Etelecki, *Nutr. Res.* **23** (2003) 465
59. D. Ristic Medic, V. Ristic, A. Arsic, M. Postic, G. Ristic, V. Blazencic Mladenovic, J. Tepsic, *Nutr. Met. Cardiovasc. Dis.* **16** (2006) 395
60. D. Ristic-Medic, S. Suzic, V. Vucic, M. Takic, J. Tepsic, M. Glibetic, *Gen. Physiol. Biophys.* **28** (2009) 190

61. Z. Cvetković, V. Vučić, B. Cvetković, M. Petrović, D. Ristić-Medić, J. Tepšić, M. Glibetić, *Ann. Hematol.* **89** (2010) 775
62. V. Risic, V. Tepšic, D. Ristic-Medic, G. Perunicic, Z. Rasic, M. Poštic, A. Arsic, V. Blazencic, G. Ristic, *Renal Failure* **28** (2006) 211
63. Z. Rasic-Milutinovic, G. Perunicic, S. I. Pljesa S, Z. Gluvic, S. Sobajic, I. Djuric, D. Ristic, *Renal Failure* **29** (2007) 321
64. G. B. Perunicic-Pekovic, Z. R. Rasic, S. I. Pljesa, S. Sobajic, I. Djuric, R. Maletic, D. Ristic-Medic, *Nephrology* **12** (2007) 331
65. A. M. Koorts, M. Viljoen, M. C. Kruger, *Prostaglandins Leukot. Essent. Fatty Acids* **67 (**2002) 13
66. T. Popovic, M. Ranic, P. Bulajic, M. Milicevic, A. Arsic, V. Vucic, M. Glibetic, *J. Clin. Biochem. Nutr.* **45** (2009) 1
67. M. Takić, D. Ristić-Medić, Lj. Mandić, M. Glibetić, A. Arsić, J. Debeljak-Martačić, G. Petrović-Oggiano, *Arch. Biol. Sci.* **61** (2009) 37
68. R. De Caterina, R. Madonna, A. Bertolotto, E. B. Schmidt. *Diabetes Care* **30** (2007) 1012
69. B. M. Forman, J. Chen, R. M. Evans, *Proc. Natl. Acad. Sci. USA* **94** (1997) 4312
70. Y. A. Carpentier, I. Portois, W. J. Malaisse, *Am J. Clinic. Nutr.* **83** (2006) 1449S
71. P. M. Kris-Etherton, W. S. Harris, L. J. Apell, *Circulation* **106** (2002) 2747
72. A. Saifullah, B. A. Watkins, S. Saha, Y. Li, S. Moe, A. N. Friedman, *Nephrol. Dial. Transplan.* **22** (2007) 3561
73. A. Lapillonne, S. D. Clarke, W. C. Heird, *Curr. Opin. Clin. Nutr. Metab. Care* **7** (2004) 151
74. M. H. Davidson, *Am. J. Cardiol.* **98** (2006) 27
75. S. A. Kliewer, S. S. Sundseth, S. A. Jones, P. J. Brown, G. B. Wisely, C. S. Koble, P. Devchand, W. Wahli, T. M. Willson, J. M. Lenhard, J. M. Lehmann, *Proc. Natl. Acad. Sci. USA* **94** (1997) 4318
76. F. B. Hu, M. J. Stampfer, J. E. Manson, A. Ascherio, G. A. Colditz, F. E. Speizer, C. H. Hennekens, W. C. Willett, *Am. J. Clin. Nutr.* **70** (1999) 1001
77. D. B. Jump, *Curr. Opin. Lipidol.* **13** (2002) 155
78. W. S. Harris, *Am. J. Clin. Nutr.* **65** (1997) S1645
79. T. Popovic, S. Borozan, A. Arsic, J. Debeljak-Martacic, V. Vucic, A. Trbovic, Lj. Mandic, M. Glibetic, *J. Anim. Physiol. Anim. Nutr.* **96** (2012) 1020
80. D. Chan, G. F. Watts, M. N. Nguyen, P. H. R. Barrett, *Am. J. Clin. Nutr.* **84** (2006) 37
81. C. Torrejon, U. J. Jung, R. J. Deckelbaum, *Prostaglandins, Leukot. Essent. Fatty Acids* **77** (2007) 319
82. Y. Park, W. S. Harris, *J. Lipid Res.* **44** (2003) 455
83. I. Ikeda, J. Kumamaru, N. Nakatani, M. Sakono, I. Murota. K. Imaizumi, *J. Nutr.* **131** (2001) 1159
84. H. Bays, *Am. J. Cardiol.* **98** (2006) 71
85. R. P. Mensink, P. L. Zock, A. D. Kester, M. B. Katan, *Am. J. Clin. Nutr.* **77** (2003) 1146
86. S. Czernichow, D. Thomas, E. Bruckert, *Br. J. Nutr.* **107** (2012) S 171
87. M. U. Jakobsen, E. J. O'Reilly, B. L. Heitmann, M. A. Pereira, K. Bälter, G. E. Fraser, U. Goldbourt, G. Hallmans, P. Knekt, S. Liu, P. Pietinen, D. Spiegelman, J. Stevens, J. Virtamo, W. C. Willett, A. Ascherio, *Am. J. Clin. Nutr.* **89** (2009) 1425
88. L. Hodson L, C. M. Skeaff, W. A. Chisholm, *Eur. J. Clin. Nutr.* **55** (2001) 908
89. G. Peruničić-Peković, Z. Rašić-Milutinović, Z. Gluvić, M. Lačković, D. Ristić-Medić, M. Glibetić, *Arch. Biol. Sci.* **64** (2012) 1173

90. J. H. Wu, R. Micha, F. Imamura, A. Pan, M. L. Biggs, O. Ajaz, L. Djousse, F. B. Hu, D. Mozaffarian, *J. Nutr.* **107** (2012) S214
91. M. P. Cleary, F. C. Phillips, R. A. Morton *Proc. Soc. Exp. Biol. Med.* **220** (1999) 153
92. F. Massiera, P. Saint-Marc, J. Seydoux, T. Murata, T. Kobayashi, S. Narumiya, P. Guesnet, E. Z. Amri, R. Negrel, G. Ailhaud, *J. Lipid. Res.* **44** (2003) 271
93. C. W. Miller, D. A. Casimir, J. M. Ntambi, *Endocrinology* **137** (1996) 5641
94. G. Serrero, N. M. Lepak, S. P. Goodrich, *Biochem. Biophys. Res. Commun.* **183** (1992) 183
95. G. Ailhaud, P. Guesnet, S. C. Cunnane, *Br. J. Nutr.* **100** (2008) 467
96. K. Okuno, S. Kajiwara, S. Imai, T. Kobayashi, N. Honma, T. Maki, K. Suruga, T. Goda, S. Takase, Y. Muto, H. Moriwaki, *J. Nutr.* **127** (1997) 1752
97. S. A. Khan, J. P. Vanden Heuvel, *J. Nutr. Biochem.* **14** (2003) 554
98. P. C. Calder, *Proc. Nutr. Soc.* **61** (2002) 345
99. R. De Caterina, P. Libby, *Lipids* **31** (1996) S57
100. P. C. Calder, *Lipids* **38** (1996) 343
101. S. Endres, S. N. Meydani, R. Ghorbani, R. Schindler, C. A. Dinarello, *J. Leukoc. Biol.* **54** (1993) 599
102. E. Mantzioris, L. G. Cleland, R. A. Gibson, M. A. Neumann, M. Demasi, M. J. James, *Am. J. Clin. Nutr.* **72 (**2000) 42
103. A. Geelen, I. A. Brouwer, E. G. Schouten, C. Kluft, M. B. Katan, L. Zock, *Eur. J. Clin. Nutr.* **58** (2004) 1440
104. B. Baggio, E. Musacchio, G. Priante, *J. Nephrol.* **18** (2005) 362
105. R. Graber, C. Sumunda, E. A. Nunez, *J. Lipid. Mediat. Cell Signal.* **9** (1994) 91
106. V. Di Marzo, *Prostanlandins Leukot. Essent. Fatty Acids* **53** (1995) 239
107. U. N. Das. *Eur. J. Clin. Nutr.* **58** (2004) 195
108. P. C. Calder, *Mol. Nutr. Food Res.* **52** (2008) 885
109. E. A. Miles, P. C. Calder, *Br. J. Nutr.* **107** (2012) S171
110. H. Rupp, D. Wagner, T. Rupp, L. M. Schulte, B. Maisch, *Herz* **29** (2004) 673
111. L. Ferrucci, A. Cherubini, S. Bandinelli, B. Bartali, A. Corsi, F. Lauretani, A. Martin , C. Andres-Lacueva, U. Senin, J. M. Guralnik, *J. Clin. Endocrinol. Metab.* **91** (2006) 439
112. F. Thies, E. A. Miles, G. Nebe-von-Caron, J. R. Powell, T. L. Hurst, E. A. Newsholme, P. C. Calder, *Lipids* **36** (2001) 1183
113. M. Abbey, G. B. Belling, M. Noakes, F. Hirata, P. J. Nestel, *Am. J. Clin. Nutr.* **57** (1993) 391
114. P. Kleemola, R. Freese, M. Jauhiainen, R. Pahlman, G. Alfthan, M. Mutanen, *Atherosclerosis* **160** (2002) 425
115. C. T. Damsgaard, H. Frokiaer, A. D. Andersen, L. Lauritzen, *J. Nutr.* **138** (2008) 1061
116. W. L. Hall, *Nutr. Res. Rev.* **22** (2009) 18
117. J. A. Simon, J. Fong, J. T. Bernert, *Hypertension* **27** (1996) 303
118. M. C. Morris, F. Sacks, B. Rosner, *Circulation* **88** (1993) 523
119. J. C. McGiff, J. Quilley, *Curr. Opin. Nephrol. Hypertens.* **10** (2001) 231
120. J. M. Geleijnse, E. J. Giltay, D. E. Grobbee, A. R. Donders, F. J. Kok, *J. Hypertens.* **20** (2002) 1493
121. W. S. Harris, W. C. Poston, C. K. Haddock, *Atherosclerosis* **193** (2007) 1
122. R. C. Block, W. S. Harris, K. J. Reid , J. A. Spertus, *Am. Heart J.* **156** (2008) 1117
123. N. G. Kutner, P. W. Clow, R. Zhang, A. Aviles, *Am. J. Kidney Dis.* **39 (**2002) 1018
124. M. Svensson, E. Schmidt, K. Jorgensen, J. Christensen, *Clin. J. Am. Soc. Nephrol.* **1** (2006) 780

125. M. Svensson, E. B. Schmidt, K. A. Jørgensen, J. H. Christensen, *J. Ren. Nutr.* **17** (2007) 243
126. E. Kirkegaard, M. Svensson, C. Strandhave, K. Schmidt, A. Jørgensen, C. Hagstrup, *Br. J. Nutr.* **26** (2011) 1
127. E. C. Rizos, E. E. Ntzani, E. Bika, M. S. Kostapanos, M. S. Elisaf, *JAMA* **308** (2012) 1024
128. I. J. Cartwright, A. G. Pockley, J. H. Galloway, M. Greaves, F. E. Preston, *Atherosclerosis* **55** (1985) 267
129. R. G. Bowden, R. L. Wilson, M. Gentile, S. Ounpraseuth, P. Moore, B. C. Leutholtz, *J. Ren. Nutr.* **17** (2007) 126
130. T. A. Mori, L. Beilin, V. Burke, J. Morris, J. Ritchie, *Arterioscler. Thromb. Vasc. Biol.* **17** (1997) 279
131. W. E. Kaminski, R. Jendraschak, R. Kiefl, C. von Schacky, *Blood* **81**(1993) 1871
132. G. Kaur, D. Cameron-Smith, M. Garg, A. J. Sinclair, *Prog. Lipid. Res.* **50** (2011) 28
133. R. A. Murphy, T. F. Bureyko, M. Mourtzakis, Q. S. Chu, M. T. Clandinin, T. Reiman, V. C. Mazurak, *Lipids* **47** (2012) 363
134. S. D. Zuijdgeest-van Leeuwen, M. S. van der Heijden, T. Rietveld, J. W. van den Berg, H. W. Tilanus, J. A. Burgers, J. H. Wilson, P. C. Dagnelie, *Clin. Nutr.* **21** (2002) 225
135. R. A. Murphy, M. Mourtzakis, Q. S. Chu, T. Reiman, V. C. Mazurak, *J. Nutr.***140** (2010) 1602
136. H. Weisburger, *J. Am. Diet Assoc.* ***97*** (1997) S16
137. T. T. Brown, D. L. Zelnik, A. S. Dobs, *Int. J. Gastrointest. Cancer* **34 (**2003) 143
138. V. Vucic, D. Ristic-Medic, *Eicosapentaenoic Acid: Sources, Health Effects and Role in Disease Prevention*, Nova Publishers, New York, 2012, p. 99.

Journal of the Serbian Chemical Society
JSCS-info@shd.org.rs • www.shd.org.rs/JSCS
J. Serb. Chem. Soc. 78 (9) 1291–1299 (2013)
JSCS–4497
UDC 547.815+542.9:547.7+
542.913:546.185'226–32
Original scientific paper

Phosphosulfonic acid, an efficient solid acid catalyst for the one-pot preparation of 14-aryl-14*H*-dibenzo[*a,j*]xanthenes and 1,8-dioxooctahydroxanthenes under solvent-free conditions

ALI REZA KIASAT*, ARASH MOURADZADEGUN and SEYYED JAFAR SAGHANEZHAD

Chemistry Department, College of Science, Shahid Chamran University, P. O. Box 61357-4-3169, Ahvaz, Iran

(Received 8 October 2012, revised 16 January 2013)

Abstract: An expeditious procedure for the synthesis of 14-aryl-14*H*-dibenzo[*a,j*]xanthenes and 1,8-dioxooctahydroxanthenes through a one-pot pseudo three component condensation of *β*-naphthol or dimedone with various aromatic aldehydes is described. This green protocol is catalyzed by phosphosulfonic acid, and proceeds efficiently in the absence of any organic solvent under optimized, mild, green and environmentally benign reaction conditions in high yields within 20–55 min.

Keywords: xanthenes; one-pot reaction; dimedone; *β*-naphthol; solvent-free; phosphosulfonic acid.

INTRODUCTION

The synthesis of new heterocyclic compounds has always been a subject of great interest due to their wide applicability. Among a large variety of heterocyclic compounds, heterocyclic compounds with oxygen-containing moieties are industrially very important as they serve as precursors. Xanthene derivatives, which have one oxygen atom in a fused ring system, possess antibacterial,[1] antiviral[2] and anti-inflammatory[3] activities. Moreover, these compounds have been used as leuco dyes[4] and found application in laser technology[5] and as sensitizers in photodynamic therapy.[6] Thus, the synthesis of xanthenes is of paramount importance in organic synthesis.

A literature search revealed that many procedures have been developed for the preparation of the biologically important xanthene derivatives, 14-aryl-14*H*--dibenzo[*a,j*]xanthenes, through the dehydration of *β*-naphthol and aromatic alde-

* Corresponding author. E-mail: akiasat@scu.ac.ir
doi: 10.2298/JSC121108008K

hydes in the presence of various catalysts, such as AcOH–H_2SO_4,[7] selectfluor (1-(chloromethyl-4-fluoro-1,4-diazoniabicyclo[2.2.2]octane bis(tetrafluoroborate)),[8] wet cyanuric chloride,[9] $Sc[N(SO_2C_8F_{17})_2]_3$ in a fluorine-containing solvent,[10] silica gel supported $H_6P_2W_{18}O_{62}\cdot 24H_2O$ or $H_3PW_{12}O_{40}\cdot 6H_2O$,[11] I_2,[12] sulfamic acid,[13] a Preyssler-type heteropolyacid ($H_{14}[NaP_5W_{30}O_{110}]$),[14] potassium dodecatungstocobaltate trihydrate ($K_5CoW_{12}O_{40}\cdot 3H_2O$),[15] poly(4-vinylpyridinium) hydrogen sulfate,[16] an acid-functionalized mesoporous silica sieve (SBA-15)[17] and sulfonic acid-functionalized silica (SiO_2–Pr-SO_3H).[18]

In the same manner, the synthesis of 1,8-dioxooctahydroxanthenes was achieved through the dehydration of dimedone (5,5-dimethylcyclohexane-1,3--dione) and aromatic aldehydes in pseudo three-component reactions in the presence of a catalyst, such as, tetrabutylammonium hydrogen sulfate,[19] Sc^{3+}–montmorillonite,[20] $HClO_4$–SiO_2 and polyphosphoric acid (PPA)–SiO_2,[21] phosphomolybdic acid (PMA)–SiO_2,[22] acidic ionic liquids,[23] heteropoly tungstic acid (HPWA) loaded Si-mobile crystalline material (HPWA–MCM-41) mesoporous molecular sieves,[24] silica-supported Preyssler nanoparticles (SPNP),[25] MCM--41–RSO_3H,[26] acid functionalized SBA-15 and MCM-41,[27] and silica-bonded *N*-propylsulfamic acid (SBNPSA).[28]

Although these methods may be effective, some of them have relatively long reaction times and unsatisfactory yields. Due to their wide application, further development of an efficient and useful method for the synthesis of xanthenes derivatives were considered advantageous. These findings prompted further investigations in the search for a new catalyst that would assist in the synthesis of 14*H*-dibenzo[*a*,*j*]xanthenes and 1,8-dioxooctahydroxanthenes under a simpler experimental set up and eco-friendly conditions.

Furthermore, the application of environmentally benign, solid acid catalysts, especially under solvent-free conditions, in organic synthesis provides some advantages, such as ease of handling, mild reaction conditions, decreasing reactor and plant corrosion problems, easier work-up and ease of transportation and storage.[29]

Thus, in continuation of previous studies on the applications of reusable acid catalysts in organic synthesis,[30,31] it was decided to investigate the synthesis of 14-aryl-14*H*-dibenzo[*a*,*j*]xanthenes and 1,8-dioxooctahydroxanthenes in the presence of catalytic amounts of phosphosulfonic acid under solvent-free conditions (Scheme 1).

RESULTS AND DISCUSSION

Phosphosulfonic acid, PSA, was easily prepared by simple mixing of diammonium hydrogen phosphate and chlorosulfonic acid in CH_2Cl_2 at room temperature (Scheme 2).[32]

The FT-IR spectrum of the catalyst (Fig. 1) was recorded using the KBr disc technique. The O=S=O asymmetric and symmetric stretching modes of the sulfonic acid functional groups were found in the ranges 1141–1316 and 1010–1020 cm^{-1}, respectively, and that of the S–O stretching mode at 695 cm^{-1}. The spectrum also showed a broad OH stretching absorption around 2700 and 3600 cm^{-1}.

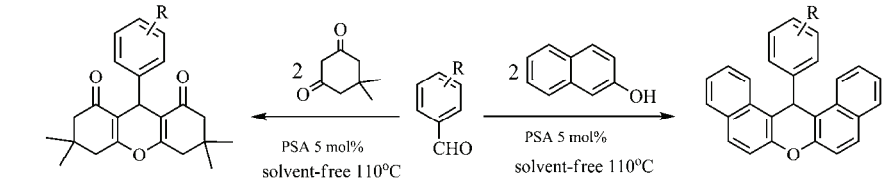

1,8-dioxooctahydroxanthenes **5a-h**

14- aryl-14H-dibenzo[*aj*]xanthenes **3a-l**

Scheme 1. One-pot preparation of 14-aryl-14*H*-dibenzo[*a*,*j*]xanthenes (**3a**–**l**) and 1,8-dioxooctahydroxanthenes (**5a**–**h**).

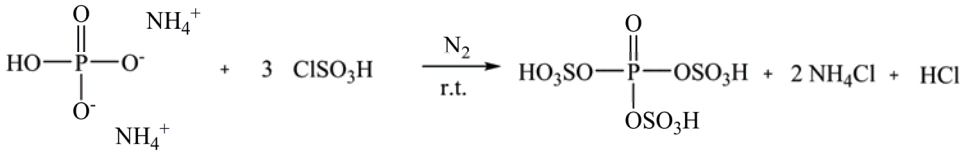

Scheme 2. Preparation of phosphosulfonic acid.

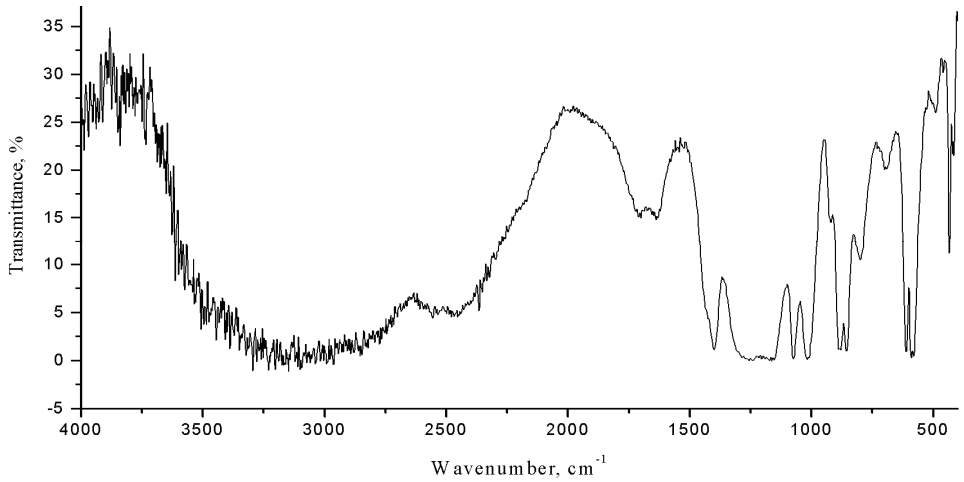

Fig. 1. The FT-IR spectrum of phosphosulfonic acid (KBr disc).

To evaluate the catalytic activity of PSA in the preparation of 14-aryl-14*H*--dibenzo[*a*,*j*]xanthenes derivatives, a model reaction of 2 mmol of *β*-naphthol and 1 mmol of benzaldehyde under solvent-free conditions at 110 °C in the

absence and presence of PSA was examined. It was found that in the absence of solid acid catalyst, only a trace amount of the desired product was produced even after 6 h of heating (Table I). When the reaction was performed in the presence of PSA, it proceeded rapidly to give the desired product.

TABLE I. Determination of the optimum conditions for the pseudo three-component coupling reaction of *β*-naphthol (2 mmol) and benzaldehyde (1 mmol) under thermal solvent-free conditions

Entry	Catalyst, mol %	Temperature, °C	Time, min	Yield, %
1	0	100	360	11
2	3.5	100	55	65
3	3.5	110	45	65
4	5	110	35	93
5	7	110	30	90
6	9	110	30	80

In order to evaluate the appropriate catalyst loading, the model reaction was performed using 3.5 to 9 mol % PSA at 110 °C without solvent (Table I). It was found that 5 mol % of the catalyst afforded the maximum yield in minimum time. Higher percentages of catalyst loading (7 and 9 mol %) neither increased the yield nor lowered the conversion time. Next, the effect of temperature was evaluated for the model reaction. It was observed that the reaction did not proceed at room temperature. Elevating the reaction temperature proved helpful, and the yield of desired product increased considerably.

To investigate the feasibility of this synthetic methodology for the synthesis of xanthenes derivatives, the reaction of *β*-naphthol was extended to a range of aromatic aldehydes under similar conditions, furnishing the respective 14-aryl--14*H*-dibenzo[*a*,*j*]xanthenes derivatives in high to excellent isolated yields. The optimized results are summarized in Table II. The method has the ability to tolerate a variety of functional groups, such as fluro-, chloro-, nitro- and methoxy-substituents. The products were characterized by FT-IR, ^{1}H-NMR, ^{13}C-NMR and physical constants. The results of the characterization of the synthesized xanthenes are given in the Supplementary material to this paper. The physical and spectral data of the known compounds were in agreement with those reported in the literature.

As seen from Table II, electron-withdrawing substituents on the aromatic ring retarded the reaction while electron-donating groups promoted it. This effect of the substituents is comprehendible according to the plausible mechanism for the one-pot preparation of 14-aryl-14*H*-dibenzo[*a*,*j*]xanthenes (Scheme 3). First, the aldehyde is activated by PSA, and subsequently nucleophilic attack of the *β*-naphthol occurs. After stepwise rearrangement and dehydration, the intermediate X is formed. According to this, electron-withdrawing substituents destabilize the positive charge and consequently increase the activation energy and retard

the reaction, while electron-donating groups stabilize the positive charge and promote the reaction.

TABLE II. One-pot preparation of 14-aryl-14*H*-dibenzo[*a*,*j*]xanthenes promoted by PSA under solvent-free conditions at 110 °C

Entry	R	Time, min	Yield, %	Melting point, °C	
				Found	Literature
3a	H	35	93	183–185	183[8]
3b	4-NO_2	55	88	310–312	312[8]
3c	3-NO_2	55	90	211–212	213[8]
3d	2-Cl	45	95	214–216	215[8]
3e	4-CH_3	30	91	226–228	228[8]
3f	4-Cl	40	98	285–287	287[8]
3g	2-NO_2	40	96	294–295	293[8]
3h	4-OH	30	89	140–142	140[8]
3i	4-CF_3	40	97	258–259	258–259[33]
3j	3-CH_3	40	94	198–200	198[18]
3k	3-F	45	96	258–260	259[8]
3l	4-OMe	45	65	203–205	205[8]

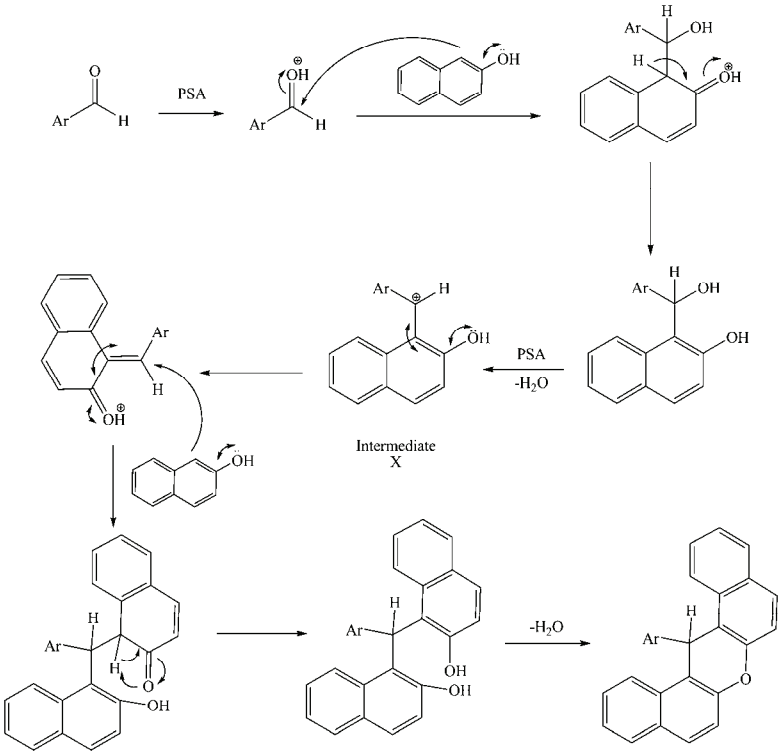

Scheme 3. Plausible mechanism for the one-pot preparation of 14-aryl-14*H*-dibenzo[*a*,*j*]xanthenes.

After the success of phosphosulfonic acid in the preparation of 14-aryl-14*H*--dibenzo[*a*,*j*]xanthenes, it was decided to explore the catalytic activity of this catalyst in the preparation of 1,8-dioxooctahydroxanthenes. Thus, the condensation of various aromatic aldehydes with dimedone was performed using phosphosulfonic acid as the solid acid catalyst under the above optimized reaction condition. All the aldehydes reacted almost equally well to afford the corresponding 1,8-dioxooctahydroxanthenes in high to excellent yields (Table III).

TABLE III. One-pot preparation of 1,8-dioxo-octahydro-xanthenes promoted by PSA under solvent-free conditions at 110 °C

Product	R	Time, min	Yield, %	Melting point, °C	
				Found	Literature
5a	H	20	96	206–207	204–206[19]
5b	4-NO_2	30	95	220–222	221–223[19]
5c	3-NO_2	30	93	172–174	170–172[19]
5d	2-NO_2	35	95	249–250	248–249[19]
5e	4-CH_3	25	97	216–218	217–218[19]
5f	4-OMe	30	98	241–242	240–242[19]
5g	2-Cl	25	96	224–225	225–227[19]
5h	4-CN	35	88	224–226	217–218[34]

With the increasing interest in human health and environmental protection, more attention is being paid to green chemistry. With this view, the recyclability and reusability of the catalyst were studied. After completion of the reaction, the separated catalyst was washed with hot ethanol and dried. The catalyst was used for two more subsequent cycles. Surprisingly, a consistent performance of the catalyst was observed in all the cycles, Table IV.

TABLE IV. The reusability of the catalyst in the pseudo three-component coupling reaction of *β*-naphthol (2 mmol) and benzaldehyde (1 mmol) under thermal solvent-free conditions at 110 °C

Run	Time, min	Yield, %
1	35	93
2	38	91
3	40	90

To compare the advantage of the use of PSA over other reported catalysts, the pseudo three-component coupling reaction of *β*-naphthol and benzaldehyde was considered as a representative example (Table V). While in most of these cases (except entry 2), comparative yields of the desired product were obtained following the PSA-catalyzed procedure, the reported procedures required long reaction times (entry 1, 2, 4 and 5), or high catalyst loading (entry 1 and 3). These results clearly demonstrate that PSA is an equally or more efficient catalyst for this three-component reaction.

TABLE V. Comparison of PSA with reported catalysts in the pseudo three-component coupling reaction of *β*-naphthol and benzaldehyde

Entry	Catalyst/Temperature, °C	Catalyst loading, mol %	Time, h	Yield, %	Ref.
1	AcOH–H_2SO_4/0 then 80	100	73	60	7
2	Selectfluor/125	10	8	93	8
3	Cyanuric chloride/110	20	0.7	94	9
4	$Sc[N(SO_2C_8F_{17})_2]_3$/110	1	5	93	10
5	I_2/90	10	2.5	90	12
6	Phosphosulfonic acid/110	5	0.6	93	This work

EXPERIMENTAL

All commercially available chemicals were purchased from Fluka or Merck and used without further purification. The IR spectra were recorded on a Bomem MB-Series 1998 FT-IR spectrophotometer. The ^{1}H- and ^{13}C-NMR spectra were recorded in $CDCl_3$ or DMSO-d_6 on a Bruker Advance DPX 400 MHz spectrometer using TMS as an internal standard. Monitoring of the reactions was accomplished by TLC on silica gel polygram SILG/UV 254 plates. Phosphosulfonic acid was prepared according to the recently reported procedure.[32]

Determination of the acidity of the catalyst

The acidity of the catalyst was determined by titration with standard NaOH. Catalyst (0.5 g) required 8.9 mL of 0.05 M NaOH to reach neutralization, as witnessed by an indicator. The titration verified that the amount of base consumed was 3 equivalents per 1 mole of the catalyst.

*Typical procedure for the preparation of 14-aryl-14*H*-dibenzo[*a,j*]xanthenes/1,8-dioxo-octahydroxanthenes derivatives*

A mixture of aromatic aldehyde (1.0 mmol), *β*-naphthol or dimedone (2.0 mmol), and PSA (0.05 g) was heated at 110 °C for 20–55 min. Completion of the reaction was indicated by TLC (ethyl acetate/*n*-hexane, 2:5). After completion of the reaction (as indicated in Tables II and III), the insoluble crude product was dissolved in hot ethanol and the phosphosulfonic acid was filtered off. The filtrate was concentrated to dryness, and the crude product was purified by recrystallization from ethanol.

CONCLUSION

In conclusion, a simple, facile and green protocol is described for the synthesis of 14-aryl-14*H*-dibenzo[*a,j*]xanthenes and 1,8-dioxooctahydroxanthenes by a one-pot pseudo three-component condensation reaction of aromatic aldehydes and *β*-naphthol or dimidone using phosphosulfonic acid as a novel, environmentally safe, heterogeneous solid acid catalyst under solvent-free conditions. This method offers several advantages, including high yields, inexpensive catalyst, short reaction times, easy work-up and realization of the reaction under green, solvent-free conditions.

SUPPLEMENTARY MATERIAL

Spectroscopic data for the prepared xanthenes are available electronically at http://www.shd.org.rs/JSCS/, or from the corresponding author on request.

Acknowledgement. We gratefully acknowledge the support of this work by the Shahid Chamran University Research Council.

И З В О Д

ФОСФОСУЛФОНСКА КИСЕЛИНА: ЕФИКАСАН ЧВРСТ КИСЕЛИ КАТАЛИЗАТОР ЗА СИНТЕЗУ 14-АРИЛ-14*H*-ДИБЕНЗО[*a*,*j*]КСАНТЕНА И 1,8-ДИОКСООКТАХИДРОКСАНТЕНА У ЈЕДНОМ РЕАКЦИОНОМ КОРАКУ У ОДСУСТВУ РАСТВАРАЧА

ALI REZA KIASAT, ARASH MOURADZADEGUN и SEYYED JAFAR SAGHANEZHAD

Chemistry Department, College of Science, Shahid Chamran University, P. O. Box 61357-4-3169, Ahvaz, Iran

Описана је синтеза 14-арил-14*H*-дибензо[*a*,*j*]ксантена и 1,8-диоксооктахидроксантена из псеудо-трокомпонентне реакционе смеше кондензацијом β-нафтола или димедона са различитим ароматичним алдехидима. Поступак катализован фосфосулфонском киселином, одиграва се без присуства органских растварача, под оптимизованим, благим и еколошки прихватљивим условима, у високом приносу и током 20–55 min.

(Примљено 8. октобра 2012, ревидирано 16. јануара 2013)

REFERENCES

1. T. Hideu, JP 56005480 (1981) (*CA* **95** 80922b)
2. R. W. Lamberk, J. A. Martin, J. H. Merrett, K. E. B. Parkes, G. J. Thomas, PCT Int. Appl. WO 9706178 (1997) (*CA* **126** P212377y)
3. J. P. Poupelin, G. Saint-Rut, O. Fussard-Blanpin, G. Narcisse, G. Uchida-Ernouf, R. Lakroix, *Eur. J. Med. Chem.* **13** (1978) 67
4. A. Banerjee, A. K. Mukherjee, *Stain Technol.* **56** (1981) 83
5. O. Sirkecioglu, N. Tulinli, A. Akar, *J. Chem. Res. Synop.* (1995) 502
6. R. M. Ion, D. Frackowiak, A. Planner, K. Wiktorowicz, *Acta Biochim. Pol.* **45** (1998) 833
7. R. J. Sarma, J. B. Baruah, *Dyes Pigm.* **64** (2005) 91
8. P. S. Kumara, B. S. Kumara, B. Rajithaa, P. N. Reddya, N. Sreenivasulua, Y. T. Reddy, *ARKIVOC* (2006) 46
9. M. A. Bigdeli, M. M. Heravi, G. H. Mahdavinia, *Catal. Commun.* **8** (2007) 1595
10. M. Hong, C. Cai, *J. Fluorine Chem.* **130** (2009) 989
11. M. Mohammadpour Amini, M. Seyyedhamzeh, A. Bazgir, *Appl. Catal., A.* **323** (2007) 242
12. B. Das, B. Ravikanth, R. Ramu, K. Laxminarayana, B. V. Rao, *J. Mol. Catal., A* **255** (2006) 74
13. B. Rajitha, B. S. Kumar, Y. T. Reddy, P. N. Reddy, N. Sreenivasulu, *Tetrahedron Lett.* **46** (2005) 8691
14. M. M. Heravi, K. Bakhtiari, Z. Daroogheha, F. F. Bamoharramb, *J. Mol. Catal., A* **273** (2007) 99
15. L. Nagarapu, S. Kantevari, V. C. Mahankhali, S. Apuri, *Catal. Commun.* **8** (2007) 1173
16. N. Ghaffari Khaligh, *Ultrason. Sonochem.* **19** (2012) 736
17. M. Nandi, J. Mondal, K Sarkar, Y. Yamauchi, A. Bhaumik, *Chem. Commun.* **47** (2011) 6677
18. G. Mohammadi Ziarani, A. R. Badiei, M. Azizi, *Scientia Iranica, C* **18** (2011) 453
19. H. N. Karade, M. Sathe, M. P. Kaushik, *ARKIVOC* (2007) 252
20. S. Sato, Y. Naito, K. Aoki, *Carbohydr. Res.* **342** (2007) 913
21. S. Kantevari, R. Bantu, L. Nagarapu, *J. Mol. Catal., A* **269** (2007) 53

22. P. Srihari, S. S. Mandal, J. S. S. Reddy, R. Srinivasa Rao, J. S. Yadav, *Chin. Chem. Lett.* **19** (2008) 771
23. D. Fang , K. Gong , Z. Liu, *Catal. Lett.* **127** (2009) 291
24. G. Karthikeyana, A. Pandurangan, *J. Mol. Catal., A* **311** (2009) 36
25. A. Javid, M. M. Heravi, F. F. Bamoharram, *E-J. Chem*. **8** (2011) 910
26. G. H. Mahdavinia , M. M. Ghanbari, H. Sepehrian, F. Kooti, *J. Iran. Chem. Res*. **3** (2010) 117
27. J. Mondal, M. Nandi, A. Modak, A. Bhaumik, *J. Mol. Catal., A* **363**–**364** (2012) 254
28. F. Rashedian, D. Saberi, K. Niknam, *J. Chin Chem. Soc.* **57** (2010), 998
29. P. Salehi, M. A. Zolfigol, F. Shirini, M. Baghbanzadeh, *Curr. Org. Chem*. **10** (2006) 2171
30. A. R. Kiasat, M. Fallah-Mehrjardi, *J. Braz. Chem. Soc*. **19** (2008) 1595
31. A. R. Kiasat, M. Fallah-Mehrjardi, *Synth. Commun.*, **40** (2010) 1551
32. A. R. Kiasat, A. Mouradezadegun, S. J. Saghanezhad, *J. Serb. Chem. Soc.* **78** (2013) 469
33. S. Ko, C. F. Yao, *Tetrahedron Lett.* **47** (2006) 8827
34. Z. H. Zhang, Y. H. Liu, *Catal. Commun.* **9** (2008) 1715.

Journal of the Serbian Chemical Society
JSCS@tmf.bg.ac.rs • www.shd.org.rs/JSCS
J. Serb. Chem. Soc. 78 (9) S99–S101 (2013) *Supplementary material*

SUPPLEMENTARY MATERIAL TO

Phosphosulfonic acid, an efficient solid acid catalyst for the one-pot preparation of 14-aryl-14*H*-dibenzo[*a,j*]xanthenes and 1,8-dioxooctahydroxanthenes under solvent-free conditions

ALI REZA KIASAT*, ARASH MOURADZADEGUN
and SEYYED JAFAR SAGHANEZHAD

Chemistry Department, College of Science, Shahid Chamran University, P. O. Box 61357-4-3169, Ahvaz, Iran

J. Serb. Chem. Soc. 78 (9) (2013) 1291–1299

SPECTROSCOPIC DATA FOR THE PREPARED XANTHENES

*14-Phenyl-14*H-*dibenzo[*a,j*]xanthene* (***3a***). IR (KBr, cm^{-1}): 3068, 3020, 2885, 1620, 1590, 1512, 1488, 1457; ^{1}H-NMR (400 MHz, DMSO-d_6, δ / ppm): 8.70 (2H, *d*, *J* = 8.8 Hz), 7.91–7.93 (4H, *m*), 7.62–7.66 (4H, *m*), 7.57 (2H, *d*, *J* = 8.8 Hz), 7.45 (2H, *t*, *J* = 7.2 Hz), 7.14 (2H, *t*, *J* = 7.6 Hz), 6.97 (1H, *t*, *J* = 7.6 Hz), 6.74 (1H, *s*); ^{13}C-NMR (100 MHz, DMSO-d_6, δ / ppm): 148.5, 146.0, 131.4, 131.1, 129.5, 129.1, 128.8, 128.4, 127.4, 126.7, 124.9, 123.9, 124.9, 123.9, 118.2, 117.9, 37.0.

*14-(4-Nitrophenyl)-14*H-*dibenzo[*a,j*]xanthene* (***3b***). IR (KBr, cm^{-1}): 3070, 2930, 1621,1591, 1614, 1457, 1400, 1340; ^{1}H -NMR (400 MHz, DMSO-d_6, δ / ppm): 8.72 (2H, *d*, *J* = 8.4 Hz), 8.45 (1H, *s*), 8.14 (1H, *d*, *J* = 7.8 Hz), 7.90–7.95 (4H, m), 7.81 (1H, *d*, *J* = 7.5 Hz), 7.58–7.65 (4H, *m*), 7.43 (3H, *t*, *J* = 7.2 Hz), 6.95 (1H, *s*); ^{13}C-NMR (100 MHz, DMSO-d_6, δ / ppm): 148.6, 148.3, 147.9, 134.7, 131.11, 130.4, 130.0, 129.1, 127.7, 125.2, 123.6, 122.0, 118.2, 116.9, 36.4.

*14-(4-Methylphenyl)-14*H-*dibenzo[*a,j*]xanthene* (***3e***). IR (KBr, cm^{-1}) 3020, 2908, 1620, 1591, 1509, 1457, 1430, 1247, 959, 837, 810, 739; ^{1}H-NMR (400 MHz, $CDCl_3$, δ / ppm): 8.36 (2H, *d*, *J* = 9.4 Hz) , 7.32–7.80 (12H, *m*), 6.90 (2H, *d*, *J* = 9.6 Hz), 6.39 (1H, *s*), 2.18 (3H, *s*); ^{13}C-NMR (100 MHz, $CDCl_3$, δ / ppm): 147.9, 147.8, 142.5, 135.9, 130.8, 128.8, 128.4, 127.7, 126.7, 124.3, 123.3, 117.5, 117.4, 117.3, 37.1, 20.2.

* Corresponding author. E-mail: akiasat@scu.ac.ir

*14-(4-Chlorophenyl)-14*H-*dibenzo[*a,j*]xanthene* (***3f***). IR (KBr, cm^{-1}): 3033, 1618, 1580; ^{1}H-NMR (400 MHz, $CDCl_3$, δ / ppm): 7.10–8.34 (16H, *m*, Ar), 6.48 (1H, *s*, CH); ^{13}C-NMR (100 MHz, $CDCl_3$, δ / ppm): 148.7, 143.5, 132.1, 131.24, 131.0, 129.5, 129.1, 128.9, 128.6, 126.9, 124.4, 122.4, 118.0, 116.7, 37.4.

*14-(2-Nitrophenyl)-14*H-*dibenzo[*a,j*]xanthene* (***3g***). IR (KBr, cm^{-1}): 3400, 3058, 1593, 1523, 1350, 1240, 1142, 810, 748; ^{1}H-NMR (400 MHz, $CDCl_3$, δ / ppm): 7.52 (1H, *s*) 7.10–8.70 (16H, *m*); ^{13}C-NMR (100 MHz, $CDCl_3$, δ / ppm): 149.8, 147.5, 141.3, 134.5, 132.6, 132.1, 130.8, 129.9, 129.5, 129.4, 128.0, 127.8, 125.3, 125.0, 124.6, 123.0, 118.4, 118.0, 32.9.

*14-(4-Hydroxyphenyl)-14*H-*dibenzo[*a,j*]xanthene* (***3h***). IR (KBr, cm^{-1}): 3404, 1592, 1511, 1401, 1250, 1242, 816; ^{1}H-NMR (400 MHz, $CDCl_3$, δ / ppm): 6.56–8.36 (16H, *m*, Ar-H), 6.42 (1H, *s*, CH), 4.97 (1H, *brs*, OH); ^{13}C-NMR (100 MHz, $CDCl_3$, δ / ppm): 154.2, 149.1, 137.9, 131.8, 131.5, 129.8, 129.2, 129.1, 127.2, 124.6, 123.1, 118.4, 117.9, 115.7, 37.5.

*14-(4-(Trifluoromethyl)phenyl)-14*H-*dibenzo[*a,j*]xanthene* (***3i***). IR (KBr, cm^{-1}): 3021, 2919, 1591, 1513, 1458; ^{1}H-NMR (400 MHz, $CDCl_3$, δ / ppm): 8.33 (2H, *d*, *J* = 8.4 Hz), 7.82–7.86 (4H, *m*), 7.58–7.65 (4H, *m*), 7.50 (2H, *d*, *J* = 8.8 Hz), 7.39–7.46 (4H, *m*), 6.61 (1H, *s*); ^{13}C-NMR (100 MHz, $CDCl_3$, δ / ppm): 148.8, 131.2, 131.1, 129.3, 129.0, 128.5, 127.0, 125.54, 125.50, 124.5, 122.3, 118.0, 116.4, 37.8.

*14-(3-Fluorophenyl)-14*H-*dibenzo[*a,j*]xanthene* (***3k***). IR (KBr, cm^{-1}): 3154, 1594, 1403, 1240, 1207, 1069, 817, 747; ^{1}H-NMR (400 MHz, $CDCl_3$, δ / ppm): 6.72–8.38 (16H, *m*), 6.51 (1H, *s*); ^{13}C-NMR (100 MHz, $CDCl_3$, δ / ppm) 165.0, 161.7, 149.2, 147.8 ($J_{C–F}$ = 6.2 Hz), 131.6 ($J_{C–F}$ = 19.4 Hz), 130.1 ($J_{C–F}$ = 8.3 Hz), 129.5, 129.3, 127.4, 124.8, 124.3 ($J_{C–F}$ = 2.8 Hz), 122.9, 118.2, 117.1, 115.7 ($J_{C–F}$ = 21.5 Hz), 113.9 ($J_{C–F}$ = 21.5 Hz), 38.1.

*14-(4-Methoxyphenyl)-14*H-*dibenzo[*a,j*]xanthene* (***3l***). IR (KBr, cm^{-1}): 2999, 2833, 1734, 1591, 1508, 1457; ^{1}H-NMR (400 MHz, $CDCl_3$, δ / ppm): 8.35 (2H, *d*, *J* = 9.6 Hz), 7.32–7.85 (12H, *m*), 6.65 (2H, *d*, *J* = 9.7 Hz), 6.40 (1H, *s*), 3.58 (3H, *s*); ^{13}C-NMR (100 MHz, $CDCl_3$, δ / ppm): 158.2, 149.3, 137.2, 133.7, 131.4, 129.4, 129.1, 127.4, 124.1, 123.5, 118.3, 117.2, 114.3, 53.2, 36.9.

*3,4,5,6,7,9-Hexahydro-3,3,6,6-tetramethyl-9-phenyl-1*H-*xanthene-1,8(2*H*)-dione* (***5a***). IR (KBr, cm−1): 3032, 2952, 1670, 1471; ^{1}H-NMR (400 MHz, DMSO-d_6, δ / ppm): 7.21 (2H, *t*, *J* = 7.20 Hz), 7.18 (2H, *d*, *J* = 7.0 Hz), 7.10 (1H, *t*, *J* = 7.0 Hz), 2.58 (2H, *d*, *J* = 17.7 Hz), 4.53 (1H, *s*), 2.53 (2H, *d*, *J* = 17.1 Hz), 2.27 (2H, *d*, *J* = 16.2 Hz), 2.09 (2H, *d*, *J* = 16.1 Hz), 1.04 (6H, *s*), 0.90 (6H, *s*); ^{13}C-NMR (100 MHz, DMSO-d_6, δ / ppm): 196.8, 162.7, 144.5, 128.8, 128.4, 126.8, 116.1, 51.2, 41.3, 32.6, 32.3, 29.6, 27.7.

*3,4,5,6,7,9-Hexahydro-3,3,6,6-tetramethyl-9-(4-nitrophenyl)-1*H-*xanthene-1,8(2*H*)-dione* (***5b***). IR (KBr, cm−1): 3032, 2960, 1664, 1462; ^{1}H-NMR (400 MHz, $CDCl_3$, δ / ppm): 8.08 (2H, *d*, *J* = 8.2 Hz), 7.48 (2H, *d*, *J* = 8.2 Hz), 4.83

(1H, *s*), 2.51 (4H, *t*, *J* = 18.7 Hz), 2.26 (2H, *d*, *J* = 16.3 Hz), 2.16 (2H, *d*, *J* = 16.3 Hz), 1.12 (6H, s), 0.99 (6H, *s*); ^{13}C-NMR (100 MHz, $CDCl_3$, δ / ppm): 196.7, 163.5, 152.0, 146.8, 129.8, 123.8, 114.9, 51.0, 41.2, 32.8, 32.6, 29.6, 27.7.

*3,4,5,6,7,9-Hexahydro-3,3,6,6-tetramethyl-9-(3-nitrophenyl)-1*H*-xanthene--1,8(2*H*)-dione (**5c**)*. IR (KBr, cm−1): 3021, 2962, 1662, 1466, 1363; ^{1}H-NMR (400 MHz, $CDCl_3$, δ / ppm): 8.06 (1H, *s*), 7.99 (1H, *d*, *J* = 8.2 Hz), 7.81 (1H, *d*, *J* = 7.5 Hz), 7.41 (1H, *t*, *J* = 7.9 Hz), 4.85 (1H, *s*), 2.53 (4H, *t*, *J* = 18.5 Hz), 2.27 (2H, *d*, *J* = 16.3 Hz), 2.18 (2H, *d*, *J* = 16.3 Hz), 1.13 (6H, s), 1.01 (6H, s); ^{13}C--NMR (100 MHz, $CDCl_3$, δ / ppm): 196.8, 163.5, 148.7, 146.8, 136.0, 129.2, 123.1, 122.0, 114,9, 51.0, 41.2, 32.7, 32.5, 29.6, 27.7.

*3,4,5,6,7,9-Hexahydro-3,3,6,6-tetramethyl-9-(2-nitrophenyl)-1*H*-xanthene--1,8(2*H*)-dione (**5d**)*. IR (KBr, cm−1): 3026, 2964, 1662, 1471, 1361; ^{1}H-NMR (400 MHz, $CDCl_3$, δ / ppm): 7.21–7.73 (4H, *m*, Ar-H), 5.51 (1H, *s*), 2.45 (4H, *s*), 2.21 (2H, *d*, *J* = 16.2 Hz), 2.13 (2H, *d*, *J* = 16.2 Hz), 1.07 (6H, *s*), 0.98 (6H, *s*); ^{13}C-NMR (100 MHz, $CDCl_3$, δ / ppm): 196.7, 163.4, 150.3, 138.5, 132.4, 131.5, 127.6, 125.0, 114.6, 51.0, 41.3, 32.5, 29.4, 29.2, 28.0.

*3,4,5,6,7,9-Hexahydro-3,3,6,6-tetramethyl-9-(4-methylphenyl)-1*H*-xanthene--1,8(2*H*)-dione (**5e**)*. IR (KBr, cm−1): 3021, 2961, 1662, 1466; ^{1}H-NMR (400 MHz, $CDCl_3$, δ / ppm): 7.20 (2H, *d*, *J* = 6.9 Hz), 7.04 (2H, *d*, *J* = 7.5 Hz), 4.74 (1H, *s*), 2.49 (4H, *s*), 2.17–2.27 (7H, *m*), 1.25 (6H, s), 1.02 (6H, *s*); ^{13}C-NMR (100 MHz, $CDCl_3$, δ / ppm); 196.8, 162.5, 141.6, 136.1, 129.2, 128.7, 116.2, 51.2, 41.3, 32.6, 31.9, 29.7, 27.8, 21.5.

*3,4,5,6,7,9-Hexahydro-9-(4-methylphenyl)-3,3,6,6-tetramethyl-1*H*-xanthene--1,8(2*H*)-dione (**5f**)*. IR (KBr, cm−1):: 3031, 2959, 1665, 1460, 1361, 1200, 1170, 855; ^{1}H-NMR (400 MHz, $CDCl_3$, δ / ppm): 7.22 (2H, *d*, *J* = 8.8 Hz), 6.77 (2H, *d*, *J* = 8.8 Hz), 4.72 (1H, *s*), 3.75 (3H, *s*), 2.48 (4H, *s*), 2.25 (2H, *d*, *J* = 16.4 Hz), 2.18 (2H, *d*, *J* = 16.4 Hz), 1.12 (6H, *s*), 1.01 (6H, *s*); ^{13}C-NMR (100 MHz, $CDCl_3$, δ / ppm): 196.5, 162.1, 157.9, 136.5, 129.3, 115.8, 113.5, 55.1, 50.8, 40.9, 32.2, 30.9, 29.3, 27.3.

*9-(4-Chlorophenyl)-3,4,5,6,7,9-hexahydro-3,3,6,6-tetramethyl-1*H*-xanthene--1,8(2*H*)-dione (**5g**)*. IR (KBr, cm^{-1}): 3018, 2971, 1661, 1466; ^{1}H-NMR (400 MHz, $CDCl_3$, δ / ppm): 7.09–7.46 (*m*, 4H, Ar-H), 5.03 (1H, *s*), 2.48 (4H, *s*), 2.26 (2H, *d*, *J* = 16.2 Hz), 2.19 (2H, *d*, *J* = 16.2 Hz), 1.13 (6H, *s*), 1.05 (6H, *s*); ^{13}C--NMR (100 MHz, $CDCl_3$, δ / ppm) 196.8, 163.4, 140.3, 133.9, 133.3, 130.6, 128.2, 126.7, 114.1, 51.1, 41.2, 32.4, 32.3, 29.7, 27.8.

*4-(2,3,4,5,6,7,8,9-Octahydro-3,3,6,6-tetramethyl-1,8-dioxo-1*H*-xanthene-9--yl)benzonitrile (**5h**)*. IR (KBr, cm^{-1}): 3015, 2960, 2224, 1662, 1500, 1471; ^{1}H-NMR (400 MHz, $CDCl_3$, δ / ppm): 0.98 (6H, *s*, 2 × CH_3), 1.11 (6H, *s*, 2 × CH_3), 2.13–2.26 (4H, *dd*, *J* = 19.6 Hz, 2 × CH_2), 2.49 (4H, *t*, 2 × CH_2), 4.76 (1H, *s*), 7.40–7.51 (4H, *dd*, *J* = 4.9 Hz, Ar-H); ^{13}C-NMR (100 MHz, $CDCl_3$, δ / ppm) 196.3, 163.0, 149.5, 131.9, 129.3, 119.0, 114.5, 110.1, 50.6, 40.8, 32.5, 32.2, 29.2, 27.3.

J. Serb. Chem. Soc. 78 (9) 1301–1308 (2013) UDC 547.532'815+542.913:57–188:615.277
JSCS–4498 *Original scientific paper*

Synthesis and biological evaluation of novel benzo[*b*]xanthone derivatives as potential antitumor agents

LIN LUO[1], JIANG-KE QIN[1]*, ZHI-KAI DAI[2]** and SHI-HUA GAO[1]

[1]*Key Laboratory for the Chemistry and Molecular Engineering of Medicinal Resources, School of Chemistry & Chemical Engineering of Guangxi Normal University, Guilin 541004, China and* [2]*Department of Pharmacology, Pharmaceutical Institute of Guilin Medical University, Guilin 541004, China*

(Received 25 September 2012, revised 2 May 2013)

Abstract: Nine novel aminoalkoxy substituted benzo[*b*]xanthones (**3a**–**i**) were synthesized. Their antitumor activities were evaluated in five human solid tumor cell lines, including Hep-G2, BEL-7402, HeLa, MGC-803 and CNE, by the MTT (2-(4,5-dimethyl-thiazol-2-yl)-3,5-diphenyl-2*H*-tetrazolium bromide) method. The results showed that most of the compounds displayed moderate to good inhibitory activities on the tested cancer cell lines *in vitro*, among them compounds **3a** and **3h** showed higher antitumor activity than the other tested compounds against most cell lines. The influences of two kinds of structural factors, *i.e.*, the terminal amino group and length of the carbon spacers, on the anticancer activities were explored to discuss preliminary structure–activity relationships.

Keywords: xanthone; benzo[*b*]xanthone; *in vitro* anticancer activity.

INTRODUCTION

Xanthones, a class of oxygen-containing heterocyclic compounds widely distributed in nature,[1] have diverse pharmacological activities, such as antioxidant activity,[2,3] topoisomerase II inhibitory activity,[4] antitumor activity,[5] α-glucosidase inhibitory activity,[6–9] cholesterol acyltransferase (ACAT) inhibitory activity,[10] antibacterial and antifungal activity,[11] based on their diverse structures. Their interesting structural scaffolds and pharmacological importance have attracted many scientists to isolate or synthesize these compounds as novel drug candidates. Especially, the effective inhibitory activity against human cancer cell lines has attracted considerable attention and many xanthone derivatives with excellent anticancer activity have been obtained.[12–15] For example, Shen *et al.* reported xanthone derivatives substituted by six different groups, of which the

*,** Corresponding authors. E-mails: (*)jiangkeq@sina.com; (**)dzhk110@126.com
doi: 10.2298/JSC120925060L

piperidinylethoxy-substituted xanthone could efficiently prohibit the growth of cancer cells.[16] Although preliminary work has highlighted the high class of the potent anticancer potentials of xanthone as a promising building motif for the development of new drugs, more efforts on structural modification of xanthone as well as on their pharmacological activity should be realized.

In the past few decades, medicinal chemistry researchers have mainly focused on the introduction of various side chains onto the aromatic ring core of xanthone in attempts to improve its bioactivity; however, little attention was paid to the structural modifications and anticancer activities of benzoxanthone, which possesses an extended π-system. Considering that a pharmacophore might improve its physicochemical and biological activities by the introduction of a nitrogen-containing side chain[17] and the structure of 1,3-dihydroxybenzoxanthone, in the herein reported study, a series of novel benzo[*b*]xanthone derivatives with terminal amines linked by different carbon spacers were prepared and their effect on the growth of five human cancer cell lines, *i.e.*, Hep-G2, BEL-7402, HeLa, MGC-803 and CNE, evaluated.

The primary aim of this work was to gain some insight into the effect of various terminal amines and different carbon lengths on benzo[*b*]xanthones on antitumor activities and an interesting structure–activity relationship. The obtained results revealed that aminoalkoxy-substituted benzo[*b*]xanthones provided interesting scaffolds in the search for potential anticancer drugs. The chemical structures of xanthone and benzo[*b*]xanthone are shown in Fig. 1.

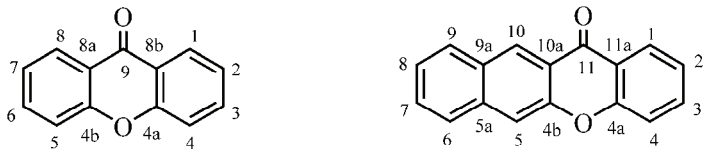

Fig. 1. Chemical structures of xanthone and 12*H*-benzo[*b*]xanthen-12-one.

RESULTS AND DISCUSSION

Chemistry

The synthetic route of benzoxanthone derivatives **3a**–**i** is shown in Scheme 1. Compound **1** was synthesized in 35 % yield from the condensation of 3-hydroxy-2-naphthoic acid with phloroglucinol (1,3,5-trihydroxybenzene) in the presence of anhydrous zinc chloride and phosphorus oxychloride as a condensing agent.[7] Compounds **2a**–**e**, which could be prepared from 1,3-dihydroxy-12*H*--benzo[*b*]xanthen-12-one with α,ω-dibromoalkane using K_2CO_3 as the base in anhydrous acetone.[5,8,9] were the key intermediates for the synthesis of the investigated compounds, Finally, amination of compounds **2a**–**e** with appropriate

amines in ethanol afforded the novel benzo[*b*]xanthone derivatives **3a**–**i**,[3,18] which could be purified by chromatography on a silica gel column, as yellow solids. The synthetic compounds gave satisfactory analytical and spectroscopic data, which were in full accordance with their depicted structures.

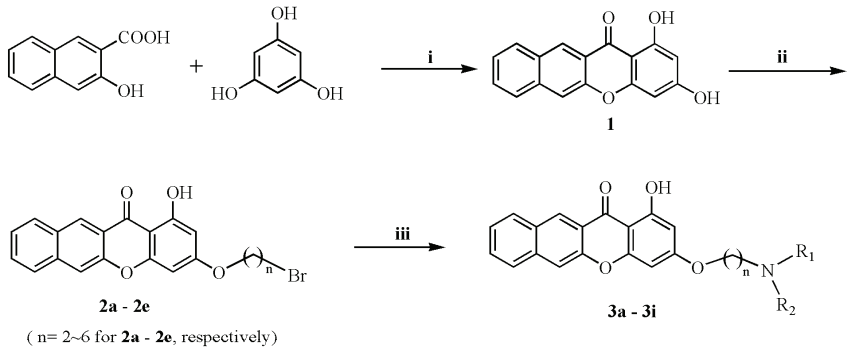

Compound	3a	3b	3c	3d	3e	3f	3g	3h	3i
n	4	4	4	4	4	2	3	5	6
$-NR^1R^2$									

Regents and conditions: (i) $ZnCl_2$, $POCl_3$, 70℃, 2-3 h; (ii) $Br(CH_2)_nBr$, K_2CO_3, acetone, 55℃, 24 h; (iii) R^1R^2NH, MeOH, 78℃, 6 h

Scheme 1. Synthetic route to the benzo[*b*]xanthone derivatives.

Antiproliferative activities

In the present study, the antiproliferative activity of the synthesized compounds was tested *in vitro* on five human tumor cell lines, *i.e.*, human hepatocarcinoma (Hep-G2 and BEL-7402), human cervix tumor (HeLa), human gastric cancer (MGC-803) and human nasopharyngeal carcinoma (CNE). 5-Flurouracil (5-Fu) was used as a positive control. The typical MTT (2-(4,5-dimethyl-thiazol--2-yl)-3,5-diphenyl-2*H*-tetrazolium bromide) assay procedure was applied for this assessment. The inhibitory activities of the compounds are given in Table I.

The results depicted in Table I indicated that most of the prepared compounds exhibited moderate to good inhibitory activities with the IC_{50} values at micromole level concentration against all of the cancer cell lines and all of the compounds demonstrated selective cytotoxicity against MGC-803 cells, except for compound **3e**. To optimize the structure favorable for anticancer activities, two kinds of structural factors, *i.e.*, the terminal amino substituent and the length of

TABLE I. IC_{50} values, determined by the MTT assay, for the benzoxanthone derivatives towards Hep-G2, BEL-7402, HeLa, MGC-803 and CNE cells

Compd./cell	IC_{50}[a] / μM				
	Hep-G2	BEL-7402	HeLa	MGC-803	CNE
5-Fu	21.30±2.53	20.95±1.90	51.88±2.53	7.76±1.09	51.00±2.82
3a	3.51±0.72	1.64±0.33	1.59±0.14	0.85±0.15	5.47±2.10
3b	7.56±1.09	5.74±1.37	6.22±0.56	0.76±0.09	12.39±0.88
3c	4.08±0.50	1.41±0.70	3.72±0.57	0.49±0.05	6.51±0.44
3d	5.70±0.39	5.53±0.58	8.45±1.97	0.39±0.06	20.29±1.14
3e	>100	>100	>100	>100	>100
3f	9.86±0.20	16.73±3.36	19.24±1.49	1.92±0.21	>100
3g	5.49±0.54	8.18±0.90	8.93±0.88	0.70±0.08	5.11±0.44
3h	1.72±0.67	10.08±1.46	3.41±0.17	0.86±0.14	4.41±0.31
3i	2.35±0.69	6.81±1.11	4.26±0.95	1.48±0.12	9.61±0.86

[a]The drug concentration required to inhibit tumor cell proliferation by 50 % after continuous exposure of 48 h; each value represents the mean ± *SD* from three independent experiments

the carbon spacer, were considered. First, compounds **3a**–**e**, in which the benzoxanthone ring system was linked to different terminal amino substituents by a 4-carbon spacer at the C-3 position, were investigated to determine the influence of the different amino substituents on the antiproliferative activity. It was shown that the dimethylamine-substituted compound **3a** holds the best inhibitory activity on the cancer cell lines in most cases. Compound **3a** has best activities against the cancer cell lines of Hep-G2, HeLa and CNE in this series, with IC_{50} values of 3.51, 1.59 and 5.47 μM, respectively. However, for the cell lines BEL-7402 and MGC-803, compounds **3c** and **3d**, which have *N*-heterocyclic rings at the C-3 position of 1,3-dihydroxy-12*H*-benzo[*b*]xanthen-12-one, were more active than compound **3a**. Interestingly, no notable activities were observed for the morpholino-substituted compound **3e** at a concentration of 100 μM against any of the tested cancer cell line. Compound **3b** also exhibited weaker inhibitory activities than compound **3a**, except for the cell line MGC-803. From the above comparisons, it is obvious that compound **3a** was the most potent compound of the derivatives **3a**–**e**, which indicated that the terminal dimethylamino group was favorable for the growth inhibitory activity in this series. Next, compounds **3f**–**i** as well as **3a**, in which the benzoxanthone ring system was linked to dimethylamino group by different carbon spacers, were investigated to explore the influence of the different length of carbon spacers on the anticancer activity. In this series, compounds **3a** and **3h**, which contained a four or five carbon spacer at position C-3 position respectively, showed higher inhibitory activities than the other compounds. Meanwhile, compound **3f**, which had two carbon spacers in between benzoxanthone and the terminal dimethylamino group, displayed the lowest activities. Comparing the IC_{50} values of compounds **3a** and **3h**, compound **3a** showed greater anticancer activities against the cancer cell line BEL-7402 and

HeLa, but lower activities against the Hep-G2/ and CNE cell lines, and equivalent activities for the MGC-803 cell line; thus they had almost equivalent anticancer activities. Although more studies are required to establish a structure–activity relationship, these preliminary results suggest that a four or five carbon spacer and a terminal dimethylamino group at position C-3 of the benzoxanthone scaffold (compounds **3a** and **3h**) are favorable for growth inhibitory activity against most cancer cell lines.

EXPERIMENTAL

All the solvents and reactants were of analytical grade and were used without further purification unless stated. Melting points were determined on a WRS-IA apparatus without correction. The elemental analyses were realized using an Elementar Vario EL CHNS elemental analyzer. The ^{1}H-NMR and ^{13}C-NMR spectra were recorded in DMSO-d_6 or $CDCl_3$ on a Bruker Avance AV500 spectrometer using TMS as an internal standard. The IR spectra were recorded on a Nicolet ESP 360 FTIR instrument. The mass spectra were obtained on a Bruker Esquire HCT spectrometer. Analytic and spectroscopic data for compounds **1** and **2a**–**e** are given in Supplementary material to this paper.

*Synthesis of 1,3-dihydroxy-12*H*-benzo[*b*]xanthen-12-one (**1**)*

Compound **1** was synthesized by an improved literature method.[7] Thus, to a mixture of 3-hydroxy-2-naphthoic acid (9.4 g, 0.050 mol), phloroglucinol (6.3 g, 0.050 mol) and freshly fused zinc chloride (20 g) was added phosphoryl chloride (50–60 mL). The reaction mixture was stirred at 70 °C for 2–3 h until the starting material had disappeared as controlled by TLC. On completion of the reaction, the mixture was cooled to room temperature, poured onto crushed ice and allowed to stand overnight. The solid was collected by filtration, washed with saturated aqueous sodium bicarbonate and water, and dried to give a red solid. The crude products were purified by silica gel column chromatography eluting with petroleum ether (PE):EtOAc = 3:1 (v/v) to afford compound **1** as a yellow solid.

*General procedure for the synthesis of ω-bromoalkoxy-substituted benzo[*b*]xanthones (**2a**–**e**)*

With improved methods based on literatures procedures,[5,8,9] to a mixture of compound **1** (1.112 g, 4 mmol) and anhydrous K_2CO_3 (1.656 g, 12.0 mmol) in anhydrous acetone (30 mL) was added 1,2-dibromoethane or 1,3-dibromopropane or 1,4-dibromobutane or 1,5-dibromopentane or 1,6-dibromohexane (20 mmol) with a syringe. The reaction mixture was stirred overnight at 55 °C. The mixture was filtered, washed with water, then the solvent was removed under reduced pressure and the residue was purified by silica gel column chromatography eluting with PE:EtOAc = 25:1 (v/v) to give compounds **2a**–**e** as yellow solid, respectively.

*Synthesis of aminoalkoxy substituted benzo[*b*]xanthones (**3a**–**i**)*

General procedure. To a solution of **2a**–**e** in 15 mL of anhydrous ethanol was added dimethylamine, diethylamine, pyrrolidine, piperidine or morpholine, followed by heating at 78 °C for 6 h until the starting material had disappeared as evidenced by TLC and then cooled to room temperature. The mixture was filtered, washed with water, dried over Na_2SO_4 and concentrated. The crude products were purified by column chromatography.

*Compound **3a***. Reactants: **2c** (0.06 g, 0.15 mmol) and an aqueous solution of dimethylamine (30 %, 2 mL, 9.97 mmol); elution solvent for column chromatography, chloroform:methanol, 100:8 (v/v).

*Compound **3b***. Reactants: **2c** (0.060 g, 0.15 mmol) and diethylamine (2 mL, 19.4 mmol); elution solvent for column chromatography, chloroform:methanol, 100:4 (v/v).

*Compound **3c***: Reactants: **2c** (0.060 g, 0.15 mmol) and pyrrolidine (0.25 mL, 3 mmol); elution solvent for column chromatography, chloroform:methanol, 100:6 (v/v).

*Compound **3d***. Reactants: **2c** (0.060 g, 0.15 mmol) and piperidine (0.25 mL, 2.52 mmol); elution solvent for column chromatography, chloroform:methanol, 100:1 (v/v).

*Compound **3e***. Reactants: **2c** (0.060 g, 0.15 mmol) and morpholine (0.25 mL, 2.88 mmol); elution solvent for column chromatography, chloroform:methanol, 100:1 (v/v).

*Compound **3f***: Reactants: **2a** (0.060 g, 0.16 mmol) and an aqueous solution of dimethylamine (30 %, 2 mL, 9.97 mmol); elution solvent for column chromatography, chloroform:methanol, 100:3 (v/v).

*Compound **3g***. Reactants: **2b** (0.060 g, 0.15 mmol) and dimethylamine aqueous solution (2 mL, 30%, 9.97 mmol); elution solvent for column chromatography, chloroform:methanol, 100:8 (v/v).

*Compound **3h***. Reactants: **2d** (0.060 g, 0.14 mmol) and dimethylamine aqueous solution (30%, 2 mL, 9.97 mmol); elution solvent for column chromatography, chloroform:methanol, 100:8 (v/v).

*Compound **3i***. Reactants: **2e** (0.060 g, 0.14 mmol) and dimethylamine aqueous solution (30%, 2 mL, 9.97 mmol); elution solvent for column chromatography, chloroform:methanol, 100:8 (v/v).

Growth of cell and chemicals

The human hepatocarcinoma cell lines (Hep-G2 and BEL-7402), human cervix tumor cell line (HeLa), human gastric cancer cell line (MGC-803) and human nasopharyngeal carcinoma cell line (CNE) were obtained from the Shanghai Institutes for Biological Sciences, Chinese Academy of Sciences (Shanghai, China). All cell lines were maintained in RPMI 1640 medium supplemented with 10 % fetal bovine serum and 100 U mL^{-1} penicillin and 100 μg mL^{-1} streptomycin. The cells were kept at 37 °C in a humidified atmosphere containing 5 % CO_2. The nine benzo[*b*]xanthone derivatives **3a**–**i** were applied in DMSO to 10 mM and stored at −80 °C. MTT (2-(4,5-dimethylthiazol-2-yl)-3,5-diphenyl-2*H*-tetrazolium bromide) was obtained from Amresco Chemical Corp (USA) and was dissolved in 0.01 M PBS to 5 mg mL^{-1}. Deionized water was used in all experiments.

Cell proliferation assay (MTT assay)

Inhibition of cell proliferation by the benzo[*b*]xanthone derivatives was measured using the MTT assay. Briefly, cells were plated in 96-well culture plates at the density of 5000 cells per well in RPMI 1640 medium in 200 μL aliquots. After 24 h incubation, the cells were treated with the benzo[*b*]xanthone derivatives (0.3, 1, 3, 10 and 30 μM, four wells per concentration) for 48 h. Then 20 μL of a 5 mg mL^{-1} MTT solution was added to each well and the cells were further incubated at 37 °C for another 4 h. The supernatant was discarded, 150 μL DMSO per well was added and the absorbance (*A*) was measured at 490 nm. The cell inhibition (*IR*) was calculated using the following equation:

$$IR\ (\%) = \left[\frac{(A_c - A_t)}{A_c}\right] \times 100$$

where A_c and A_t are the absorption of the control and treated samples, respectively.

The IC_{50}, values, calculated by the logit method,[19] were taken as the concentrations of the benzo[*b*]xanthone derivatives causing 50 % inhibition of cell viabilities.

CONCLUSIONS

In this work, nine novel aminoalkoxy substituted benzo[*b*]xanthone were synthesized and their *in vitro* antitumor activities evaluated. The results suggested that a four or five carbon spacer and a terminal dimethylamino group at position C-3 of benzo[*b*]xanthone scaffold were favorable for the growth inhibitory activity. Thus, compounds **3a** and **3h** were the most potent compounds, which possess potential as future antitumor agents. The molecular mechanisms of their antitumor action will be reported in due course.

SUPPLEMENTARY MATERIAL

Analytical and spectral data of the synthesized compounds are available electronically at http://www.shd.org.rs/JSCS/, or from the corresponding author on request.

Acknowledgments. This work was financially supported by grants from the National Natural Science Foundation of PRC (21002015), the Natural Science Foundation of Guangxi (2010GXNSFB013013, 0639030, 2010GXNSFF013001) and the Key Laboratory for the Chemistry and Molecular Engineering of Medicinal Resources (Guangxi Normal University), Ministry of Education of China (07109001-14).

И З В О Д

СИНТЕЗА И ИСПИТИВАЊЕ БИОЛОШКЕ АКТИВНОСТИ НОВИХ ДЕРИВАТА БЕНЗОКСАНТОНА КАО ПОТЕНЦИЈАЛНИХ АНТИТУМОРСКИХ АГЕНАСА

LIN LUO[1], JIANG-KE QIN[1], ZHI-KAI DAI[2] и SHI-HUA GAO[1]

[1]*Key Laboratory for the Chemistry and Molecular Engineering of Medicinal Resources, School of Chemistry & Chemical Engineering of Guangxi Normal University, Guilin 541004, China и* [2]*Department of Pharmacology, Pharmaceutical Institute of Guilin Medical University, Guilin 541004, China*

Описана је синтеза и карактеризација девет нових супституисаних деривата бензо[*b*]ксантона (**3a–i**). Испитивана је њихова антитуморска активност према пет типова ћелијских линија хуманог тумора, Hep-G2, BEL-7402, HeLa, MGC-803 и CNE, MTT методом. Резултати су показали да већина деривата показује умерену до добру *in vitro* инхибиторну активност према ћелијским линијама канцера, од којих једињења **3a** и **3h** показују највећу активност. Испитиван је утицај терминалне амино групе и дужине низа на антиканцерску активност и дискутована је прелиминарна веза између структуре и активности.

(Примљено 25. септембра 2012, ревидирано 2. маја 2013)

REFERENCES

1. L. Hu, H. Hu, W. Wu, X. Chai, J. Luo, Q. Wu, *Bioorg. Med. Chem. Lett.* **21** (2011) 4013
2. B. W. Lee, J. H. Lee, S. T. Lee, H. S. Lee, W. S. Lee, T. S. Jeong, K. H. Park, *Bioorg. Med. Chem. Lett.* **15** (2005) 5548
3. J. H. Cheng, A. M. Huang, T. C. Hour, S. C. Yang, Y. S. Pu, C. N. Lin, *Eur. J. Med. Chem.* **46** (2011) 1222
4. K.-Y. Jun, E.-Y. Lee, M.-J. Jung, O.-H. Lee, E.-S. Lee, H.-Y. P. Choo, Y. Na, Y. Kwon, *Eur. J. Med. Chem.* **46** (2011) 1964

5. E. Sousa, A. Paiva, N. Nazareth, L. Gales, A. M. Damas, M. S. Nascimento, M. Pinto, *Eur. J. Med. Chem.* **44** (2009) 3830
6. G. L. Li, J. Y. He, A. Zhang, Y. Wan, B. Wang, W. H. Chen, *Eur. J. Med. Chem.* **46** (2011) 4050
7. Y. Liu, L. Ma, W. H. Chen, B. Wang, Z. L. Xu, *Bioorg. Med. Chem.* **15** (2007) 2810
8. Y. Liu, Z. F. Ke, J. F. Cui, W. H. Chen, L. Ma, B. Wang, *Bioorg. Med. Chem.* **16** (2008) 7185
9. Y. Liu, *PhD Thesis*, Sun Yat-sen University, Guangzhou, P. R. China, 2007, p. 103 (in Chinese)
10. H. Hu, H. Liao, J. Zhang, W. Wu, J. Yan, Y. Yan, Q. Zhao, Y. Zou, X. Chai, S. Yu, Q. Wu, *Bioorg. Med. Chem. Lett.* **20** (2010) 3094
11. J. J. Omolo, M. M. Johnson, S. F. van Vuuren, C. B. de Koning, *Bioorg. Med. Chem. Lett.* **21** (2011) 7085
12. R. A. Heald, T. S. Dexheimer, H. Vankayalapati, A. Siddiqui-Jain, L. Z. Szabo, M. C. Gleason-Guzman, L. H. Hurley, *J. Med. Chem.* **48** (2005) 2993
13. K. Matsumoto, Y. Akao, K. Ohguchi, T. Ito, T. Tanaka, M. Iinuma, Y. Nozawa, *Bioorg. Med. Chem.* **13** (2005) 6064
14. C. Sittisombut, S. Boutefnouchet, H. Trinh Van-Dufat, W. Tian, S. Michel, M. Koch, F. Tillequin, B. Pfeiffer, A. Pierre, *Chem. Pharm. Bull.* **54** (2006) 1113
15. S. Woo, J. Jung, C. Lee, Y. Kwon, Y. Na, *Bioorg. Med. Chem. Lett.* **17** (2007) 1163
16. R. Shen, P. Wang, N. Tang, *J. Fluoresc.* **20** (2010) 1287
17. K. L. Kirk, R. Filler, *ACS Symp. Ser.* **639** (1996) 1
18. H. Q. Li, L. Shi, Q. S. Li, P. G. Liu, Y. Luo, J. Zhao, H. L. Zhu, *Bioorg. Med. Chem.* **17** (2009) 6264
19. M. Wang, L. Zhang, X. Han, J. Yang, J. Qian, S. Hong, F. Samaniego, J. Romaguera, Q. Yi, *Blood* **109** (2007) 5455.

Journal of the Serbian Chemical Society
JSCS@tmf.bg.ac.rs • www.shd.org.rs/JSCS
J. Serb. Chem. Soc. 78 (9) S102–S106 (2013) *Supplementary material*

SUPPLEMENTARY MATERIAL TO

Synthesis and biological evaluation of novel benzo[*b*]xanthone derivatives as potential antitumor agents

LIN LUO[1], JIANG-KE QIN[1]*, ZHI-KAI DAI[2]** and SHI-HUA GAO[1]

[1]*Key Laboratory for the Chemistry and Molecular Engineering of Medicinal Resources, School of Chemistry & Chemical Engineering of Guangxi Normal University, Guilin 541004, China and* [2]*Department of Pharmacology, Pharmaceutical Institute of Guilin Medical University, Guilin 541004, China*

J. Serb. Chem. Soc. 78 (9) (2013) 1301–1308

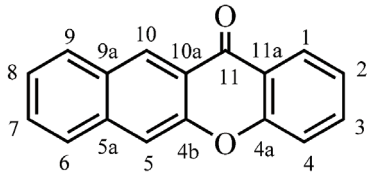

Fig. S-1. Chemical structure of benzo[*b*]xanthone with atomic numbering.

ANALYTIC AND SPECTROSCOPIC DATA FOR COMPOUNDS **1** AND **2a–e**

*1,3-Dihydroxy-12*H*-benzo[*b*]xanthen-12-one (**1**)*. Yield: 35 %; m.p.: 278––279 °C; ^{1}H-NMR (500 MHz, DMSO-d_6, δ / ppm): 12.92 (1H, *s*, HO-1), 8.86 (1H, *s*, H-10), 8.25 (1H, *d*, *J* = 8.4 Hz, H-9), 8.08 (1H, *s*, H-5), 8.07 (1H, *d*, *J* = 8.3 Hz, H-6), 7.71 (1H, *t*, *J* = 7.2 Hz, H-7), 7.58 (1H, *t*, *J* = 7.6 Hz, H-8), 6.43 (1H, *s*, H-2), 6.23 (1H, *s*, H-4).

*3-(2-Bromoethoxy)-1-hydroxy-12*H*-benzo[*b*]xanthen-12-one (**2a**)*. Yield: 14.9 %; m.p.: 236–238 °C; ^{1}H-NMR (500 MHz, $CDCl_3$, δ / ppm): 12.95 (1H, *s*, HO-1), 8.88 (1H, *s*, H-10), 8.08 (1H, *d*, *J* = 8.2 Hz, H-9), 7.93 (1H, *d*, *J* = 8.3 Hz, H-6), 7.84 (1H, *s*, H-5), 7.65 (1H, *t*, *J* = 7.1 Hz, H-7), 7.55 (1H, t, *J* = 7.2 Hz, H-8), 6.49 (1H, *s*, H-2), 6.37 (1H, *s*, H-4), 4.42 (2H, *t*, *J* = 6.1 Hz, OCH_2), 3.71 (2H, *t*, *J* = 6.0 Hz, CH_2Br).

*3-(3-Bromoethoxy)-1-hydroxy-12*H*-benzo[*b*]xanthen-12-one (**2b**)*. Yield: 32 %; m.p.: 190–192 °C; ^{1}H-NMR (500 MHz, $CDCl_3$, δ / ppm): 8.86 (1H, *s*, H-10), 8.06 (1H, *d*, *J* = 8.3 Hz, H-9), 7.91 (1H, *d*, *J* = 8.3 Hz, H-6), 7.82 (1H, *s*, H-5), 7.64 (1H, *t*, *J* = 7.5 Hz, H-7), 7.53 (1H, *t*, *J* = 7.4 Hz, H-8), 6.46 (1H, *s*, H-2),

*,** Corresponding authors. E-mails: (*)jiangkeq@sina.com; (**)dzhk110@126.com

6.36 (1H, *s*, H-4), 4.25 (2H, *t*, *J* = 6.0 Hz, OCH_2), 3.65 (2H, *t*, *J* = 6.4 Hz, CH_2Br), 2.43-2.38 (2H, *m*, $OCH_2C\mathbf{H}_2CH_2Br$).

*3-(4-Bromoethoxy)-1-hydroxy-12*H-*benzo[*b*]xanthen-12-one* (***2c***). Yield: 14.5 %; m.p.: 177–179 °C; ^{1}H-NMR (500 MHz, $CDCl_3$, δ / ppm): 12.94 (1H, *s*, HO-1), 8.85 (1H, *s*, H-10), 8.06 (1H, *d*, *J* = 8.3 Hz, H-9), 7.91 (1H, *d*, *J* = 8.4 Hz, H-6), 7.82 (1H, *s*, H-5), 7.64 (1H, *t*, *J* = 7.2 Hz, H-7), 7.52 (1H, *t*, *J* = 7.3 Hz, H-8), 6.43 (1H, *s*, H-2), 6.33 (1H, *s*, H-4), 4.12 (2H, *t*, *J* = 6.0 Hz, OCH_2), 3.54 (2H, *t*, *J* = 6.4 Hz, CH_2Br), 2.14–2.09 (2H, *m*, $OCH_2C\mathbf{H}_2CH_2CH_2Br$), 2.06–2.02 (2H, *m*, $OCH_2CH_2C\mathbf{H}_2CH_2Br$).

*3-[(5-Bromopentyl)oxy]-1-hydroxy-12*H-*benzo[*b*]xanthen-12-one* (***2d***). Yield: 20.5 %; m.p.: 167–169 °C; ^{1}H-NMR (500 MHz, $CDCl_3$, δ / ppm): 12.95 (1H, *s*, HO-1), 8.88 (1H, *s*, H-10), 8.08 (1H, *d*, *J* = 8.2 Hz, H-9), 7.93 (1H, *d*, *J* = 8.1 Hz, H-6), 7.85 (1H, *s*, H-5), 7.65 (1H, *t*, *J* = 7.6 Hz, H-7), 7.54 (1H, *t*, *J* = 7.9 Hz, H-8), 6.46 (1H, *d*, *J* = 1.8 Hz, H-2), 6.36 (1H, *d*, *J* = 1.8 Hz, H-4), 4.12 (2H, *t*, *J* = 6.3 Hz, OCH_2), 3.49 (2H, *t*, *J* = 6.6 Hz, CH_2Br), 2.01–1.96 (2H, *m*, $OCH_2C\mathbf{H}_2CH_2CH_2CH_2Br$), 1.92–1.87(2H, *m*, $OCH_2CH_2CH_2C\mathbf{H}_2CH_2Br$), 1.72–1.68 (2H, *m*, $OCH_2CH_2C\mathbf{H}_2CH_2CH_2Br$).

*3-[(6-Bromohexyl)oxy]-1-hydroxy-12*H-*benzo[*b*]xanthen-12-one* (***2e***). Yield: 15.3 %, m.p.: 156–158 °C; ^{1}H-NMR (500 MHz, $CDCl_3$, δ / ppm): 12.94 (1H, *s*, HO-1), 8.87 (1H, *s*, H-10), 8.07 (1H, *d*, *J* = 8.2 Hz, H-9), 7.92 (1H, *d*, *J* = 8.6 Hz, H-6), 7.84 (1H, *s*, H-5), 7.64 (1H, *t*, *J* = 7.6 Hz, H-7), 7.53 (1H, *t*, *J* = 7.5 Hz, H-8), 6.45 (1H, *s*, H-2), 6.35 (1H, *s*, H-4), 4.10 (2H, *t*, *J* = 6.5 Hz, OCH_2), 3.45 (2H, *t*, *J* = 6.9 Hz, CH_2Br), 1.96–1.93 (2H, *m*, $OCH_2C\mathbf{H}_2CH_2CH_2CH_2CH_2Br$), 1.89–1.88 (2H, *m*, $OCH_2CH_2CH_2CH_2C\mathbf{H}_2CH_2Br$), 1.58–1.56 (4H, *m*, $OCH_2CH_2C\mathbf{H}_2C\mathbf{H}_2CH_2CH_2Br$).

ANALYTIC AND SPECTROSCOPIC DATA OF COMPOUNDS **3a–i**

*3-[4-(Dimethylamino)butoxy]-1-hydroxy-12*H-*benzo[*b*]xanthen-12-one* (***3a***). Yield: 17.8 %; Color: Yellow; m.p.: 148–150 °C; Anal. Calcd. for $C_{23}H_{23}NO_4$: C, 73.19; H, 6.14; N, 3.71 %. Found: C, 73.28; H, 6.18; N, 3.63 %; IR (KBr, cm^{-1}): 3429 (O–H), 3054 (Ar-H), 2940 (C–H str. of $–CH_3$ and $–CH_2–$), 1656 (C=O), 1600 (Ar), 1512 (Ar), 1469 ($–CH_2–$); ^{1}H-NMR (500 MHz, DMSO-d_6, δ / ppm): 12.90 (1H, *s*, HO-1), 8.90 (1H, *s*, H-10), 8.28 (1H, *d*, *J* = 8.5 Hz, H-9), 8.12 (1H, *s*, H-5), 8.10 (1H, *d*, *J* = 8.4 Hz, H-6), 7.74 (1H, *t*, *J* = 7.9 Hz, H-7), 7.62 (1H, *t*, *J* = 7.8 Hz, H-8), 6.67 (1H, *s*, H-2), 6.42 (1H, *s*, H-4), 4.18 (2H, *t*, *J* = 6.6 Hz, OCH_2), 2.46 (2H, *brs*, CH_2N), 2.35 (6H, *s*, $2NCH_3$), 1.79–1.77 (2H, *m*, $OCH_2C\mathbf{H}_2CH_2CH_2N$), 1.65–1.62 (2H, *m*, $OCH_2CH_2C\mathbf{H}_2CH_2N$); ^{13}C-NMR (125 MHz, DMSO-d_6, δ / ppm): 181.7 (C-11), 167.0 (C-3), 163.6 (C-1), 158.2 (C-4a), 151.8 (C-4b), 136.9 (C-5a), 130.1 (C-9a), 130.0 (C-10), 129.7 (C-9), 127.7 (C-7), 127.6 (C-6), 126.4 (C-10a), 120.1 (C-8), 113.6 (C-5), 103.0 (C-11a), 97.5 (C-4), 94.0 (C-2), 68.9 (OCH_2), 58.5 (CH_2N), 44.9 ($2NCH_3$), 26.5

(OCH_2**C**$H_2CH_2CH_2N$), 23.1 (OCH_2CH_2**C**H_2CH_2N); ESI-MS (*m*/*z*): 378.15 $[M+H]^+$.

*3-[4-(Diethylamino)butoxy]-1-hydroxy-12*H*-benzo[*b*]xanthen-12-one* (***3b***). Yield: 8.3 %; Color: yellow; m.p.: 128–130 °C; Anal. Calcd. for $C_{25}H_{27}NO_4$: C, 74.05; H, 6.71; N, 3.45 %. Found: C, 74.16; H, 6.80; N, 3.36 %; IR (KBr, cm^{-1}): 3417 (O–H), 3050(Ar-H), 2929 (C–H str. of $–CH_3$ and $–CH_2–$), 1646 (C=O), 1599 (Ar), 1506 (Ar), 1468 ($–CH_2–$); ^{1}H-NMR (500 MHz, DMSO-d_6, δ / ppm): 8.88 (1H, *s*, H-10), 8.26 (1H, *d*, *J* = 8.5 Hz, H-9), 8.09 (1H, *s*, H-5), 8.08 (1H, *d*, *J* = 8.5 Hz, H-6), 7.73 (1H, *t*, *J* = 7.4 Hz, H-7), 7.60 (1H, *t*, *J* = 7.8 Hz, H-8), 6.66 (1H, *s*, H-2), 6.42 (1H, *s*, H-4), 4.20 (2H, *t*, *J* = 6.1 Hz, OCH_2), 2.99 (6H, *s*, $3CH_2N$), 1.85–1.76 (4H, *m*, OCH_2C**H**$_2C$**H**$_2CH_2N$), 1.17 (6H, *s*, *J* = 7.1 Hz, $2CH_3$); ^{13}C-NMR (125 MHz, DMSO-d_6, δ / ppm): 181.2 (C-11), 167.0 (C-3), 163.6 (C-1), 158.2 (C-4a), 151.8 (C-4b), 136.9 (C-5a), 130.2 (C-9a), 129.7 (C-10), 129.7 (C-9), 127.7 (C-7), 127.6 (C-6), 126.5 (C-10a), 120.1 (C-8), 113.7 (C-5), 103.1 (C-11a), 97.6 (C-4), 94.0 (C-2), 68.6 (OCH_2), 51.3 (CH_2N), 46.8 ($2NCH_2$), 26.2 (OCH_2**C**$H_2CH_2CH_2N$), 21.2 (OCH_2CH_2**C**H_2CH_2N), 9.7 (NCH_2**C**H_3), 8.8 (NCH_2**C**H_3); ESI-MS (*m*/*z*): 406.15 $[M+H]^+$.

*1-Hydroxy-3-[4-(pyrrolidin-1-yl)butoxy]-12*H*-benzo[*b*]xanthen-12-one* (***3c***). Yield: 20 %; Color: yellow; m.p.: 150–152 °C; Anal. Calcd. for $C_{25}H_{25}NO_4$: C, 74.42; H, 6.25; N, 3.47 %. Found: C, 74.55; H, 6.34; N, 3.38 %; IR (KBr, cm^{-1}): 3429 (O–H), 3044 (Ar-H), 2940 (C–H str. of $–CH_2–$), 1655 (C=O), 1598 (Ar), 1509 (Ar), 1471 ($–CH_2–$); ^{1}H-NMR (500 MHz, DMSO-d_6, δ / ppm): 12.89 (1H, *s*, HO-1), 8.90 (1H, *s*, H-10), 8.27 (1H, *d*, *J* = 8.4 Hz, H-9), 8.10 (1H, *s*, H-5), 8.09 (1H, *d*, *J* = 8.3 Hz, H-6), 7.73 (1H, *t*, *J* = 7.4 Hz, H-7), 7.60 (1H, *t*, *J* = 7.6 Hz, H-8), 6.67 (1H, *s*, H-2), 6.43 (1H, *s*, H-4), 4.20 (2H, *t*, *J* = 6.6 Hz, OCH_2), 3.07 (6H, *br*, CH_2N), 1.90 (4H, *s*, OCH_2C**H**$_2C$**H**$_2CH_2N$), 1.83–1.80 (4H, *m*, H-2' and 3'); ^{13}C-NMR (DMSO-d_6, 125 MHz, δ / ppm): 181.7 (C-11), 167.0 (C-3), 163.6 (C-1), 158.2 (C-4a), 151.8 (C-4b), 136.9 (C-5a), 130.1 (C-9a), 130.0 (C-10), 129.7 (C-9), 127.7 (C-7), 127.6 (C-6), 126.5 (C-10a), 120.1 (C-8), 113.7 (C-5), 103.0 (C-11a), 97.5 (C-4), 94.0 (C-2), 68.7 (OCH_2), 54.9 (CH_2N), 53.9 (C-1' and 4'), 26.4 (OCH_2**C**H_2CH_2C H_2N), 23.8 (OCH_2CH_2**C**H_2CH_2N), 23.3 (C-2' and 3'); ESI-MS (*m*/*z*): 404.17 $[M+H]^+$.

*1-Hydroxy-3-[4-(piperidin-1-yl)butoxy]-12*H*-benzo[*b*]xanthen-12-one* (***3d***). Yield: 25.1 %; Color: yellow; m.p.: 154–156 °C; Anal. Calcd. for $C_{26}H_{27}NO_4$: C, 74.80; H, 6.52; N, 3.35 %. Found: C, 74.68; H, 6.65; N 3.43 %; IR (KBr, cm^{-1}): 3441 (O–H), 2924 (C–H str. of $–CH_2–$), 1641 (C=O), 1597 (Ar), 1506 (Ar), 1470 ($–CH_2–$); ^{1}H-NMR (500 MHz, DMSO-d_6, δ /ppm): 12.89 (1H, *s*, HO-1), 8.90 (1H, *s*, H-10), 8.27 (1H, *d*, *J* = 8.2 Hz, H-9), 8.09 (1H, *s*, H-5), 8.08 (1H, *d*, *J* = 8.2 Hz, H-6), 7.73(1H, *t*, *J* = 7.6 Hz, H-7), 7.60 (1H, *t*, *J* = 7.5 Hz, H-8), 6.67 (1H, *s*, H-2), 6.42 (1H, *s*, H-4), 4.20 (2H, *t*, *J* = 6.6 Hz, OCH_2), 3.05 (6H, *s*,

CH_2N), 1.81 (4H, *s*, $OCH_2C\mathbf{H}_2C\mathbf{H}_2CH_2N$), 1.72 (6H, brs, H-2', 3' and 4'); ESI-MS (*m*/*z*): 418.13 $[M+H]^+$.

*1-Hydroxy-3-[4-(morpholin-1-yl)butoxy]-12*H*-benzo[*b*]xanthen-12-one (**3e**)*. Yield: 16.7 %; Color: yellow; m.p.: 183–185 °C; Anal. Calcd. for $C_{25}H_{25}NO_5$: C, 71.58; H, 6.01; N, 3.34 %. Found: C, 71.49; H, 6.04; N, 3.38 %; IR (KBr, cm^{-1}): 3440 (O–H), 2956 (C–H str. of $–CH_2–$), 1658 (C=O), 1601 (Ar), 1512 (Ar), 1471 ($–CH_2–$); ^{1}H-NMR (500 MHz, DMSO-d_6, δ / ppm): 12.94 (1H, *s*, HO-1), 8.87(1H, *s*, H-10), 8.08 (1H, *d*, *J* = 8.3 Hz, H-9), 7.92 (1H, *d*, *J* = 8.3 Hz, H-6), 7.84 (1H, *s*, H-5), 7.65 (1H, *t*, *J* = 7.4 Hz, H-7), 7.53 (1H, *t*, *J* = 7.7 Hz, H-8), 6.46 (1H, *s*, H-2), 6.35 (1H, *s*, H-4), 4.13 (2H, *t*, *J* = 6.3 Hz, OCH_2), 3.76 (4H, *t*, *J* = 4.5 Hz, H-2' and 4'), 2.49 (4H, *s*, H-1' and 5'), 2.45 (2H, *t*, *J* = 7.3 Hz, CH_2N), 1.91–1.87 (2H, *m*, $OCH_2C\mathbf{H}_2CH_2CH_2N$), 1.75–1.71 (2H, *m*, $OCH_2CH_2C\mathbf{H}_2CH_2N$); ^{13}C-NMR ($CDCl_3$, 125 MHz, δ / ppm): 181.7 (C-11), 166.7 (C-3), 164.0 (C-1), 158.1 (C-4a), 151.8 (C-4b), 136.7 (C-5a), 129.6 (C-9a), 129.5 (C-10), 129.2 (C-9), 127.5 (C-7), 127.0 (C-6), 125.6 (C-10a), 120.2 (C-8), 113.1 (C-5), 103.2 (C-11a), 97.0 (C-4), 93.4 (C-2), 68.4 (OCH_2), 67.0 (C-2' and 4'), 58.5 (CH_2N), 53.8 (C-1' and 5'), 26.9 ($OCH_2\mathbf{C}H_2CH_2CH_2N$), 23.0 ($OCH_2CH_2\mathbf{C}H_2CH_2N$); ESI-MS (*m*/*z*): 420.13 $[M+H]^+$.

*3-[2-(Dimethylamino)ethoxy]-1-hydroxy-12*H*-benzo[*b*]xanthen-12-one (**3f**)*. Yield: 27.6 %; Color: yellow; m.p.: 148–150 °C; Anal. Calcd. for $C_{21}H_{19}NO_4$: C, 72.19; H, 5.48; N, 4.01 %. Found: C, 72.28; H, 5.53; N, 3.96 %; IR (KBr, cm^{-1}): 3363 (O–H), 3044 (Ar-H), 2925 (C–H str. of $–CH_3$ and $–CH_2–$), 1658 (C=O), 1596 (Ar), 1572 (Ar), 1509 (Ar), 1467 ($–CH_2–$); ^{1}H-NMR ($CDCl_3$, 500 MHz, δ / ppm): 8.83 (1H, *s*, H-10), 8.05 (1H, *d*, *J* = 8.3 Hz, H-9), 7.90 (1H, *d*, *J* = 8.4 Hz, H-6), 7.81(1H, *s*, H-5), 7.63 (1H, t, *J* = 7.7 Hz, H-7), 7.51 (1H, *t*, *J* = 7.8 Hz, H-8), 6.47 (1H, *d*, *J* = 2.1 Hz, H-2), 6.36 (1H, *d*, *J* = 2.2 Hz, H-4), 4.19 (2H, *t*, *J* = 5.7 Hz, OCH_2), 2.81 (2H, *t*, *J* = 5.7 Hz, CH_2N), 2.39 (6H, *s*, $2NCH_3$); ^{13}C-NMR (CDCl3, 125 MHz, δ / ppm): 181.3 (C-11), 166.5 (C-3), 164.1 (C-1), 158.1 (C-4a), 151.9 (C-4b), 136.8 (C-5a), 129.7 (C-9a), 129.6 (C-10), 129.2 (C-9), 127.6 (C-7), 127.1 (C-6), 125.6 (C-10a), 120.3 (C-8), 113.2 (C-5), 103.4 (C-11a), 97.0 (C-4), 93.7 (C-2), 66.8 (OCH_2), 57.9 (CH_2N), 45.9 ($2NCH_3$); APCI-MS (*m*/*z*): 350.09 $[M+H]^+$.

*3-[3-(Dimethylamino)propoxy]-1-hydroxy-12*H*-benzo[*b*]xanthen-12-one (**3g**)*. Yield: 27.6 %; Color: yellow; m.p.: 148–150 °C; Anal. Calcd. for $C_{22}H_{21}NO_4$: C, 72.71; H, 5.82; N, 3.85 %. Found: C, 72.78; H, 6.04; N, 3.76 %; IR (KBr, cm^{-1}): 3418 (O–H), 3055 (Ar-H), 2945 (C–H str. of $–CH_3$ and $–CH_2–$), 1656 (C=O), 1600 (Ar), 1506 (Ar), 1467 ($–CH_2–$); ^{1}H-NMR ($CDCl_3$, 500 MHz, δ / ppm): 8.82 (1H, *s*, H-10), 8.04 (1H, *d*, *J* = 8.4 Hz, H-9), 7.89 (1H, *d*, *J* = 8.4 Hz, H-6), 7.79 (1H, *s*, H-5), 7.62 (1H, *t*, *J* = 7.3 Hz, H-7), 7.50 (1H, *t*, *J* = 7.5 Hz, H-8), 6.44 (1H, *d*, *J* = 1.9 Hz, H-2), 6.34 (1H, *d*, *J* = 1.9 Hz, H-4), 4.15 (2H, *t*, *J* = 6.4 Hz, OCH_2), 2.50 (2H, *t*, *J* = 7.1 Hz, CH_2N), 2.31 (6H, *s*, $2NCH_3$). 2.05–2.00

(2H, *m*, $OCH_2CH_2C\mathbf{H}_2N$); ^{13}C-NMR (125 MHz, $CDCl_3$, δ / ppm): 181.2 (C-11), 166.8 (C-3), 164.0 (C-1), 158.2 (C-4a), 151.9 (C-4b), 136.7 (C-5a), 129.7 (C-9a), 129.6 (C-10), 129.2 (C-9), 127.6 (C-7), 127.1 (C-6), 125.6 (C-10a), 120.3 (C-8), 113.1 (C-5), 103.3 (C-11a), 97.1 (C-4), 93.5 (C-2), 66.9 (OCH_2), 56.1 (CH_2N), 45.5 ($2NCH_3$), 27.3 ($OCH_2\mathbf{C}H_2$); APCI-MS (*m*/*z*): 364.11 $[M+H]^+$.

*3-{5-[(Dimethylamino)pentyl]oxy}-1-hydroxy-12*H*-benzo[*b*]xanthen-12-one* (***3h***). Yield: 36.4 %; Color yellow; m.p.: 130–132 °C; Anal. Calcd. for $C_{24}H_{25}NO_4$: C, 73.64; H, 6.44; N, 3.58 %. Found: C, 73.48; H, 6.52; N, 3.63 %; IR (KBr, cm^{-1}): 3423 (O–H), 3093 (Ar-H), 3055 (Ar-H), 2936 (C–H str. of $–CH_3$ and $–CH_2–$), 1655 (C=O), 1601 (Ar), 1506 (Ar), 1468 ($–CH_2–$); ^{1}H-NMR (500 MHz, $CDCl_3$, δ/ppm): 8.82 (1H, *s*, H-10), 8.04 (1H, *d*, *J* = 8.4 Hz, H-9), 7.89 (1H, *d*, *J* = 8.4 Hz, H-6), 7.79 (1H, *s*, H-5), 7.62 (1H, *t*, *J* = 7.2 Hz, H-7), 7.50 (1H, *t*, *J* = 7.5 Hz, H-8), 6.41 (1H, *d*, *J* = 2.0 Hz, H-2), 6.32 (1H, *d*, *J* = 2.0 Hz, H-4), 4.08 (2H, *t*, *J* = 6.5 Hz, OCH_2), 2.35 (2H, *t*, *J* = 7.0 Hz, CH_2N), 2.28 (6H, *s*, $2NCH_3$), 1.90–1.85 (2H, *m*, $OCH_2C\mathbf{H}_2$), 1.62–1.52 (4H, *m*, $C\mathbf{H}_2C\mathbf{H}_2CH_2N$); ^{13}C-NMR (125 MHz, $CDCl_3$, δ / ppm): 181.2 (C-11), 166.8 (C-3), 164.1 (C-1), 158.1 (C-4a), 151.9 (C-4b), 136.7 (C-5a), 129.7 (C-9a), 129.6 (C-10), 129.2 (C-9), 127.6 (C-7), 127.1 (C-6), 125.6 (C-10a), 120.3 (C-8), 113.1 (C-5), 103.2 (C-11a), 97.0 (C-4), 93.5 (C-2), 66.8 ($O\mathbf{C}H_2$), 59.6 (CH_2N), 45.4 ($2NCH_3$), 28.9 ($OCH_2\mathbf{C}H_2$), 27.3 ($\mathbf{C}H_2CH_2N$), 23.9 ($OCH_2CH_2\mathbf{C}H_2$); APCI-MS (*m*/*z*): 392.13 $[M+H]^+$.

*3-{6-[(dimethylamino)hexyl]oxy}-1-hydroxy-12*H*-benzo[*b*]xanthen-12-one* (***3i***). Yield: 29.1 %; Color: yellow; m.p.: 156–158 °C; Anal. Calcd. for $C_{25}H_{27}NO_4$: C, 74.05; H, 6.71; N, 3.45 %. Found: C, 74.10; H, 6.82; N, 3.41 %; IR (KBr, cm^{-1}): 3418 (OH), 3088 (Ar-H), 3055 (Ar-H), 2924 (C-H str. of $-CH_3$ and $-CH_2-$), 1659 (C=O), 1601 (Ar), 1509 (Ar), 1468 ($-CH_2-$); ^{1}H-NMR (500 MHz, $CDCl_3$, δ / ppm): 8.83 (1H, *s*, H-10), 8.05 (1H, *d*, *J* = 8.3 Hz, H-9), 7.90 (*d*, *J* = 8.4 Hz, H-6), 7.80 (*s*, 1H, H-5), 7.62 (*t*, *J* = 7.2 Hz, 1H, H-7), 7.51(1H, *t*, *J* = = 7.4 Hz, 1H, H-8), 6.43 (1H, *d*, *J* = 2.1 Hz, H-2), 6.33 (1H, *d*, *J* = 2.2 Hz, H-4), 4.08 (2H, *t*, *J* = 6.5 Hz, OCH_2), 2.37 (2H, *t*, *J* = 7.5 Hz, CH_2N), 2.31 (6H, *s*, $2NCH_3$), 1.89–1.83 (2H, *m*, $OCH_2C\mathbf{H}_2$), 1.59–1.51 (4H, *m*, $OCH_2C\mathbf{H}_2C\mathbf{H}_2CH_2CH_2CH_2N$), 1.46–1.41 (2H, *m*, $C\mathbf{H}_2CH_2N$); ^{13}C-NMR (125 MHz, $CDCl_3$, δ / ppm): 181.2 (C-11), 166.9 (C-3), 164.1 (C-1), 158.2 (C-4a), 152.0 (C-4b), 136.7 (C-5a), 129.7 (C-9a), 129.6 (C-10), 129.2 (C-9), 127.6 (C-7), 127.1 (C-6), 125.6 (C-10a), 120.3 (C-8), 113.1 (C-5), 103.2 (C-11a), 97.0 (C-4), 93.5 (C-2), 68.6 (OCH_2), 59.6 (CH_2N), 45.3 ($2NCH_3$), 28.9 ($OCH_2\mathbf{C}H_2$), 27.4 ($\mathbf{C}H_2CH_2N$), 27.1 ($OCH_2CH_2\mathbf{C}H_2$), 25.9 ($\mathbf{C}H_2CH_2CH_2N$); APCI-MS (*m*/*z*): 406. 14 $[M+H]^+$.

Journal of the Serbian Chemical Society
JSCS-info@shd.org.rs • www.shd.org.rs/JSCS
J. Serb. Chem. Soc. 78 (9) 1309–1322 (2013)
JSCS–4499
UDC 663.222:663.251:547.973:543.544
Original scientific paper

Characterisation of Vranec, Cabernet Sauvignon and Merlot wines based on their chromatic and anthocyanin profiles

MAJA DIMITROVSKA[1]*, ELENA TOMOVSKA[2] and MIRJANA BOCEVSKA[2]

[1]*Institute of Public Health, 50 Divizija 6, 1000 Skopje, FYR Macedonia and* [2]*Faculty of Technology and Metallurgy, Ss. Cyril and Methodius University, Rudjer Boskovic 16, 1000 Skopje, FYR Macedonia*

(Received 1 January, revised 21 February 2013)

Abstract: Wines of three different grape varieties, Vranec, Cabernet Sauvignon and Merlot, were characterised in terms of their anthocyanin and chromatic profiles, total polyphenols and antioxidant potential. The total, monomeric, polymeric and co-pigmented anthocyanins were determined by spectrophotometry and the individual anthocyanin compounds were quantified using HPLC–DAD. The chromatic profile was evaluated according to colour density, hue, % red, % blue, % yellow and brilliance (*dA*). The established data were submitted to analysis of variance and principle component analysis in order to evaluate their potential for differentiation of wines according to variety and vintage. The Vranec wines showed distinctive characteristics, with the highest content of anthocyanins and values of colour intensity, % red and *dA*, compared to the other two studied varieties. The content of petunidin-3-glucoside, peonindin-3-glucoside and anthocyanin acetates were established as possible markers for the differentiation of Vranec wines from Cabernet Sauvignon and Merlot wines. However, none of the assayed parameters could be used for the differentiation of Cabernet Sauvignon from Merlot wines. It was observed that wine age limits the successful classification of the wines by variety according to anthocyanins. The chromatic parameters allowed young (aged up to 1 year) to be distinguished from old Vranec wines.

Keywords: wine; anthocyanins; Vranec; colour; differentiation.

INTRODUCTION

Wine is a complex product composed of various compounds of different nature. One of the most important components of wines that influence their quality parameters are polyphenols. Polyphenols contribute to the organoleptic characteristics, such as colour, astringency and bitterness and also exert antimicrobial and antioxidant properties.[1] Anthocyanins are polyphenols of the flavo-

* Corresponding author. E-mail: m.dimitrovska@iph.mk
doi: 10.2298/JSC130101026D

noid family that play a key role in the colour characteristics and colour stability of wines.[2] Anthocyanins are transferred into the wine from grape skins during the process of vinification. The free monomeric anthocyanins are responsible for the bluish-red colour of young wines, however, during maturation and ageing, the colour of wines transforms to brick-red as a result of the development of polymeric pigments. The extent of red colour in wines depends on the type and concentration of anthocyanins, pH, level of free SO_2 and the degree of polymerisation and co-pigmentation.[3]

Knowledge of the chemical composition of wine and its relation to the grape variety is of great importance in oenology. Several groups of compounds have been proposed for authentication purposes of wines and anthocyanins are among them. The amount of anthocyanins in wines is affected by several factors, such as grape variety, soil, climate, the winemaking techniques, *etc*. However, there are indications that the anthocyanin pattern or fingerprint of grapes is relatively constant and independent of the environmental conditions. As a result, anthocyanins are considered as markers of variety and are used for the differentiation and classification of grapes and wines.[4,5]

There are many publications in which the anthocyanin composition of wines produced from the international grape varieties Cabernet Sauvignon and Merlot is studied,[6–10] but, to the best of our knowledge, there has been almost no detailed research on the anthocyanin profile of wines obtained from these grape varieties cultivated in R. Macedonia. There are also little data on the composition of Vranec wines,[11,12] which is an indigenous Balkan variety.

The aim of this research was to study and compare the colour characteristics, anthocyanin composition, content of total phenolics and antioxidative potential of red wines obtained from three grape varieties, Vranec, Cabernet Sauvignon and Merlot, and produced in four consecutive vintages (2005–2008). Furthermore, based on the considerable number of data obtained from the analysed chemical parameters, the possibility for the classification of the wines according to age and variety was evaluated.

EXPERIMENTAL

Wine samples. A set of 32 monovarietal red wines of vintage ranging from 2005 to 2008, produced and bottled in different local wineries were taken directly from the producers. Most of the samples were of Vranec, an autochthonous Balkan variety (17), then Merlot (8) and Cabernet Sauvignon (7). All wines were collected during the first three months of 2009 and were immediately analysed for their total phenolic content, individual anthocyanins, colour components and antioxidant capacity.

Chemicals. For the chromatographic determinations, acetonitrile (gradient grade, HPLC) and potassium dihydrogen phosphate (*p.a.*) were obtained from Merck (Darmstadt, Germany). Malvidin-3-glucoside purchased from Extrasynthese (Genay Cedex, France) was used for anthocyanin quantification. 2,2-Diphenyl-1-picrylhydrazyl (DPPH$^{\bullet}$) and gallic acid were from Sigma–Aldrich (St. Louis, MO, USA). Nitric acid, 60 % (*puriss*), used for the determination

of the elements was also purchased from Sigma–Aldrich (St. Louis, MO, USA). Deionised water was obtained from an ultra pure water system TKA Lab micro (Niederelbert, Germany).

Total phenolic content. The total phenols in the wines were determined spectrophotometrically (Cary 50 SCAN, Varian, Inc., USA) at 765 nm, according to the method of Slinkard and Singleton[13] using Folin–Ciocalteu reagent and gallic acid as a standard substance. The results were calculated as the mean of three measurements and are expressed as gallic acid equivalents (*GAE*, mg L^{-1}).

Determination of the colour components. The colour components, colour intensity (*CI*), hue (*H*), brilliance (*dA*), percent red (%*R*), percent yellow (%*Y*) and percent blue (%*B*) were determined by direct measurement of the absorbance of the wines at 420, 520 and 620 nm in 2 mm cuvette after filtering of the samples. *CI* was calculated as the sum of the absorbances at 420, 520 and 620 nm and *H* as the ratio between the absorbance at 420 nm and the absorbance at 520 nm. The other colour variables, *dA*, %*R*, %*Y* and %*B* were calculated according to Glories.[14]

Determination of co-pigmented, monomeric, polymeric and total anthocyanins. The content of monomeric, co-pigmented, polymeric and total anthocyanins was determined according to the method based on the colorimetric effects that wines exert after addition of SO_2 and acetaldehyde.[15] The spectrophotometric measurements were performed in a 2 mm cuvette at 520 nm. The obtained readings were corrected for a 10 mm optical path and used for the calculation of the co-pigmented, monomeric, polymeric and total anthocyanins expressed as absorption units (a.u.) and percents.

Antioxidant activity. The antioxidant capacity of the wines was determined as their antiradical DPPH• activity ($I_{50\%}$). The stable 2,2-diphenyl-1-picrylhydrazyl radical (DPPH•) was used in the procedure described by Brand–Williams.[16] The effect of distinct wine aliquots on DPPH• inhibition (*I*%) was calculated using Eq. (1):

$$I\% = 100\frac{A_0 - A_i}{A_0} \quad (1)$$

where A_0 is the absorbance of the blank and A_i is the absorbance of the sample.

According to the calculated values, a graph was constructed relating the DPPH• inhibition (%) and the wine quantity (mL). From the graph, the quantity of wine (mL) that caused 50 % inhibition of the DPPH radical was determined and expressed as $I_{50\%}$.

Determination of anthocyanins by HPLC. The anthocyanins were determined using a Shimadzu Prominence liquid chromatography system comprising a quaternary pump LC-|-20AT, a photodiode detector SPD-M20A, a column oven CTO-20AC, an autosampler SIL--20AC, an on-line degasser DGU-20A5 and a bus communications module CBM-20A. The system was controlled by Class VP 7.3 software. Separation of the compounds was achieved using a Purospher STAR RP-18e column (250 mm×4 mm I.D, 5 μm particle size) supplied by Merck, Darmstadt, Germany, protected with a guard column of the same packing material (4 mm×4 mm). The chromatographic conditions were as described in a previous study.[17] The anthocyanins were identified by the retention time, elution order and the spectral characteristics of the compounds. The amounts of the anthocyanins identified in the samples are expressed as malvidine-3-glucoside equivalents.

Statistical analysis. The means and standard deviations were calculated using Microsoft Excel® 2003. For comparison of the means, one-way ANOVA and Tukey's post-hoc test were applied at the 95 % significance level ($p < 0.05$). In addition, multivariate analysis including Principal Component Analysis (PCA) was performed using SPSS® 18.0 software.

RESULTS AND DISCUSSION

Chemical profile of the wines

The mean values of the colour components, content of anthocyanins and total phenols, and the antioxidant capacity of the wines (2005–2008 vintages) of Vranec, Cabernet Sauvignon and Merlot varieties are summarized in Table I, while Table II presents the mean values of the analyzed parameters of wines grouped by vintage.

TABLE I. Colour components, content of anthocyanins and total phenols and antioxidant capacity of the red wines grouped by grape variety, Vranec, Cabernet Sauvignon and Merlot; the results are expressed as means ± *SD*; different letters in the superscript in a same row indicate statistically significant means ($p < 0.05$)

Wine characteristic	Vranec (n=17)	Cabernet Sauvignon (n=7)	Merlot (n=8)
Colour intensity (*CI*)	15.4±4.3[a]	10.6±1.8[b]	9.15±2.3[b]
Hue (*H*)	0.66±0.12[a]	0.77±0.11[a]	0.76±0.12[a]
%*R*	54.1±4.0[a]	50.7±3.0[a]	51.1±3.0[a]
%*B*	10.8±0.8[a]	10.7±1.1[a]	10.4±1.6[a]
%*Y*	35.1±3.8[a]	38.6±3.3[a]	38.5±4.0[a]
dA / %	57.2±6.8[a]	51.1±5.7[a]	51.8±5.8[a]
Monomeric anthocyanins, a.u.	1.84±1.01[a]	1.12±0.55[a]	1.2±0.7[a]
Co-pigmented anthocyanins, a.u.	1.12±0.68[a]	0.71±0.39[a]	0.83±0.42[a]
Polymeric anthocyanins, a.u.	5.6±1.6[a]	3.9±0.7[b]	3.2±0.8[b]
Total anthocyanins, a.u.	8.6±2.6[a]	5.7±1.6[b]	5.1±1.4[b]
Monomeric anthocyanins, %	20.5±6.55[a]	19.04±5.05[a]	21.37±7.60[a]
Co-pigmented anthocyanins, %	12.92±7.25[a]	11.78± 3.95[a]	16.43±7.71[a]
Polymeric anthocyanins, %	66.58±9.33[a]	69.18±5.64[a]	62.20±9.50[a]
Total phenols, GAE, mg L^{-1}	2383±596[a]	2323±279[a]	2023±188[a]
Antiradical $DPPH^{\bullet}$ activity $I_{50\%}$, µL wine	21.2±6.3[a]	20.6±5.0[a]	23.0±2.8[a]

Differences in average values of the studied parameters were observed amongst the wines of different variety (Table I). The Vranec variety wines had the highest colour intensity compared to the Cabernet Sauvignon and Merlot wines. This is due to the higher content of total and polymeric anthocyanins observed in Vranec wines, since anthocyanins are related and contribute to the colour intensity of wines.[3] Vranec wines have also shown the highest values for percent red (%*R*), brilliance (*dA*) and monomeric anthocyanins. However, although they were the wines richest in anthocyanins, their content of total phenols was not markedly higher compared to the Cabernet Sauvignon and Merlot wines. The lowest average phenolic content (2023 mg L^{-1} GAE) was measured in the Merlot wines, but this value did not differ significantly from the other two studied wine varieties. ANOVA and the Tukey post hoc test used on the obtained data for the wine characteristics revealed statistically significant differences among the wines only for three parameters: colour intensity and contents of polymeric and total

anthocyanins. These parameters allow differentiation of Vranec wines from the Cabernet Sauvignon and Merlot varieties, but not between the Merlot and Cabernet Sauvignon wines. Regarding the antioxidant capacity, Vranec, Cabernet Sauvignon and Merlot wines exhibited very similar values of DPPH• activity ($I_{50\%} \approx 20$), which did not change with ageing of the wines (Table II).

TABLE II. Colour components, content of anthocyanins and total phenols and antioxidant capacity of the red wines of Vranec, Cabernet Sauvignon and Merlot variety grouped by vintage, 2005–2008; the results are expressed as means ± *SD*; different letters in the superscript in a same row indicate statistically significant means ($p < 0.05$)

Wine characteristic	2005 (n=3)	2006 (n=6)	2007 (n=6)	2008 (n=17)
Colour intensity (*CI*)	14.4±2.5^a	9.7±2.2^a	13.1±4.8^a	13.4±4.9^a
Hue (*H*)	0.80±0.10^a	0.79±0.12^a	0.74±0.09^a	0.65±0.12^a
%*R*	49.5±2.7^a	50.6±3.4^a	51.1±2.5^a	54.4±3.8^a
%*B*	10.8±0.2^a	9.8±0.7^a	11.1±0.8^a	10.8±1.3^a
%*Y*	39.6±3.0^a	39.6±3.4^a	37.8±2.8^a	34.8±3.9^a
dA / %	48.8±5.6^a	50.8±6.5^a	51.9±4.7^a	57.7±6.4^a
Monomeric anthocyanins, AU	1.0±0.2^a	0.87±0.19^a	1.4±0.7^a	1.9±1.0^a
Co-pigmented anthocyanins AU	0.53±0.3^a	0.42±0.18^a	1.1±0.6^a	1.2±0.6^a
Polymeric anthocyanins AU	5.6±1.1^a	3.6±1.1^a	4.9±2.2^a	4.8±1.7^a
Total anthocyanins AU	7.2±1.0^a	4.9±1.0^a	7.3±3.0^a	7.8±2.8^a
Monomeric anthocyanins, %	14.4±1.4^a	18.1±3.7^a	18.3±4.7^a	23.0±7.1^a
Co-pigmented anthocyanins, %	7.9±5.8^a	9.4±5.3^a	14.8±6.9^a	15.5±6.7^a
Polymeric anthocyanins, %	77.7±4.4^a	72.5±6.0^{ab}	66.9±7.6^{ab}	61.4±7.4^b
Total phenols, GAE, mg L^{-1}	2105±86^a	1982±211^a	2469±682^a	2370±482^a
Antiradical DPPH activity $I_{50\%}$, µL wine	20.1±2.2 ^{a}	27.4±6.2^a	20.3±5.1^a	20.0±4.3^a

Additionally, the Pearson's coefficients of correlation were calculated from the data of the analysed characteristics of the wine samples. It was found that the total anthocyanins showed highly positive correlations with the colour intensity (r = 0.967), %*R* (r = 0.743) and brilliance, *dA* (r = 0.740), and negative correlations with hue (r = –0.780) and %*Y* (r = –0.811).

Comparing the average values of wine characteristics grouped by vintage (Table II), it was observed that the %*R* and *dA* were higher in younger wines than in older wines, while older wines were characterized by higher %*Y* and hue values. The younger wines were also richer in monomeric and co-pigmented anthocyanins (Table II). In young red wines, a co-pigmentation phenomenon occurs that involves molecular association between anthocyanins and other, usually, non-coloured organic molecules. The colour exhibited by these co-pigmented complexes could be 30–50 % higher than that of the anthocyanin free forms.[18] On the other hand, during storage and ageing of wines, the co-pigmented complexes break up and polymerization reactions and condensation of anthocyanins with other wine constituents occur. As a result, the concentration of

the monomeric anthocyanins decreases in favour of the polymeric anthocyanins. The newly formed polymeric pigments are compounds with different spectral characteristics that affect the chromatic properties of the wines, changing the hue to higher values.[9,19] In addition, the proportion of yellow colour of aged wines was simultaneously enhanced with increasing degree of polymerization.[20] The data obtained in this study for the analysed colour parameters are in agreement with the results reported by Cliff *et al.*,[21] who compared 4 different wine varieties over 7 vintages and found higher contents of monomeric, co-pigmented and total anthocyanins in the younger wines, regardless of the variety.

The applied ANOVA and Tukey's post-hoc test showed that among the wines of different vintages, statistically significant difference existed only in the content of polymeric anthocyanins. Actually, clear differentiation was possible only between wines produced in 2005 and 2008 or between mature wines with considerable content of polymeric anthocyanins and younger wines in which the polymerization processes were still in an early phase. The wines of 2006 were neither significantly different from the wines of 2007, nor from the wines produced in 2005 and 2008. Concerning the content of total phenols and the antioxidant capacity, statistically significant differences were not evidenced among the wines of different vintages. This indicates that the antioxidant activity of the wines was not related to the age of the wine, but rather with the concentration of phenolic compounds present in the wine. It is known that the antioxidant capacity and the content of phenolics strongly correlate and that wines containing higher levels of phenolic compounds are usually associated with stronger antioxidant activity.[22–24]

In the wine samples, 14 anthocyanin compounds were unambiguously detected and quantified and the average values of individual anthocyanins grouped according to variety are presented in Table III. In order to facilitate the comparison of anthocyanin profiles of the wines, the anthocyanin concentrations were normalized, *i.e.*, the compounds were expressed as percent of the total. The anthocyanin profiles of the analysed wine samples were submitted to statistical tests for wine differentiation.

It was observed that the profiles of the monomeric anthocyanins of the wines were distinctive and related to the grape variety. Malvidine-3-glucoside was the predominant compound in the wines of all grape varieties, which is in agreement with literature data.[4,10] Malvidine acetyl and coumaroyl derivatives were also found in abundance compared to the other anthocyanins. The proportion of malvidine-3-glucoside in the Cabernet Sauvignon wines (36.5 %) was lower compared to the Vranec (44.1 %) and Merlot (40.3 %) wines. On account of this, the proportion of malvidine acetate was substantially higher in the Cabernet Sauvignon (14.3 %) than in Vranec (7.9 %) wines, but almost the same as in the Merlot (14.4 %) wines. The relative content of malvidine-3-glucoside that was

found in the analysed wine samples was slightly lower compared to the Cabernet Sauvignon wines studied by Burns *et al.*[6] and Arozarena *et al.*[19]

TABLE III. Antocyanin composition of Vranec, Cabernet Sauvignon and Merlot wines produced in 2006–2008; De-3-gl (delphinidin-3-*O*-glucoside), Cy-3-gl (cyanidin-3-*O*-glucoside), Pt-3-gl (petunidin-3-*O*-glucoside), Pn-3-gl (peonidin-3-*O*-glucoside), Mv-3-gl (malvidin-3-*O*--glucoside), De-ac (delphinidin-3-*O*-acetylglucoside), Cy-ac (cyanidin-3-*O*-acetylglucoside), Pt-ac (petunidins-3-*O*-acetylglucoside), Pn-ac (peonidin-3-*O*-acetylglucoside), De-coum (delphinidin-3-*O*-*p*-coumarylglucoside), Mv-ac (malvidin-3-*O*-acetylglucoside), Pt-coum (petunidin-3-*O*-*p*-coumarylglucoside), Pn-coum (peonidin-3-*O*-*p*-coumarylglucoside), Mv-coum (malvidin-3-*O*-*p*-coumarylglucoside); the results are expressed as means ± *SD*; different letters in superscript in the same row indicate statistically significant means ($p < 0.05$)

Antho-cyanin	Vranec		Cabernet Sauvignon		Merlot	
	mg L^{-1}	%	mg L^{-1}	%	mg L^{-1}	%
De-3-gl	7.01±3.72	5.93±1.01^a	3.69±0.54	5.92±1.00^a	6.37±2.67	6.01±1.45^a
Cy-3-gl	3.12±1.01	2.63±1.45^a	1.92±0.18	3.09±0.96^a	2.40±0.35	2.27±1.44^a
Pt-3-gl	10.09±6.22	8.53±0.79^a	3.89±0.61	6.24±1.29^b	7.12±3.98	6.73±0.69^b
Pn-3-gl	9.91±6.11	8.38±0.70^a	3.13±0.80	5.02±1.81^b	6.08±3.08	5.74±1.24^b
Mv-3-gl	52.11±35.57	44.07±9.43^a	22.74±7.40	36.50±4.43^a	42.72±31.64	40.34±7.58^a
De-ac	2.81±0.53	2.37±1.87^a	2.31±0.15	3.71±0.86^a	2.97±0.78	2.80±1.35^a
Cy-ac	2.39±0.35	2.02±0.46^a	1.95±0.13	3.13±0.68^a	2.23±0.36	2.11±1.48^a
Pt-ac	2.61±0.77	2.21±1.39^a	2.20±0.31	3.53±0.47^a	2.93±1.04	2.77±0.88^a
Pn-ac	3.43±1.25	2.90±1.18^a	2.17±0.27	3.48±0.54^a	3.30±1.51	3.12±0.79^a
Mv-ac	9.31±5.35	7.88±1.79^a	8.90±5.28	14.29±5.68^a	15.20±12.22	14.35±4.41^a
De-coum	2.43±0.67	2.06±1.53^a	1.87±0.07	3.00±0.77^a	2.22±0.38	2.10±1.17^a
Pt-coum	2.63±0.79	2.22±1.45^a	1.84±0.05	2.95±0.92^a	2.31±0.44	2.18±1.17^a
Pn-coum	3.12±1.19	2.63±1.31^a	1.93±0.12	3.10±0.83^a	2.69±0.72	2.54±1.08^a
Mv-coum	7.30±3.98	6.17±1.08^a	3.77±0.64	6.04±0.60^a	7.36±4.01	6.95±0.88^a
Glucosides	82.23±52.62	69.54±13.38^a	35.37±9.53	56.77±9.49^a	64.69±41.72	61.08±12.40^a
Acetates	14.73±2.90	17.38±4.90^b	8.63±0.85	28.14±2.56^a	11.44±3.70	25.15±4.50^a
Couma-rates	15.47±6.63	13.08±5.37^a	9.40±0.89	15.09±3.12^a	14.58±5.55	13.76±4.30^a
Total	112±62	100±24	53±11	100±15	91±51	100±21

The proportion of malvidine-3-glucoside in the Vranec wines varied in the range 22.4–48.8 %, depending on the wine age. Older wines contained significantly lower levels of this anthocyanin, which indicated its degradation or transformation during the processes of wines ageing. One assumption is that malvidine-3-glucoside in the presence of fermenting yeasts is involved in addition reactions with pyruvate molecules forming vitisin A, a compound that is not detected in grapes but exists in abundance in young wines and decreases with their maturation.[25,26] Mv-3-glucoside also reacts with caffeic acid building pinotin A, the concentration of which increases with ageing and reaches a maximum in about 5-year-old wines.[27]

The highest content of total anthocyanins expressed as malvidin-3-glucoside equivalents was found in the Vranec wines, with an average value of 112.4 mg L^{-1}. Very large variations in the concentrations of total anthocyanins among samples of this variety were observed as a result of the different age of the wines. In general, younger wines were richer in monomeric anthocyanins, detectable by liquid chromatography, than older ones. For Cabernet Sauvignon wines, the average concentration of total monomeric anthocyanins was 53.4 mg L^{-1}, a value lower in comparison to the data reported by González-Neves *et al.*[7,28] A possible explanation for this discrepancy is the domination of older wine samples in the set of Cabernet Sauvignon wines analysed in the present study and the fact that the mentioned literature values referred to wines analysed immediately after completion of the alcoholic fermentation or wines of maximum 1-year old. In the Merlot wines, the content of total monomeric anthocyanins varied from 70 mg L^{-1} for mature wines (3 years) to 185 mg L^{-1} for young wines (1 year).

Statistical analysis of the anthocyanin components with ANOVA ($p < 0.05$) and the Tukey's post hoc test showed possible differentiation of Vranec from Merlot and Cabernet Sauvignon wines according to the content of petunidin-3--glucoside and peonidin-3-glucoside, but not between Cabernet Sauvignon and Merlot wines (Table III). Between wines of Vranec and the other two varieties, Cabernet Sauvignon and Merlot, statistically significant differences were also verified in the proportion of anthocyanin acetates, which agrees with the results published by Arozarena *et al.*[29] According to these authors, differentiation of several varieties of Spanish wines was possible based on their anthocyanin fingerprint, with malvidine-3-glucoside being the most discriminating compound. On the other hand, Kallithraka *et al.*[30] did not obtain consistent anthocyanin profiles even for monovarietal wines and thus considered the anthocyanin composition inappropriate for establishing wine authenticity. According to their study, significant changes in anthocyanins distribution occurs during vinification and particularly during maturation of wines as a consequence of considerable transformations of the monomeric anthocyanins to co-pigmented and polymeric forms.

Anthocyanin ratios in the wines

Genetic factors are determinant for every grape cultivar to have its own specific anthocyanin pattern.[4,31,32] It is assumed that the anthocyanin pattern is constant and independent of the environmental conditions, so it was proposed that it could be used for discrimination of the grape varieties. Moreover, the established ratios between some anthocyanins were considered as parameters upon which the identity of the grape could be verified[7] and the same principle could be used in certifying the authenticity of single variety wines.[33]

Based on the measured concentrations of individual anthocyanins in the studied wines, several anthocyanin ratios were calculated and are presented in Table

IV. These ratios were statistically analysed to identify variations that could be used for differentiation of the wine varieties. Analysis of variance showed that the ratios ΣGluc/ΣAcet, Pt3gl/De3gl, De3gl/Pn3gl and Mv3gl/Mvac in Vranec wines differed significantly from those of Cabernet Sauvignon and Merlot wines, but they did not differ between Merlot and Cabernet Sauvignon wines. These findings indicate that Vranec wines are characterized by a specific anthocyanin profile that distinguishes them from other international varieties of wines, such as Cabernet Sauvignon and Merlot.

TABLE IV. Ratios of anthocyanin compounds detected in Vranec, Cabernet Sauvignon and Merlot wines; De – delphinidins, Pt – petunidins, Pn – peonidins, Mv – malvidins, Coum – coumaroyl derivatives, Acet – acetyl derivatives and Gluc – monoglucosides; different letters in superscript in the same row indicate statistically significant means ($p < 0.05$)

Anthocyanin ratios	Vranec	Cabernet Sauvignon	Merlot
ΣMv/ΣPn	3.98±1.0	4.90±1.78	4.89±2.06
ΣDe/ΣPn	0.86±0.25	1.10±0.11	0.99±0.11
ΣPt/ΣPn	0.78±0.30	0.43±0.40	0.45±0.38
(ΣMv+ΣPt+ΣDe)/ΣPn	5.84±0.90	7.06±1.97	6.89±2.06
ΣGluc/ΣAcet	3.91±1.01^{a}	2.11±0.48^{b}	2.37±0.17^{b}
ΣGluc/ΣCoum	4.84±1.59	3.90±0.78	4.11±1.27
ΣCoum/ΣAcet	0.86±0.24	0.55±0.14	0.61±0.14
Mv3gl/ΣGLuc	0.60±0.09	0.63±0.08	0.62±0.09
Pt3gl/De3gl	1.37±0.18^{a}	1.06±0.10^{b}	1.09±0.18^{b}
De3gl/Pn3gl	0.76±0.12^{b}	1.21±0.24^{a}	1.07±0.16^{a}
Pt3gl/Pn3gl	1.02±0.06^{b}	1.26±0.16^{a}	1.15±0.13^{ab}
Mv3gl/Pn3gl	4.86±1.18	7.49±2.79	6.40±2.47
Mv3gl/Mvac	5.29±1.40^{a}	3.08±1.29^{b}	3.10±0.59^{b}
Mv3gl/Mvcoum	6.44±2.07	5.90±1.19	5.34±1.40
Mvac/Mvcoum	1.24±0.45	2.25±1.14	1.80±0.68

Differentiation of the wines

In order to further study the possibilities for classification and differentiation of wines, Principle Component Analysis (PCA) was performed. PCA is a multivariate method that produces new set of variables obtained as a result of the linear combination of the original descriptors. The new variables or principal components are calculated so as to retain most of the information present in the original data set, but reduced in the least number of variables.[34]

PCA was applied to the data of individual anthocyanins determined in the studied wines. Of the fourteen variables, three components with eigenvalues greater than 1 were obtained, accounting for 87.5 % of the variation. The first component explained 54.1 %, the second 23.1 %, and the third component explained 12.2 % of the total variation. After the third component, the percentage of explained variation drastically decreased, so it could be concluded that the most relevant information is obtainable from the first three components. The

component matrix showing the distribution of variables in the three components is presented in Table V. The predominant variables grouped into the first component include: peonidin coumarate, cyanidin-3-glucoside, delphinidin-coumarate, delphinidin acetate, malvidin-3-glucoside and petunidin acetate. The second component contained peonidin-3-glucoside and petunidin-3-glucoside. Cyanidin acetate dominated in the third component.

TABLE V. Component matrix (coefficients) of the three principal components used for grouping of Vranec, Cabernet Sauvignon and Merlo by anthocyanins

Variables	Component		
	1	2	3
pncoum	0.988	0.027	–0.016
cy3gl	0.980	0.086	0.055
decoum	0.976	–0.128	–0.046
deac	0.962	–0.198	–0.038
mv3gl	–0.950	0.300	–0.023
ptac	0.917	–0.359	–0.053
ptcoum	0.809	–0.115	–0.250
de3gl	0.715	0.272	0.253
mvcoum	0.630	0.110	–0.524
pt3gl	0.233	0.949	0.147
pn3gl	0.216	0.938	0.176
mvac	–0.482	–0.807	–0.289
cyac	0.027	–0.483	0.773
pnac	0.352	–0.434	0.539

The score plot of the first two components is shown in Fig. 1. The principle component analysis confirmed that wines of the local Vranec variety could be easily distinguished from Merlo and C. Sauvignon, while the latter two were harder to separate. The first group, located in the positive part of the principal component 2 (PC 2) and the negative part of the principal component 1 (PC 1) consisted of samples of Vranec wines. The second group, in the central part, with negative values for PC 2, covered the Merlot wines, while a third group was located in the negative part of PC 2 and contained the Cabernet Sauvignon wines. Difficulties achieving ideal varietal classification of Cabernet Sauvignon and Merlot wines according to anthocyanins were also reported by other authors.[24] On the other hand, González-Neves *et al.*[7] obtained satisfactory differentiation of Cabernet Sauvignon from Merlot and Tannat wines, but not between the latter two varieties.

Deviation from the correct grouping was observed in two samples of Vranec wine and one sample of the Cabernet Sauvignon variety. Since these three wines were produced in the 2006 vintage unlike the rest that were of recent date, it was supposed that the observed deviations were due to the age of the samples. This finding tends to support the results published by De Villiers *et al.*,[2] who did not

achieve a successful classification of South African wines of a large range of vintages by their anthocyanin profile. These data may support the assumption that the variety characteristics are obscured as a result of changes in the anthocyanin pattern during ageing and the age of wines becomes a limiting factor in their classifications by anthocyanins.

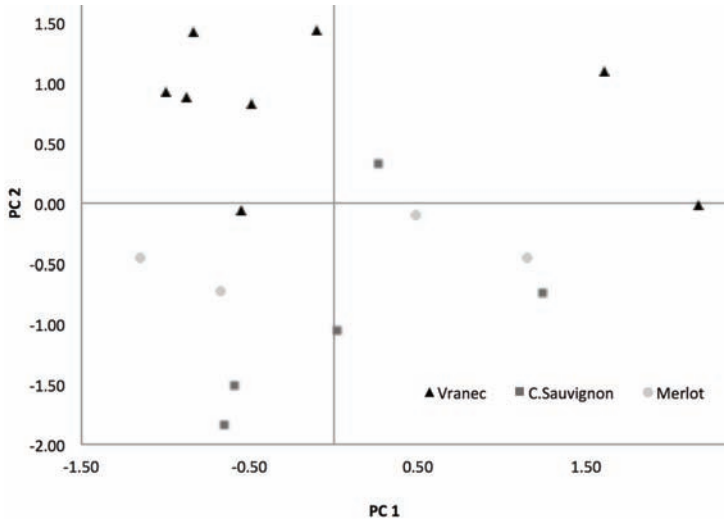

Fig. 1. Score plot of the principal components PC 1 and PC 2 of the wines according to variety.

Since statistical analyses (ANOVA) of the wine colour characteristics and type of anthocyanins obtained by spectrophotometric measurements (Table I) showed that colour intensity and content of total and polymeric anthocyanins could be used as indicators for differentiation of Vranec wines from other wine varieties, an attempt was made to group the wines of the Vranec variety according to age using multivariate methods based on spectrophotometric data.

The component matrix of the variables used for the classification of Vranec wines is presented in Table VI. Of the total number of variables, three main components were extracted that together described 94.5 % of the variation. Most of the variables, such as %*Y*, hue, total anthocyanins, monomeric anthocyanins, brightness, %*R*, colour intensity and polymeric anthocyanins were located in the first component. Percent blue (%*B*) dominated in the second component, while the co-pigmented anthocyanins were descriptors of the third component.

The best segmentation of wine samples according to age was obtained by the loading plot of the first (PC1) and third (PC3) component, as shown in Fig. 2. Relatively clear differentiation of older wines (produced in vintages 2005–2007) was observed in the lower left part of the plane, along the negative parts of PC1 and PC3. In the upper right part of the plane, mostly in the positive part of PC3,

were grouped wines produced in the 2008 harvest (aged 1 year at the time of analysis). Hue and %*Y* emerged as descriptors for the old wines, while young wines correlated with monomeric and total anthocyanins, %*R* and brightness (*dA*).

TABLE VI. Component matrix of the three principal components used for grouping Vranec wines according to age by chromatic parameters; AC – anthocyanins

Variables	Component		
	1	2	3
%*Y*	–0.957	0.220	–0.083
Hue	–0.935	0.294	–0.085
Total AC	0.890	0.435	–0.019
Monomeric AC	0.927	–0.036	–0.049
dA	0.909	–0.386	0.073
%*R*	0.886	–0.422	0.098
Colour intensity	0.849	0.359	–0.347
Polymeric AC	0.701	0.575	–0.363
Co-pigmented AC	0.355	0.362	0.832
%*B*	0.022	0.898	0.169
Monomeric AC	0.927	–0.036	–0.049

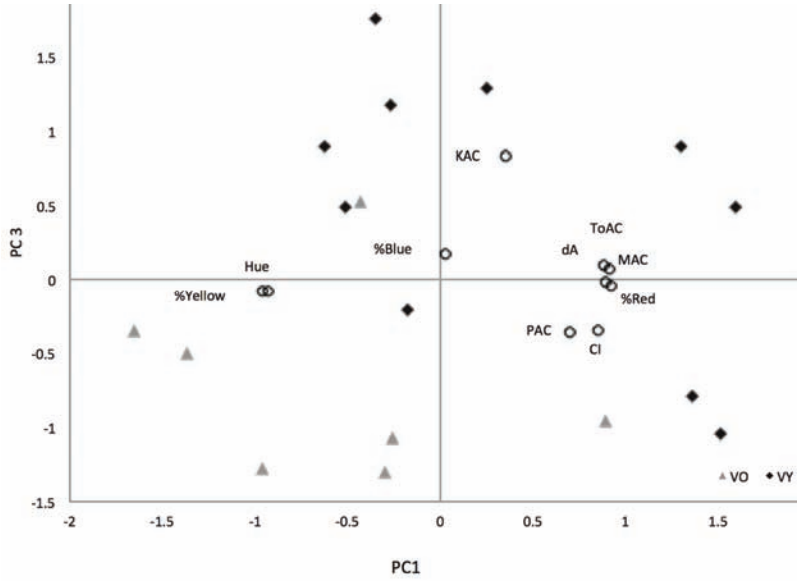

Fig. 2. Distribution of Vranec wines according to age - Score plot and superimposed loading plot of PC 1 and PC 3 using the chromatic characteristics determined by spectrophotometry; VO – old wines (2005, 2006 and 2007) and VY – young wines (2008).

CONCLUSIONS

The results of this study represent a certain contribution to a database of the chemical properties of red wines obtained from the most common grape varieties

grown in Macedonia. The wines of the autochthonous grape variety Vranec were distinguished from Cabernet Sauvignon and Merlot wines by their specific chromatic and anthocyanin profiles, particularly highest colour intensity, %*R*, %*dA*, monomeric, co-pigmented and total anthocyanins. Concerning the individual anthocyanins, Vranec wines contained higher percentage of petunidin-3-glucoside and peonidin-3-glucoside and lower percentage of acetates. The content of total phenols among the investigated wine varieties did not vary significantly, although it was slightly higher in Vranec. The antioxidative potential was similar for all the wine varieties and independent of the wine age. The results obtained using principal component analysis showed that differentiation of the Vranec wines from Cabernet Sauvignon and Merlot varieties could be feasible according individual anthocyanins. Chromatic properties allowed the differentiation of Vranec wines into two groups, young (aged to 1 year) and old. However, further studies are necessary to compile data of a greater number of wines corresponding to several vintages to confirm these observations.

ИЗВОД

КАРАКТЕРИСТИКЕ ВИНА ВРАНЕЦ, КАБЕРНЕ СОВИЊОН И МЕРЛО У ПОГЛЕДУ БОЈЕ И САДРЖАЈА АНТОЦИЈАНА

MAJA DIMITROVSKA[1], ELENA TOMOVSKA[2] И MIRJANA BOCEVSKA[2]

[1]Institute of Public Health, 50 Divizija 6, 1000 Skopje, FYR Macedonia и [2]Faculty of Technology and Metallurgy, Ss. Cyril and Methodius University, Rudjer Boskovic 16, 1000 Skopje, FYR Macedonia

Три врсте вина, Вранец, Каберне Совињон и Мерло, су испитане у погледу садржаја антоцијана, карактеристика боје, количине укупних полифенола и антиоксидативног потенцијала. Спектрофотометријски су одређивани укупни, мономерни, полимерни и копигментисани антоцијани, а поједина једињења су квантификована методом HPLC–DAD. Хроматни профил је одређен према интензитету боје, као % црвене, плаве и жуте боје и % сјаја (*dA*). Добијени подаци су анализирани у циљу процене њихове примене у разликовању вина према врсти и години. Вина Вранец су имала најкарактеристичнија својства, са највећим садржајем антоцијана и највећим интензитетом црвене боје и сјаја у односу на друге две врсте вина. Као могући маркери у диференцијацији вина Вранец од вина Каберне Совињон и Мерло могли би послужити петунидин-3-глукозид, пеонидин-3-глукозид и ацетати антоцијана. Са друге стране, ни један од анализираних параметара није могао разликовати вина Каберне Совињон и Мерло. Одређивање врсте вина према садржају антоцијана ипак има своја ограничења, повезана са старошћу вина. Параметри боје могу да послуже у разликовању младих (до 1 године старости) од старих вина само у случају врсте Вранец.

(Примљено 1. јануара, ревидирано 21. фебруара 2013)

REFERENCES

1. M. S. Fernández-Pachón, D. Villaño, M. C. García-Parrilla, A. M. Troncoso, *Anal. Chim. Acta* **513** (2004) 113
2. A. De Villiers, G. Vanhoenacker, P. Majek, P. Sandra, *J. Chromatogr., A* **1054** (2004) 195

3. A. Versari, G. P. Parpinello, A. U. Mattioli, *S. Afr. J. Enol. Vitic.* **28** (2007) 6
4. E. Revilla, E. García-Beneytez, F. Cabello, *Aust. J. Grape Wine Res.* **15** (2009) 70
5. H. Otteneder, R. Marx, M. Zimmer, *Aust. J. Grape Wine Res.* **10** (2004) 3
6. J. Burns, W. Mullen, N. Landrault, P. Teissedre, M. E. J. Lean, A. Crozier, *J. Agric. Food Chem.* **50** (2002) 4096
7. G. González-Neves, J. Franco, L. Barreiro, G. Gil, M. Moutounet, A. Carbonneau, *Eur. Food Res. Technol*. **225** (2007) 111
8. J. M. Ryan, E. Revilla, *J. Agric. Food Chem.* **51** (2003) 3372
9. H. Wang, E. J. Race, A. J. Shrikhande, *J. Agric. Food Chem.* **51** (2003) 7989
10. M. J. Aguirre, M. Isaacs, B. Matsuhiro, L. Mendoza, L. S. Santos, S. Torres, *Food Chem.* **129** (2011) 514
11. V. Ivanova, A. Dörnyei, L. Márk, B. Vojnoski, T. Stafilov, M. Stefova, F. Kilár, *Food Chem.* **124** (2011) 316
12. A. Radovanović, B. Radovanović, B. Jovančićević, *Food Chem.* **117** (2009) 326
13. K. Slinkard, V. L. Singleton, *Am. J. Enol. Vitic.* **28** (1977) 49
14. Y. Glories, *Connaiss. Vigne Vin* **18** (1984) 195
15. G. Mazza, L. Fukumoto, P. Delaquis, B. Girard, B. Ewert, *J. Agric. Food Chem.* **47** (1999) 4009
16. W. Brand-Williams, M. E. Cuvelier, C. Berset, *Lebensm. Wiss. Technol.* **28** (1995) 25
17. M. Dimitrovska, M. Bocevska, D. Dimitrovski, M. Murkovic, *Eur. Food Res. Technol*. **232** (4) (2011) 591
18. R. Boulton, *Am. J. Enol. Vitic.* **52** (2001) 67
19. I. Arozarena, A. Casp, R. Marín, M. Navarro, *J. Sci. Food Agric.* **80** (2000) 1909
20. S. Tsanova-Savova, S. Dimov, F. Ribarova, *J. Food Compos. Anal.* **15** (2002) 647
21. M. A. Cliff, M. C. King, J. Schlosser, *Food Res. Int.* **40** (2007) 92
22. E. Maletić, J. K. Kontić, D. Preiner, A. Jeromel, C. D. Patz, H. Dietrich, *J. Food Agric. Environ.* **7** (2009) 48
23. H. P. V. Rupasinghe, S. Clegg, *J. Food Compos. Anal.* **20** (2007) 133
24. J. Pazourek, D. Gajdošova, M. Spanilá, M. Farková, K. Novotná, J. Havel, *J. Chromatogr., A* **1081** (2005) 48
25. N. Mateus, A. M. S. Silva, J. Vercauteren, V. De Freitas, *J. Agric. Food Chem*. **49** (2001) 4836
26. A. L. Waterhouse, A. Zimman, *The Fate of Malvidin-3-glucoside in New Wine*, in *Red Wine Color - Revealing the Mysteries*, A. L. Waterhouse, J. Kennedy, Eds., ACS Symposium Series, 886, American Chemical Society, Washington DC, 2004, p. 217
27. D. Von Baer, M. Rentzsch, M. A. Hitschfeld, C. Mardones, C. Vergara, P. Winterhalter, *Anal. Chim. Acta* **621** (2008) 52
28. G. González-Neves, C. Gómez-Cordovés, L. Barreiro, *J. Wine Res.* **12** (2001) 125
29. I. Arozarena, A. Casp, R. Marín, M. Navarro, *Eur. Food Res. Technol*. **212** (2000) 108
30. S. Kallithraka, A. A. Mohdaly, D. P. Makris, P. Kefalas, *J. Food Compos. Anal.* **18** (2005) 375
31. M. A. Esteban, M. J. Villanueva, J. R. Lissarrague, *J. Sci. Food Agric.* **81** (2001) 409
32. I. Arozarena, B. Ayesterán, M. J. Cantalejo, M. Navarro, M. Vera, I. Abril, A. Casp, *Eur. Food Res. Technol.* **214** (2002) 303
33. C. Casavecchia, R. Magnisi, L. La Pera, R. Maisano, G. Dugo, *Am. J. Enol. Vitic.* **58** (2007) 286
34. J. Saurina, *Trends Anal. Chem.* **29** (2010) 234.

Journal of the Serbian Chemical Society
JSCS-info@shd.org.rs • www.shd.org.rs/JSCS
J. Serb. Chem. Soc. *78* (9) 1323–1333 (2013) UDC 546.814+547.563+543.422.25:615.28
JSCS–4500 *Original scientific paper*

Reactions of tin and triorganotin(IV) isopropoxides with thymol derivative: synthesis, characterization and *in vitro* antimicrobial screening

GARIMA MATELA[1]*, ROBINA AMAN[1], CHETAN SHARMA[2] and SMITA CHAUDHARY[3]

[1]*Department of Chemistry, Kumaun University, S. S. J. Campus Almora-263 601, India,* [2]*Department of Microbiology, Kurukshetra University, Kurukshetra, Haryana-136 119, India and* [3]*Institute of Environmental Studies, Kurukshetra University, Kurukshetra, Haryana-136 119 India*

(Received 17 September 2012, revised 6 March 2013)

Abstract: New series of diisopropoxytin and triorganotin(IV) complexes of H_2hbgl (**1**) of the general formula $Sn(OPr^i)_2$(hbgl) (**2**), $Sn(OPr^i)_2$(Hhbgl)$_2$ (**3**), Ph_3Sn(Hhbgl) (**4**), Bu_3Sn(Hhbgl) (**5**) and Me_3Sn(Hhbgl) (**6**), where H_2hbgl is a ligand of a thymol derivative, namely, *N*-(2-hydroxy-3-isopropyl-6-methyl-benzyl)glycine, were synthesized by reacting tin and triorganotin(IV) chloride with the ligand, with the aid of sodium isopropoxide in appropriate stiochiometric ratios (1:1 and 1:2). These complexes were characterized by elemental analysis, IR and ^{1}H-NMR. The spectral data suggest that the carboxylate group, in complexes **2**–**5**, was bonded in a bidentate manner, while a unidentate bonding was observed in complex **6**. All five complexes were tested *in vitro* for their antibacterial activity against Gram-positive bacteria, namely, *Staphylococcus aureus* MTCC 96, *Bacillus subtilis* MTCC 121, and two Gram-negative bacteria, namely, *Escherichia coli* MTCC 1652 and *Pseudomonas aeruginosa* MTCC 741. All five complexes were also tested against three pathogenic fungal strains, namely, *Aspergillus niger*, *Aspergillus flavus* and *Penicillium* sp.

Keywords: tri-organotin(IV) complexes; IR, NMR spectral studies; antifungal activity; antibacterial activity.

INTRODUCTION

Organotin(IV) complexes show a spectrum of biological effects and have been extensively studied in various biological fields as anticancer, antiviral, antibacterial and antifungal agents, wood preservatives, pesticides, *etc*.[1–12] It is noteworthy that, for a long time, organotin(IV) complexes have been widely used in a variety of industrial and agricultural applications.[13–15] A unique fluorescent pro-

* Corresponding author. E-mail: matelagarima28@yahoo.in
doi: 10.2298/JSC120917030M

perty of organotin carboxylates has also been investigated in the last few years.[16,17] Thymol, a *p*-cymene-derived compound, is widely used in medicine for its antimicrobial, antiseptic, disinfectant and wound-healing properties.[18–23] As derivatives of *p*-cymene have leishmanicidal activity and are considered important basic structures for the development of novel antiparasitic drugs, in the present study, a new ligand of a thymol derivative derived from glycine was synthesized and investigated for its ligating properties. The interaction of tin metal with the organic groups *via* O–Sn and N–Sn bonds has attracted considerable interest in several research fields.[24] Regarding this, some tin compounds with a thymol derivative were synthesized as potential antibacterial and antifungal agents.

EXPERIMENTAL

Materials and methods

All the reagents, *viz*., tin (Merck), triphenyltin(IV) chloride (Merck), tributyltin(IV) chloride (Merck), trimethyltin(IV) chloride (Merck) and thymol (Sigma–Aldrich) were used as received. All the chemicals and solvents used were dried and purified by standard methods, and moisture was excluded from the glass apparatus using $CaCl_2$ drying tubes. The melting points were determined in open capillaries with an electronic melting point apparatus. C, H and N analyses of the ligand and complexes were performed on a Vario-EL, CHNS elemental analyzer. The tin contents in the synthesized complexes were determined gravimetrically as SnO_2. Infrared spectra of the solid compounds were recorded on a Perkin-Elmer 1600 series FT-IR spectrophotometer over the range 4000–500 cm^{-1} in KBr discs and over 500–200 cm^{-1} in CsI discs. The ^{1}H-NMR spectra were recorded on a Bruker DRX 300 (300 MHz FT-NMR) spectrometer at the Central Drug Research Institute, Lucknow, India, using DMSO or MeOD as solvents with TMS as the internal standard. The conductivity measurements were performed using an Ecotestr EC Low conductometer in 10^{-3} M DMSO solutions at room temperature. The antibacterial and antifungal activities of the synthesized complexes were evaluated by the agar well diffusion method and the poison food technique, respectively.

*Synthesis of H_2hbgl (**1**)*

An equimolar mixture of thymol (11.86 g, 0.05 mol), glycine (3.75 g, 0.05 mol), sodium acetate crystals (6.8 g, 0.05 mol) was dissolved in glacial acetic acid (25 mL). Formalin solution (37 % (w/v), 4.05 mL) was added to it dropwise under stirring and the contents were heated at 60–80 °C, until a viscous mass was obtained. The viscous mass was then added dropwise with brisk stirring into an excess of water. The thus obtained crude product was purified by dissolving it in a requisite quantity of *ca*. 7 M sodium hydroxide solution followed by its reprecipitation by 6 M hydrochloric acid. It was further purified by recrystallisation from ethanol.

Synthesis of the complexes

*[Sn(OPr^i)$_2$(hbgl)] (**2**).* A solution of tin(IV) tetrachloride (1.300 g, 0.005 mol) in benzene (10 mL) was treated with sodium isopropoxide (1.64 g, 0.020 mol) to produce tin(IV) tetraisopropoxide and sodium chloride. The sodium chloride precipitate was removed by filtration and the solvent by distillation. The solution of tin(IV) tetraisopropoxide (1.770 g, 0.005 mol) and H_2hbgl (1.067 g, 0.0045 mol) was refluxed in benzene (20 mL) for 8–10 h at 95–100 °C. The liberated 2-propanol was fractionated out azeotropically with benzene. The complex,

[$Sn(OPr^i)_2$(hbgl)], isolated as a yellow brown solid, was purified by recrystallisation from ethanol at room temperature and dried under reduced pressure.

*[$Sn(OPr^i)_2(Hhbgl)_2$] (**3**).* Complex **3** was prepared in the similar way as complex **2**. Tin(IV) tetraisopropoxide (1.770 g, 0.005 mol) and H_2hbgl (2.135 g, 0.009 mol).

*[$Ph_3Sn(Hhbgl)$] (**4**).* A solution of triphenyltin(IV) isopropoxide (2.045 g, 0.005 mol) and H_2hbgl (1.067 g, 0.0045 mol) was refluxed in benzene (20 mL) for 8–10 h at 95–100 °C. The complex, [Ph_3Sn(Hhbgl)], isolated as a brown solid, was purified by recrystallisation from ethanol at room temperature and dried under reduced pressure.

*[$Bu_3Sn(Hhbgl)$] (**5**).* Complex **5** was prepared in the similar way as complex **4**. Tributyltin(IV) isopropoxide (1.745 g, 0.005 mol) and H_2hbgl (1.067 g, 0.0045 mol).

*[$Me_3Sn(Hhbgl)$] (**6**).* A solution of trimethyltin(IV) isopropoxide (1.115 g, 0.005 mol) and H_2hbgl (1.067 g, 0.0045 mol) was refluxed in toluene (20 mL) for 16–18 h at 95–100 °C. The complex, [Me_3Sn(Hhbgl)], isolated as a yellow solid, was purified by recrystallisation from ethanol at room temperature and dried under reduced pressure.

Antimicrobial assays

Antibacterial activity. The antibacterial activities of the synthesized complexes were evaluated by the agar well diffusion method. All the bacterial cultures were adjusted to 0.5 McFarland standards, which is visually comparable to a bacterial suspension of approximately 1.5×10^8 cfu mL^{-1}. 20 mL of Mueller Hinton agar medium was poured into each Petri plate and plates were swabbed with 100 µL inocula of the test micro-organisms and kept for 15 min for adsorption. Using a sterile cork borer of 8 mm diameter, wells were bored into the seeded agar plates and these were loaded with a 100 µL of each complex reconstituted in dimethyl sulphoxide (DMSO) at a concentration of 2.0 mg mL^{-1}. All the plates were incubated at 37 °C for 24 h. The antibacterial activity of each organotin complex was evaluated by measuring the zone of growth inhibition against the test organisms with a zone reader (HiAntibiotic zone scale). DMSO was used as a negative control whereas ciprofloxacin was used as positive control. This procedure was performed in three replicate plates for each organism.[24-27]

Determination of the minimum inhibitory concentration (MIC) of the synthesized complexes. The *MIC* value is the lowest concentration of an antimicrobial complex that will inhibit the visible growth of a micro-organism after overnight incubation. The *MIC* of the various complexes against the bacterial strains was evaluated through a modified agar well diffusion method.[28] In this method, a twofold serial dilution of each complex was prepared by first reconstituting the complex in DMSO followed by dilution in sterile distilled water to achieve a decreasing concentration range of 256 to 0.5 µg mL^{-1}. A 100 µL volume of each dilution was introduced into the wells (in triplicate) in the agar plates already seeded with 100 µL of standardized inoculum (10^6 cfu mL^{-1}) of the test bacterial strains. All the test plates were incubated aerobically at 37 °C for 24 h and observed for an inhibition zone. The *MIC* of an organotin(IV) complex, taken as the lowest concentration that completely inhibited the growth of the bacteria, showed by a clear zone of inhibition, was recorded for each test organism. Ciprofloxacin was used as the positive control while DMSO was the negative control.

Antifungal activity. The antifungal activities of the five organotin complexes were evaluated by the poisoned food technique.[27,29] The moulds were grown on Sabouraud dextrose agar (SDA) at 25 °C for 7 days and used as inoculates. The 15 mL of molten SDA (45 °C) was poisoned by the addition of 100 µL of each organotin complex reconstituted in the DMSO at a concentration of 2.0 mg mL^{-1}, poured into a sterile Petri plate and allowed it to solidify at room temperature. The solidified poisoned agar plates were inoculated at the centre

with fungal plugs (8 mm diameter) obtained from the colony margins and incubated at 25 °C for 7 days. DMSO was used as the negative control whereas fluconazole was used as the positive control. The experiments were performed in triplicates. The diameter of fungal colonies was measured and expressed as percent mycelial inhibition by applying the formula:

$$\text{Inhibition} = \frac{(d_c - d_t)}{d_c} \times 100$$

where d_c is the average diameter of fungal colony in the negative control sets and d_t is the average diameter of the fungal colony in the experimental sets.

RESULTS AND DISCUSSION

The ligand of the thymol derivative was prepared adopting a procedure almost identical to that described by Mehrotra *et al.*[30] The synthetic route used to synthesise the ligand and its complexes is outlined in Schemes 1 and 2, respectively. A new methodology was used to synthesise the tin and triorganotin(IV) complexes. Organotin complexes are usually prepared by reacting organotin hydroxide or organotin oxide with the corresponding ligand and by reacting organotin halide with the sodium or potassium salt of the ligand. In present study, the halogen of tin or organotin was replaced with the isopropoxide group by reacting them with sodium isopropoxide (Scheme 2). The tin and triorganotin isopropoxides were isolated and reacted with the ligand. These reactions proceeded with the liberation of 2-propanol, which was fractionated out azeotropically and estimated to monitor the completion of reaction. The obtained values are given in Table S-I of the Supplementary material to this paper. Owing to highly hydroscopic nature of tin and tri-organotin(IV) alkoxides, all the reactions were performed under strictly anhydrous conditions.

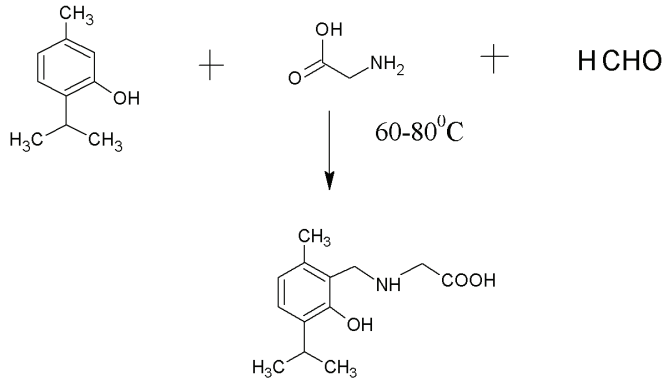

Scheme 1. Synthesis of the ligand **1**.

Characterisation of the ligand and its complexes

The physical, analytical and spectral data for the ligand and the synthesised complexes are given in the Supplementary material to this paper.

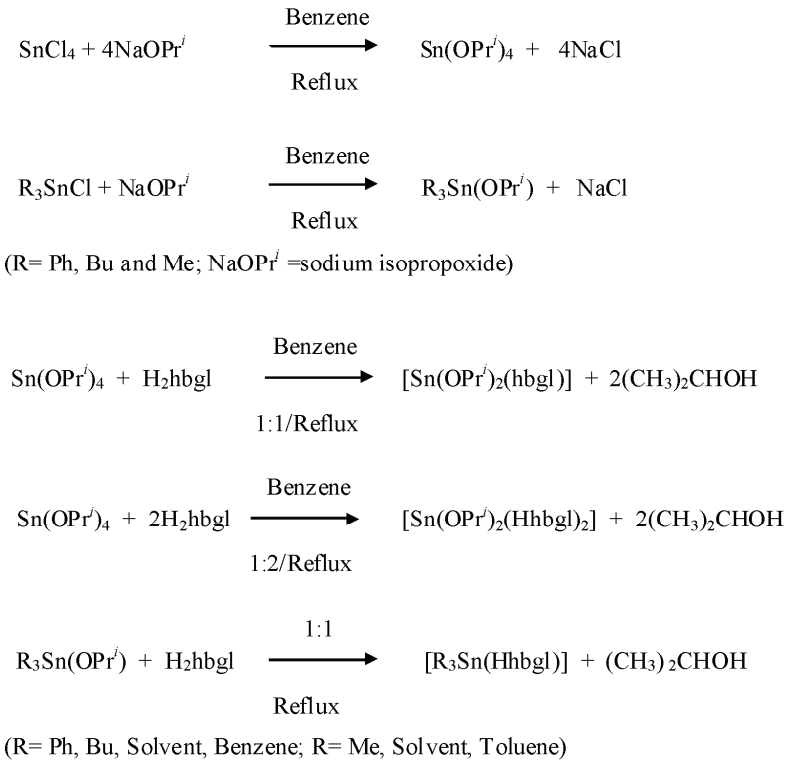

Scheme 2. Synthesis of the complexes.

Elemental analysis. The analytical data were in good agreement with the proposed stoichiometry of the complexes.

Molar conductance. The molar conductance values of the synthesized complexes showed very low values indicating their non-electrolytic nature.[31]

Infrared spectra. The IR spectra of the complexes displayed a broad vibrational band at 3000–3500 cm^{-1}, which is assignable to the unbonded –OH stretching of the phenolic group.[32,33]

These complexes gave a strong asymmetric stretching frequency ν_{as}(COO) near 1588–1626 cm^{-1} and a medium symmetrical stretching frequency ν_{s}(COO) near 1406–1417 cm^{-1}. The magnitude of $\nu_{as}-\nu_{s}$ ($\Delta\nu$) was used to explain the type of boding of the carboxylate group to tin metal.[34,35] For complex **2**, Fig. 1, the $\Delta\nu$ value of 201 cm^{-1} was attributed to a bidentate carboxyl group.[36] The magnitude of $\Delta\nu$ for **3**–**5** (Fig. 1) were smaller than 200 cm^{-1}, indicating bridged tin and triorganotin(IV) carboxylates. While, for the complex **6** (Fig. 1), the values of $\Delta\nu$ exceeded 210 cm^{-1}, which clearly demonstrated that these complexes adopt a monodentate carboxylate structure.

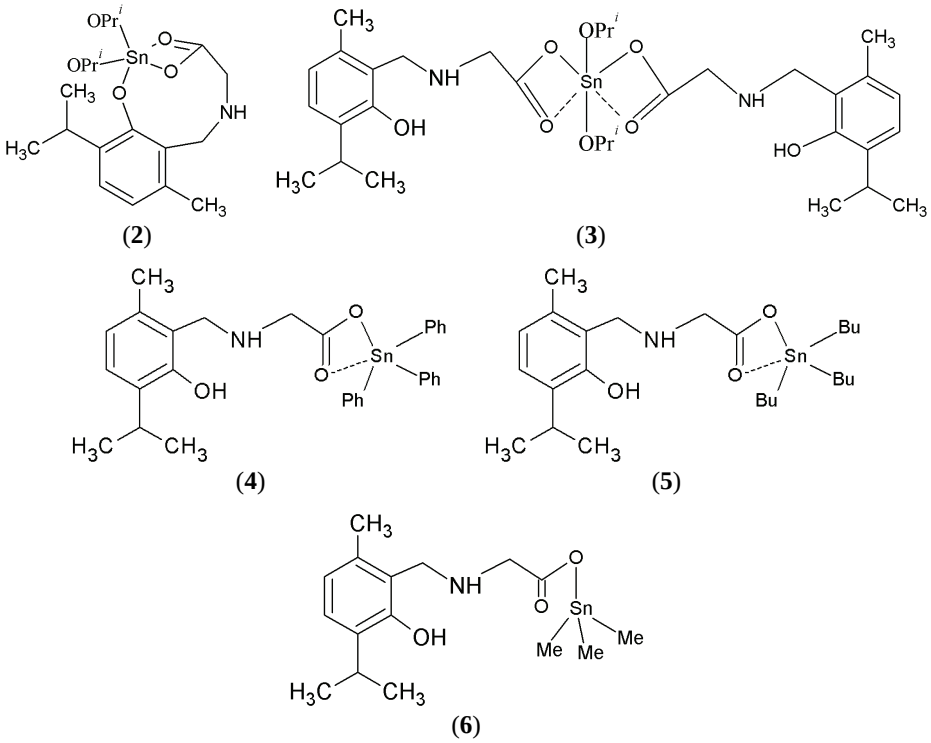

Fig. 1. Proposed structures of the metal complexes of *N*-(2-hydroxy-3-isopropyl-6-methyl-benzyl)glycine.

The bonding of the carboxylate group to the tin metal was further confirmed by the appearance of a band at 500–558 cm^{-1}, assignable to the Sn–O stretching frequency.[37] The far IR spectrum of triphenyltin(IV) complex showed bands at 279 and 207 cm^{-1}, which may be assigned to the ν_{as}(Sn–C) and ν_s(Sn–C), respectively, whereas the corresponding peaks at 528 and at 469 cm^{-1} were found in the spectrum of tributyltin(IV) complex.[38] In the case of trimethyltin(IV) complex the appearance of ν(Sn–C) bands were not certain due to overlapping with the Sn–O stretching vibration.

^{1}H-NMR spectra. The absence of a signal due to the –OH proton at δ 12.00––13.00 ppm suggested deprotonation of the carboxylic oxygen atom of the ligand on complexation.[39] The ^{1}H-NMR spectra of the complexes displayed signals in the region δ 6.45–7.58 ppm due to the aromatic protons of the ligand. A signal at δ 7.80–8.54 ppm may be attributed to the unbonded phenolic group proton.[40] In the complexes, the $–NH_2$ resonances were observed either as a broad weak signal at δ 4.90–6.88 ppm or in conjugation with the phenyl protons.[41,42] The values of coupling constants $^2J(^{117/119}Sn–C–^1H)$ provides important information regarding the coordination number.[38,43] The two-band coupling $^2J(^{117/119}Sn–C–H)$ of tri-

methyltin(IV) complex in DMSO was 68.0 Hz. Using the Lockhart equation,[44] the estimated value of C–Sn–C bond angle for complex **6** was 116.62°, implying a four-coordinated tetrahedral geometry. The $^{2}J(^{117/119}\text{Sn–C–}^{1}\text{H})$ value for **5** was not visible since the protons of butyl group were multiplets in the range of 0.90––1.21 ppm, however a triplet was observed at δ 0.78 ppm.[45,46] In the spectrum of complex **4**, the signals for the phenyl group attached to tin were observed in the δ range 7.22–7.58 ppm, in conjugation with phenyl protons of the ligand.

Antimicrobial evaluation

Antibacterial activity. All the newly synthesized complexes were evaluated for their antibacterial activity against two Gram-positive bacteria (*Staphylococcus aureus* and *Bacillus subtilis*) and two Gram-negative bacteria (*Escherichia coli* and *Pseudomonas aeruginosa*). The results revealed that all the tested organotin(IV) complexes possessed variable antibacterial activity against both Gram-positive and Gram-negative bacteria.

Based on the maximum inhibitory activity shown against Gram-positive bacteria, the complexes **4** and **6** were found to be most effective against *S. aureus*, with inhibition zones of 27 and 25.6 mm, respectively, whereas complex **4** was found to be most effective against *B. subtilis*, with an inhibition zone of 25 mm. However, in case of Gram-negative bacteria, two complexes, **4** and **3**, were found to be most effective against *E. coli* with the zone of inhibition ranging between 21 and 24 mm and one complex, **4**, against *P. aeruginosa* with zone of inhibition of 22 mm (Table I). The synthesized complexes showed comparatively better activity against Gram-positive bacteria.

TABLE I. Antibacterial activity of the metal complexes of *N*-(2-hydroxy-3-isopropyl-6--methylbenzyl)glycine; values of the zone of inhibition include the diameter of the well (8 mm)

Complex	Diameter of the growth of inhibition zone, mm			
	S. aureus	*B. subtilis*	*E. coli*	*P. aeruginosa*
2	22	22	19	16
3	24	22	21	17
4	27	25	24	22
5	22	22	19	15
6	26	22	20	17
Ciprofloxacin	28	26	25	25

In the whole series, the *MIC* values of organotin complexes ranged between 8 and 32 μg mL^{-1} against the Gram-positive bacteria. Complex **4** was found to be best as it exhibited the lowest MIC of 8 μg mL^{-1} against *S. aureus*. In case of the Gram-negative bacteria, the *MIC* values of complexes ranged from 32 to 128 μg mL^{-1}. Complex **4** showed lowest *MIC* of 32 μg mL^{-1} against *E. coli* and *P. aeruginosa* (Table II). Ciprofloxacin was used as the standard antibiotic. The

positive controls produced significantly sized inhibition zones against the tested bacteria; however, the negative control produced no observable inhibitory effect against any of the tested bacteria.

TABLE II. Minimum inhibitory concentration (*MIC* / μg mL^{-1}) of the metal complexes of *N*-(2-hydroxy-3-isopropyl-6-methyl benzyl)glycine

Complex	Bacterium			
	S. aureus	*B. subtilis*	*E. coli*	*P. aeruginosa*
2	32	32	64	128
3	32	32	64	128
4	8	16	32	32
5	32	32	64	128
6	16	16	64	128
Ciprofloxacin	5	5	5	5

Antifungal activity. All the newly synthesized complexes were evaluated for their antifungal activity against three fungal pathogens, *Aspergillus niger*, *A. flavus* and *Penicillium* sp., isolated from ear patients of Kurukshetra.[47] The complexes **3** and **4** showed a more than 60 % inhibition level of mycelial growth against *A. niger* and *Penicillium* sp., whereas complex **4** showed highest inhibition level of 69 %, of fungal mycelium against *A. flavus*. Fluconazole was used as the standard antibiotic (Table III).

TABLE III. Antifungal activity of the metal complexes of *N*-(2-hydroxy-3-isopropyl-6-methyl-benzyl)glycine; all the values are the means of three replicates

Complex	Mycelial growth inhibition, %		
	A. niger	*A. flavus*	*Penicillium* sp.
2	57	56	59
3	63	58	61
4	61	69	66
5	51	44	50
6	56	53	59
Fluconazole	81	78	83

CONCLUSIONS

Based on various studies, such as elemental analysis, IR and ^{1}H-NMR spectroscopy, five- and six-coordinate geometry are proposed for complexes **2**–**5**, while four-coordinate geometry is proposed for complex **6**. The synthesized complexes were screened against various fungi and bacteria to assess their potential as antimicrobial agents. The antimicrobial data revealed that the triphenyltin(IV) complex (**4**) was superior to the other complexes. The synthesized complexes showed remarkable antimicrobial activity.

SUPPLEMENTARY MATERIAL

Table S-I, as well as physical, analytical and spectral data of the ligand and complexes are available electronically from http://www.shd.org.rs/JSCS/, or from the corresponding author on request.

Acknowledgements. One of the authors (R. A.) thanks the U-COST, Dehradun, India, for financial support in the form of a Research Project and another of the authors (G. M.) for the award of Project Fellowship under the same project.

И З В О Д

РЕАКЦИЈЕ КАЛАЈ(IV)- И ТРИОРГАНОКАЛАЈ(IV)-ИЗОПРОПОКСИДА СА ДЕРИВАТОМ ТИМОЛА: СИНТЕЗА, КАРАКТЕРИЗАЦИЈА И *IN VITRO* АНТИМИКРОБНО ИСПИТИВАЊЕ

GARIMA MATELA[1], ROBINA AMAN[1], CHETAN SHARMA[2] и SMITA CHAUDHARY[3]

[1]Department of Chemistry, Kumaun University, S. S. J. Campus Almora-263 601, India, [2]Department of Microbiology, Kurukshetra University, Kurukshetra, Haryana-136 119 India и [3]Institute of Environmental Studies, Kurukshetra University, Kurukshetra, Haryana-136 119 India

У реакцијама калај(IV)- и триорганокалај(IV)-хлорида са H_2hbgl лигандом (**1**; H_2hbgl је дериват тимола, *N*-(2-хидрокси-3-изопропил-6-метилбензил)глицин), уз додатак натријум-изопропоксида у одговарајућим стехиометријским односима (1:1 и 1:2), синтетизовани су нови комплекси опште формуле $Sn(OPr^i)_2$(hbgl) (**2**), $Sn(OPr^i)_2(Hhbgl)_2$ (**3**), Ph_3Sn(Hhbgl) (**4**), Bu_3Sn(Hhbgl) (**5**) и Me_3Sn(Hhbgl) (**6**). Добијени комплекси су окарактерисани применом елементалне анализе, као и IR и ^{1}H-NMR спектроскопије. На основу спектроскопских података, претпостављено је да је у комплексима **2**–**5** карбоксилна група бидентатно координована, док је у комплексу **6** монодентатно координована за јон метала. Испитивана је *in vitro* антибактеријска активност на две грам-позитивне бактерије, *Staphylococcus aureus* MTCC 96 и *Bacillus subtilis* MTCC 121, и на две грам-негативне бактерије, *Escherichia coli* MTCC 1652 и *Pseudomonas aeruginosa* MTCC 741. Поред тога, испитивана је антифунгална активност на три врсте гљива, *Aspergillus niger, Aspergillus flavus* и *Penicillium* sp.

(Примљено 17. септембра 2012, ревидирано 6. марта 2013)

REFERENCES

1. M. Nath, P. K. Saini, *Dalton Trans.* **40** (2011) 7077
2. G. Matela, R. Aman, *Cent. Eur. J. Chem.* **10** (2012) 1
3. K. C. Molloy, in *The Chemistry of Metal Carbon Bond*, Vol. 5, F. Hartley, Ed., Wiley, New York, 1989, Ch. 11
4. E. L. Torres, F. Zani, M. A. Mendiola, *J. Inorg. Biochem.* **105** (2011) 600
5. M.-L. Sun, B.-F. Ruan, Q. Zhang, Z.-D. Liu, S.-L. Li, J.-Y. Wu, B.-K. Jin, J.-X. Yang, S.-Y. Zhang, Y.-P. Tian, *J. Organomet. Chem.* **696** (2011) 3180
6. C. K. Yap, L. T. Hong, R. Hill, K. M. Lo, S. W. Nig, V. G. Kumar-das, *J. Trop. Forest Sci.* **1** (1989) 390
7. J. S. Casas, M. D. Couce, A. Sanchez, J. Sordo, E. M. V. Lopez, *J. Organomet. Chem.* **696** (2012) 4236
8. S. G. Ruiz, J. C. Torres, S. Prashar, M. Fajardo, Z. Zizak, Z. D. Juranic, G. N. Kaluderovic, *J. Organomet. Chem.* **696** (2011) 3023

9. K. S. Prasad, L. S. Kumar, M. Prasad, H. D. Revanasiddappa, *Bioinorg. Chem. Appl.* 2010 (2010) ID 854514; doi: 10.1155/2010/854514
10. A. Alama, B. Tasso, F. Novelli, F. Sparatore, *Drug Discov. Today* **14** (2009) 500
11. A. Alama, M. Viale, M. Cilli, C. Bruzzo, F. Novelli, B. Tasso, F. Sparatore, *Invest. New Drugs* **27** (2009) 124
12. N. Kobakhidze, N. Farfan, M. Romero, J. M. Mendez-Stivalet, M. G. Ballinas-Lopez, H. Garcia-Ortega, O. Dominguez, R. Santillan, F. Sanchez-Bartez, I. Gracia-Mora, *J. Organomet. Chem.* **695** (2010) 1189
13. A. G. Davies, P. J. Smith, in *Comprehensive Organometallic Chemistry*, Vol. 2, G. Wilkinson, F. G. A. Stone, E. W. Abel, Eds., Pergamon Press, Oxford, 1982, p. 519
14. P. J. Smith, *Chemistry of tin*, 2nd ed., Blackie Academic and Professional, London, 1997
15. M. X. Li, D. Zhang, L. Z. Zhang, J. Y. Niu, B. S. Ji, *J. Organomet. Chem.* **696** (2011) 852
16. S. L. Cai, Y. Chen, W. X. Sun, H. Li, Y. Chen, S. S. Yuan, *Bioorg. Med. Chem. Lett.* **20** (2010) 5649
17. E. L. Torres, A. L. Medina-Castillo, J. F. Fernandez-Sanchez, M. A. Mendiola, *J. Organomet. Chem.* **695** (2010) 2305
18. R. Aeschbach, J. Loliger, B. C. Scott, A. Murcia, J. Butler, B. Halliwell, O. I. Aruoma, *Food Chem. Toxicol.* **32** (1994) 31
19. N. Cenas, A. Nemeikaite, E. Sergediene, H. Nivinskas, Z. Anusevicius, J. Sarlauskas, *Biochim. Biophys. Acta* **1528** (2001) 31
20. N. Didry, L. Dubreuil, M. Pinkas, *Pharm. Acta Helv.* **69** (1994) 25
21. S. Kulevanova, A. Kaftandzieva, A. Dimitrovska, G. Stefkov, T. Grdanoska, N. Panovski, *Boll. Chim. Farm.* **139** (2000) 276
22. B. Ogaard, E. Larsson, R. Glans, T. Henriksson, D. Birkhed, *J. Orofac. Orthop.* **58** (1997) 206
23. S. Shapiro, B. Guggenheim, *Oral Microbiol. Immunol.* **10** (1995) 241
24. E. L. Torres, F. Zani, M. A. Mendiola, *J. Inorg. Biochem.* **105** (2011) 600
25. J. M. Andrews, *J. Antimicrob. Chemother.* **48** (2001) 5
26. D. P. Singh, K. Kumar, C. Sharma, K. R. Aneja, *J. Enz. Inhib. Med. Chem.* **25** (2010) 544
27. O. Prakash, D. K. Aneja, K. Hussain, P. Lohan, P. Ranjan, S. Arora, C. Sharma, K. R. Aneja, *Eur. J. Med. Chem.* **46** (2011) 5065
28. M. I. Okeke, C. U. Iroegbu, E. N. Eze, A. S. Okoli, C. O. Esimone, *J. Ethnopharmacol.* **78** (2001) 119
29. S. K. S. Al-Burtamani, M. O. Fatope, R. G. Marwah, A. K. Onifade, S. H. Al-Saidi, *J. Ethnopharmocol.* **96** (2005) 107
30. K. Kumar, N. D. Pandey, J. K. Mehrotra, *J. Indian Chem.* Soc. **51** (1974) 944
31. K. Jamil, R. Wajid, M. Bakhtiar, M. Danish, *J. Iran. Chem. Soc.* **7** (2010) 495
32. M. Singh, *Synth. React. Inorg. Met.–Org. Chem.* **15** (1985) 235
33. M. A. Abdellah, S. K. Hadjikakou, N. Hadjiliadis, M. Kubicki, T. Bakas, N. Kourkoumelis, Y. V. Simos, S. Karkabounas, M. M. Barsan, I. S. Butler, *Bioinorg. Chem. Appl.* 2009 (2009) ID 542979; doi:10.1155/2009/542979
34. G. K. Sandu, S. P. Verma, L. S. Moore, R. V. Parish, *J. Organomet. Chem.* **321** (1987) 15
35. G. Eng, X. Song, A. Zapata, A. C. de Dios, L. Casabianca, R. D. Pike, *J. Organomet. Chem.* **692** (2007) 1398
36. M. Gielen, A. E. Khloufi, M. Biesemans, F. Kayser, R. Willem, B. Mahieu, D. Maes, J. N. Lisgarten, L. Wyns, *Organometallics* **13** (1994) 2849
37. M. Nath, R. Yadav, *Bull. Chem. Soc. Jpn.* **70** (1997) 1331
38. M. Nath, S. Pokharia, R. Yadav, *Coord. Chem. Rev.* **215** (2001) 99

39. M. Nath, C. L. Sharma, N. Sharma, *Synth. React. Inorg. Met.–Org. Chem.* **21** (1991) 807
40. D. H. Williams, I. Fleming, *Spectroscopic methods in organic chemistry*, 5th ed., Tata McGraw Hill, India, 2004, p. 161
41. M. Nath, R. Yadav, *Bull. Chem. Soc. Jpn.* **71** (1998) 1355
42. R. M. Silverstein, F. X. Webster, D. J. Kiemle, *Spectrometric Identification of Organic Compounds*, 7th ed., Wiley, New York, 2005
43. M. M. Amini, A. Azadmeher, H. R. Khavasi, S.W. Ng, *J. Organomet. Chem.* **692** (2007) 3922
44. T. P. Lockhart, W. F. Manders, *Inorg. Chem.* **25** (1986) 892
45. M. Nath, R. Yadav, M. Gielen, H. Dalil, D. de Vos, G. Eng, *Appl. Organomet. Chem.* **11** (1997) 727
46. S. Shahzadi, K. Shahid, S. Ali, M. Bakhtiar, *Turk. J. Chem.* **32** (2008) 333
47. K. R. Aneja, C. Sharma, R. Joshi, *Int. J. Otorhinolaryngol.* **74** (2010) 604.

Journal of the Serbian Chemical Society
JSCS@tmf.bg.ac.rs • www.shd.org.rs/JSCS
J. Serb. Chem. Soc. 78 (9) S107–S109 (2013) *Supplementary material*

SUPPLEMENTARY MATERIAL TO

Reactions of tin and triorganotin(IV) isopropoxides with thymol derivative: synthesis, characterization and *in vitro* antimicrobial screening

GARIMA MATELA[1]*, ROBINA AMAN[1], CHETAN SHARMA[2] and SMITA CHAUDHARY[3]

[1]*Department of Chemistry, Kumaun University, S. S. J. Campus Almora-263 601, India,* [2]*Department of Microbiology, Kurukshetra University, Kurukshetra, Haryana-136 119, India and* [3]*Institute of Environmental Studies, Kurukshetra University, Kurukshetra, Haryana-136 119 India*

J. Serb. Chem. Soc. 78 (9) (2013) 1323–1333

TABLE S-I. Amount of 2-propanol in the azeotropic mixture formed during the preparation of the complexes

Complex	Calculated, g	Found, g
2	0.598	0.538
3	0.598	0.538
4	0.300	0.270
5	0.300	0.272
6	0.299	0.269

PHYSICAL, ANALYTICAL AND SPECTRAL DATA OF THE LIGAND AND COMPLEXES

*H_2hbgl (**1**)*. Yield: 5.9 g, 80 %; Colour: yellow; m.p.: 70 °C; Anal. Calcd. for $C_{13}H_{19}NO_3$: C, 65.74; H, 8.00; N 6.04 %. Found: C, 65.84; H, 8.10; N, 5.80 %; IR (KBr/CsI, cm^{-1}): 3390 (–OH stretching of phenolic group), 3056 (–CH stretching of aromatic ring), 2956, 2856 (asymmetric and symmetric stretching of $–CH_3$ or $–CH_2$), 1582 (asymmetric stretching of carboxylate group), 1413 (symmetric stretching of carboxylate group); ^{1}H-NMR (300 MHz, DMSO, δ / ppm): 6.50 (1H, *d*, *J* = 7.8 Hz, Ar-H), 6.90 (1H, *d*, *J* = 8 Hz, Ar-H); 8.38 (1H, *s*, phenolic –OH), 7.15 (1H, *br*, –NH), 2.13 (3H, *s*, $–CH_3$), 1.81 (2H, *s*, Ar–C$\mathbf{H}_2$–), 3.10 (2H, *s*, $–CH_2$–), 1.12 (6H, *d*, *J* = 6.9 Hz, -CH(C$\mathbf{H}_3$)$_2$); ESI-MS (*m/z* (relative abundance (%)): $[C_{13}H_{19}NO_3]^+$ 237.9 (48), $[C_{11}H_{15}O]^+$ 163.1 (30).

* Corresponding author. E-mail: matelagarima28@yahoo.in

*[Sn(OPr^i)$_2$(hbgl)] (**2**).* Yield: 1.42 g, 67 %; Colour: yellowish brown; m.p.: 155 °C; Anal. Calcd for $C_{19}H_{31}NO_5Sn$: C, 48.28; H, 6.56; N, 3.09; Sn, 25.13 %. Found: C, 48.34; H, 6.59; N, 2.99; Sn, 25.19 %; IR (KBr/CsI, cm^{-1}): 3100 (N–H stretching of amine), 2963, 2868 (asymmetric and symmetric stretching of –CH_3 or –CH_2 groups), 1613 (asymmetric stretching of carboxylate group), 1412 (symmetric stretching of carboxylate group), $\Delta\nu$: 201, 500 (Sn–O stretching); ^{1}H-NMR (300 MHz, DMSO, δ / ppm): 7.13 (1H, *d*, *J* = 7.8 Hz, Ar-H), 6.77 (1H, *d*, *J* = 7.8 Hz, Ar-H), 6.58 (1H, *d*, –NH), 2.30 (3H, *s*, –CH_3), 1.15 (3H, *d*, *J* = 2.7 Hz, –CH(C**H**$_3$)$_2$), 1.76 (3H, *d*, *J* = 2.7 Hz, -CH(C**H**$_3$)$_2$); molar conductance (10^{-3} M DMSO, µS cm^{-1}): 21.

*[Sn(OPr^i)$_2$(Hhbgl)$_2$] (**3**).* Yield: 2.057 g, 64 %; Colour: brown; m.p.: 160 °C; Anal. Calcd. for $C_{32}H_{50}N_2O_8Sn$: C, 54.12; H, 7.04; N, 4.07; Sn, 16.73 %. Found: C, 54.22; H, 7.14; N, 4.01; Sn 16.79 %; IR (KBr/CsI, cm^{-1}): 3394 (–OH stretching of phenolic group), 3200–3000 (–NH/–CH stretching of amine and aromatic ring), 2961, 2871 (asymmetric and symmetric stretching of –CH_3 or –CH_2 group), 1588 (asymmetric stretching of carboxylate group), 1415 (symmetric stretching of carboxylate group), $\Delta\nu$:173, 503 (Sn–O stretching); ^{1}H-NMR (300 MHz, MeOD, δ / ppm): 6.45–6.96 (4H, *m*, Ar-H), 8.06 (1H, *s*, phenolic –OH), 8.54 (1H, *s*, phenolic –OH), 2.20 (6H, *s*, CH_3); molar conductance (10^{-3} M DMSO, µS cm^{-1}): 25.

*[Ph$_3$Sn(Hhbgl)] (**4**).* Yield: 1.764 g, 67 %; Colour: brown; m.p.: >300 °C; Anal. Calcd. for $C_{31}H_{33}NO_3Sn$: C, 63.41; H, 5.80; N, 2.39; Sn, 20.23 %. Found: C, 63.46; H, 5.84; N, 2.34; Sn, 20.28 %; IR (KBr/CsI, cm^{-1}): 3426 (–OH stretching of phenolic group), 3056 (–CH stretching of aromatic ring), 2958, 2868 (asymmetric and symmetric stretching of –CH_3 or –CH_2 groups), 1604 (asymmetric stretching of carboxylate group), 1417 (symmetric stretching of carboxylate group), $\Delta\nu$: 187, 558 (Sn–O stretching), 279, 207 (asymmetric and symmetric stretching of Sn–C); ^{1}H-NMR (300 MHz, DMSO, δ / ppm): 7.22––7.58 (17H, *m*, Ar-H and Sn–C_6H_5), 7.76 (1H, *br*, phenolic –OH), 7.33 (1 H, *br*, –NH), 2.13 (3H, *s*, –CH_3), 1.08 (3H, *d*, *J* = 5.1 Hz, –CH(C**H**$_3$)$_2$), 1.05 (3H, *d*, *J* = = 5.1 Hz, -CH(C**H**$_3$)$_2$); molar conductance (10^{-3} M DMSO, µS cm^{-1}): 17.

*[Bu$_3$Sn(Hhbgl)] (**5**).* Yield: 1.644 g, 69 %; Colour: brown; m.p.: >300 °C; Anal. Calcd. for $C_{25}H_{45}NO_3Sn$: C, 57.06; H, 8.56; N, 2.67; Sn, 22.58 %. Found: C, 57.15; H, 8.61; N, 2.61; Sn, 22.62 %; IR (KBr/CsI, cm^{-1}): 3500–3000 (–OH stretching of phenolic group), 2962, 2863 (asymmetric and symmetric stretching of –CH_3 or –CH_2 groups), 1591 (asymmetric stretching of carboxylate group), 1406 (symmetric stretching of carboxylate group), $\Delta\nu$: 185, 501 (Sn–O stretching), 528, 469 (asymmetric and symmetric stretching of Sn–C); ^{1}H-NMR (300 MHz, DMSO, δ / ppm): 7.12 (1H, *d*, *J* = 7.8 Hz, Ar-H), 6.77 (1H, *d*, *J* = 7.5 Hz, Ar-H), 8.00 (1H, *s*, phenolic –OH), 6.88 (1H, *s*, –NH), 2.30 (3H, *s*, CH_3), 0.78

and 0.90–1.21 (27 H, *t*, *m*, Sn–C_4H_9); molar conductance (10^{-3} M DMSO, µS cm^{-1}): 18.

*[$Me_3Sn(Hhbgl)$] (**6**)*. Yield: 1.304 g, 72 %; Colour: cream; m.p.: >300 °C; Anal. Calcd for $C_{16}H_{27}NO_3Sn$: C, 47.99; H, 6.75; N, 3.50; Sn, 29.67 %. Found: C, 47.91; H, 6.71; N, 3.46; Sn, 29.70 %; IR (KBr/CsI, cm^{-1}): 3404 (–OH stretching of phenolic group), 2959, 2863 (asymmetric and symmetric stretching of $–CH_3$ or $–CH_2$ groups), 1626 (asymmetric stretching of carboxylate group), 1410 (symmetric stretching of carboxylate group), $\Delta\nu$: 216, 555 (Sn–O stretching); ^{1}H-NMR (300 MHz, DMSO, δ / ppm): 6.89 (1H, *d*, *J* = 6 Hz, Ar-H), 6.48 (1H, *d*, *J* = 6.09 Hz, Ar-H), 7.80 (1H, *s*, phenolic –OH), 4.90 (1H, *br*, –NH), 0.99 (3H, *d*, *J* = 5.13 Hz, –CH(C**H**$_3$)$_2$), 1.07 (3H, *d*, *J* = 4.44 Hz, –CH(C**H**$_3$)$_2$), 0.42 (9H, *s*, Sn–CH_3, ^2J $^{117/119}$Sn- ^{1}H = 68.0 Hz); molar conductance (10^{-3} M DMSO, µS cm^{-1}): 32.

Journal of the Serbian Chemical Society
JSCS-info@shd.org.rs • www.shd.org.rs/JSCS
J. Serb. Chem. Soc. 78 (9) 1335–1349 (2013)
JSCS–4501
UDC 546.650.3+546.13+547.586.2–384:542.913:536.5.004.12
Original scientific paper

Magnetic, thermal and spectroscopic properties of lanthanide(III) 2-(4-chlorophenoxy)acetates, $Ln(C_8H_6ClO_3)_3 \cdot nH_2O$

WIESŁAWA FERENC[1]*, BEATA CRISTÓVÃO[1] and JAN SARZYŃSKI[2]

[1]*Faculty of Chemistry, Maria Curie-Skłodowska University, 20–031 Lublin, Poland and* [2]*Institute of Physics, Maria Curie-Skłodowska University, 20–031, Lublin, Poland*

(Received 3 December 2012, revised 6 April 2013)

Abstract: 2-(4-Chlorophenoxy)acetates of lanthanides(III) were synthesized as polycrystalline hydrated solids with the general formulae: $Ln(C_8H_6ClO_3)_3 \cdot 2H_2O$ (Ln = La(III), Pr(III), Sm(III), Eu(III) or Tb(III)); $Ln(C_8H_6ClO_3)_3 \cdot H_2O$ (Ln = = Dy(III)) and $Ln(C_8H_6ClO_3)_3 \cdot 3H_2O$ (Ln = Er(III), Tm(III), Yb(III) and Lu(III). The complexes were characterized by elemental analysis, FTIR spectroscopy, magnetic and thermogravimetric studies and X-ray diffraction (XRD) analysis. The complexes have colours typical for the lanthanide(III) ions. The carboxylate groups bind as bidentate chelating agents. On heating to 1273 K in air, the complexes decompose in three steps. First they dehydrate in one stage to form anhydrous salts that then decompose to the oxides of the respective metals with the intermediate formation of their oxychlorides. The gaseous products of the thermal decomposition of the compounds under nitrogen were also determined. The magnetic susceptibilities of the complexes were measured over the ranges 76–303 K and 1.8–303 K, and their magnetic moments were calculated. The results showed that the 2-(4-chlorophenoxy)acetates of lanthanides(III) are high-spin complexes with weak ligand fields.

Keywords: 2-(4-chlorophenoxy)acetates; thermal stability; magnetic properties; lanthanides.

INTRODUCTION

Many metal carboxylates have been known from ancient times and since that moment the interest in their chemistry has been growing.[1] This type of compounds show the tendency to form various bondings in their molecules, hence they may be used in biotechnology, bioengineering and medicine.[1–4] Depending on their magnetic properties, they are used in modern branches of techniques and technology as electric materials. Some are useful reagents for the synthesis of

* Corresponding author. E-mail: wetafer@poczta.umcs.lublin.pl
doi: 10.2298/JSC121203043F

organic compounds, being applied in metallation and oxymetallation reactions. Transition metal carboxylates are used as catalysts in many industrial processes and as selective oxidizing agents in organic chemistry. They also play an important role in inorganic and bioinorganic chemistry and in some areas of daily life.[1,3,5] Many of them are components of several vitamins and drugs.[1] They serve for the production of biomedical materials and as the therapeutic agents being used in anti-cancer therapy. Carboxylic acids are applied for the absorption, preservation and separation of many gases. Having luminescence properties, their complexes with 4f electron elements find application in optical and electronic industries.[1,6] They play significant roles in crystal engineering and serve for the production of paramagnetic organic materials.[4,7–12] Their compounds form interesting group of single-molecule magnets (SMMs) that exhibit magnetization hysteresis at low temperatures, yielding special properties of macroscopic magnets.[1,4,7–13]

2-(4-Chlorophenoxy)acetic acid is a white solid sparingly soluble in water. Its melting point temperature is 157 °C. It may be easily decomposed to CO, CO_2 and HCl. Therefore it has toxic properties. It belongs to the herbicide group of substances and may be used as a hormone for plant growth regulation.[14,15]

In previous papers, studies of the 2-(4-chlorophenoxy)acetic acid anion with Mo, Li, Cu, Mn, Co, Ni, Nd, Gd and Ho were reported in which the complexes were characterized by elemental analysis, FTIR spectroscopy, thermogravimetric studies and X-ray diffraction measurements.[14,15] In continuation of ongoing investigations on the carboxylates of transition metal ions, the synthesis of complexes of lanthanides(III) with the 2-(4-chlorophenoxy)acetic acid anion and an examination of some of their properties, such as thermal stability in air at 293–1273 K, magnetic properties in the range of 77–303 K and 1.8–300 K, and their FTIR spectra, are reported herein.

EXPERIMENTAL

Materials

All the chemicals and solvents used for the synthesis were commercially available and of reagent grade. They were used without further purification. A solution of the ammonium 2-(4--chlorophenoxy)acetate (0.1 mol L^{-1}, pH ~5) was prepared by the addition of an aqueous NH_3 solution (25 %, Polish Chemical Reagents, Gliwice, Poland) to an aqueous solution of 2-(4-chlorophenoxy)acetic acid (99 %, Aldrich). In order to obtain the chlorides of the rare earth element(III), 0.8 g of the oxides of lanthanides(III) (99.9 % pure, Aldrich) were digested in the equivalent amount of concentrated HCl (35–38 %, Polish Chemical Reagents, Gliwice, Poland). The solutions were constantly heated and evaporated to dryness. The residues of lanthanide(III) chlorides were dissolved in water, forming solutions of lanthanide(III) chlorides, the concentration of which was equal to 0.1 mol L^{-1} and pH ~5.

Synthesis of the compounds

The 2-(4-chlorophenoxy)acetates of lanthanides(III) were prepared by adding equivalent quantities of 0.1 mol L^{-1} ammonium 2-(4-chlorophenoxy)acetate (pH ~5) to hot solutions of

the lanthanide(III) chlorides. The solutions were heated for 1 h at 333–343 K under constant stirring to reach the equilibrium state. The solids were then filtered off, washed with hot water to remove ammonium ions, recrystallised and dried at 303 K to constant mass.

Sodium 2-(4-chlorophenoxy)acetate was prepared by the addition of an equivalent amount of a 0.1 mol L^{-1} ammonium 2-(4-chlorophenoxy)acetate solution to a solution containing 0.1 g NaOH (analytically pure, Polish Chemical Reagents, Gliwice, Poland) and crystallizing.

Methods and apparatus applied

The contents of carbon and hydrogen in the complexes were determined by elemental analysis using a Perkin–Elmer CHN 2400 analyser. The content of chloride was determined by the Schöniger method.[16] The amounts of M(III) metals were established by the X-ray fluorescence (XRF) method with energy dispersion using an ED XRF-1510 spectrophotometer (Canberra-Packard).

The FTIR spectra of complexes and the products of the final complex decompositions were recorded over the range of 4000–400 cm^{-1} using an M–80 Perkin–Elmer spectrometer. The samples were prepared as KBr discs. The FIR spectra of complexes in Nujol mulls sandwiched between polyethylene plates were recorded over the range of 600–100 cm^{-1} using the Perkin–Elmer 180 spectrometer.

The X-ray diffraction patterns of compounds and the products of decomposition process were taken on a HZG-4 (Carl-Zeiss, Jena) diffractometer using Ni filtered CuK_α radiation. The measurements were made within the range of 2θ 4–80° by means of the Bragg–Brentano method.[17]

The thermal stability and decomposition of the complexes were studied using a Setsys 16/18 (Setaram) TG, DTG and DSC instrument. The experiments were performed under a under air, flow rate of 1 L h^{-1}, in the temperature range of 297–1273 K at a heating rate of 5 K min^{-1}. The initial mass of the samples of the lanthanides(III) 2-(4-chlorophenoxy)acetates used for the measurements ranged from 7.87 to 4.56 mg. The samples were heated in Al_2O_3 crucibles. The TG–FTIR measurements were also made under a nitrogen atmosphere in order to know the complex behaves under neutral, reduction atmosphere while in air under oxidation atmosphere, using a Q 5000 instrument (TA Instruments) with a Nicolet 6700 spectrophotometer. The experiments were performed in Pt crucibles under a nitrogen flow of 25 mL min^{-1} at a heating rate of 20 K min^{-1}. The masses of the samples were in the range of 8.98–4.54 mg.

Magnetic susceptibilities of polycrystalline samples of the lanthanide(III) 2-(4-chlorophenoxy)acetates were investigated at 76–303 K and 1.8–303 K. The measurements were realised using the Gouy method on a Quantum Design SQUID-VSM magnetometer. The superconducting magnet is generally operated at a field strength ranging from 0 to 7 T. Measurement of the studied samples were made at a magnetic field 0.1 T. The SQUID magnetometer was calibrated with a palladium rod sample. In the case of the Gouy method, the mass changes were obtained using a Cahn RM-2 electrobalance. The employed calibrant was $Hg[Co(SCN)_4]$, for which the magnetic susceptibility was assumed to be 1.644×10^{-5} cm^3 g^{-1}. Correction for diamagnetism of the constituent atoms was calculated by the use of Pascal constants.[4,18]

The effective magnetic moment values were calculated from the equation:

$$\mu_{\text{eff}} = 2.83(\chi_{\text{M}}T)^{1/2}$$

where μ_{eff} is the effective magnetic moment, χ_M is the magnetic susceptibility per molecule and T is the absolute temperature.

The solubility of 2-(4-chlorophenoxy)acetates of lanthanides(III) in water was determined at 298 K by the ASA method.[19]

RESULTS AND DISCUSSION

The lanthanides(III) 2-(4-chlorophenoxy)acetates were obtained as crystalline products of the general formula: $Ln(C_8H_6ClO_3)_3 \cdot nH_2O$, where Ln = lanthanide, n = 2 for La(III), Pr(III), Sm(III), Eu(III) and Tb(III); n = 1 for Dy(III) and n = 3 for Er(III), Tm(III), Yb(III) and Lu(III).

Their colours are typical for Ln(III), which is connected with the similar electron density in the complexes. In their molecules, the f–f electronic transitions of the metal ions are those of the lowest energy and absorption occurs at relatively high wavelengths, the value depending on the nature of the metal ion.[20]

The results of the elemental analyses are given in Table I.

TABLE I. Elemental analysis data (%) for the lanthanide(III) 2-(4-chlorophenoxy)acetates

Complex (L = $C_8H_6ClO_3$)	C		H		Cl		M	
	Calcd.	Found	Calcd.	Found	Calcd.	Found	Calcd.	Found
$LaL_3 \cdot 2H_2O$	39.40	39.20	3.00	2.95	14.60	14.50	19.00	18.90
$PrL_3 \cdot 2H_2O$	39.29	39.07	3.02	2.78	14.50	14.30	19.20	19.12
$SmL_3 \cdot 2H_2O$	38.79	38.85	2.98	2.76	14.31	14.20	20.23	20.60
$EuL_3 \cdot 2H_2O$	38.68	38.50	2.96	2.81	14.30	14.25	20.42	20.30
$TbL_3 \cdot 2H_2O$	38.35	38.27	2.93	2.79	14.15	14.53	21.14	22.00
$DyL_3 \cdot H_2O$	39.09	38.90	2.71	2.62	14.42	14.80	22.04	22.80
$ErL_3 \cdot 3H_2O$	37.05	36.99	3.11	2.98	13.67	13.70	21.49	21.60
$TmL_3 \cdot 3H_2O$	36.97	36.70	3.10	2.86	13.64	13.82	21.66	21.10
$YbL_3 \cdot 3H_2O$	36.75	35.90	3.06	3.00	13.59	13.40	22.08	22.00
$LuL_3 \cdot 3H_2O$	36.67	36.50	3.06	2.99	13.56	13.50	22.29	22.20

Infrared spectra

The Ln(III) 2-(4-chlorophenoxy)acetates exhibited similar solid state FTIR spectra (Table II). The band at 1708 cm^{-1}, originating from the RCOOH group, present in the spectrum of the acid is replaced in the spectra of complexes by two bands, one at 1608–1567 cm^{-1} and the other 1340–1322 cm^{-1}, which are ascribed to the asymmetric and symmetric vibrations of the COO^- groups, respectively.[5,21–33]

The bands with the maxima at 3429–3410 cm^{-1}, characteristic for ν(OH) vibrations confirmed the presence of crystallization water molecules in the complexes. The bands of C–H were observed at 2929–2918 cm^{-1} and those of the ν(C=C) ring vibrations at 1624–1622, 1496, 1177–1174, 1111–1104 and 1068–1066 cm^{-1}. The ν(C–Cl) vibration bands occurred at 736–704 cm^{-1} while those of the asymmetric and symmetric ν(C–O–C) vibrations are at 1082–1068 cm^{-1}

and 1060–1058 cm^{-1}, respectively. The bands at 508–449 cm^{-1} confirmed the ionic metal–oxygen bond vibrations.[1,19] They change their positions in the FTIR spectra of complexes, which may suggest that the metal–ligand bonding have different stabilities. The O–H···O stretching vibrations bands[5] were in the range 118–106 cm^{-1}. Their shapes changed according to the increase in the atomic number of elements and the degree of hydration in the 4-chlorophenoxyacetates. The bands at 138–122 cm^{-1} indicate internal C–C torsion vibrations and those at 283–267cm^{-1} arise from vibrations of the aromatic ring. The values of the two band frequencies of the asymmetrical and symmetrical vibrations of the carboxylate groups of analysed complexes, and those of C–Cl and M–O stretching vibrations are presented in Table II.

TABLE II. Wavenumbers ($\tilde{\nu}$ / cm^{-1}) of OCO^-, C–Cl and M–O in the FTIR spectra of lanthanides(III) and Na 2-(4-chlorophenoxy)acetates and that of the COOH band in 2-(4-chlorophenoxy)acetic acid

Compound (L = $C_8H_6ClO_3$)	ν(C=O)	ν_{as}(OCO)	ν_s(OCO)	$\Delta\nu$(OCO)	ν(C–Cl)	ν(M–O)
$LaL_3{\cdot}2H_2O$	–	1596	1332	264	724	504
$PrL_3{\cdot}2H_2O$	–	1568	1322	246	720	508
$SmL_3{\cdot}2H_2O$	–	1572	1336	236	720	500
$EuL_3{\cdot}2H_2O$	–	1572	1336	236	716	504
$TbL_3{\cdot}2H_2O$	–	1608	1340	268	704	524
$DyL_3{\cdot}H_2O$	–	1580	1336	244	716	504
$ErL_3{\cdot}3H_2O$	–	1580	1328	252	736	504
$TmL_3{\cdot}3H_2O$	–	1580	1328	252	736	504
$YbL_3{\cdot}3H_2O$	–	1596	1336	260	724	508
$LuL_3{\cdot}2H_2O$	–	1596	1328	268	736	504
NaL	–	1620	1340	280	722	–
HL	1708	–	–	–	–	–

The separations of the ν_{as}(OCO) and ν_s(OCO) modes in the FTIR spectra of the complexes ($\Delta\nu$(OCO) from 268 to 236 cm^{-1}) are smaller than that of the sodium salt ($\Delta\nu$(OCO) = 280 cm^{-1}), indicating that the degree of ionic nature of the M–O bond in the 2-(4-chlorophenoxy)acetates is smaller compared to that of the sodium salt. For the complexes, the shifts of the frequencies of bands ν_{as}(OCO) and ν_s(OCO) were lower and lower or the same, respectively, in comparison with those of the sodium salt. Accordingly, taking into account the spectroscopic criteria, especially the Nakamoto criterion,[1,5,20,31,33,34] the carboxylate ions in the analysed complexes appear to be bidentate chelating groups. The structure of the carboxylate groups is bidentate chelating when the bands of ν_{as}(OCO) and ν_s(OCO) in the FTIR spectrum of the analysed complex are shifted to lower and higher wavenumbers compared to those for the sodium salt; or the $\Delta\nu$(OCO) value of studied complex << than the $\Delta\nu$(OCO) value of the sodium salt.[1,5,31] A bidentate bridging structure exists when the bands of ν_{as}(OCO) and ν_s(OCO) in the FTIR spectrum of studied complex are shifted to higher wavenumbers, com-

pared to those for the sodium salt; or the $\Delta\nu$(OCO) value of the studied complex ≈ $\Delta\nu$(OCO) value of the sodium salt.[5] For monodentate geometry of carboxylate group, the bands of ν_{as}(OCO)and ν_s(OCO) in the FTIR spectrum of the complex are shifted to higher and lower wavenumbers, respectively, in comparison with those for sodium salt; or the $\Delta\nu$(OCO) value of the studied complex is considerably larger than the $\Delta\nu$(OCO) of the sodium salt.

X-Ray powder diffraction

From the X-ray powder diffraction of 2-(4-chlorophenoxy)acetates of lanthanides(III), it follows that they are crystalline compounds (Fig. 1). The structures of 2-(4-chlorophenoxy)acetates were not determined since suitable single crystals were not obtained.

Thermal analysis

The thermal stability of the lanthanide(III) 2-(4-chlorophenoxy)acetates was studied in air in the temperature range of 293–1273 K (Fig. 2, Tables III and IV). The TG, DTG and DSC curves were recorded using the DSC/TG technique. When heated to 1273 K, the complexes decomposed in three steps. They were stable up to 312–365 K. Next, in the range of 312–433 K, all the studied 2-(4--chlorophenoxy)acetates dehydrated in one step, exhibiting endothermic peaks on the DSC curves, losing one, two or three molecules of water to form anhydrous compounds. The mass losses calculated from the TG curves, being equal to 2.27–6.93 %, correspond to the loss of 1, 2 or 3 molecules of water (theoretical values 2.44–6.95 %). From the temperature data, it follows that Pr(III) complex with the highest value of initial decomposition temperature is the most thermally stable compound, whereas the Tm(III) complex is the least stable one in the series of the analysed lanthanide(III) 2-(4-chlorophenoxy)acetates. The energetic effects accompanying the dehydration processes were also determined. The enthalpy values, ΔH, change from 60.20–21.43 kJ mol^{-1} per one molecule of water. These values may indicate that the water molecules are coordinated to the central ions with different strengths depending on their various positions in the complex coordination spheres.[22] The anhydrous lanthanide(III) complexes first form oxychlorides in the second step of their decomposition,[1,35–37] as intermediate products formed by the gradual loss of the ligands (463–923 K). This process is accompanied by a strong exothermic effect on the DSC curves. The mass losses calculated from TG curves indicated oxychloride formation. In the third stage of decomposition, the intermediate LnOCl products decomposed to the oxides of appropriate metals: Ln_2O_3 (where Ln = La, Sm, Eu, Dy, Er, Tm, Yb or Lu) and Pr_6O_{11} and Tb_4O_7, which were verified by comparing their FTIR spectra and powder diffractograms with those of the pure oxide. The final temperature values of their formation were in the range of 1073–1273 K. The masses of resi-

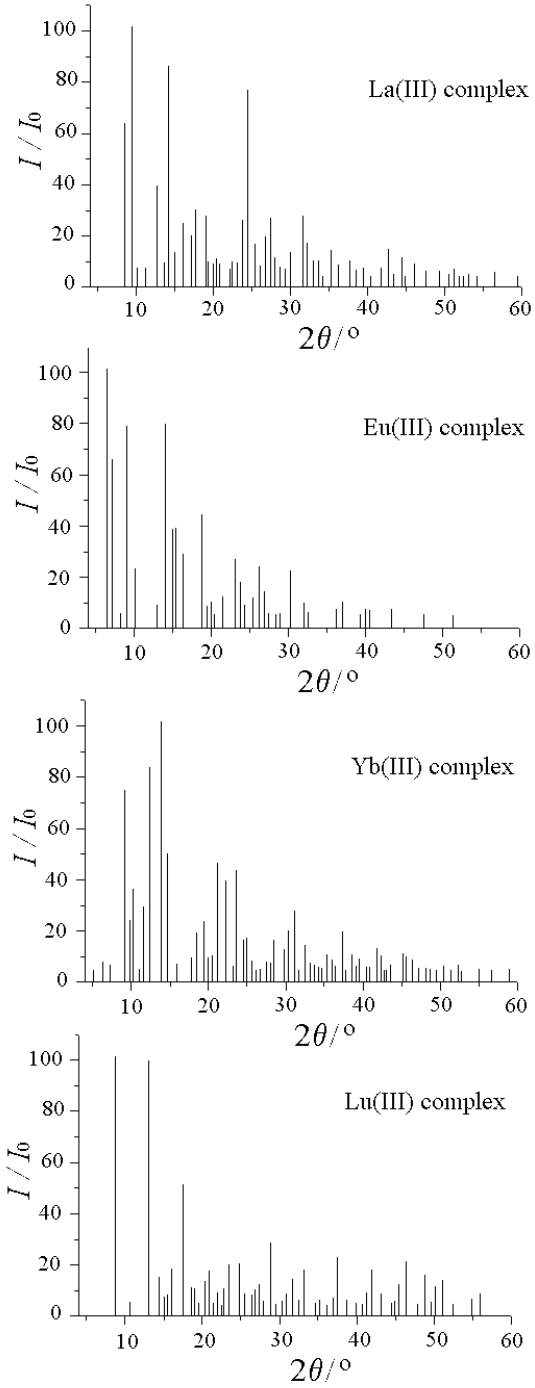

Fig. 1. Dependence of I/I_0 *vs.* 2θ for La(III), Eu(III), Yb(III) and Lu(III) 2-(4-chlorophenoxy)acetates.

dues determined from TG curve were 22.48–25.00 % (theoretical value 22.22––25.33 %). The results indicate that the thermal decomposition of lanthanide(III) 2-(4-chlorophenoxy)acetates in air proceeds in the following manner:

$$LnL_3 \cdot nH_2O \rightarrow LnL_3 \rightarrow LnOCl \rightarrow \begin{matrix} Ln_2O_3 \\ Pr_6O_{11} \\ Tb_4O_7 \end{matrix} \quad (Ln = La, Sm, Eu, Dy, Er, Tm, Yb, Lu)$$

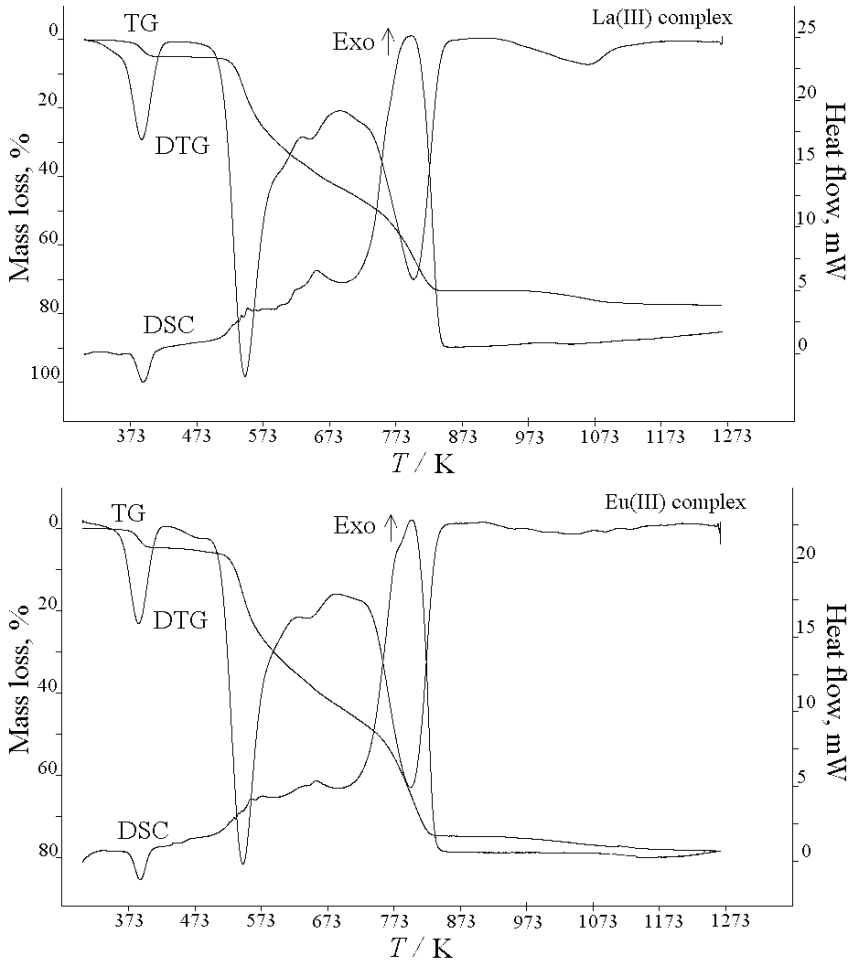

Fig. 2. TG, DTG and DSC curves for La(III) and Eu(III) complexes under an air atmosphere.

From the obtained data, it appears that the coordination number of the central ions is probably 7, 8 or 9. The molecules of water may be coordinated with the central ions despite their loss at a low temperature.[38–41]

TABLE III. Temperature ranges of the thermal mass losses of lanthanide(III) 2-(4-chlorophenoxy)acetates in air at 293–1273 K

Complex ($L = C_8H_6ClO_3$)	T^a / K	Mass loss, %		n^b	T^c / K	Mass loss, %		T^d / K	Residue mass, %	
		Calcd.	Found			Calcd.	Found		Calcd.	Found
$LaL_3·2H_2O$	353–413	4.92	4.92	2	523–858	73.96	73.12	1223	22.22	22.55
$PrL_3·2H_2O$	365–390	4.91	4.85	2	580–898	73.90	74.86	1073	23.19	23.62
$SmL_3·2H_2O$	339–389	4.85	4.78	2	563–877	72.84	73.29	1273	23.46	22.56
$EuL_3·2H_2O$	358–423	4.83	4.68	2	463–853	72.68	74.77	1173	23.63	22.56
$TbL_3·2H_2O$	328–393	4.79	4.52	2	503–923	72.00	71.83	1203	24.87	22.48
$DyL_3·H_2O$	363–433	2.44	2.27	1	483–893	70.97	68.69	1188	25.30	24.06
$ErL_3·3H_2O$	331–394	6.95	6.62	3	519–886	71.88	71.45	1273	24.59	25.00
$TmL_3·3H_2O$	327–381	6.31	6.93	3	573–857	71.74	72.25	1273	24.58	23.76
$YbL_3·3H_2O$	338–365	6.80	6.40	3	560–850	71.35	70.40	1250	25.14	24.90
$LuL_3·3H_2O$	348–368	6.87	6.54	3	573–848	71.17	72.45	1123	25.33	24.80

[a]Temperature range of dehydration process; [b]number of water molecules lost in the single step; [c]temperature range of the decomposition of the anhydrous complex; [d]final temperature of decomposition process

TABLE IV. Enthalpy values of the dehydration process for the lanthanide(III) 2-(4-chlorophenoxy)acetates and their solubility in water at 293 K

Complex ($L = C_8H_6ClO_3$)	ΔH^a / kJ·mol^{-1}	$\Delta H_1{}^b$ / kJ·mol^{-1}	Solubility, 10^{-4} mol·dm^{-3}
$LaL_3·2H_2O$	48.20	24.10	4.70
$PrL_3·2H_2O$	45.03	22.50	4.60
$SmL_3·2H_2O$	42.87	21.43	5.30
$EuL_3·2H_2O$	120.40	60.20	6.00
$TbL_3·2H_2O$	78.48	39.24	7.60
$DyL_3·H_2O$	59.99	59.99	3.80
$ErL_3·3H_2O$	90.22	30.07	9.00
$TmL_3·3H_2O$	80.54	26.84	9.50
$YbL_3·3H_2O$	78.30	26.10	9.80
$LuL_3·2H_2O$	83.30	27.76	9.90

[a]Enthalpy value; [b]enthalpy value for one molecule of water

The data obtained from the determination of the complete structures of these complexes can give fair information on the positions of water molecules in the compounds, but their monocrystals have not yet been determined. However, attempts to prepare them have still to be made.

The FTIR spectra recorded of the gaseous products released during complex decompositions revealed them to be molecules of H_2O, CO_2, CO, CH_4 hydrocarbons and hydrogen chloride. For all the analysed complex decompositions, the bands at 4000–3500 and 1700–1500 cm^{-1} (348–481 K) confirmed the presence of H_2O molecules in the products. At higher temperatures, the bands at 2250–2500 and 600–750 cm^{-1} result from CO_2 vibrations, whereas the bands observed at 2000–2200 cm^{-1} are characteristic for CO. The absorbance peak of methane (CH_4) appears around 3000 cm^{-1} and HCl in the range of 3059–2650 cm^{-1}.[41,42]

Solubility in water

The solubilities of lanthanide(III) 2-(4-chlorophenoxy)acetates in water (at 293 K) were also determined (Table IV). They were of the order of 1×10^{-4} mol dm^{-3}. Lu(III) 2-(4-chlorophenoxy)acetate was the most soluble salt, while the Dy(III) complex was the least soluble. Taking into account the values of the solubilities, it could be said that 2-(4-chlorophenoxy)acetic acid cannot be used for separation of lanthanide(III) ions by ion-exchange chromatography or by extraction methods because of their low solubility.

Magnetic properties

To estimate the nature of metal–ligand bonding in the analysed compounds and to try to find the reasons why their colours are typical for Ln(III) ions, the magnetic susceptibilities of the lanthanide(III) 2-(4-chlorophenoxy)acetates were determined over the range of 76–303 K. In order to determine whether the nature of atomic magnetic interactions changed at low temperatures, the magnetic susceptibilities of the complexes were investigated between 1.8 and 303 K.

The complexes obey the Curie–Weiss law.[3,4] For all compounds, the values of the Weiss constant, Θ_m, had a negative sign, which may result from the antiferromagnetic spin or from a crystal field splitting of the paramagnetic spin state.[3,4,43–46] The experimentally determined effective magnetic moment, μ_{eff}, values for the 2-(4-chlorophenoxy)acetates at 76 and 303 K are given in Table V.

TABLE V. The effective magnetic moment, μ_{eff} / μ_B, values for the Ln(III) 2-(4-chlorophenoxy)acetates at 76 and 303 K

Trivalent ion	T = 76 K	T = 303 K	Trivalent ion	T = 76 K	T = 303 K
Pr	2.75	3.26	Dy	10.45	10.69
Sm	1.09	1.56	Er	9.48	9.74
Eu	2.12	3.08	Tm	7.70	8.14
Tb	9.19	9.44	Yb	2.00	3.54

In the lanthanide(III) 2-(4-chlorophenoxy)acetates, the paramagnetic central ions remain practically unaffected by the diamagnetic ligands coordinated around them. The 4f orbitals, partly occupied by the magnetically active electrons, are very efficiently shielded by the fully occupied 5s and 5p orbitals. These 4f orbitals are almost uninvolved in the bonds between a rare earth(III) ion and its nearest neighbours. The lanthanide ion in a molecular compound behaves as free ion and its energy levels are the same as those in the free ion. The energy separation between the state of lowest energy and the first excited state varies from a few hundred to several thousands of wavenumbers. When this energy separation is small, the first excited state may be thermally populated, while only the ground state is thermally populated when the separation is large. The magnetic properties can be taken as those of the ground state alone and the lanthanide(III) ions in the

complexes act in the same manner as free ions. The values of μ_{eff} determined for all 2-(4-chlorophenoxy)acetates (except for europium) (Table V) were similar to those calculated for Ln(III) ions by Hund and Van Vleck (Table VI).[43] The values of magnetic moments determined for the complexes indicate that the energies of the 4f electrons in the central ions are not changed compared to those in the free lanthanide ions. Therefore the colours of these complexes determined by rare earth element(III) ions remain the same as those in the free lanthanides. The electron density in the molecules makes the f–f electronic transitions of the central ions to be those of the lowest energy and the absorption occurs at relatively high wavelengths. The 4f orbitals of lanthanide(III) ions are effectively shielded by the $5s^2 5p^6$ octet. Therefore the metal–ligand bonding in the analysed lanthanide(III) complexes is mainly electrostatic in nature.[46]

TABLE VI. Magnetic moment values (μ_{eff}) of lanthanide(III) ions calculated by Hund and Van Vleck[4,22,43,47] and those obtained experimentally for the Ln(III) 4-chlorophenoxyacetates of at room temperature

Trivalent ion	Configuration	μ_{eff}/μ_B		
		Calculated by Hund	Calculated by Van Vleck	Experimental
Pr	f^2	3.58	3.62	3.26
Sm	f^5	0.84	1.55–1.65	1.56
Eu	f^6	0.00	3.40–3.51	3.08
Tb	f^8	9.70	9.70	9.44
Dy	f^9	10.60	10.60	10.69
Er	f^{11}	9.60	9.60	9.74
Tm	f^{12}	7.60	7.60	8.14
Yb	f^{13}	4.50	4.50	3.54

The magnetic properties of Er(III) were also studied over the temperature range of 1.8–300 K. Plots of magnetic susceptibility, χ_m^{-1}, and of the product $\chi_m T$ *vs.* T are shown in Fig. 3. The thermal dependence of χ_m^{-1} obeys the Curie–Weiss law over the whole temperature range. From the shape of the dependence of the $\chi_m T$ *vs.* T curve, it follows that it decreases on cooling in the range 303–1.8 K. Between 303 and 48 K, the decrease is very slow showing the saturation paramagnetic state, while the decrease is drastic between 48 and 1.8 K.

The value of $\chi_m T$ for Er(III) 2-(4-chlorophenoxy)acetate at room temperature was 11.28 $cm^3\ mol^{-1}$ K, which is similar to that calculated theoretically for the free Er(III) ion, 11.48 $cm^3\ mol^{-1}$ K.[4,47,48] At 1.8 K, the $\chi_m T$ value was 6.14 $cm^3\ mol^{-1}$ K. The decrease of the $\chi_m T$ *vs.* T curve in the range 48–1.8 K indicates a negative θ value, which may confirm antiferromagnetic intermolecular interactions. Therefore, the magnetic moment value of the Er(III) complex was equal to 7.01 (1.8 K) and 8.94 μ_B (48 K). Further, this value increases to 9.50 μ_B (303 K),

which is connected with the change in the unpaired electron order. This value is similar to that of the free Er(III) ion value (9.59 μ_B).[4,47]

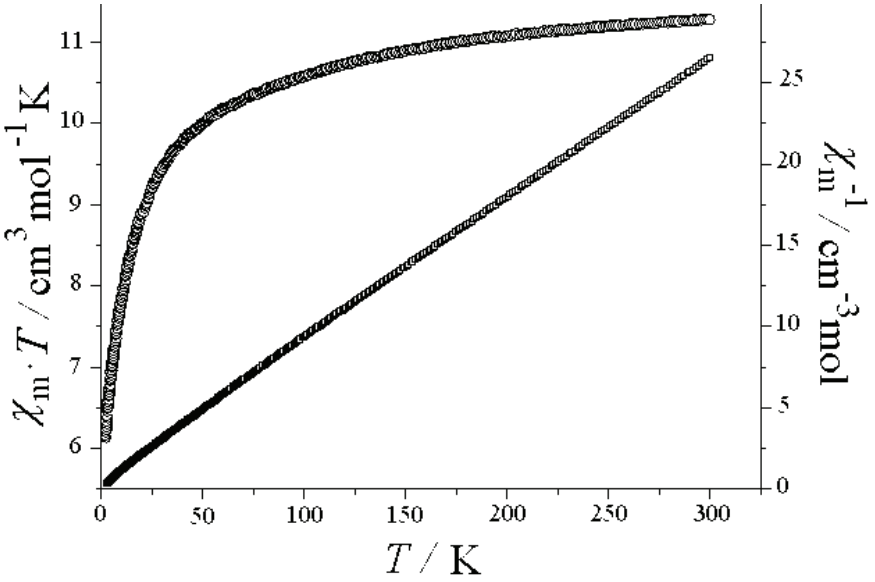

Fig. 3. Dependence of $\chi_m T$ (○) and χ_m^{-1} (□) *vs.* T for 2-(4-chlorophenoxy)acetate of Er(III).

CONCLUSIONS

From the obtained results, it follows that the lanthanide(III) 2-(4-chlorophenoxy)acetates were prepared as mono-, di- or trihydrates with colours typical for the respective Ln(III) ions, having their origin in the lowest energy f–f electronic transitions of the central ions. The Ln–O bonds are electrostatic in nature. The compounds are crystalline complexes that on heating in air to 1273 K decompose in three steps. In the first step, all 2-(4-chlorophenoxy)acetates dehydrate to form anhydrous complexes, which further decomposed to the oxides of the corresponding metal(III), with the intermediate formation of LnOCl. The values of μ_{eff} calculated for all compounds were close theoretically calculated by Hund and Van Vleck for Ln(III) ions. There was no influence of the ligand field on the 4f electrons of the lanthanide(III) ions. The solubility of 2-(4-chlorophenoxy)acetates of lanthanides(III) in water was of the order of 10^{-4} mol dm^{-3}.

The complexes of Nd(III), Gd(III) and Ho(III) ions with the 2-(4-chlorophenoxy)acetic acid anion are di- and trihydrates[14,15] and they exhibited properties similar to those of the complexes described in this paper. The Ln–O bonds were mainly electrostatic in nature. The complexes are crystalline compounds that on heating in air to 1173 K decompose in three steps. They dehydrate to form anhydrous complexes that further decompose to the oxides of the respective

metal, with the intermediate formation of LnOCl. The enthalpy values of dehydration processes were in the range 120.4–42.9 and 60.2–21.4 kJ mol^{-1} per one molecule of water. The values of μ_{eff} calculated for these compounds were similar to those calculated theoretically by Hund and Van Vleck for Ln(III) ions. Their solubilities in water at 293 K were of the order of 10^{-4} mol dm^{-3}.

И З В О Д

МАГНЕТНА, ТЕРМАЛНА И СПЕКТРОСКОПСКА СВОЈСТВА КОМПЛЕКСА ЛАНТАНИДА(III) СА 2-(4-ХЛОРОФЕНОКСИ)АЦЕТАТОМ, $Ln(C_8H_6ClO_3)_3 \cdot nH_2O$

WIESŁAWA FERENC[1], BEATA CRISTÓVÃO[1] и JAN SARZYŃSKI[2]

[1]*Faculty of Chemistry, Maria Curie-Skłodowska University, 20–031 Lublin, Poland и* [2]*Institute of Physics, Maria Curie-Skłodowska University, 20–031, Lublin, Poland*

Синтетисани су различити комплекси лантанида(III) са 2-(4-хлорофенокси)ацетатом као хидратисане поликристалне супстанце опште формуле: $Ln(C_8H_6ClO_3)_3 \cdot 2H_2O$ (Ln = La(III), Pr(III), Sm(III), Eu(III) или Tb(III)), $Ln(C_8H_6ClO_3)_3 \cdot H_2O$ (Ln = Dy(III)) и $Ln(C_8H_6ClO_3)_3 \cdot 3H_2O$ (Ln = Er(III), Tm(III), Yb(III) или Lu(III)). За карактеризацију ових комплекса употребљени су елементална микроанализа, FTIR спектроскопија, магнетна и термогравиметријска мерења, као и метода дифракције рендгенских зрака (XRD). Боја комплекса је карактеристична за лантанид(III) јоне, а карбоксилатне групе у овим комплексима су бидентатно координоване. Загревањем на температури од 1273 K у атмосфери ваздуха комплекси се разграђују у три фазе. У првој фази комплекси губе кристалну воду, док се у следећој фази разлажу до оксида одговарајућих метала, чему претходи грађење одговарајућих оксихлорида као интермедијарних производа. Магнетна мерења су вршена у опсегу 76–303 K и 1,8–303 K и израчунате су вредности магнетних момената. Нађено је да 2-(4-хлорофенокси)ацетати са лантанидима граде високоспинске комплексе слабог лигандног поља.

(Примљено 3. децембра 2012, ревидирано 6. априла 2013)

REFERENCES

1. R. C. Mehrotra, R. Bohra, *Metal Carboxylates*, Academic Press, London, 1983
2. R. L. Martin, in *New Pathways in Inorganic Chemistry*, E. A. V. Ebsworth, A. G. Maddock, A. G. Sharpe, Eds., Cambridge University Press, Cambridge, 1968, Ch. 9
3. Ch. J. O'Connor, *Progress in Inorganic Chemistry*, Wiley, New York, 1982
4. O. Kahn, *Molecular Magnetism*, VCH Publisher, New York, 1993
5. K. Nakamoto, *Infrared and Raman Spectra of Inorganic and Coordination Compounds*, Wiley, Toronto, 1997
6. G. Liu, X. Li, X. Ren, *J. Rare Earths* **29** (2011) 511
7. G. R. Desiraju, *Angew. Chem. Int. Ed.* **34 (**1995) 2311
8. N. Ishikawa, M. Sugita, W. Wernsdorfer, *Angew. Chem. Int. Ed.* **44** (2005) 2931
9. N. Ishikawa, M. Sugita, N. Tanaka, T. Ishikawa, S. Koshihara, Y. Kaizu, *Inorg. Chem.* **43** (2004) 5498

10. N. Ishikawa, M. Sugita, T. Ishikawa, S. Koshihara, Y. Kaizu, *J. Phys. Chem., B* **108** (2004) 11265
11. J. Q. Liu, Y. Y. Wang, L. F. Ma, W. H. Zhang, X. R. Zeng, F. Zang, Q. Z. Shi, S. M. Peng, *Inorg. Chim. Acta* **361** (2008) 173
12. N. Ishikawa, M. Sugita, T. Ishikawa, Y. Kaizu, *J. Am. Chem. Soc.* **125** (2003) 8694
13. R. Świsłocka, M. Kalinowska, W. Ferenc, J. Sarzyński, W. Lewandowski, *Cent. Eur. J. Chem.* **10** (2012) 1095
14. W. Ferenc, M. Bernat, J. Sarzyński, H. Głuchowska, *Ecl. Quim.* **33** (2010) 67
15. W. Ferenc, M. Bernat, J. Sarzyński, B. Paszkowska, *Ecl. Quim.* **33** (2008) 7
16. M. Franzini, L. Leoni, M. Saitta, *X-Ray Spectrom.* **1** (1972)151
17. Z. Bojarski, *Krystalografia*, PWN, Warszawa, 2007
18. B. N. Figgis R. S. Nyholm, *J. Chem. Soc.* (1958) 4190
19. D. Glotzel, B. Segall, O.K. Anderson, *Solid State Commun.* **36** (1980)403
20. W. Ferenc, B. Bocian, D. Mazur, *Croat. Chem. Acta* **72** (1999) 779
21. R. M. Silverstein, G. C. Bassler, T. C. Morrill, *Spectrometric Identification of Organic Compounds*, Wiley, New York, 1991
22. K. Burger, *Coordination Chemistry: Experimental Methods*, Akadémiai Kiadó, Budapest, 1973
23. W. Lewandowski, H. Barańska, *Vibr. Spectr.* **2** (1991) 211
24. W. Lewandowski, *J. Mol. Struct.* **101** (1983) 79
25. E. Pretsch, T. Clerc, J. Seibl, W. Simon, *Tables of Spectral Data for Structure Determination of Organic Compounds*, Springer, Berlin, 1989
26. L. J. Bellamy, *The Infrared Spectra of Complex Molecules*, Chapman & Hall, London, 1975
27. G. Varsányi, *Assignments for Vibrational Spectra of 700 Benzene Derivatives*, Akadémiai Kiadó, Budapest, 1973
28. R. Łyszczek, *J. Therm. Anal. Calorim.* **108** (2012)1101
29. A. K. Bridson, *Inorganic Spectroscopic Methods*, Oxford University Press, New York, 1998
30. A. Cross, A. R. Jones, *An Introduction to Practical Infrared Spectroscopy*, Butterworths, London, 1969
31. B. S. Manhas, A. K Trikha, *J. Indian. Chem. Soc.* **59** (1982) 315
32. S. Xiao, J. Zang, X. Li, Q. Li, I. V. Ren, H. Li, *J. Rare Earths* **28 (**2010) 12
33. Z. Lei, K. Zhao, Y. Gu, X. Li, *J. Rare Earths* **29 (**2010) 303
34. G. B. Deacon, R. J. Philips, *Coord. Chem. Rev.* **33** (1980) 227
35. W. Brzyska, *Lanthanides and Actinides*, Scientific –Technical Publishers, Warsaw, 1996
36. B. Czajka, B. Bocian, W. Ferenc, *J. Therm. Anal. Calorim.* **67** (2002) 631
37. W. Ferenc, A. Dziewulska-Kulaczkowska, J. Sarzyński, B. Paszkowska, *J. Therm. Anal. Calorim.* **91** (2008) 285
38. W. Ferenc, B. Cristóvão, J. Sarzyński, H. Głuchowska, *J. Rare Earths* **30** (2012) 257
39. A. V. Nikolaev, V. A. Logvinienko, L. I. Myachina, *Thermal Analysis*, Academic Press, New York, 1969
40. F. Paulik, *Special Trends in Thermal Analysis*, Wiley, Chichester, 1995
41. T. Xu, X. Huang, *Fuel* **89** (2010) 2185
42. L. Tao, G. B. Zhao, *J. Hazard. Mater.* **175** (2010) 754
43. J. H. Van Vleck, *The Theory of Electronic and Magnetic Susceptibilities*, Oxford University Press, Oxford, 1932

44. S. F. A. Kettle, *Physical Inorganic Chemistry: A Coordination Chemistry Approach*, Oxford University Press, Oxford, 2000
45. A. Earnshaw, *Introduction to magnetochemistry*, Academic Press, New York, 1968
46. S. P. Sinha, *Systematic and Properties of the Lanthanides*, Reidel, Dordrecht, The Netherlands, 1983
47. C. Benelli, D. Gatteschi, *Chem. Rev.* **102** (2002) 2369
48. C. Meyer, B. J. Ruck, A. R. H. Preston, S. Granville, G. V. M. Williams, H. J. Trodahl, *J. Magn. Magn. Mater.* **322** (2010) 1973.

Journal of the Serbian Chemical Society
JSCS-info@shd.org.rs • www.shd.org.rs/JSCS
J. Serb. Chem. Soc. 78 (9) 1351–1357 (2013)
JSCS–4502
UDC 547.53+547.535:544.112:548.1.023:548.115
Original scientific paper

On benzenoid systems with a minimal number of inlets

ROBERTO CRUZ[1], IVAN GUTMAN[2,3*#] and JUAN RADA[1]

[1]Instituto de Matemáticas, Universidad de Antioquia, Medellín, Colombia, [2]Faculty of Science, University of Kragujevac, P. O. Box 60, 34000 Kragujevac, Serbia and [3]Department of Chemistry, Faculty of Science, King Abdulaziz University, Jeddah 21589, Saudi Arabia

(Received 18 February, revised 21 March 2013)

Abstract. Inlets are features on the perimeter of a benzenoid system that determine numerous of its electronic and topological properties. A class of large benzenoid systems is constructed, having a small number of inlets. It is shown that the minimal number of inlets in a benzenoid system with h hexagons is less than or equal to $\sqrt{3(h-1)}$.

Keywords: benzenoid molecule; benzenoid hydrocarbon; perimeter (of benzenoid system); hexagonal system; inlet; number of inlets.

INTRODUCTION

Recent experimental methods have made it possible to synthesize very large benzenoid molecules, sometimes referred to as "graphenes".[1–3] These have found unprecedented applications as organic materials for electronic and optoelectronic devices.[2,3] As large benzenoid systems have countless possible isomers,[4–6] it is a task of theoretical chemistry to help indicate those species that may possess interesting properties.

The fact that numerous electronic and topological properties of benzenoid systems are determined by the structural features on their perimeter was established a long time ago.[7–9] These features are shown in Fig. 1; their more precise definitions are given in the literature.[10] The total number of fissures, bays, coves and fjords in a benzenoid system B is called[11] its number of inlets and is denoted by $r = r(B)$.

By means of $r(B)$, several topological properties of B are directly determined. Thus, let B be a benzenoid molecule with n carbon atoms and h hexagons. If m_{ij} denotes the number of edges of the molecular graph of B, connecting vertices of degree i and j, then:[11]

* Corresponding author. E-mail: gutman@kg.ac.rs
# Serbian Chemical Society member.
doi: 10.2298/JSC130218033C

$$m_{22} = n - 2h - r + 2 \quad (1)$$

$$m_{23} = 2r \quad (2)$$

$$m_{33} = 3h - r - 3 \quad (3)$$

Recall that m_{22}, m_{23} and m_{33} are the number of carbon–carbon bonds of the type CH–CH, CH–C and C–C, respectively.[10]

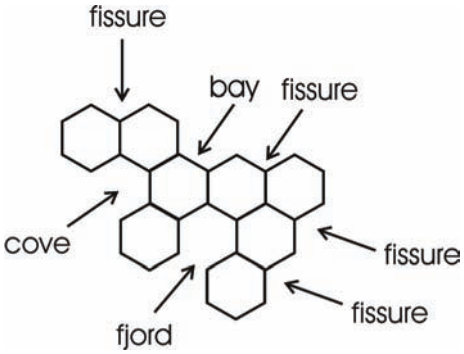

Fig. 1. Structural features on the perimeter of a benzenoid molecule.[10] The total number of fissures, bays, coves, and fjords is the number of inlets r. In this example, $r = 7$.

Equations (1)–(3) enable a large number of molecular structure descriptors of a benzenoid molecule to be expressed as a function of r. For instance:

$$GA(B) = n + h - 1 - \left(2 - \frac{4\sqrt{6}}{5}\right) r$$

$$ABC(B) = n + \left(\sqrt{8} - 2\right)(h - 1) + \frac{3 - \sqrt{8}}{3} r$$

$$H(B) = \frac{1}{2} n - \frac{1}{30} r$$

for the geometric–arithmetic,[12–14] atom–bond connectivity[15–17] and harmonic[18] indices, respectively; for more details see elsewhere.[11,19–23] Evidently, benzenoid molecules of a given size (*i.e.*, with fixed values of n and h), for which the number of inlets r is extremal (maximal or minimal), will possess extremal values of these structure descriptors and, therefore, may be expected to have extremal (or at least, outstanding) electronic and physicochemical properties. In this paper, the problem of constructing benzenoid systems with a minimal number of inlets and estimating its value as a function of h are considered.

The benzenoid system with maximal r-value is easy to characterize:[20] this is the linear acene with h hexagons, for which $r = r_{\max} = 2(h - 1)$. In Fig. 2 this is the benzenoid system denoted by R_{p1}, for which $h = p$.

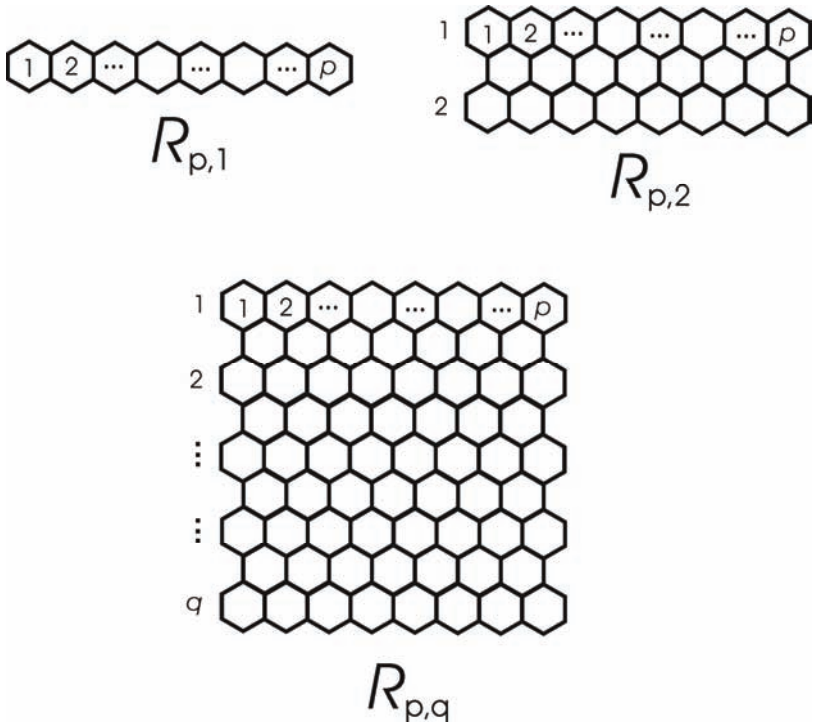

Fig. 2. Prolate rectangles,[24] consisting of $h(R_{pq}) = qp + (q-1)(p-1)$ hexagons. These possess $2(p-1)$ fissures and $2(q-1)$ bays, and thus, $r(R_{pq}) = 2(p-1) + 2(q-1)$ inlets.

CONSTRUCTING LARGE BENZENOID SYSTEMS WITH FEW INLETS

Consider the benzenoid systems R_{pq}, general formula of which is depicted in Fig. 2. These benzenoids are sometimes referred to[24] as "prolate rectangles".

As already pointed out, among the benzenoids with a fixed number of hexagons, the prolate rectangle with q = 1, namely R_{p1}, has the maximal number of inlets. First, one needs to observe that the transition from R_{p1} to R_{p2} (Fig. 2) almost triples the number of hexagons: $h(R_{p2}) = 3h(R_{p1}) - 1 = 3p - 1$, whereas the number of inlets is increased by only two: $r(R_{p2}) = r(R_{p1}) + 2 = 2p$. Continuing this rationale, one arrives at R_{pq} ; $q \geq 3$, for which:

$$h(R_{pq}) = 2pq - p - q + 1 \text{ and } r(R_{pq}) = 2p + 2q - 4$$

At this point, it is noteworthy that recent studies revealed that benzenoid systems of the form R_{p2} ; $p \geq 4$ possess unusual, "anomalous", π-electron[25,26] and magnetic[27] properties.

By means of the transformations indicated in Fig. 3, the number of hexagons was increased, but the *r*-value was decreased. Namely, by adding a new hexagon in a "dent" position, $R_{pq} \Rightarrow R'_{pq}$ (Fig. 3), the number of inlets was diminished by one. If p is even, then $p/2 - 1$ such "dents" could be added on the top of R_{pq}

(see R_{pq} in Fig. 3), and the same number on its bottom, a total of $p - 2$ "dents". By this, the number of hexagons was increased by $p - 2$, whereas the number of inlets was decreased by $p - 2$.

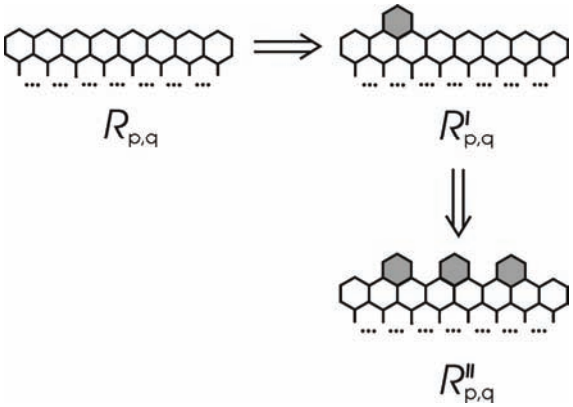

Fig. 3. Adding "dents" at the top (and bottom) of a prolate rectangle diminishes the number of inlets; for details, see text.

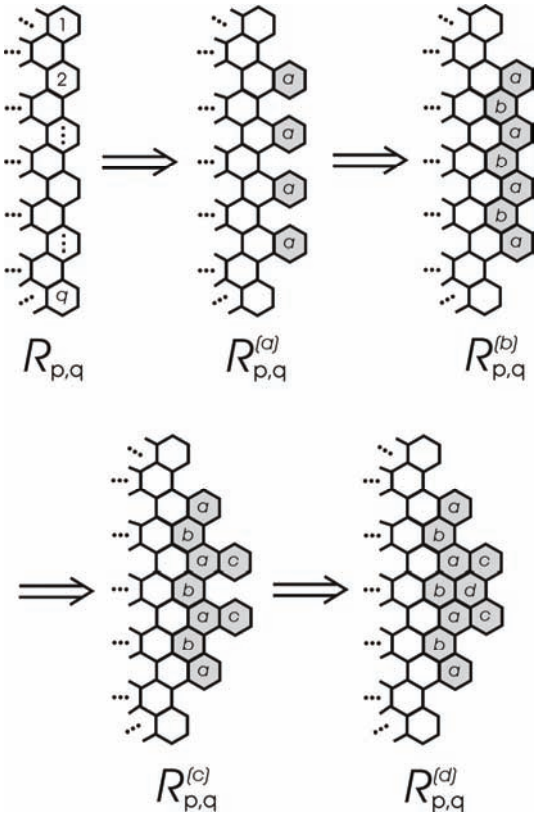

Fig. 4. Adding hexagons on to a prolate rectangle whereby the number of inlets remains the same.

A further series of transformations, indicated in Fig. 4, increases the number of hexagons, but leaves the number of inlets of R_{pq} unchanged.

First, $q-2$ hexagons are to be added to one side of R_{pq}, resulting in $R_{pq}^{(a)}$. Then an additional $q-3$ hexagons could be added, resulting in $R_{pq}^{(b)}$. Continuing this transformation, one arrives at $R_{pq}^{(c)}$, $R_{pq}^{(d)}$, *etc*. Thus:

$$(q-2)+(q-3)+\cdots+2+1=\frac{1}{2}(q-1)(q-2)$$

hexagons can be added on one side of R_{pq} without increasing its *r*-value. The same can also be realized on the other side of R_{pq}, and thus a total of $(q-1)(q-2)$ hexagons are added.

Combining the transformations indicated in Figs. 3 and 4, a class of benzenoid systems is arrived at, the general formula B_{pq} of which is shown in Fig. 5.

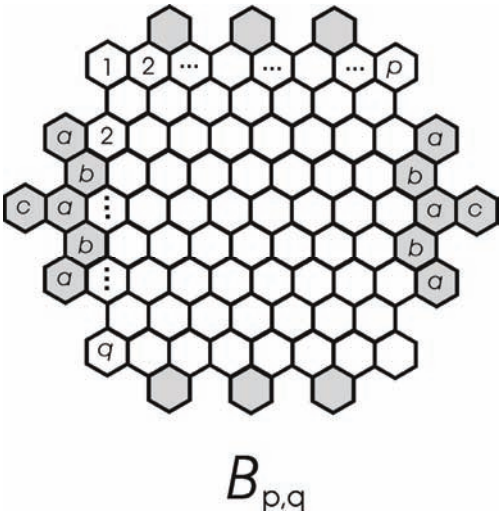

Fig. 5. A large benzenoid system with a small number of inlets. It has $h(R_{pq})+(p-2)+(q-1)(q-2)$ hexagons, but only $r(R_{pq})-(p-2)$ inlets, *cf*. Fig. 2.

By direct calculation (*cf*. Figs. 2 and 5), it could be shown that:

$$h(B_{pq})=2pq+q^2-4q+1 \text{ and } r(B_{pq})=p+2q-2$$

and B_{pq} may be considered as a candidate for a large benzenoid system, which for a given number of hexagons has the smallest number of inlets.

What remains is to choose the parameters *p* and *q*, in order to minimize the *r*-value for some fixed value of *h*. This is achieved by a standard Lagrange multiplier method, in which it is required that both derivatives:

$$\frac{\partial}{\partial p}\left[(p+2q-2)+\lambda\left(2pq+q^2-4q+1-h\right)\right]$$

and

$$\frac{\partial}{\partial q}\left[(p+2q-2)+\lambda\left(2pq+q^2-4q+1-h\right)\right]$$

are simultaneously equal to zero. This yields:

$$1+\lambda(2q)=0 \qquad \text{and} \qquad 2+\lambda(2p+2q-4)=0$$

which, by eliminating the multiplier λ, results in $q=p-2$. Consequently,

$$h=h(B_{p,p-2})=3p^2-12p+13 \tag{4}$$

and

$$r=r(B_{p,p-2})=3p-6 \tag{5}$$

Solving Eq. (4) in the parameter p, one obtains $p=2+\sqrt{(h-1)/3}$, which substituted back into Eq. (5) yields $r=\sqrt{3(h-1)}$.

CONCLUDING REMARKS

It has been shown how a large benzenoid system $B_{p,p-2}$ with h hexagons can be constructed, the number of inlets of which is only $\sqrt{3(h-1)}$. It was not proven that $B_{p,p-2}$ has the smallest possible number of inlets (for a given value of h), but – at least – it is deemed to be not too far from the true minimum. Nevertheless, what has been proven is that $r\le\sqrt{3(h-1)}$ for any benzenoid system with h hexagons. It is believed that this result could be useful in the design of graphenes with the desired properties.

И З В О Д

О БЕНЗЕНОИДНИМ СИСТЕМИМА СА МИНИМАЛНИМ БРОЈЕМ УСЕКА

ROBERTO CRUZ[1], ИВАН ГУТМАН[2,3] и JUAN RADA[1]

[1]Instituto de Matemáticas, Universidad de Antioquia, Medellín, Colombia, [2]Природно–математички факултет Универзитета у Крагујевцу и [3]Department of Chemistry, Faculty of Science, King Abdulaziz University, Jeddah 21589, Saudi Arabia

Усеци су структурни детаљи на периметру бензеноидног система који одређују његова бројна електронска и тополошка својства. Конструисана је класа великих бензеноидних система који имају мали број усека. Показано је да је минималан број усека бензеноидног система са h хексагона мањи од или једнак $\sqrt{3(h-1)}$.

(Примљено 18. фебруара, ревидирано 21. марта 2013)

REFERENCES

1. M. D. Watson, A. Fechtenkötter, K. Müllen, *Chem. Rev.* **101** (2001) 1267
2. J. Wu, A. Pisula, K. Müllen, *Chem. Rev.* **107** (2007) 718
3. T. M. Figueira-Duarte, K. Müllen, *Chem. Rev.* **111** (2011) 7260
4. G. Brinkmann, G. Caporossi, P. Hansen, *MATCH Commun. Math. Comput. Chem.* **43** (2001) 133
5. M. Vöge, A. J. Guttmann, I. Jensen, *J. Chem. Inf. Comput. Sci.* **42** (2002) 456

6. G. Brinkmann, C. Grothaus, I. Gutman, *J. Math. Chem.* **42** (2007) 909
7. K. Balasubramanian, J. J. Kauffman, W. S. Koski, A. T. Balaban, *J. Comput. Chem.* **1** (1980) 149
8. I. Gutman, G. G. Hall, S. Marković, Z. Stanković, V. Radivojević, *Polyc. Arom. Comp.* **2** (1991) 275
9. D. Babić, I. Gutman, *J. Math. Chem.* **9** (1992) 261
10. I. Gutman, S. J. Cyvin, *Introduction to the Theory of Benzenoid Hydrocarbons*, Springer, Berlin, 1989
11. J. Rada, O. Araujo, I. Gutman, *Croat. Chim. Acta* **74** (2001) 225
12. D. Vukičević, B. Furtula, *J. Math. Chem.* **46** (2010) 1369
13. M. Mogharrab, G. H. Fath-Tabar, *MATCH Commun. Math. Comput. Chem.* **65** (2011) 33
14. K. C. Das, I. Gutman, B. Furtula, *MATCH Commun. Math. Comput. Chem.* **65** (2011) 595
15. E. Estrada, L. Torres, L. Rodríguez, I. Gutman, *Indian J. Chem.* **37A** (1998) 849
16. E. Estrada, *Chem. Phys. Lett.* **463** (2008) 422
17. I. Gutman, J. Tošović, S. Radenković, S. Marković, *Indian J. Chem., A* **51** (2012) 690
18. L. Zhong, *Appl. Math. Lett.* **25** (2012) 561
19. J. Rada, *MATCH Commun. Math. Comput. Chem.* **52** (2004) 167
20. R. Cruz, I. Gutman, J. Rada, *MATCH Commun. Math. Comput. Chem.* **68** (2012) 97
21. I. Gutman, B. Furtula, *J. Serb. Chem. Soc.* **77** (2012) 1031
22. R. Cruz, H. Giraldo, J. Rada, *MATCH Commun. Math. Comput. Chem.* **70** (2013) 501
23. I. Gutman, J. Tošović, *J. Serb. Chem. Soc.* **78** (2013) 805
24. S. J. Cyvin, I. Gutman, *Kekulé Structures in Benzenoid Hydrocarbons*, Springer, Berlin, 1988
25. I. Gutman, J. Đurđević, Z. Matović, M. Marković, *J. Serb. Chem. Soc.* **77** (2012) 1401
26. I. Gutman, J. Đurđević, S. Radenković, Z. Matović, *Monatsh. Chem.* **143** (2012) 1649
27. S. Radenković, P. Bultinck, I. Gutman, J. Đurđević, *Chem. Phys. Lett.* **552** (2012) 151.

Journal of the Serbian Chemical Society
JSCS-info@shd.org.rs • www.shd.org.rs/JSCS
J. Serb. Chem. Soc. 78 (9) 1359–1372 (2013)
JSCS–4503
UDC 547.426.1+66.094.3+544.478+546.92:547.474.3:66.061
Original scientific paper

Selective liquid phase oxidation of glycerol to glyceric acid over novel supported Pt catalysts

ELINA SPROGE[1]*, SVETLANA CHORNAJA[1], KONSTANTINS DUBENCOVS[1], SVETLANA ZHIZHKUN[1], VALDIS KAMPARS[1], VERA SERGA[2], LIDIJA KULIKOVA[2] and ERIKS PALCEVSKIS[2]

[1] *Faculty of Material Science and Applied Chemistry, Riga Technical University, Azenes Str. 14/24, Riga, LV-1048, Latvia and* [2] *Institute of Inorganic Chemistry, Riga Technical University, Miera str. 34, Salaspils, LV-2169, Latvia*

(Received 3 December 2012, revised 26 February 2013)

Abstract: Several supported platinum catalysts were prepared by the extractive–pyrolytic method for the selective production of glyceric acid from glycerol. Al_2O_3, Y_2O_3, Lu_2O_3, ZrO_2–Y_2O_3 TiO_2, SG, Fe_2O_3, γ-AlO(OH) and C were used as the catalyst supports. Glycerol oxidation was performed in alkaline solutions and oxygen was used as the oxidant. The optimal catalyst preparation parameters and glycerol oxidation conditions to obtain glyceric acid were determined. The best result (57 % selectivity to glyceric acid with 92 % glycerol conversion) was achieved on a 4.8 % Pt/Al_2O_3 catalyst.

Keywords: glycerol oxidation; supported platinum catalysts; glyceric acid; extractive–pyrolytic method.

INTRODUCTION

Glycerol, which is potentially a valuable building block, is obtained as a by-product in the production of biodiesel. Glycerol is produced in large amounts during the transesterification of fatty acids into biodiesel – its yield can reach approximately 10 %.[1,2] In recent years, because of increasing biodiesel production, glycerol utilization has become a significant problem. The possibilities of glycerol transformation into useful compounds,[1–28] materials,[5,29–31] or energy sources[5,32–34] are being investigated. With green chemistry and environmentally friendly manufacturing in mind, the selective oxidation of glycerol using supported noble metal catalysts has attracted much attention. Liquid phase oxidation of glycerol with oxygen or air over heterogeneous Pt, Pd or Au catalysts affords many important compounds – glyceric acid (GLYA), lactic acid (LACT), tartronic acid (TART), glycolic acid (GLYC), dihydroxyacetone (DIHA), glyceral-

* Corresponding author. E-mail: Elina.Sproge@rtu.lv
doi: 10.2298/JSC121203037S

dehyde (GLYAD), *etc*.[1,6–12,14–26] Glyceric acid and its derivatives are important compounds as raw materials for chemical products, such as bioplastics, pharmaceuticals for acceleration of alcohol metabolism or liver disease treatment and cosmetics.[3,9,11]

Most of the studies concerning the heterogeneous oxidation of glycerol were dedicated to the selective oxidation of glycerol over supported gold catalysts using oxygen as the oxidant.[12–14] Gold catalysts are very selective to glyceric acid. Using an Au/C catalyst, Carretin *et al*. reported a selectivity to glyceric acid of 100 % at a glycerol conversion of 56 %.[14] For gold catalysts, many supports have been investigated, *i.e*., carbon materials, several metal oxides and polymers.[8,15,16] The main drawback of gold catalysts is that they are active only in the presence of base, whereas platinum catalysts work in basic, acidic and neutral conditions.[17–19]

Liang *et al*.[6] reported that multi-wall carbon nanotubes (MWNT)-supported Pt catalysts were more active and selective than Pt/activated carbon (AC) catalysts, but this type of support is expensive and the preparation of catalyst is complicated, so in further studies, the authors returned to activated carbon. Liang *et al*. compared glycerol oxidation over 5 % Pt/MWNT catalyst under alkaline and base-free conditions.[8] The 5 % Pt/MWNT catalyst in a base-free aqueous solution was more selective to glyceric acid (68 %) at the same glycerol conversion (90 %). The authors also concluded that the activity and selectivity to glyceric acid increased with decreasing particle size of the carbon support (from 253 to 9 μm). The most active were catalysts with a Pt particle size of less than 6 nm.[1,6,8]

A general drawback of platinum-containing catalysts is poisoning with molecular oxygen and deactivation. Therefore, Pt catalysts are used in oxidation processes at low partial pressures of oxygen or the platinum is alloyed with gold, thereby allowing higher oxygen partial pressures. Prati *et al*.[20–23] reported that in the alkaline solutions at 3 atm bimetallic Pt–Au/C catalysts were more active and selective to glyceric acid compared with Pt/C catalysts. For example, in the presence of 1 %Pt–Au/C, the glycerol conversion was 46 % higher than in the presence of 1 %Pt/C and the selectivity to glyceric acid was increased by 13 %.[22]

It is obvious that during the past years, many authors dedicated their time to the investigation of glycerol oxidation only in base-free solutions because these, together with recyclable catalysts, are the environmentally friendly route.[1,8,23–25]

Since 1993, when Kimura *et al*.[17] reported glycerol oxidation over Pt/C, mainly carbon material supports have been studied for monometallic Pt catalysts, *i.e*., activated carbon, graphite and MWNT. Recently, several authors reported about selective glycerol oxidation over bimetallic Au–Pt catalysts supported on MgO, $Mg(OH)_2$,[35,36] H-mordenite[37] and Al_2O_3.[38] The preparations of Pt catalysts are based on 3 methods – impregnation, immobilization and ion

exchange.[1,6,8,11,18] Recently, a new extractive–pyrolytic method was described[39] for the preparation of a fine-disperse platinum coating on nanopowder supports, such as Al_2O_3, γ-AlO(OH), Y_2O_3, CeO_2 and SiO_2. It was determined that the Pt particles were spherical and depending on the nature of the supports nature and parameters for the preparation of the catalyst, the sizes of the Pt crystallites range from 5 to 35 nm.

Herein, the results of an investigation of glycerol oxidation by molecular oxygen over novel Pt catalysts to obtain glyceric acid are reported. The catalysts were prepared by the new extractive–pyrolytic method and Al_2O_3, Y_2O_3, Lu_2O_3, ZrO_2–Y_2O_3 TiO_2, silica gel (SG), Fe_2O_3, γ-AlO(OH) and AC were used as the supports.

EXPERIMENTAL

Materials

The following reagents were used for the preparation of the catalysts precursors: platinum powder (99.99 %; Sigma–Aldrich), HCl (35 %; Lachema); HNO_3 (65 %; Lachema), trioctylamine ($(C_8H_{17})_3N$) (95 %; Fluka) and toluene (analytical grade; Stanchem). For the synthesis of the catalysts, several powders were used as supports – Al_2O_3 and Y_2O_3 (nanopowders of aluminium and yttrium oxide obtained in plasma by procedure described in the literature[39]), ZrO_2–Y_2O_3 (nanopowder of zirconium oxide (86 %), which was stabilized with yttrium oxide (14 %) and prepared by a literature procedure[40]), Fe_2O_3 (nanopowder of iron (III) oxide prepared by the extractive–pyrolytic method described in the literature[41]), TiO_2 (nanopowder of titanium dioxide prepared by the sol–gel method described previously[42]), Lu_2O_3 nanopowder (Sigma–Aldrich), γ-AlO(OH) nanopowder (boehmite, PURAL® SB, Sasol, Germany); γ-Al_2O_3 (nanopowder of aluminium oxide obtained in burning commercial γ-AlO(OH), C (Norit®, Sigma–Aldrich), SG – silica gel obtained through sol–gel technology from S. I. Vavilov State Optical Institute (St. Petersburg, Russia)[43]. Glycerol (≥98 %; Fluka), NaOH (reagent grade, Sigma–Aldrich) and oxygen (98 %; AGA SIA) were used in the glycerol oxidation experiments. H_2SO_4 (95–98 %; Sigma–Aldrich) was used in the samples of the reaction mixture preparation and analysis. For the identification of the glycerol oxidation, several possible products were used: DL-glyceraldehyde dimer (≥97 %; Aldrich), 1,3-dihydroxyacetone dimer (≥97 %; Aldrich), glyceric acid calcium salt hydrate (≥99 %; Fluka), sodium β–hydroxypyruvate hydrate (≥97 %; Fluka), lithium lactate (≥97 %; Fluka), tartronic acid (≥98 %; Alfa Aesar), sodium mesoxalate monohydrate (≥98 %; Aldrich), glycolic acid (≥99 %; Acros Organics), glyoxylic acid monohydrate (≥98 %; Aldrich), oxalic acid (98 %; Aldrich), acetate standard for IC (1.000 g L^{-1}; Fluka) and formate standard for IC (1.000 g L^{-1}; Fluka).

Catalyst preparation and characterization

Supported platinum catalysts were prepared by the extractive–pyrolytic method.[39,44]. In order to obtain platinum-containing organic extracts by the liquid extraction method, chloroplatinic acid (H_2PtCl_6) solution in hydrochloric acid (2 M HCl) was added to the trioctylamine ($(C_8H_{17})_3N$) solution in toluene. After shaking the mixture for 3 min, the organic phase was separated from the aqueous phase and filtered. The analysis of the aqueous solution after extraction using a Hitachi 180-50 atomic absorption spectrometer evidenced that the platinum had been completely extracted into the organic phase. The obtained organic phase, which was a solution of $[(C_8H_{17})_3NH]_2PtCl_6$ in toluene, is a precursor. The precursor was added to the

support. Alkylammonium salts are typical cationic surfactants and wet properly surfaces of different nature.[45] To uniformly distribute the precursor over the carrier surface, the mixture was thoroughly stirred, then dried to remove the solvent and calcinated. In the preparation of the catalyst, several parameters, *i.e.*, the concentration of the precursor (0.016–0.4 M), impregnation time of the supports with the precursor (5–180 min), the temperature and time of drying (18–110 °C and 3–120 min, respectively) and the temperature and time of calcination (300–500 °C and 5–120 min, respectively), were varied.

Example of catalyst precursor preparation. To 48.25 mL of 1 M trioctylamine solution in toluene, 38.7 mL of 0.5 M chloroplatinic acid solution in 2 M HCl was added. After shaking the mixture for 3 min, organic phase was separated and filtrated. During extraction, the precursor, which was a 0.4 M solution of $[(C_8H_{17})NH]_2PtCl_6$ in toluene was formed.

Example of 2.4 % Pt/Al_2O_3 catalyst preparation. To 1.0 g Al_2O_3 powder, 0.32 mL of a 0.4 M precursor solution was added. The obtained mixture was stirred until the support had been completely impregnated with precursor and then dried for 5 min at a temperature between 80–100 °C. After drying, the mixture was heated at a rate of 10 °C min^{-1} and calcinated at 300 °C for 5 min under atmospheric pressure.

Catalyst characterization

The prepared catalysts were characterized by X-ray diffraction (XRD) analysis using a Bruker AXS D-8 Advance diffractometer with CuK_α radiation (λ = 1.5418 Å) over a wide range of Bragg angles ($10° < 2\theta < 75°$) at a scanning rate of 0.02° s^{-1} at room temperature. Specific surface area (*SSA*) of the powders was measured using HROM-3 chromatograph (Laboratorni Pristroje, Praha) at the liquid nitrogen temperature and calculated by the Brunauer–Emmett–Teller (BET) method.

Glycerol oxidation

The oxidation was performed at elevated temperatures using a thermostatted slurry bubble reactor (50 mL capacity), equipped with gas supply system. After the catalyst had been fed into the reactor, the desired amount of distilled water and an aqueous solution of glycerol were added. If necessary, an aqueous solution of NaOH was added to the reaction mixture. When the required temperature had been reached, the oxygen supply to the reactor was turned on (300 mL min^{-1}). Samples were removed periodically and analysed by high-performance liquid chromatograph (HPLC). Several glycerol oxidation process parameters like NaOH initial concentration (0–1.5 M), glycerol and platinum molar ratio (300–500 mol/mol) as well as oxidation temperature (50–65 °C) were varied.

Example of glycerol oxidation over 4.8 % Pt/Al_2O_3 catalyst in basic solution. Oxidation conditions: initial concentration of glycerol $c_0(C_3H_8O_3)$ = 0.3 mol dm^{-3}; initial concentration of sodium hydroxide c_0(NaOH) = 0.7 mol dm^{-3}; glycerol and platinum molar ratio $n(C_3H_8O_3)/n$(Pt) = 300; oxygen partial pressure p_{O_2} = 1 atm; oxidation temperature 60 °C. 0.0585 g of dry 4.8 % Pt/Al_2O_3 catalyst, 11.77 mL of distilled water and 1.13 mL of 3.99 M aqueous glycerol solution were added into the reactor on the thermostatted stage (10 min). After that an oxygen supply to the reactor was turned on (300 mL min^{-1}) and 2.10 mL of an aqueous 5.00 M NaOH solution was added.

Product analysis

Analysis of the reaction mixture was performed on a Waters 2487 HPLC instrument equipped with an ultraviolet (UV 210 nm) and a refractive index (RI) detector.

The reactants and the products were separated on an anion exclusion column (IC–PAK Ion–Exclusion 50 A, 7 μm (300 mm×7.8 mm)) maintained at 60 °C. The eluent was 2.5 mM

H_2SO_4 solution. Filtered samples of the reaction mixtures (20 μL) were diluted 50 times with eluent. The injection volume was 10 μL, and run time and eluent flow rate were set at 20 min and 0.6 mL min^{-1}, respectively. The possible products were identified by comparison with original samples.

RESULTS AND DISCUSSION

Influence of catalyst support and Pt loading on glycerol oxidation

Several products were obtained in the oxidation process, *i.e.*, glyceric acid, tartronic acid, lactic acid, glyceraldehyde, dihydroxyacetone, glycolic acid, oxalic acid and formic acid. The reaction pathways are presented in Scheme 1.

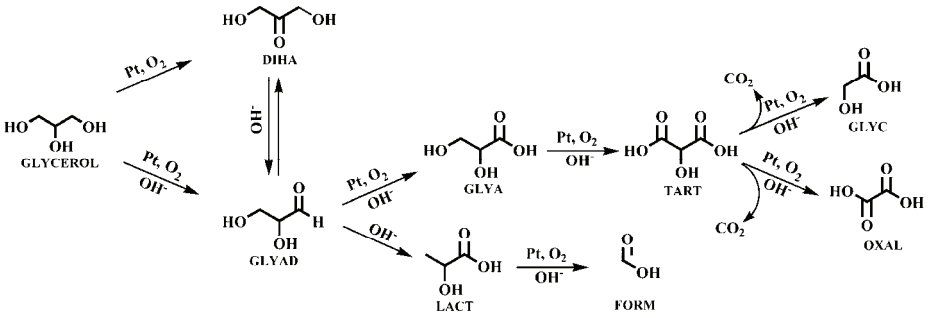

Scheme 1. Reaction pathway for glycerol oxidation in the presence of Pt-supported catalysts.

The results for the oxidation of glycerol over the different novel Pt catalysts are given in Table I. The activity of the catalysts was estimated by glycerol conversion. The most active catalysts with glycerol conversion above 83 % were 1.2 % Pt/Y_2O_3, $Pt/ZrO_2–Y_2O_3$, Pt/γ-Al_2O_3, 1.2 % Pt/SG, 4.8 % Pt/γ-AlO(OH) and 2.4 % Pt/Lu_2O_3. For almost all these catalysts, the Pt crystallite size d_{Pt} was less than 10 nm. As was reported previously,[39] X-ray diffraction analyses showed that with increasing Pt loading, the characteristic peak Pt(111) became more apparent. In the case of Pt loading less than 2.4 %, this Pt peak was almost fully overlapped by peaks arising from some of the supports, which makes the determination of the average crystallite size of the metal in the catalyst impossible. As was mentioned above, Liang *et al.*[1,6,8] who investigated the influence of Pt particle size on the activity and selectivity of Pt/C and Pt/MWNTs catalysts, concluded that catalysts with Pt particle sizes less than 6 nm were the most active. Simultaneously, the selectivity to glyceric acid gradually increased with increaseing size of the Pt particles. They considered that the lower activity of the larger-sized Pt particles was due to their lower metal surface area, which restricted the adsorption of substrate. In the study, the specific surface area (*SSA*) of the supports and catalysts, determined by the BET method, were different depending on the nature of the support. The data presented in Table I show that the carbon support (337 $m^2\ g^{-1}$) and the Pt catalysts on the carbon support (161–213 $m^2\ g^{-1}$) have the

TABLE I. Effect of the nature of the catalyst support and the platinum loading on glycerol conversion and oxidation product selectivity; reaction conditions: $c_0(C_3H_8O_3)$ = 0.3 M, c_0(NaOH) = 1.5 M, $n(C_3H_8O_3)/n$(Pt) = 300, T = 60 °C, p_{O_2} = 1 atm and reaction time = 7 h; Catalyst calcination temperature and time: 300 °C and 5 min, respectively

Catalyst support	Pt wt. %	d_{Pt} nm	SSA of catalyst $m^2\ g^{-1}$	SSA of support $m^2\ g^{-1}$	Glycerol conversion %	Selectivity, mol %					
						GLYA	TART	LACT	GLYC	OXAL	FORM
Al_2O_3	0.6	–	–	41	64	41	27	17	10	3	2
	1.2	–	41		69	51	17	16	12	2	2
	2.4	>15	42		69	49	9	24	13	2	3
	4.8	20	44		73	53	14	19	10	2	2
Y_2O_3	0.6	–	18	21	65	14	28	42	3	13	0
	1.2	–	16		88	38	11	42	6	2	1
	2.4	–	20		66	54	9	27	6	3	1
	4.8	7	–		70	50	8	30	8	2	2
ZrO_2–Y_2O_3	1.2	8	60	65	87	20	31	34	8	5	2
	2.4	10	58		91	39	22	24	10	3	2
	4.8	10	56		85	47	14	24	12	2	1
γ-Al_2O_3	1.2	–	105	122	87	19	40	25	7	8	1
	2.4	5	100		94	48	19	20	10	2	1
	4.8	10	102		89	46	17	22	11	3	1
C	1.2	–	213	337	49	62	6	19	11	2	0
	4.8	20	161		68	37	18	30	9	4	2
Lu_2O_3	2.4	–	14	16	84	44	13	28	12	2	1
	4.8	23	14		65	55	11	20	11	2	1
Fe_2O_3	2.4	–	34	39	31	37	2	0	60	1	0
	4.8	8	30		56	36	2	8	53	1	0
SG	1.2	9	51	51	93	35	23	25	9	4	4
	2.4	12	56		58	36	22	26	9	3	4
TiO_2	4.8	25	66	135	76	62	7	19	8	2	2
γ-AlO(OH)	4.8	5	115	146	83	47	19	18	11	3	1

largest surface areas. However, catalysts of this type were less active than catalysts with Y_2O_3, ZrO_2–Y_2O_3, γ-Al_2O_3, SG, γ-AlO(OH) and Lu_2O_3 as supports. It was shown in earlier investigations of glycerol oxidation in the presence of gold catalysts supported on different carbons,[46,47] CeO_2,[48] Nb_2O_5, V_2O_5, Ta_2O_5 and Al_2O_3[46] that there was no direct dependency between specific surface area of the support and the catalytic properties of gold. The results presented in Table I confirm this statement. For example, the glycerol conversions with the 4.8 % Pt/ZrO_2–Y_2O_3 and 4.8 % Pt/γ-Al_2O_3 catalysts, having d_{Pt} =10 nm, are the same (85–89 %) but the specific surface areas of the supports and catalysts differ two-fold. Moreover, the activities of the 4.8 % Pt/Al_2O_3 and 4.8 % Pt/Y_2O_3 catalysts were similar, but the d_{Pt} of the 4.8 % Pt/Al_2O_3 catalyst was 3 times greater and the SSA of the support was 2 times greater than the corresponding values for the 4.8 % Pt/Y_2O_3 catalyst.

The data in Table I show that depending on the nature of the catalyst support and the loading of Pt on the support, glyceric acid, lactic acid, tartronic acid or glycolic acid were produced as the main product. It is visible from Table I that in the presence of catalysts with Al_2O_3, Lu_2O_3, TiO_2, SG, γ-AlO(OH) and C as supports, glyceric acid was the main product regardless of the Pt loading. The Pt/Fe_2O_3 catalyst was selective to glycolic acid. When Y_2O_3, ZrO_2–Y_2O_3 and γ-Al_2O_3 were used as supports, the selectivity of the catalyst was dependent on the Pt loading. If the Pt loading was 2.4–4.8 %, the main product of glycerol oxidation was glyceric acid. Decreasing the Pt content in the catalyst from 2.4 to 0.6 % led to changes in the main product of the reaction. Over the 0.6–1.2 % Pt/Y_2O_3 catalyst, the main product was lactic acid with a selectivity of 42 %, but the 1.2 % Pt/γ-Al_2O_3 catalyst was the most selective to tartronic acid (40 %). 1.2 % Pt/(ZrO_2–Y_2O_3) catalyst was not selective; the amounts of formed glyceric, tartronic and lactic acids were similar.

It could be concluded from Table I that the most effective Pt catalysts to produce glyceric acid are Pt/TiO_2, Pt/Al_2O_3, Pt/Y_2O_3, Pt/Lu_2O_3, Pt/ZrO_2–Y_2O_3 and Pt/γ-Al_2O_3. The catalysts with a Pt loading of 2.4–4.8 % were both active (glycerol conversion for these catalysts was 65–94 %) and selective to glyceric acid (39–62 %). The Pt/Al_2O_3 and Pt/Y_2O_3 catalysts were used in the further investigation to determine how the catalyst preparation and glycerol oxidation parameters affect the activity and selectivity of the catalysts.

Effect of the catalyst preparation parameters on the activity and selectivity of the catalyst

The experiment results showed that some catalyst preparation parameters, such as concentration of precursor, impregnation time of the supports with the precursor, temperature and drying time did not significantly influence the activity and selectivity of the catalyst. In the further investigation these preparation para-

meters were kept constant: concentration of precursor 0.4 M, support impregnation time with precursor 10 min, temperature and drying time 80–100 °C and 10 min, respectively. The calcination temperature and time considerably influenced the activity and selectivity of the catalyst, as given in Table II.

TABLE II. Effect of catalysts calcination temperature on glycerol conversion and oxidation product selectivity; reaction conditions: $c_0(C_3H_8O_3)$ = 0.3 mol dm^{-3}, c_0(NaOH) = 1.5 mol dm^{-3}, $n(C_3H_8O_3)/n$(Pt) = 300, T = 60 °C, p_{O_2} = 1 atm and reaction time = 7 h; Pt catalyst calcination time = 5 min

Catalyst	Calcination temperature, °C	Glycerol conversion, %	Selectivity, %					
			GLYA	TART	LACT	GLYC	OXAL	FORM
1.2 % Pt/Al_2O_3	300	69	51	17	16	12	1	3
	400	54	7	26	57	0	6	4
	500	61	18	23	49	0	4	6
2.4 % Pt/Al_2O_3	300	69	50	9	24	13	1	3
	400	56	6	26	57	0	6	5
	500	54	20	14	58	0	2	6
4.8 % Pt/Al_2O_3	300	75	53	13	19	10	3	2
	400	16	15	2	65	15	0	3
	500	22	15	3	67	12	0	3
1.2 % Pt/Y_2O_3	300	88	38	11	42	6	2	1
	400	87	8	18	62	6	5	1
	500	85	10	16	62	6	5	1
2.4 % Pt/Y_2O_3	300	66	54	9	27	6	3	1
	400	59	12	29	49	0	6	4
	500	87	25	15	48	8	3	1

From Table II it is visible that the 4.8 % Pt/Al_2O_3 catalyst prepared with a calcination temperature of 300 °C demonstrated the highest activity and selectivity to glyceric acid. On increasing the catalyst calcination temperature from 300 to 500 °C, the glycerol conversion for the 4.8 % Pt/Al_2O_3 catalyst decreased from 75 to 22 % and the selectivity to glyceric acid decreased from 53 to 15 %. Meanwhile, the selectivity to lactic acid rose from 19 to 67 %. The changes in the glycerol conversion in the presence of the 1.2–2.4 % Pt/Al_2O_3 catalysts were not so drastic (69–54 %) in comparison with those observed in the presence of the 4.8 % Pt/Al_2O_3 catalyst. The data presented in Table III showed the Pt/Al_2O_3 catalysts became more active when the catalyst calcination time was extended from 5 to 120 min. The glycerol conversion increased by 9–19 %. The selectivity of the 4.8 %Pt/Al_2O_3 catalyst to glyceric acid also increased from 53 to 59 % with increasing calcination time, but the 1.2–2.4 % Pt/Al_2O_3 catalysts became non-selective.

It can be seen from the data presented in Tables II and III that in the glycerol oxidation processes over the Pt/Y_2O_3 catalysts, the effect of calcination temperature and time on catalyst activity and selectivity was different and depended on

the Pt loading. Using the 1.2 % Pt/Y_2O_3 catalyst, the glycerol conversion was in the range from 83 to 88% and was independent of the temperature and time of calcination. The main product of the reaction was lactic acid and the selectivity increased with increasing temperature and time of calcination. The 1.2 % Pt/Y_2O_3 catalyst calcinated at 400–500 °C was the most selective catalyst to lactic acid (62 %, with a glycerol conversion of 85–87 %). In the presence of the 2.4 % Pt/Y_2O_3 catalyst, the main product obtained was glyceric acid and the glycerol conversion was higher when the catalyst was prepared with a calcination temperature of 300 °C and a calcination time of 120 min.

TABLE III. Effect of catalyst calcination time on glycerol conversion and oxidation product selectivity; reaction conditions: $c_0(C_3H_8O_3)$ = 0.3 mol dm^{-3}, c_0(NaOH) = 1.5 mol dm^{-3}, $n(C_3H_8O_3)/n$(Pt) = 300, T = 60 °C; p_{O_2} = 1 atm and reaction time = 7 h; Pt catalyst calcination temperature: 300 °C

Catalyst	Calcination time, °C	Glycerol conversion, %	Selectivity, %					
			GLYA	TART	LACT	GLYC	OXAL	FORM
1.2 %Pt/Al_2O_3	5	69	51	17	16	12	1	3
	30	86	26	27	29	11	7	0
	120	88	27	31	24	11	6	1
2.4 %Pt/Al_2O_3	5	69	50	9	24	13	1	3
	30	89	36	20	28	12	3	1
	120	88	35	21	29	11	3	1
4.8 %Pt/Al_2O_3	5	73	53	14	19	10	2	2
	120	82	59	10	20	7	1	3
1.2 %Pt/Y_2O_3	5	88	38	11	42	6	2	1
	30	83	18	25	43	8	5	1
	120	83	8	23	55	7	7	0
2.4 %Pt/Y_2O_3	5	66	54	9	27	6	3	1
	30	87	41	21	24	11	2	1
	120	84	46	14	27	10	2	1

By comparing the data presented in Tables II and III, it could be concluded that the most effective catalyst for glycerol oxidation to glyceric acid was the 4.8 % Pt/Al_2O_3 catalyst that had been calcinated at 300 °C for 120 min.

Effect of glycerol oxidation parameters on the glycerol conversion and oxidation selectivity in the presence of the 4.8 % Pt/Al_2O_3 catalyst

It was reported[23,49–51] that catalysts based on platinum group metals suffered oxygen poisoning proportional to the oxygen partial pressure. When using Pt catalysts, a low oxygen partial pressure must be applied to limit the rate of oxygen supply to the surface of such catalysts. Under these conditions, the oxidation process must be performed in the oxygen transport limited region when the temperature effect on the oxidation ratio is insignificant. To investigate influence of oxygen partial pressure on glycerol oxidation, experiments were performed under the following conditions: $c_0(C_3H_8O_3)$ = 0.3 mol dm^{-3};

TABLE IV. Glycerol oxidation; effect of p_{O_2}, $n(C_3H_8O_3)/n(Pt)$ and initial NaOH concentration; reaction conditions: T = 60 °C; reaction time, 7 h; catalyst: 4.8 % Pt/Al_2O_3; catalyst calcination temperature and time: 300 °C and 120 min, respectively

$n(C_3H_8O_3)/n(Pt)$	c_0(NaOH) mol dm^{-3}	Glycerol conversion %	Selectivity, %						
			GLYA	GLYAD	DIHA	TART	LACT	GLYC	OXAL	FORM
300	0.7	92	57	–	–	12	17	9	3	2
500		92	52	–	–	12	21	12	2	1
500[a]		44	55	–	–	3	29	10	2	1
500[b]		85	50	–	–	23	10	9	7	1
300	1.5	82	59	–	–	10	20	7	1	3
500		57	63	–	–	7	17	9	1	3
300	–	49	47	32	8	–	–	9	2	2

[a]p_{O_2} = 0.2 atm; [b]p_{O_2} = 3 atm

c_0(NaOH) = 0.7 mol dm^{-3}; $n(C_3H_8O_3)/n$(Pt) = 500. From the data presented in Table IV, it could be seen that the best result was attained when p_{O_2} = 1 atm was applied. The glycerol conversion increased by 7 % when the oxidation was realized at p_{O_2} = 3 atm in comparison with that at p_{O_2} = 1 atm. Moreover, it was found that with further oxidation, the glycerol conversion did not change but the selectivity to glyceric acid decreased. It was impossible to reach a conversion above 45 % when glycerol was oxidised at p_{O_2} = 0.2 atm. Atmospheric oxygen pressure was used in the further studies on the effect of other oxidation parameters on glycerol conversion and oxidation selectivity.

Data from Table IV show that at p_{O_2} = 1 atm, a higher glycerol conversion of 92 % was reached when the initial concentration of NaOH was 0.7 M, which was not dependent on the $n(C_3H_8O_3)/n$(Pt) ratio. In a 1.5 M NaOH solution, the glycerol conversion decreased by 25 % if the $n(C_3H_8O_3)/n$(Pt) was increased from 300 to 500. Selectivity to the main product, glyceric acid, was similar and ranged from 52 to 59 % in both aqueous 0.7 and 1.5 M NaOH solutions when the glycerol conversion was 82–92 %, respectively. In addition, in the base-free solution, the glycerol conversion decreased noticeably to 49 % and the selectivity to glyceric acid decreased from 59–57 to 47 % with new products, such as glyceraldehyde and dihydroxyacetone, being formed. As was mentioned above, Liang *et al.*[8] reported that a 5 % Pt/MWNTs catalyst in a base-free aqueous solution was more selective to glyceric acid (68 %) at the same glycerol conversion (90 %). This apparent contradiction with the present results could be explained by an effect of the nature of the support on glycerol oxidation.

The influence of temperature on the oxidation rate of glycerol data is shown in Fig. 1, from which it could be seen that temperature had almost no effect.

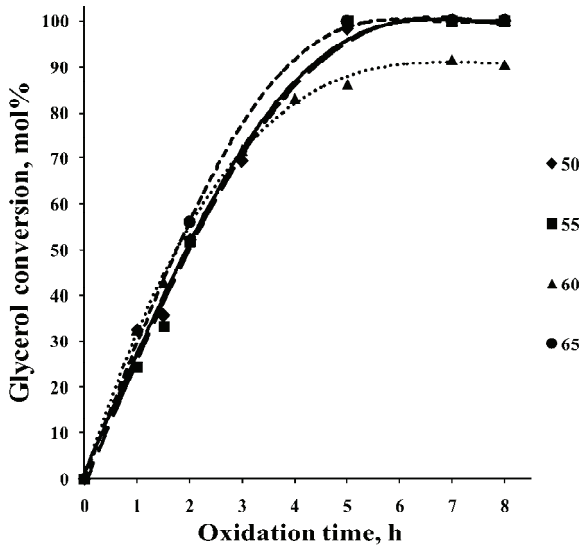

Fig. 1. Effect of temperature on glycerol oxidation over the 4.8 % Pt/Al_2O_3 catalyst. Reaction conditions: $c_0(C_3H_8O_3)$ = 0.3 mol dm^{-3}, c_0(NaOH) = 1.5 mol dm^{-3}, $n(C_3H_8O_3)/n$(Pt) = 300 and p_{O_2} = 1 atm.

The changes in selectivity to glyceric acid with oxidation time at different temperatures are shown in Fig. 2. Analyzing the data shown in Figs. 1 and 2, it could be concluded that at a glycerol conversion of 90 %, the selectivity to glyceric acid was similar (50–56 %) at 50–60 °C. At the higher temperature (65 °C), the selectivity to glyceric acid was only 40 % at the same glycerol conversion. It should be noted that only at 60 °C was the selectivity to glyceric acid higher and independent of glycerol conversion.

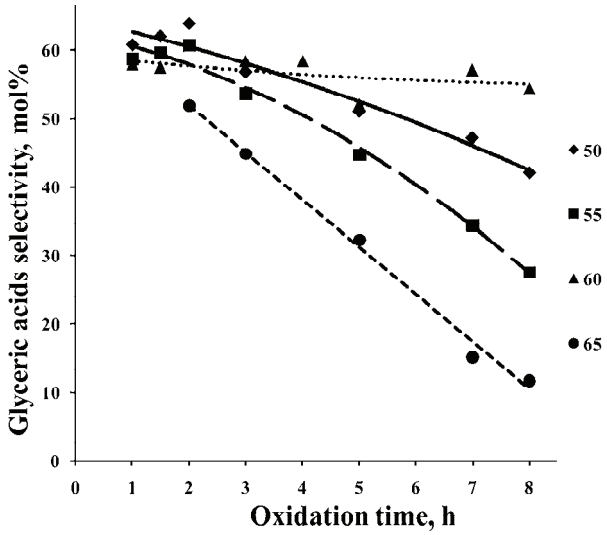

Fig. 2. Effect of temperature on the selectivity to glyceric acid during glycerol oxidation over the 4.8 % Pt/Al_2O_3 catalyst. Reaction conditions: $c_0(C_3H_8O_3)$ = 0.3 mol dm^{-3}, c_0(NaOH) = 1.5 mol dm^{-3}, $n(C_3H_8O_3)/n$(Pt) = 300 and p_{O_2} = 1 atm.

CONCLUSIONS

It was demonstrated that the extractive–pyrolytic method could be employed for the preparation of supported platinum catalysts for the selective oxidation of glycerol. By optimization of catalyst preparation and glycerol oxidation process parameters, the optimal conditions for the selective production of glyceric acid were found for the most effective novel 4.8 % Pt/Al_2O_3 catalyst to be: catalyst calcination temperature, 300 °C; calcination time, 120 min; $c_0(C_3H_8O_3)$, 0.3 mol dm^{-3}; c_0(NaOH), 0.7 mol dm^{-3}; $n(C_3H_8O_3)/n$(Pt), 300; temperature, 60 °C and P_{O_2}, 1 atm, when a glycerol conversion of 92 % and a selectivity to glyceric acid of 57 % were achieved..

Acknowledgment. This work was supported by the European Regional Development Fund – Project No. 2010/0304/2DP/2.1.1.1.0/10/APIA/VIAA/087.

ИЗВОД

СЕЛЕКТИВНА ОКСИДАЦИЈА ГЛИЦЕРОЛА ДО ГЛИЦЕРИНСКЕ КИСЕЛИНЕ У ТЕЧНОЈ ФАЗИ СА Pt КАТАЛИЗАТОРИМА

ELINA SPROGE[1], SVETLANA CHORNAJA[1], KONSTANTINS DUBENCOVS[1], SVETLANA ZHIZHKUN[1], VALDIS KAMPARS[1], VERA SERGA[2], LIDIJA KULIKOVA[2] и ERIKS PALCEVSKIS[2]

[1]Faculty of Material Science and Applied Chemistry, Riga Technical University, Azenes str 14/24, Riga, LV-1048, Latvia и [2]Institute of Inorganic Chemistry, Riga Technical University, Miera str 34, Salaspils, LV-2169, Latvia

Неколико чврстих Pt катализатора за селективно добијање глицеринске киселине из глицерола су припремљени поступком који је комбинација екстракције и пиролизе. Al_2O_3, Y_2O_3, Lu_2O_3, ZrO_2–Y_2O_3, TiO_2, SG, Fe_2O_3, γ-AlO(OH) и C су коришћени као носачи катализатора. Оксидација глицерола је вршена у алкалним растворима и кисеоник је коришћен као оксиданс. Одређени су оптимални параметри за припрему катализатора и услови оксидације глицерола при којим се добија глицеринска киселина. Најбољи резултат (селективност за глицеринску киселину 57 % са конверзијом глицерола 92 %) постигнут је у присуству катализатора 4,8 % Pt/Al_2O_3.

(Примљено 3. децембра 2012, ревидирано 26 фебрауара 2013)

REFERENCES

1. D. Liang, J. Gao, J. Wang, P. Chen, Z. Hou, X. Zheng, *Catal. Commun.* **10** (2009) 1586
2. A. B. Leoneti, V. Aragão-Leoneti, S. V. W. B. de Oliveira, *Renew. Energ.* **45** (2012) 138
3. H. Habe, *AIST Today* **34** (2009) 20
4. J. A. Posada, L. E. Rincón, C. A. Cardona, *Bioresour. Technol.* **111** (2012) 282
5. A. Crooks, *Rural Cooperatives* **74** (2007) 30
6. M. Zhang, D. Liang, R. Nie, X. Lu, P. Chen, Z. Hou, *Chin. J. Catal.* **33** (2012) 1340
7. Y. Shen, S. Zhang, H. Li, Y. Ren, H. Liu, *Chem. Eur. J.* **16** (2010) 7368
8. D. Liang, J. Gao, H. Sun, P. Chen, Z. Hou, X. Zheng, *Appl. Catal., B* **106** (2011) 423
9. E. S. Demirel-Gülen, M. Lucas, P. Claus, *Catal. Today* **102**–**103** (2005) 166
10. H. C. Liu, Y. H. Shen, H. J. Li, Beijing University, CN Patent, 101225041 (A) (2008)
11. R. Garcia, M. Besson, P. Gallezot, *Appl. Catal., A* **127** (1995) 165
12. N. Dimitratos, A. Villa, C. L. Bianchi, L. Prati, M. Makkee, *Appl. Catal., A* **311** (2006) 185
13. J. P. S. Fernández, M. E. Martins, G. A. Camara, *Electrochim. Acta* **66** (2012) 180
14. S. Carrettin, P. McMorn, P. Johnston, K. Griffin, G. J. Hutchings, *Chem. Commun.* **7** (2002) 696
15. S. Gil, M. Marchena, L. Sánchez-Silva, A. Romero, P. Sánchez, J. L. Valverde, *Chem. Eng. J.* **178** (2011) 423
16. A. Villa, C. E. Chan-Thawb, L. Prati, *Appl. Catal., B* **96** (2010) 541
17. H. Kimura, K. Tsuto, T. Wakisaka, Y. Kazumi, Y. Inaya, *Appl. Catal., A* **96** (1993) 217
18. P. Fordham, R. Garcia, M. Besson, P. Gallezot, *Stud. Surf. Sci. Catal.* **101** (1996) 161
19. R. Garcia, M. Besson, P. Gallezot, *Appl. Catal., A* **127** (1995) 165
20. N. Dimitratos, C. Messi, F. Porta, L. Prati, A. Villa, *J. Mol. Cat., A* **256** (2006) 21
21. C. L. Bianchi, P. Canton, N. Dimitratos, F. Porta, L. Prati, *Catal. Today* **102**–**103** (2005) 203
22. L. Prati, A. Villa, C. Campione, P. Spontoni, *Top. Catal.* **44** (2007) 319
23. L. Prati, P. Spontoni, A. Gaiassi, *Top. Catal.* **52** (2009) 288
24. D. Liang, A. Cui, J. Gao, J. Wang, P. Chen, Z. Hou, *Chin. J. Catal.* **32** (2011) 1831
25. R. Nie, D. Liang, L. Shen, J. Gao, P. Chen, Z. Hou, *Appl. Catal., B* **30** (2012) 212

26. N. Pachauri, B. He, in *Proceedings of ASABE Annual International Meeting*, Portland, OR, 2006
27. K. Wang, M. C. Hawley, S. J. De Athos, *Ind. Eng. Chem. Res*. **42** (2003) 2913
28. F. Jerome, Y. Pouilloux, J. Barrault, *ChemSusChem*. **1** (2008) 586
29. D. S. Rosa, M. A. G. Bardi, L. D. B. Machado, D. B. Dias, L. G. A. Silva, Y. Kodama, *J. Therm. Anal. Calorim.* **102** (2010) 181
30. F. Villamagna, B. D. Hall, BioEnergy Systems, LLC, US Patent, 20080245450 (2008)
31. C. A. Sundback, J. Y. Shyu, Y. Wang, W. C. Faquin, R. S. Langer, J. P. Vacanti, T. A. Hadlock, *Biomaterials* **27** (2005) 5454
32. S. Brady, K. Tam, G. Leung, C. Salam, *Undergraduate Res. J. Univ. California Riverside* **2** (2007) 1
33. A. Demirbas, *Energy Convers. Manage*. **43** (2002) 2349
34. T. Ito, Y. Nakashimada, S. Koichiro, T. Matsui, N. Nishio, *J. Biosci. Bioeng*. **100** (2005) 260
35. G. L. Brett, Q. He, P. J. Miedziak, N. Dimitratos, M. Conte, C. J. Kiely, D. W. Knight, S. H. Taylor, G. J. Hutchings, in *Proceedings of 15th International Congress on Catalysis* Munich, Germany, 2012
36. G. L. Brett, Q. He, C. Hammond, P. J. Miedziak, N. Dimitratos, M. Sankar, A. A. Herzing, M. Conte, J. A. Lopez-Sanchez, C. J. Kiely, D. W. Knight, S. H. Taylor, G. J. Hutchings, *Angew. Chem. Int. Ed*. **50** (2011) 10136
37. A. Villa, G. M. Veith, L. Prati, *Angew. Chem. Int. Ed*. **49** (2010) 4499
38. M. Royker, J. Case, E. van Steen, *J. South Afr. Inst. Min. Metall., A* **7** (2012) 577
39. V. Serga, L. Kulikova, A. Cvetkov, A. Krumina, *IOP Conf. Ser.* **38** (2012) 012062(1)
40. L. Kuznetsova, J. Grabis, G. Heidemane, *Latvian J. Chem.* **1** (2003) 52
41. V. Serga, M. Maiorov, A. Petrov, A. Krumina, *Integr. Ferroelectr*. **103** (2008) 18
42. Z. R. Ismagilov, L. T. Tsykoza, N. V. Shikina, V. F. Zarytova, V. V. Zinoviev, S. N. Zagrebelnyi, *Russ. Chem. Rev.* **78** (2009) 873
43. L. Grinberga, A. Sivars, L. Kulikova, V. Serga, J. Kleperis, *IOP Conf. Ser.* **23** (2011) 012009(1)
44. E. Palcevskis, L. Kulikova, V. Serga, A. Cvetkov, S. Chornaja, E. Sproge, K. Dubencovs, *J. Serb. Chem. Soc*. **77** (2012) 1799
45. V. E. Kazarinov, *The Interface Structure and Electrochemical Processes at the Boundary Between Two Immiscible Liquids*, Springer-Verlag, Berlin, 1987, p. 205
46. I. Sobczak, K. Jagodzinska, M. Ziolek, *Catal. Today* **158** (2010) 121
47. S. Demirel, K. Lehnert, M. Lucas, P. Claus, *Appl. Catal., B* **70** (2007) 637
48. S. Demirel, P. Kern, M. Lucas, P. Claus, *Catal. Today* **122** (2007) 292
49. M. Besson, P. Gallezot, *Catal. Today* **57** (2000) 127
50. T. Mallat, A. Baiker, *Catal. Today* **19** (1994) 247
51. T. Mallat, A. Baiker, *Chem. Rev*. **104** (2004) 3037.

Journal of the Serbian Chemical Society
JSCS-info@shd.org.rs • www.shd.org.rs/JSCS
J. Serb. Chem. Soc. 78 (9) 1373–1385 (2013) UDC 612.46:547.476:544.6.076.32–039.59
JSCS–4504 *Original scientific paper*

The use of a gold electrode for the determination of amphetamine derivatives and application to their analysis in human urine

MARINA M. NEVEŠĆANIN[1], MILKA L. AVRAMOV IVIĆ[2*#], SLOBODAN D. PETROVIĆ[3#], DUŠAN Ž. MIJIN[3#], SONJA N. BANOVIĆ STEVIĆ[1] and VLADISLAVA M. JOVANOVIĆ[2#]

[1]BIA, Institute of Security, Kraljice Ane bb, 11000 Belgrade, Serbia, [2]ICTM, Institute of Electrochemistry, University of Belgrade, Njegoševa 12, 11000 Belgrade, Serbia and [3]Faculty of Technology and Metallurgy, University of Belgrade, Karnegijeva 4, 11120 Belgrade, Serbia

(Received 28 December 2012, revised 7 March 2013)

Abstract: The catalytic abilities of a gold electrode were tested for the quantitative determination of amphetamine (A) and 3,4-methylenedioxy-*N*-methylamphetamine (MDMA) standards by their oxidation using cyclic voltammetry (CV). The values of the oxidative currents of A and MDMA standards at 0.80 V *vs.* SCE in 0.05 M $NaHCO_3$ at a scan rate of 50 mV s^{-1} were linear functions of the concentration in range of 110.9–258.9 μM and 38.7–229.2 μM, respectively. Square wave voltammetry (SWV) revealed a linear increase of current with the concentration of MDMA (range 30.9–91.6 μM), which enabled the quantitative determination of amphetamine derivates. SWV analysis was also successfully performed in spiked urine samples. A and MDMA in the presence of sucrose and as a content in illegally produced tablets were also determined. The voltammetric determinations of A and MDMA derivatives using CV and SWV at gold a electrode are rapid, selective and simple procedures and their accuracy was confirmed with a reference method, high performance liquid chromatography (HPLC). The analysis of spiked urine samples offers an additional possibility for the rapid detection of A and MDMA in human urine.

Keywords: amphetamine derivatives; cyclic voltammetry; square wave voltammetry; spiked urine samples.

INTRODUCTION

The abuse of amphetamine type stimulants (ATS) is on the rise worldwide. According to UNODC data, the number of ATS users is larger than the number

* Corresponding author. E-mail: milka@tmf.bg.ac.rs
# Serbian Chemical Society member.
doi: 10.2298/JSC121228032N

of heroin and cocaine users combined.[1,2] Amphetamine (Scheme 1a) and methamphetamine belong to the *β*-phenyl ethylamine structure sympathomimetic drugs that were utilized as psycho stimulants, antidepressants and appetite suppressants.[3,4] 3,4-Methylenedioxy-*N*-methylamphetamine (Scheme 1b) can induce euphoria, and diminished anxiety.

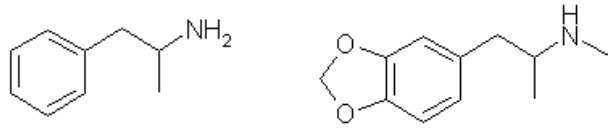

a **b**

Scheme 1. Chemical structures of a) amphetamine and b) 3,4-methylenedioxy-*N*-methylamphetamine.

There is an increasing interest in the development of rapid, selective and sensitive methods for the identification and quantification of A and MDMA in illegal market samples. This has been realized using a variety of methodologies: chromatographic techniques, such as HPLC and gas chromatography, capillary electrophoresis and infrared spectroscopy.[4,5]

Electro-analytical techniques have become powerful tools in modern analytical chemistry for the determination of amphetamine-type drugs.[6–11] The electrochemical oxidation mechanism of amphetamine-like compounds has not been clarified.[12,13]

A significant contribution to the understanding of the oxidative behavior of amphetamine derivatives in different buffer systems employing cyclic, differential pulse and square-wave voltammetry using a glassy carbon electrode was recently published. Primary amines oxidize at potentials higher than those allowed by the potential window of the glassy carbon electrode and a quantitative electroanalytical method was developed and successfully applied to the determination of MDMA in seized samples and in human serum.[13]

The oxidative behavior and determination of amphetamine derivatives on a gold electrode has not hitherto been reported. Taking into account the results obtained on glassy carbon electrode,[13] the testing of gold electrode for the oxidation of amphetamine like drugs is interesting and promising.

The aim of this work was to investigate the use of a gold electrode in the quantitative determination of A and MDMA standards, their content in illegally produced tablets and in spiked urine samples in 0.05 M $NaHCO_3$ by cyclic voltammetry. Furthermore, the voltammetric behavior of A and MDMA standards in the model systems, *i.e.*, in mixtures with sucrose, was studied. A standard analysis of MDMA was also performed by square wave voltammetry and the method was applied on spiked urine samples. The accuracy of the quantitative determination of amphetamine derivatives was confirmed with a reference method, HPLC.

EXPERIMENTAL

Materials

Amphetamine sulfate and 3,4-methylenedioxy-*N*-methylamphetamine hydrochloride were obtained from UN (Lipomed, Switzerland). Illegal amphetamine products (IAP) contain caffeine and quinine and illegal MDMAs product contain microcrystalline cellulose and lactose.[2] HPLC grade acetonitrile, methanol, ammonium acetate, sodium bicarbonate, sulfuric acid, sucrose, dichloromethane, sodium dihydrogenphosphate ($NaH_2PO_4 \cdot H_2O$), H_3PO_4 and $NaHCO_3$ (*p.a*. purity) were produced by Merck. Diethylamine, analytical grade, and ammonium hydroxide, 25 %, were produced by J. T. Baker. All the solutions were prepared with water (18 MΩ cm) obtained from a Millipore system.

Cyclic voltammetry

Standard equipment was used for the cyclic voltammetry measurements. The employed three-electrode electrochemical cell was described in detail previously.[14,15]

Polycrystalline gold served as the working electrode, a gold wire was used as the counter electrode and a saturated calomel electrode as the reference electrode. Polycrystalline gold (Pine rotating disc, used as stationary electrode, surface area 0.500 cm^2) was polished with diamond paste, cleaned with a mixture of water (18 MΩ cm) and sulfuric acid and further cleaned with deionized water (18 MΩ cm) in an ultrasonic bath. All the potentials are given *vs*. the SCE. Prior to the addition of A and MDMA, the electrolyte was deoxygenated by purging with nitrogen. All the experiments were performed at room temperature.

Square wave voltammetry

Square wave voltammetry (SWV) measurements were performed using an Autolab potentiostat–galvanostat (Metrohm, ECO Chemie, The Netherlands). The operating parameters were: step size 2 mV, pulse size 25 mV, frequency 8 Hz and scan rate 15 mV s^{-1}.

Preparation of the standard solutions for the analysis of A and MDMA as a content of a solid dosage form

Ten tablets were weighed and then the average mass per tablet was determined. The tablets were ground to a fine powder in a mortar. The required amount from the crushed tablets powder was dissolved in 10 cm^3 of deionized water by sonication for 5 min and filtered into a 100 cm^3 volumetric flask. The residue was washed three times with 0.05 M $NaHCO_3$ and the volume was completed to the mark with the same solvent. The obtained concentrations were checked by HPLC.

Preparation of urine samples

To 1 cm^3 of urine sample, 0.1 cm^3 of 25 % ammonium hydroxide and 5 cm^3 of dichloromethane were added. The samples were mixed on a mechanical shaker for 20 min and centrifuged at 3000 rpm for 10 min. After centrifugation, the organic layer was separated and evaporated in a stream of air. The dry extracts were reconstituted in methanol and analyzed by the HPLC–UV method at 200.5 nm.[15]

Preparation of standard solutions for the urine analysis

Stock standard solutions of A and MDMA tablets were prepared by dissolving 10 mg of tablet into 10 cm^3 of methanol and stored at –4 °C. Other concentrations of amphetamine as a content of tablets were made by diluting the stock standard solutions with methanol. Calibration samples were prepared by adding A and MDMA solution in blank (“drug-free”) human

urine. The calibration curves for urine spiked by A and MDMA were obtained by plotting their peak areas for the concentrations range 110.9–258.9 μM.

Equipment and chromatographic conditions

Characteristics of the HPLC instrument: HPLC Agilent 1100 (variable wavelength detector); column: Zorbax C18; mobile phase: A (85 %) – 1 % ammonium acetate, 2.5 % diethylamine in deionized water and B (15 %) - acetonitrile; column temperature 35 °C, wave length: 257 nm and injection volume 0.045 cm^3.

RESULTS AND DISCUSSION

Cyclic voltammetry of amphetamine

In order to avoid the influence of organic molecules (by their direct oxidation–reduction or adsorption on the gold electrode) either as a solvent or a component of the buffer solution in the electrolyte and hence to obtain only the anodic oxidation of A and MDMA, 0.05 M $NaHCO_3$ was chosen as the supporting electrolyte.[14,15] With a pH value of 8.4, this electrolyte is in accordance with the physiological pH value and the carbonate–bicarbonate buffer system of blood.[4] The polycrystalline gold electrode was previously selected as the optimal working electrode for the examination of pharmaceutical compounds (macrolide antibiotics)[14,15] and as such, was now selected as a possible suitable catalyst for the oxidation of amphetamine derivatives.

The selected concentration range for the CV determination of A (1.1–2.6 μM) is in complete accordance with the range of concentrations found in human body liquids (urine and blood)[1,3,4] during human sample testing.

The tested concentrations of the amphetamine standard, continuously added in the same experiment, are presented in Fig. 1 (full lines). For the five concentrations, the amphetamine oxidation began at a potential 50 mV more negative than the potential at which gold oxide formation occurs. The cyclic voltammograms show the apparent oxidative reaction with maximum current values covering the whole range in the area of oxide formation. It seems that amphetamines were strongly adsorbed on the gold electrode and that the gold oxide enabled their oxidation. It was recently published that the electro-oxidation of isomeric butylamines at a gold electrode in contact with an alkaline electrolyte solution was catalyzed by the gold oxide layer.[16] As expected, the gold oxide layer was also the catalyst in the electro-oxidation of A in contact with 0.05 M $NaHCO_3$. At higher concentrations of amphetamines, the flat plateau of the oxidative currents became sharper. An A concentration of 258.9 μM was the limiting one. With further increases in the concentration, the currents decreased. In the reverse sweep, the reduction peak of the gold oxides in the presence of amphetamine was diminished because of the reduction of A and the products of its oxidation formed in the forward sweep. The current values of this peak were not a linear function of its concentration, as was observed previously[16] for isomeric butylamines.

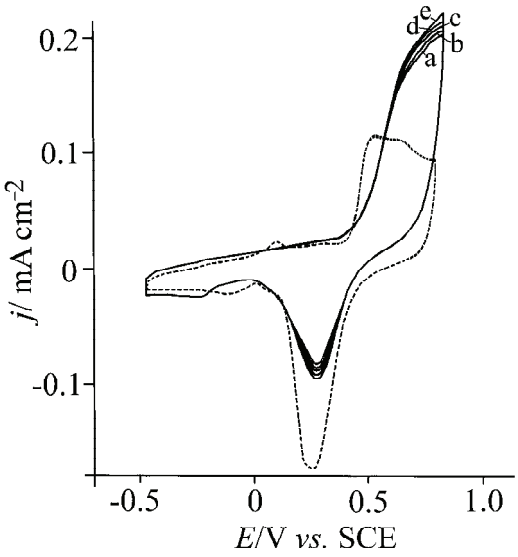

Fig. 1. Cyclic voltammogram of the gold electrode in 0.05 M $NaHCO_3$ (dashed line) and in a presence of amphetamine standard (full line) a) 110.9, b) 147.9 μM, c) 184.9 , d) 221.9 and e) 258.9 μM.
Sweep rate: 50 mV s^{-1}.

The value of the oxidative current of the amphetamine standard at 0.80 V *vs.* SCE in 0.05 M $NaHCO_3$ at the scan rate of 50 mV s^{-1} was a linear function of the concentration in a range of 110.9–258.9 μM. This linearity is presented in Fig. 2. The mentioned linear relationship corresponded to the equation:[17]

$$j_{pa} / \text{mA cm}^{-2} = 0.1112\ (\pm 0.0010) + 0.0002\ (\pm 0.000005) c / \mu\text{M} \quad (1)$$
$$r = 0.9993$$

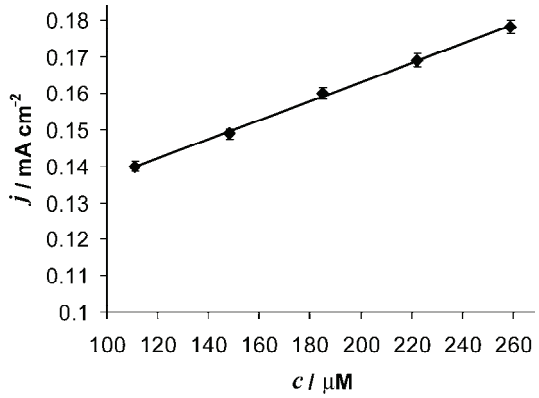

Fig. 2. Linear dependency of the anodic currents of amphetamine on its concentration, obtained from the data presented in Fig. 1.

Such equations were previously applied in the analysis of azithromycin, roxithromycin and midecamycin on a gold electrode.[14,15,18] After the first cycle, the anodic currents of the electro-oxidation of A strongly decreased with the cycling, which was attributed to poisoning of the electrode surface by the adsorption of their amine group. The most probable explanation is that amphetamine

molecules are adsorbed on the gold electrode surface in the potential range preceding the oxidation as was previously shown for isomeric butylamines.[16] This adsorptive behavior enabled a reproducible catalytic behavior of gold electrode in second sweep. After the first sweep, before the addition of the subsequent concentration, the gold electrode was prepared as is described in the Experimental.

The complete study of the MDMA dependency on pH value of electrolyte (from pH 1 to 14) is given elsewhere[13] with the suggestion that MDMA is electrochemically active on glassy carbon electrode in the range from pH 8 to 13. A is completely inactive.

In order to achieve better developed oxidation peak of A on the gold electrode, different pH values were tested in a suggested range, at pH 9 and 13. At both pH values the oxidation peak of A is less pronounced than at pH 8.

Cyclic voltammetry of 3,4-methylenedioxy-N-*methylamphetamine hydrochloride*

The tested concentrations of the MDMA standard, continuously added in the same experiment, are presented in Fig. 3 (full lines). The cyclic voltammograms show an apparent oxidative reaction, with a sharp maximum at the end of the examined oxide region and maximum current values at 0.80 V. Contrary to amphetamine, the oxidation of MDMA began at 0.1 V at the gold electrode surface, 350 mV before oxide formation. This suggests that for MDMA, the gold electrode acted as a catalyst and its molecules were not strongly adsorbed, as in the case of amphetamine. As was observed for A and isomeric butylamines,[16] the reduction peak of the gold oxides decreased markedly in the presence of MDMA.

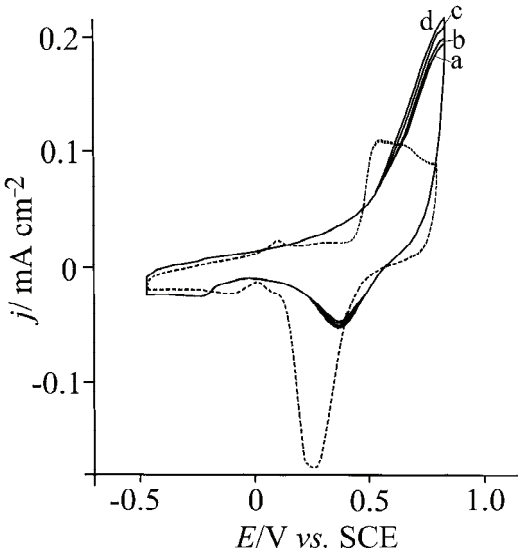

Fig. 3. Cyclic voltammogram of the gold electrode in 0.05 M $NaHCO_3$ (dashed line) and in a presence of MDMA standard (full line) a) 38.7, b) 77.1, c) 153.7 and d) 229.2 μM. Sweep rate: 50 mV s^{-1}.

The value of the oxidative current of MDMA standard at 0.80 V *vs*. SCE in 0.05 M $NaHCO_3$ at a scan rate of 50 mV s^{-1} was a linear function of the concentration in a range of (38.7–229.2 μM). This linearity is presented in Fig. 4. The obtained linear relationship corresponded to the equation:

$$j_{pa} / \text{mA cm}^{-2} = 0.1899\ (\pm 0.0005) + 0.0001\ (\pm 0.000007)c / \mu\text{M} \quad (2)$$
$$r = 0.9990$$

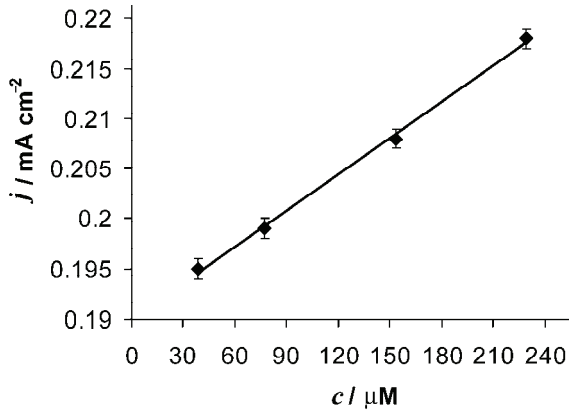

Fig. 4. Linear dependency of anodic peak currents of MDMA on its concentration, obtained from the data presented in Fig. 3.

For the determination of MDMA, only the first cycle was recorded and it is presented for all the examined concentrations. After the first cycle, the anodic currents of MDMA electro-oxidation decrease with cycling but to a smaller extent than in a case of A, which was attributed to poisoning of the electrode surface by the adsorption of its amine group. After the first sweep, before the addition of the subsequent concentration, the gold electrode was prepared as described in the Experimental.

The all tested A and MDMA concentrations are analyzed and confirmed by HPLC[5] during the electrochemical experiment and the obtained linearity was in accordance with the linearity presented in Figs. 2 and 4. The data obtained by HPLC (chromatograms) are not presented herein.

Determination of A and MDMA in illegal tablets by cyclic voltammetry

In the illegally produced samples, the basic excipient is powdered sucrose. A model experiment was performed in which samples of A and MDMA were mixed with sucrose in a concentration most often found in illegal samples (concentration: A/sucrose followed the relationship 1/6). The model samples exhibited the same electrochemical behavior as those presented in Figs. 1 and 3.

Compared to Fig. 3, the samples of MDMA mixed with sucrose exhibited an additional anodic peak (from 0.1 V to 0.5 V), which was attributed to sucrose. The oxidation of added sucrose did not influence the electro-oxidation of MDMA.

Illegal A and MDMA products containing microcrystalline cellulose, lactose and quinine were analyzed in the same manner as was presented for the A (Fig. 1) and MDMA (Fig. 3) standards. Before the electrochemical analysis, all the samples were analyzed by GC-MS and their content was confirmed as previously published.[2] The obtained cyclic voltammograms were the same as those presented in Figs. 1 and 3. The collected data are listed in Table I.

TABLE I. Application of the proposed method to the determination of A and MDMA in illegal tablets; mean of six experiments

Preparation	Amount found, mg ± *RSD* / %	
	Proposed method	Reference method
A tablets	30±3.7	24.9±1.2
MDMA tablets	60±1.7	60±1.1

The presence of microcrystalline cellulose, lactose and quinine has no influence on the catalytic properties of gold oxide in the A and MDMA determinations and cyclic voltammograms were the same as those presented in Figs. 1 and 3.

The presence of caffeine disturbed the determination of A and MDMA in the sense that the gold oxide was also a catalyst for caffeine electro-oxidation and A, MDMA and caffeine undergo the oxidation processes at the same potential values.[19] A method for caffeine separation before the electrochemical analysis should be developed in order to avoid synergetic effects. The cyclic voltammogram of illegal A tablets containing caffeine is presented in Fig. 5 (for a concen-

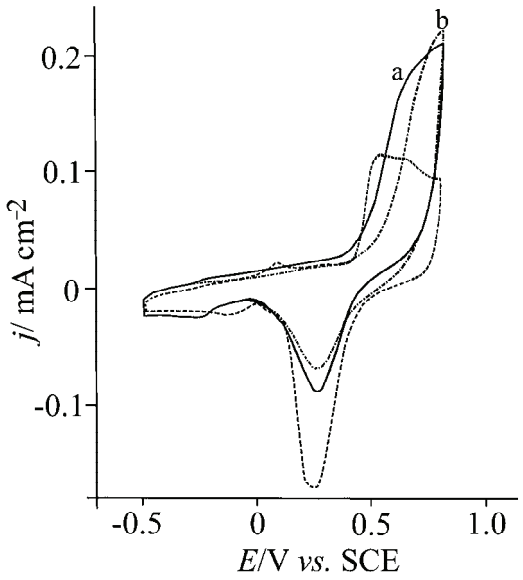

Fig. 5. Cyclic voltammogram of the gold electrode in 0.05 M $NaHCO_3$ (dashed line) and in the presence of a) amphetamine standard (full line), 184.9 μM, and b) amphetamine tablet (dashed–dotted line) 184.9 μM. Sweep rate: 50 mV s^{-1}. The concentration of A in the tablet was determined by HPLC.

tration of 184.9 μM). The found amount of A in the tablets using cyclic voltammetry (from Fig. 5) was 20 % higher in the presence of caffeine than was determined for the standard, as can be seen from Table I. The same effect was observed for MDMA.

Determination of A in urine samples using cyclic voltammetry

The urine samples spiked with amphetamine tablets (in the concentration range: 110.9–258.9 μM) were analyzed in a same manner as was presented for A.

The determination of A in the spiked urine samples was also realized by the standard addition method at two different concentration levels (110.9 and 184.9 μM). Four determinations were performed at each concentration level (Table II). The mean recoveries for the two concentrations were 98.85 and 97.36 % with relative standard deviations of 0.141 and 1.226, respectively.

TABLE II. Determination of amphetamine in spiked urine samples using the CV method

Taken concentration, μM	Recovery, %		*SD* / %		*RSD* /%	
	CV	HPLC	CV	HPLC	CV	HPLC
110.9	98.25	99.85	0.138	0.100	0.141	0.110
184.9	97.36	99.87	1.201	0.750	1.226	0.805

Different analytical methods are usually combined and compared in drug analysis[20,21] and statistical comparison of the results obtained with cyclic voltammetry and HPLC for the two concentrations are presented in Table II.[22]

Square wave voltammetry of MDMA

Being a fast and sensitive technique with a low detection limit, square wave voltammetry was tested as a possible method for the quantitative determination of A and MDMA on a gold electrode. Analysis of the A standard showed strong adsorption of the molecules on the surface of the gold electrode in the potential range preceding the oxidation,[16] blocking the surface and preventing its determination by the SW method. Contrary to A, SW voltammograms for different concentrations of the MDMA standard were recorded in 0.05 M $NaHCO_3$ in the potential range from 0 to 1.1 V at a scan rate of 15 mV s^{-1}. Before each scan, the compound was accumulated at the electrode surface at 0.1 V for 220 s. The square wave anodic stripping voltammograms for different concentrations of MDMA are presented in Fig. 6. Each voltammogram is characterized by a well-defined peak at approximately 0.7 V that was attributed to the oxidation of adsorbed MDMA. The current of the anodic stripping peak exhibited a linear dependence on the MDMA concentration as shown in Fig. 7.

The value of the oxidative peak of the MDMA standard in 0.05 M $NaHCO_3$ is linear function of the concentration in a range of (30.9–91.6 μM). This line-

arity is presented in Fig. 7. The obtained linear relationship corresponded to the equation:

$$j_{pa} / \text{mA cm}^{-2} = 0.0052\ (\pm 0.0003) + 0.00017\ (\pm 0.000006) c / \mu\text{M} \qquad (3)$$
$$r = 0.9991$$

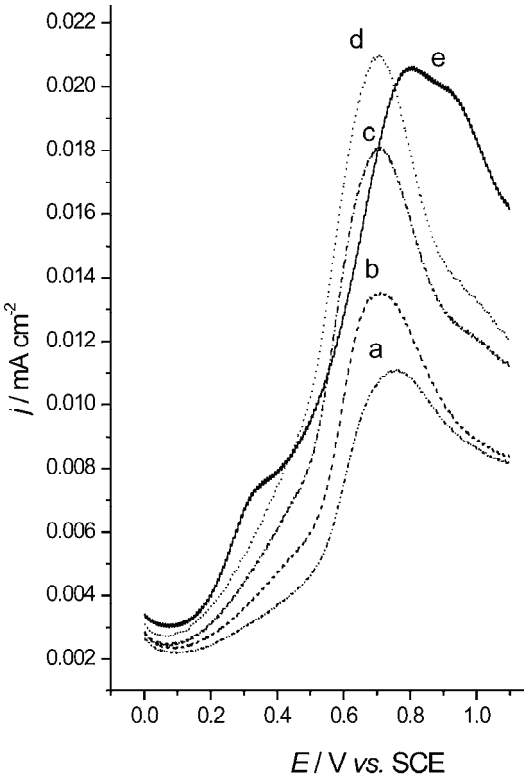

Fig. 6. Square wave anodic stripping voltammograms at the gold electrode in 0.05 M $NaHCO_3$ in a presence of MDMA standard, a) 30.9, b) 46.4 , c) 76.5, d) 91.6 and e) 91.6 μM spiked with urine. Accumulation time: 220 s at E = 0.1 V; step size 2 mV, pulse size 25 mV, frequency 8 Hz and scan rate 15 mV s^{-1}.

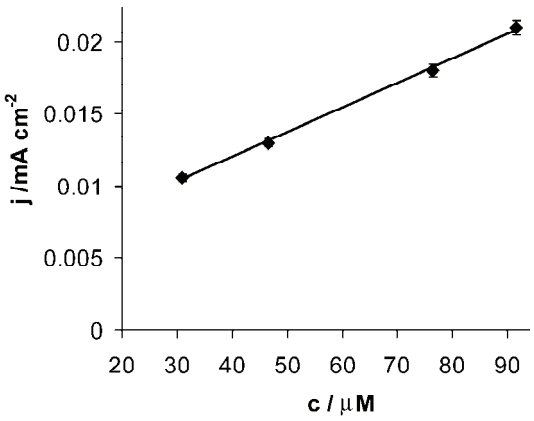

Fig. 7. Linear dependency of anodic currents of MDMA on concentration, obtained from the data presented in Fig. 6.

Determination of MDMA in urine samples using square wave voltammetry

The urine samples spiked with MDMA standard were analyzed as well and Square wave anodic stripping voltammograms of spiked urine samples for the set of concentrations of MDMA presented in Fig. 6 are the same as those observed in the absence of urine. The voltammogram for the highest tested concentration of MDMA, 91.6 μM, in Fig. 6 shows that a small shoulder that appeared at 0.35 V, attributed to the presence of the urine of healthy volunteers, did not disturb the oxidation of MDMA and had no influence on the value of the oxidation peak. The peak could be slightly shifted to positive potential values (as is presented in Fig. 6) but it does not occur with all spiked urine samples and depended on the urine content, which is common in clinical praxis. The results obtained revealed that SWV could be successfully applied for the quantitative determination of MDMA in urine.

The determination of MDMA in spiked urine samples was also performed by the standard addition method at two different concentration levels (76.5 and 91.6 μM). Four determinations were performed at each concentration level (Table III). The mean recoveries for the two concentrations were 98.32 and 98.46 % with relative standard deviations of 0.138 and 1.134, respectively.

A statistical comparison of the results obtained using cyclic voltammetry and HPLC for the two concentrations is presented in Table III.

TABLE III. Determination of MDMA in spiked urine samples using the SWV method

Taken concentration, μM	Recovery, %		*SD* / %		*RSD* /%	
	SWV	HPLC	SWV	HPLC	SWV	HPLC
76.5	98.46	99.72	1.118	0.764	1.134	0.316
91.6	98.32	99.77	0.120	0.102	0.138	0.120

CONCLUSIONS

A gold electrode as a good catalyst for amine-type molecules was successfully employed for the quantitative determination A and MDMA standards *via* their voltammetric oxidation.

The value of the oxidative current of A and MDMA standards, obtained by cyclic voltammetry at 0.80 V *vs.* SCE in 0.05 M $NaHCO_3$ at the scan rate of 50 mV s^{-1}, was a linear function of concentration in the range 110.9–258.9 μg cm^{-3} for A and 38.7–229.2 μg cm^{-3} for MDMA.

The quantitative determination of amphetamine derivatives in solid dosage form and in spiked urine samples was successfully realized using cyclic voltammetry.

The determination of an A standard in spiked urine samples was performed by the standard addition method employing cyclic voltammetry. The mean reco-

veries for the two concentrations were 98.85 and 97.36 % with relative standard deviations of 0.141 and 1.226, respectively.

Square wave voltammetry was successfully applied for quantitative determination of MDMA standard (30.9–91.6 μM) in solution and in spiked urine samples. The determination of MDMA with SWV in spiked urine samples was also performed by the standard addition method. The mean recoveries for the two concentrations were 98.32 and 98.46 % with relative standard deviations of 0.138 and 1.134, respectively.

Acknowledgement. The authors acknowledge the financial support of the Ministry of Education, Science and Technological Development of the Republic of Serbia (Grants No. 172013).

ИЗВОД

ОДРЕЂИВАЊЕ ДЕРИВАТА АМФЕТАМИНА И ПРИМЕНА У АНАЛИЗИ ХУМАНОГ УРИНА НА ЕЛЕКТРОДИ ОД ЗЛАТА

МАРИНА М. НЕВЕШЋАНИН[1], МИЛКА Л. АВРАМОВ ИВИЋ[2], СЛОБОДАН Д. ПЕТРОВИЋ[3], ДУШАН Ж. МИЈИН[3], СОЊА Н. БАНОВИЋ СТЕВИЋ[1] и ВЛАДИСЛАВА М. ЈОВАНОВИЋ[2]

[1]БИА, Институт безбедности, Краљице Ане бб, 11000 Београд, [2]ИХТМ, Центар за електрохемију, Универзитет у Београду, Његошева 12, 11000 Београд и [3]Технолошко–металуршки факултет Универзитета у Београду, Карнегијева 4, 11120 Београд

Каталитичка својства електроде од злата су тестирана за квантитативно одређивање амфетамина (A) и 3,4-метилендиокси-*N*-метиламфетамина (MDMA) стандарда. Електроксидација A и MDMA је праћена цикличном волтаметријом (CV). Вредност оксидативног пика A и MDMA стандарда је линеарна функција концентрација у опсегу 110,9––258,9 μM (A) и 38,7–229,2 μM (MDMA). Волтаметрија са правоугаоним импулсима (SWV) је показала линеарну зависност струја од концентрација за MDMA стандард (у опсегу: 30,9–91,6 μM) као и у спајкованим узорцима хуманог урина. Успешно је анализиран и садржај A и MDMA у илегално произведеним таблетама. Волтаметријско одређивање A и MDMA деривата уз помоћ CV и SWV на електроди од злата је брза, селективна и једноставна процедура. Анализа спајкованих узорака урина нуди додатну могућност за брзу детекцију A и MDMA у хуманом урину.

(Примљено 28. децембра 2012, ревидирано 7. марта 2013)

REFERENCES

1. UNODC, *Evaluation of the United Nations global initiative to fight human trafficking (un.gift)*, Vienna, 2011, pp. 1–126, http://www.globalmigrationgroup.org/ uploads/ UNCT_Corner/theme3/migrant-smuggling-and-trafficking/UN.GIFT_Evaluation_-_final_draft_24Feb2011.pdf (accessed 13 September 2012)
2. M. Nevešćanin, S. Banović, S. Petrović, V. Vajs, *J. Serb. Chem. Soc*. **73** (2008) 691
3. A. Gringauz, *Introduction to Medicinal Chemistry, How drugs act and why*, Wiley-VCH, New York, USA, 1996, p. 408
4. A. C. Moffat, M. D. Osselton, B. Widdop, *Clarke's Analysis of Drugs and Poisons*, 3rd ed., Pharmaceutical Press, Chicago, IL, 2004
5. UNODC, *Recommended methods for the identification and analysis of amphetamine, methamphetamine and their ring-substituted analogues in seized materials*, New York,

2006, p. 1–88, http://www.unodc.org/pdf/scientific/stnar34.pdf (accessed 13 September 2012)
6. R. E. Michel, A. B. Rege, W. J. George, *J. Neurosci. Methods* **50** (1993) 61
7. N. A. Santagati, G. Ferrara, A. Marrazzo, G. Ronsisvalle, *J. Pharm. Biomed. Anal*. **30** (2002) 247
8. T. Keller, M. Mutz, R. Aderjan, H. P. Latscha, *Fresenius J. Anal. Chem*. **363** (1999) 270
9. R. Gulaboski, M. N. D. S. Cordeiro, N. Milhazes, J. Garrido, F. Borges, M. Jorge, C. M. Pereira, I. Bogeski, A. H. Morales, B. Naumoski, A. F. Silva, *Anal. Biochem*. **361** (2007) 236
10. J. A. Squella, B. K. Cassels, M. Arata, M. P. Bavestrello, L. J. Nuñez-Vergara, *Talanta* **40** (1993) 1379
11. N. Milhazes, P. Martins, E. Uriarte, J. Garrido, R. Calheiros, M. P. M. Marques, F. Borges, *Anal. Chim. Acta* **596** (2007) 231
12. C. Macedo, P. S. Branco, L. M. Ferreira, A. M. Lobo, J. P. Capela, E. Fernandes, M. L. Bastos, F. Carvalho, *J. Health Sci.* **53** (2007) 31
13. E. M. P. J. Garrido, J. M. P. J. Garrido, N. Milhazes, F. Borges, A. M. Oliveira-Brett, *Bioelectrochemistry* **79** (2010) 77
14. M. L. Avramov Ivić, S. D. Petrović, D. Ž. Mijin, P. M. Živković, I. M. Kosović, K. M. Drljević, M. B. Jovanović, *Electrochim. Acta* **51** (2006) 2407
15. K. M. Drljević-Djurić, V. D. Jović, U. Č. Lačnjevac, M. L. Avramov Ivić, S. D. Petrović, D. Ž. Mijin, S. B. Djordjević, *Electrochim. Acta* **56** (2010) 47
16. T. Łuczak, *J. Appl. Electrochem*. **37** (2007) 269
17. R. Greaf, R. Peat, R. L. Peter, D. Pletcher, J. Robinson, *Instrumental Methods in Electrochemistry*, Ellis Horwood, Chichester, 1985, p. 178
18. K. M. Drljević-Djurić, M. L. Avramov Ivić, S. D. Petrović, D. Ž. Mijin, M. B. Jadranin, *Russ. J. Electrochem*. **47** (2011) 833
19. G. A. M. Mersal, *Food Anal. Method*. **5** (2012) 520
20. X. Liu, B. Li, C. Li, *J. Serb. Chem. Soc*. **76** (2011) 113
21. L.-H. Liu, C.-Q. Duan, Z.-N. Gao, *J. Serb. Chem. Soc*. **77** (2012) 483
22. J. N. Miller, J. C. Miller, *Statistics and Chemometrics for Analytical Chemistry*, 5th ed., Pearson, Harlow, 2005, pp. 18–20.

Journal of the Serbian Chemical Society
JSCS-info@shd.org.rs • www.shd.org.rs/JSCS
J. Serb. Chem. Soc. 78 (9) 1387–1395 (2013)
JSCS–4505
UDC 541.135:548.004.12+669–492.4
Original scientific paper

Influence of the type of electrolyte on the morphological and crystallographic characteristics of lead powder particles

NEBOJŠA D. NIKOLIĆ[1]*#, VESNA M. MAKSIMOVIĆ[2], GORAN BRANKOVIĆ[3], PREDRAG M. ŽIVKOVIĆ[4] and MIOMIR G. PAVLOVIĆ[1#]

[1]ICTM – Center of Electrochemistry, University of Belgrade, Njegoševa 12, P. O. Box 473, 11001 Belgrade, Serbia, [2]Vinča Institute of Nuclear Sciences, University of Belgrade, P. O. Box 522, 11001 Belgrade, Serbia, [3]Institute for Multidisciplinary Research, University of Belgrade, Kneza Višeslava 1a, Belgrade, Serbia and [4]Faculty of Technology and Metallurgy, University of Belgrade, Karnegijeva 4, P. O. Box 3503, 11001 Belgrade, Serbia

(Received 11 February, revised 13 March 2013)

Abstract: Lead electrodeposition processes from basic (nitrate) and complex (acetate) electrolytes were mutually compared by scanning electron microscopy and X-ray diffraction investigation of the produced powder particles. The shape of dendritic particles strongly depended on the type of electrolyte. Dendrites composed of a stalk and weakly developed primary branches (the primary type) were predominantly formed from the basic electrolyte. Ramified dendrites composed of a stalk and of both primary and secondary branches (the secondary type) were mainly formed from the complex electrolyte. In both types of powder particles, Pb crystallites were predominantly oriented in the (111) plane. The formation of powder particles of different shapes with strong (111) preferred orientation is discussed and explained by consideration of the general characteristics of the growth of crystals in electrocrystallization processes.

Keywords: electrodeposition; lead; powder; dendrite; scanning electron microscopy (SEM); X-ray diffraction (XRD) analysis.

INTRODUCTION

The formation of metal powders by electrolysis is an economical processing method with low capital investment and operational costs. The main advantages of this method in relation to other methods of powder production (mechanical commuting, chemical reaction and liquid metal atomization) are the high purity of the produced powder, which can be easily pressed and sintered, and the low oxygen content.[1,2] It is an environmentally friendly method of powder production that enables working in a closed-circuit.[3]

* Corresponding author. E-mail: nnikolic@tmf.bg.ac.rs
# Serbian Chemical Society active member.
doi: 10.2298/JSC130211034N

Electrodeposited metallic powders are mainly produced in a dendritic form. Although dendritic forms are the predominant shape of powder particles, powders are also obtained as flakes or needles, fibrous or spongy, cauliflower-like forms, *etc*., depending on the conditions of electrodeposition and on the nature of the metal.[2,4,5]

The shape of dendritic particles also depends on the electrodeposition conditions and the nature of the metal. The shape of the dendrites of the group of normal metals,[6] characterized by a high exchange current density ($j_0 \rightarrow \infty$) and a low melting point, T_m, such as Ag,[2,4,7,8] Sn,[9] and Pb,[10,11] is completely different from those belonging to the groups of intermediate metals (moderate T_m and a medium j_0), such as Cu,[5,12–15] Ag (complex electrolytes)[4,8,16,17] and Au,[18] or inert metals (high T_m and a low j_0), such as Co and Ni.[19,20] The composition of electrolyte strongly affects the shape of the dendritic particles. For example, the shape of lead dendrites obtained by electrodeposition from nitrate solutions is completely different from those obtained from acetate solutions.[21]

The effect of the composition of the electrolyte and the nature of the metal, as well as other electrodeposition conditions (regime of electrolysis, temperature, type of the working electrode, *etc*.) on the morphology of the powder particles has been relatively well examined and systematized.[7] However, there is not enough data concerning the crystallographic characteristics of powder particles, nor about the correlation between the morphology of powder particles and their crystallographic structure. An initial investigation was performed recently[22] for the case of lead electrodeposition from a concentrated nitrate solution and it was shown that different morphological forms, from single crystals to branchy dendrites with a strong (111) preferred orientation, were formed. The ratio of Pb crystallites oriented in the (200), (220) and (311) planes increased with increasing overpotential of the electrodeposition. The aim of this study was to continue this investigation. The effect of the type of electrolyte on the morphological and crystallographic characteristics of lead powder particles produced by potentiostatic electrodeposition will be analyzed and discussed.

EXPERIMENTAL

The electrodeposition of lead was performed in an open cell from basic (nitrate) and complex (acetate) electrolytes. The compositions of the electrolytes were: acetate electrolyte, 0.10 M $Pb(CH_3COO)_2$ + 1.5 M $NaCH_3COO$ + 0.15 M CH_3COOH and nitrate electrolyte, 0.10 M $Pb(NO_3)_2$ + 2.0 M $NaNO_3$.

Doubly distilled water and analytical grade chemicals were used for the preparation of the solutions for the electrodeposition of lead. All electrodepositions were performed on vertical cylindrical copper electrodes. The geometric surface area of the copper electrodes was 0.25 cm^2. The counter electrode was a pure lead foil of 0.80 dm^2 surface area that was placed close to the cell walls. The reference electrode was a pure lead wire, the tips of which were positioned at a distance of about 0.2 cm from the surface of the working electrodes. The working electrodes were placed in the centre of cell, at the same location for each experiment.

The electrodeposition of lead and polarization measurements were performed at a temperature of 22.0±0.5 °C.

Polarization curve for electrodeposition of lead was recorded potentiostatically by changing the overpotential in 5 mV steps. In order to obtain a reproducible shape of the polarization curves for this reaction, the following experimental procedure,[11] usual for recording the polarization curves of fast electrodeposition processes, was applied. At low overpotentials (Part (I) and (II) on the polarization curves in Fig. 1), the values of the current obtained after reaching steady-state values were used for constructing the polarization curves. Since the current increased dramatically over time at overpotentials corresponding to Part (III) on the polarization curves in Fig. 1, the values recorded immediately after setting the selected overpotential were used.

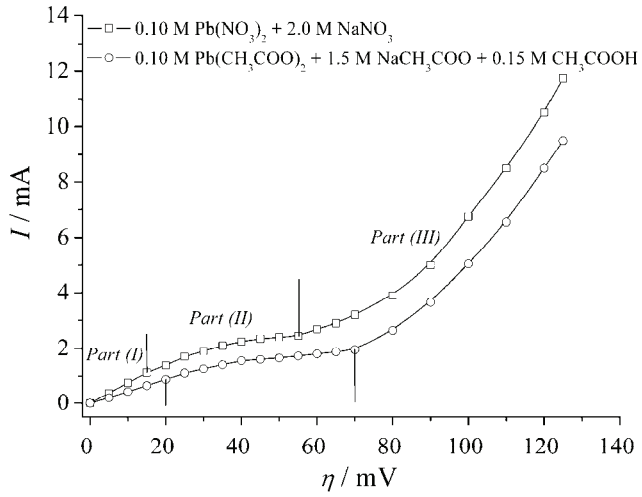

Fig. 1. The polarization curves for lead electrodeposition from 0.10 M $Pb(CH_3COO)_2$ + 1.5 M $NaCH_3COO$ + 0.15 M CH_3COOH and from 0.10 M $Pb(NO_3)_2$ + 2.0 M $NaNO_3$. The surface area of the working electrode was 0.25 cm^2.

Powder particles obtained by tapping lead deposits electrodeposited at an overpotential of 100 mV with a charge of 0.50 mA h cm^{-2} were examined using a scanning electron microscope – TESCAN Digital Microscope.

X-Ray powder diffraction (XRD) analysis performed using a Rigaku Ultima IV diffractometer with CuK_α radiation was used for examination of the crystal structures.

RESULTS AND DISCUSSION

The polarization curves for electrodeposition of lead from the basic and the complex electrolytes consisted of three parts separated by the vertical lines in Fig. 1. The characteristic of the first part (Part (I)) is the linear dependence of the current on overpotential and this part corresponds to ohmic control.[10,11,21] The intervals of overpotentials belonging to this control of the electrodeposition were between 0 and 15 mV for the nitrate and between 0 and 20 mV for the complex electrolyte. The electrodeposition processes are diffusion-controlled in the range

of overpotentials between 15 and 55 mV for the nitrate electrolyte and between 20 and 70 mV for the complex electrolyte (Part (II) on the polarization curves). The electrodeposition processes remain diffusion controlled after the inflection points (Part (III)) and the rapid increase of the current with increasing overpotential is due to the large increase in the surface area caused by the formation and growth of dendrites.

Regular single crystals were formed in the ohmic-controlled electrodeposition and their shape did not depend on the type of the electrolyte.[21] Dendritic growth was initiated at some overpotential belonging to the diffusion part of the polarization curve and this overpotential is denoted as the critical overpotential for dendritic growth initiation. Various morphological forms from single crystals to irregular crystals (precursors of dendrites) and dendrites were formed in the diffusion-controlled electrodeposition.[21] Finally, the overpotentials corresponding to the inflection points on the polarization curves represent the critical overpotentials for instantaneous dendritic growth. After these overpotential values, the currents increased rapidly (Fig. 1).

Typical powder particles obtained by tapping lead deposits electrodeposited at an overpotential of 100 mV from the nitrate electrolyte are shown in Fig. 2a and b, and those from the complex electrolyte are presented in Fig. 2c and d. At first sight, a clear difference between them is evident. The powder particles obtained from the complex electrolyte were branchier than those obtained from the basic electrolyte were. In Wranglen's classic definition of dendrites,[23] a dendrite consists of a stalk and of branches (primary, secondary, *etc*.) and resembles a tree. Dendrites consisting of only the stalk and primary branches are referred as primary (P) dendrites. If the primary branches in turn develop secondary branches, the dendrite is called secondary (S).

Analysis of the shape of dendrites obtained from the nitrate electrolyte showed that they consisted of a stalk and poorly developed branches denoted as the teeth of a saw[11] (Fig. 2a and b). It is very clear that these poorly developed branches represent primary branches in these powder particles, and hence, these dendrites are of the P type. However, the primary branches in the powder particles obtained from the complex electrolyte were very well developed (Fig. 2c and d) and the presence of the secondary branches developed from them can be easily noticed. Hence, the dendrites formed from the complex electrolyte belonged to the S type. A common characteristic of both groups of dendrites is their two-dimensional (2D) shape.

Electrochemical aspects of the formation and growth of dendrites have been very well investigated. From the electrochemical point of view, a dendrite is defined as an electrode surface protrusion that grows under activation control, while electrodeposition to a macroelectrode is predominantly under diffusion control.[7,24–26] Using this definition of a dendrite, the sudden and rapid increase

of the current with increasing the overpotential after the inflection point ((Part (III) in the polarization curves) could be mainly ascribed to activation-controlled electrodeposition at the tips of the formed dendrites,[10,11,26] where the tips of both primary and secondary branches contribute to the overall control of electrodeposition process. Formation of more branchy dendrites from the complex electrolyte than from the basic electrolyte could be ascribed to the lower exchange current density for the acetate electrolyte than for the nitrate one.[21]

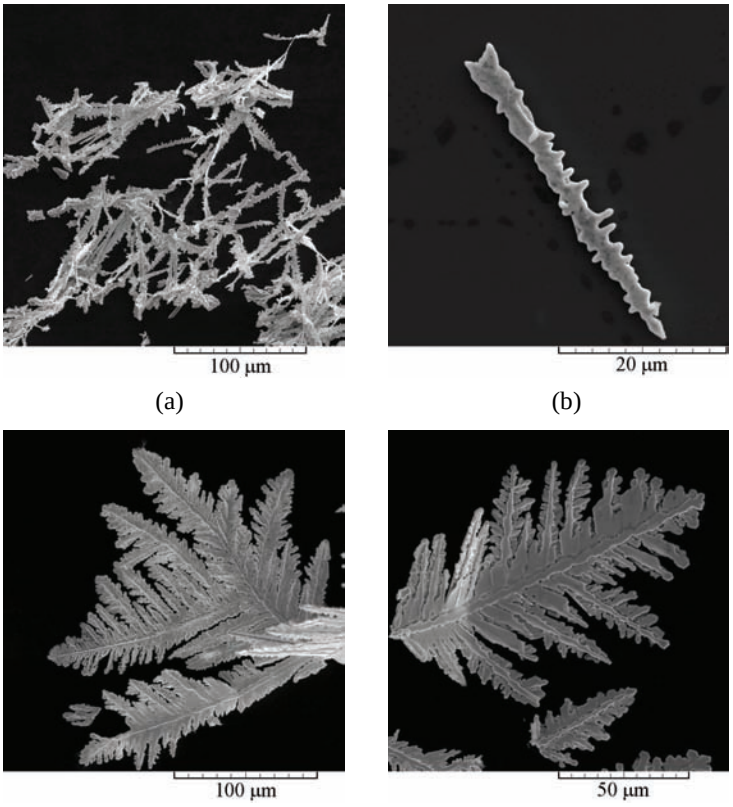

(a) (b) (c) (d)

Fig. 2. Powder particles obtained by tapping the lead powder deposits formed by electrodeposition at an overpotential of 100 mV from: (a) and (b) 0.10 M $Pb(NO_3)_2$ + 2.0 M $NaNO_3$, and (c) and (d) 0.10 M $Pb(CH_3COO)_2$ + 1.5 M $NaCH_3COO$ + 0.15 M CH_3COOH.

Unlike of systematized investigations of the effect of the type of the electrolyte on the morphology of powder particles, a correlation between the crystallographic structure of particles and the type of the electrolyte has not been sufficiently explored. The XRD patterns of the powder particles obtained by tapping the lead powder deposits electrodeposited from the basic and the complex elec-

trolytes are shown in Fig. 3, from which it is very clear that the presented XRD patterns were very similar to each other. Pb crystallites were predominately oriented in the (111) plane. Aside from Pb crystallites oriented in this plane, the presence of crystallites oriented in the (200), (220), (311) and (331) planes was also observed. Nevertheless, the strong (111) preferred orientation was characteristic of both types of powder particles.

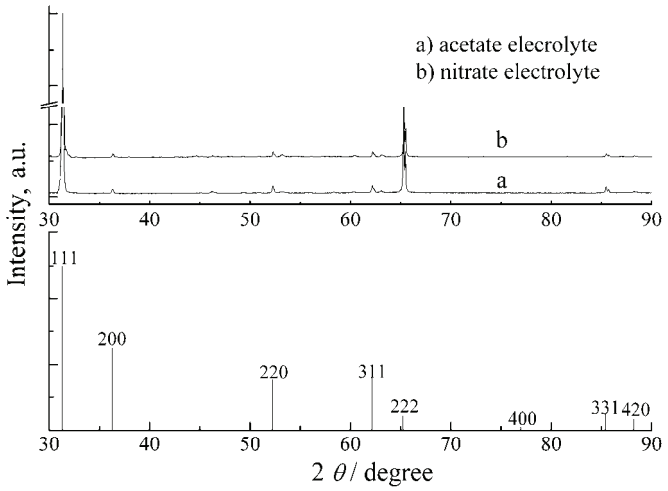

Fig. 3. The XRD patterns of the lead powder particles electrodeposited from electrolytes 0.10 M $Pb(CH_3COO)_2$ + 1.5 M $NaCH_3COO$ + 0.15 M CH_3COOH and 0.10 M $Pb(NO_3)_2$ + 2.0 M $NaNO_3$. The standard for Pb: 4-0686.

Formation of lead powders with the strong (111) preferred orientation could be explained as follows: lead crystallizes in a face-centered cubic (FCC) lattice. At constant overpotential, the rates of electrodeposition for this type of crystal lattice increase in the order of (110) > (100) > (111).[27] These different deposition rates onto different faces had an important consequence; fast-growing faces tend to grow out of existence and disappear, while slow-growing faces tend to survive,[27] as illustrated in Fig. 4. The origin of Pb crystallites oriented in the (111) plane is the growth centers present in the interior of the crystal faces.[22,23] This type of growth center is denoted as a “center type”. On the other hand, the origins of the Pb crystallites oriented in the (200), (220), (311) and (331) planes are the growth centers present on the edges and corners of the growing forms.[22] These types of growth centers are denoted as “edge and corner types”.[23] The overpotentials and current densities responsible for crystal growth based on growth centers of the “edge and corner type” are higher than those responsible for crystal growth based on growth centers of the “center type”. This means that the current densities are higher at the tips of the growing forms than at their sides. In the

growth process, slow-growing (111) face will survive constructing all elements of dendrites (both stalk and branches), and hence, causing the predominant orientation of Pb crystallites in this plane, as confirmed in Fig. 3. In the case of lead, it is clear that the (200), (220), (311) and (331) planes are fast-growing faces. In the growth process, they will disappear which explains the considerably smaller presence of Pb crystallites in these planes than in the (111) plane.

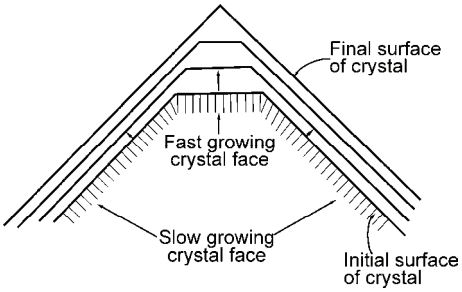

Fig. 4. The growth of a crystal, illustrating how a fast-growing face grows out of existence, while a slow-growing crystal faces remains.[27]

These processes should not been observed independently of the effect of the current density distribution at the growing surface. The current lines are primarily concentrated at the tips of growing protrusions, causing faster growth on them than in the vicinity of the electrode surface.[28] As result of all these processes, dendrites of the different shape are formed.

It is very clear from the above consideration that the crystallographic (interior) structure is determined by the characteristics (nature) of the metal and it does not depend on the type of electrolyte. Unlike the approximately same crystallographic structure, the morphology of the observed powder particles strongly depended on the type of employed electrolyte. Furthermore, the dominant orientation of Pb crystallites in the (111) plane was observed in different morphological forms, from single to irregular crystals and dendrites obtained by the potentiostatic electrodeposition from the nitrate electrolyte at the different overpotentials.[22] In addition, the application of both different regimes of electrolysis, such as the galvanostatic one, and the type of the working electrode, such as Cu, Ti and Al, did not affect the crystallographic characteristics of lead.[29]

CONCLUSIONS

Powder particles obtained by potentiostatic electrodeposition from basic (nitrate) and complex (acetate) electrolytes were analyzed using the SEM and XRD techniques.

The type of electrolyte strongly affected the surface morphology of the lead powder particles. Primary type dendrites were formed from the basic (nitrate) electrolyte. This type of dendrite consists of a stalk and weakly developed branches. The secondary type of dendrites, composed of a stalk and primary and

secondary branches, was formed by electrodeposition from the complex (acetate) electrolyte. This type of dendrite was much more ramified.

In contrast to the very different morphologies of the two types of powder particles, both of them showed the dominant presence of Pb crystallites oriented in the (111) plane. It is clear that the crystallographic structure of the powder particles did not depend on the type of electrolyte, but was only determined by the nature of the metal.

Acknowledgement. The work was supported by the Ministry of Education, Science and Technological Development of the Republic of Serbia under the research project: "Electrochemical synthesis and characterization of nanostructured functional materials for application in new technologies" (No. 172046).

И З В О Д

УТИЦАЈ ТИПА ЕЛЕКТРОЛИТА НА МОРФОЛОШКЕ И КРИСТАЛОГРАФСКЕ КАРАКТЕРИСТИКЕ ПРАШКАСТИХ ЧЕСТИЦА ОЛОВА

НЕБОЈША Д. НИКОЛИЋ[1], ВЕСНА М. МАКСИМОВИЋ[2], ГОРАН БРАНКОВИЋ[3], ПРЕДРАГ М. ЖИВКОВИЋ[4] и МИОМИР Г. ПАВЛОВИЋ[1]

[1]ИХТМ – Центар за електрохемију, Универзитет у Београду, Његошева 12, Београд, [2]Институт за нуклеарне науке „Винча", Универзитет у Београду, Београд, [3]Институт за мултидисциплинарна истраживања, Универзитет у Београду, Кнеза Вишеслава 1а, Београд и [4]Технолошко–металуршки факултет, Универзитет у Београду, Карнегијева 4, Београд

Процеси електрохемијског таложења олова из основног (нитратног) и комплексног (ацетатног) електролита су били међусобно упоређени техником скенирајуће електронске микроскопије и рендгенско-дифракционом анализом произведених честица праха. Облик дендритичних честица је снажно зависио од типа електролита. Дендрити састављени од стабла и слабо развијених грана (примарни тип) су били предоминантно формирани из основног електролита. Разгранати дендрити састављени од стабла и од примарних и секундарних грана (секундарни тип) су били углавном формирани из комплексног електролита. У оба типа прашкастих честица кристалити олова су били доминантно оријентисани у (111) равни. Формирање прашкастих честица са строгом (111) оријентацијом је било дискутовано и објашњено разматрањем општих карактеристика раста кристала у процесима електрокристализације.

(Примљено 11. фебруара, ревидирано 13. марта 2013)

REFERENCES

1. R. M. German, *Powder Metallurgy Science*, 2nd ed., Metal Powder Industries Federation, Princeton, NJ, 1994, p.p. 15–429
2. M. G. Pavlović, K. I. Popov, *Electrochem. Encyclopedia*, http://electrochem.cwru.edu/ed/encycl/, 2005
3. G. Orhan, G. Hapci, *Powder Technol.* **201** (2010) 57
4. V. D. Jović, N. D. Nikolić, U. Č. Lačnjevac, B. M. Jović, K. I. Popov, *Morphology of Different Electrodeposited Pure Metal Powders*, in *Electrochemical Production of Metal Powders*, Series: *Modern Aspects of Electrochemistry*, S. S. Djokić, Ed., Vol. 54, Springer, 2012, p.p. 63–123

5. N. D. Nikolić, K. I. Popov, Electrodeposition of Copper Powders and Their Properties, in *Electrochemical Production of Metal Powders*, Series: *Modern Aspects of Electrochemistry*, S. S. Djokić, Ed., Vol. 54, Springer, 2012, p.p. 125–185
6. R. Winand, *Electrochim. Acta* **39** (1994) 1091
7. K. I. Popov, S. S. Djokić, B. N. Grgur, *Fundamental aspects of electrometallurgy*, Kluwer Academic/Plenum Publishers, New York, 2002, p.p. 1–305
8. S. S. Djokić, N. D. Nikolić, P. M. Živković, K. I. Popov, N. S. Djokić, *ECS Trans.* **33** (2011) 7
9. K. I. Popov, M. G. Pavlović, J. N. Jovićević, *Hydrometallurgy* **23** (1989) 127
10. N. D. Nikolić, G. Branković, U. Lačnjevac, *J. Solid State Electrochem.* **16** (2012) 2121
11. N. D. Nikolić, K. I. Popov, P. M. Živković, G. Branković, *J. Electroanal. Chem.* **691** (2013) 66
12. N. D. Nikolić, Lj. J. Pavlović, M. G. Pavlović, K. I. Popov, *Powder Technol.* **185** (2008) 195
13. M. G. Pavlović, Lj. J. Pavlović, V. M. Maksimović, N. D. Nikolić, K. I. Popov, *Int. J. Electrochem. Sci.* **5** (2010) 1862
14. G. Orhan, G. G. Gezgin, *J. Serb. Chem. Soc.* **77** (2012) 651
15. N. D. Nikolić, G. Branković, M. G. Pavlović, *Powder Technol.* **221** (2012) 271
16. M. V. Mandke, S.-H. Han, H. M. Pathan, *CrystEngComm* **14** (2012) 86
17. J. Han, J. Liu, *J. Nanoeng. Nanomanuf.* **2** (2012) 171
18. T.-H. Lin, C.-W. Lin, H.-H. Liu, J.-T. Sheu, W.-H. Hung, *Chem. Commun.* **47** (2011) 2044
19. N. D. Nikolić, H. Wang, H. Cheng, C. Guerrero, E. V. Ponizovskaya, G. Pan, N. Garcia, *J. Electrochem. Soc.* **151** (2004) C577
20. J. Wang, L. Wei, L. Zhang, Y. Zhang, C. Jiang, *CrystEngComm* **14** (2012) 1629
21. N. D. Nikolić, Dj. Dj. Vaštag, P. M. Živković, B. Jokić, G. Branković, *Adv. Powder Technol.* **24** (2013) 674
22. N. D. Nikolić, V. M. Maksimović, G. Branković, *RSC Adv.* **3** (2013) 7466
23. G. Wranglen, *Electrochim. Acta* **2** (1960) 130
24. A. R. Despić, K. I. Popov, *Transport controlled deposition and dissolution of metals*, in *Modern Aspects of Electrochemistry*, B. E. Conway, J. O' M. Bockris, Eds., Vol. 7, Plenum Press, New York, 1972, p.p. 199–313
25. J. W. Diggle, A. R. Despić, J. O' M. Bockris, *J. Electrochem. Soc.* **116** (1969) 1503
26. K. I. Popov, N. D. Nikolić, *General Theory of Disperse Metal Electrodeposits Formation*, in *Electrochemical Production of Metal Powders*, Series: *Modern Aspects of Electrochemistry*, S. S. Djokić, Ed., Vol. 54, Springer, Berlin, 2012, p.p. 1–62
27. J. O' M Bockris, A. K. N. Reddy, M. Gamboa-Aldeco, *Modern Electrochemistry 2A, Fundamentals of Electrodics*, Kluwer Academic / Plenum Publishers, New York, 2000, p. 1333
28. K. I. Popov, P. M. Živković, N. D. Nikolić, *J. Serb. Chem. Soc.* **76** (2011) 805
29. C.-Z. Yao, M. Liu, P. Zhang, X.-H. He, G.-R. Li, W.-X. Zhao, P. Liu, Y.-X. Tong, *Electrochim. Acta* **54** (2008) 247.

Journal of the Serbian Chemical Society
JSCS-info@shd.org.rs • www.shd.org.rs/JSCS

J. Serb. Chem. Soc. 78 (9) 1397–1411 (2013)
JSCS–4506

UDC 547.233–304.2:544.4+544.6:
547.313'733–31+547.538+546.226
Original scientific paper

Application of commercial poly(3,4-ethylenedioxythiophene):poly(styrene sulfonate) for electrochemical sensing of dopamine

YUANYUAN YAO[1], YANGPING WEN[2], JINGKUN XU[1]*, LONG ZHANG[3] and XUEMIN DUAN[3]

[1]Jiangxi Key Laboratory of Organic Chemistry, Jiangxi Science and Technology Normal University, Nanchang 330013, China, [2]Key Laboratory of Crop Physiology, Ecology and Genetic Breeding, Ministry of Education, Jiangxi Agricultural University, Nanchang 330045, China and [3]School of Pharmacy, Jiangxi Science and Technology Normal University, Nanchang 330013, China

(Received 24 September 2012, revised 26 March 2013)

Abstract: In this paper, a simple and stable composite electrode based on the intrinsically conducting polymer poly(3,4-ethylenedioxythiophene):poly(styrene sulfonate) (PEDOT:PSS) and Nafion®, an ion-exchange polymer, was successfully fabricated by drop-coating the blended commercially available PEDOT:PSS aqueous dispersion and Nafion® solution on the surface of a glassy carbon electrode (GCE). PEDOT:PSS was used as the matrix, while Nafion® was employed to improve the immobilization stability of the composite films and adhesion to the electrode surface in comparison with PEDOT:PSS films. Cyclic voltammetry, differential pulse voltammetry, electrochemical impedance spectroscopy and scanning electron microscopy were utilized to characterize the properties of this composite electrode. The as-proposed composite electrode displayed good water-stability. Meanwhile, the composite electrode was applied to electrochemical sensing of dopamine, and the performance of PEDOT:PSS–Nafion® composite film was evaluated. The obtained results demonstrated that PEDOT:PSS–Nafion® composites are promising candidates for modification of electrode material used in electrochemical sensing and other electrocatalytic applications.

Keywords: PEDOT:PSS; Nafion®; electrocatalysis; dopamine; electrochemical sensor.

INTRODUCTION

Poly(3,4-ethylenedioxythiophene):poly(styrene sulfonate) (PEDOT:PSS), one of the most successful commercially available intrinsically conducting poly-

* Corresponding author. E-mail: xujingkun@tsinghua.org.cn
doi: 10.2298/JSC120927036Y

mers today, has been widely used as antistatic coatings, thermoelectric materials, electrically conducting coatings, hole injection layers, conducting layers in capacitors or as transparent conducting layers in photovoltaic devices and organic light-emitting diodes.[1–4] PEDOT:PSS is also an attractive material to modify electrodes foreseen for electroanalysis due to its good film forming properties, high conductivity, low redox potential, excellent electrochemical, ambient and thermal stability, and good processability,[5–8] Unfortunately, solution-cast films of commercially available PEDOT:PSS aqueous dispersions tend to swell and disintegrate in aqueous solutions,[9–11] which lead to few application in the development of chemo/bio-sensing devices. Previous studies demonstrated that water-resistant and insoluble PEDOT:PSS films could be obtained through secondary doping ionic liquids,[3] multivalent cations,[9] or bis(fluorinated phenyl azide).[12] Thus demonstrating that application of commercially available PEDOT:PSS in the field of chemo/bio sensing could be feasible.

Nafion® is a perfluorinated sulfonated ion-exchange polymer discovered in the late 1960s by Walther Grot of DuPont.[13] Its unique ionic properties are the result its hydrophobic polytetrafluoroethylene backbone chain and perfluorovinyl ether groups terminated with sulfonic cation exchange sites.[14–16] Nafion®, due to its good biocompatibility, antifouling capacity, chemical inertness, and thermal stability, as well as high permeability to water molecules and small cations,[15–21] has been widely used in electrochemistry to modify electrodes. Moreover, mixing Nafion® with other materials can improve the interface adhesion between films and electrodes.[22,23]

Dopamine (DA), one of the most important neurotransmitter in mammalian brain tissues, plays a significant role in the functioning of the central renal, nervous, hormonal and cardiovascular systems.[24,25] Deficiency of DA could be implicated in several diseases and neurological disorders, such as schizophrenia, depression, Huntington's disease, Parkinson's disease and HIV infection.[25–28] Thus, monitoring the concentration fluctuations of DA is of great importance. Among various methods that have been exploited for the determination of DA, electrochemical techniques[7,29] have been proven to be rapid, simple, sensitive, selective, and effective analytical methods. Recently, many materials have been used to fabricate modified electrode for the determination of DA, such as mesoporous silica,[25] carbon nanotubes[27,28] and gold nanoparticles.[29] However, hitherto, the electrochemical determination of DA using the commercially available intrinsically conducting polymer PEDOT:PSS has not been reported.

In this work, another strategy was adopted by directly introducing the ion-exchange polymer Nafion® to increase the hydrophobicity of PEDOT:PSS films, thereby a simple and water-stable PEDOT:PSS–Nafion® composite electrode was successfully fabricated using a glassy carbon electrode (GCE) drop-coated with a solution of a mixture of a commercially available water-dispersible

PEDOT:PSS polymer and the ion-exchange polymer Nafion®. The composite electrode was subsequently applied for the electrochemical sensing of dopamine. The performance of PEDOT:PSS–Nafion® composite films were evaluated.

EXPERIMENTAL

Chemicals

An aqueous dispersion (1.3 mass %) of PEDOT:PSS (Baytron P, Bayer AG, Germany) was used. Nafion® (5 mass %) was obtained from the DuPont Company (USA). Dopamine (DA) was purchased from Sigma–Aldrich (St. Louis, USA). Ascorbic acid was obtained from Bio Basic Inc. Uric acid was purchased from the Aladdin-Reagent Company (Shanghai, China). Glucose, citrate, cysteine, ethanol, sodium chloride, oxalate, disodium hydrogen phosphate dodecahydrate ($Na_2HPO_4 \cdot 12H_2O$) and sodium dihydrogen phosphate dihydrate ($NaH_2PO_4 \cdot 2H_2O$) were obtained from the Sinopharm Chemical Reagent Co., Ltd. 0.1 M Phosphate buffer solutions (PBS) (0.1 M) were prepared from stock solutions of 0.1 M NaH_2PO_4 and 0.1 M Na_2HPO_4. All chemicals were of analytical grade and used as received without further purification. All solutions were prepared using deionized distilled water as solvent. Dopamine solutions were prepared immediately before use in each experiment.

Apparatus

Electrochemical experiments were performed with a CHI660B electrochemical workstation (Shanghai Chenhua Instrument Company, China) and were realized in a conventional electrochemical cell containing a three-electrode arrangement at room temperature. The three-electrode cell assembly consisted of a saturated calomel electrode (SCE) reference electrode and a platinum wire counter electrode. The working electrode was a PEDOT:PSS–Nafion® composite electrode. Scanning electron microscopy (SEM) was realized with a VEGA TESCAN scanning electron microscope. The pH values were measured with a Delta 320 pH meter (Mettler-Toledo Instruments, Shanghai, China). The electrochemical impedance spectra (EIS) were recorded on an Autolab frequency response analyzer (AUT30, FRA2-Autolab, Eco Chemie, BV, Netherlands). The addition of a sample was performed with a micropipette (Dragonmed, Shanghai, China).

Preparation of the PEDOT:PSS–Nafion® composite electrodes

A commercially available aqueous dispersion of PEDOT:PSS (1.3 mass %) was thoroughly stirred for 48 h at room temperature in order to be well distributed. The counter electrode was carefully polished with abrasive paper (1500 mesh), cleaned successively with water and acetone, and then air-dried. A bare glassy carbon electrode (GCE) was carefully polished subsequently with 0.05 μm alumina slurry until a mirror-shine surface was obtained and then successively sonicated in doubly distilled deionized water and ethanol. A mixture of an aqueous dispersion of PEDOT:PSS and a 5 mass % Nafion® solution at a 1:1 volume ratio was continuously stirred for 24 h at room temperature, whereby a PEDOT:PSS–Nafion® solution was obtained. A PEDOT:PSS–Nafion® composite electrode (PEDOT:PSS––Nafion®/GCE) was prepared by directly drop-coating 5 μL PEDOT:PSS–Nafion® mixture on a GCE that was then dried at room temperature under a clean environment. All the fabricated electrodes were stored at 4 ºC until use. The fabrication procedure of PEDOT:PSS––Nafion®/GCE is schematically illustrated in Fig. 1.

RESULTS AND DISCUSSION

Surface morphology of the PEDOT:PSS–Nafion® films

SEM was employed to investigate the surface morphology of PEDOT:PSS––Nafion® films. Compared with the regular, compact and homogeneous structure of pure PEDOT:PSS films,[30] the surface morphology of PEDOT:PSS–Nafion® films were found to be slightly irregular, and there were some small pore distributed relatively homogeneous (see SEM in Fig. 1), which suggested that the mixture of water-dispersible PEDOT:PSS and Nafion® had been mixed well, and the slightly rough structure may be very beneficial for the adsorption of analytes.

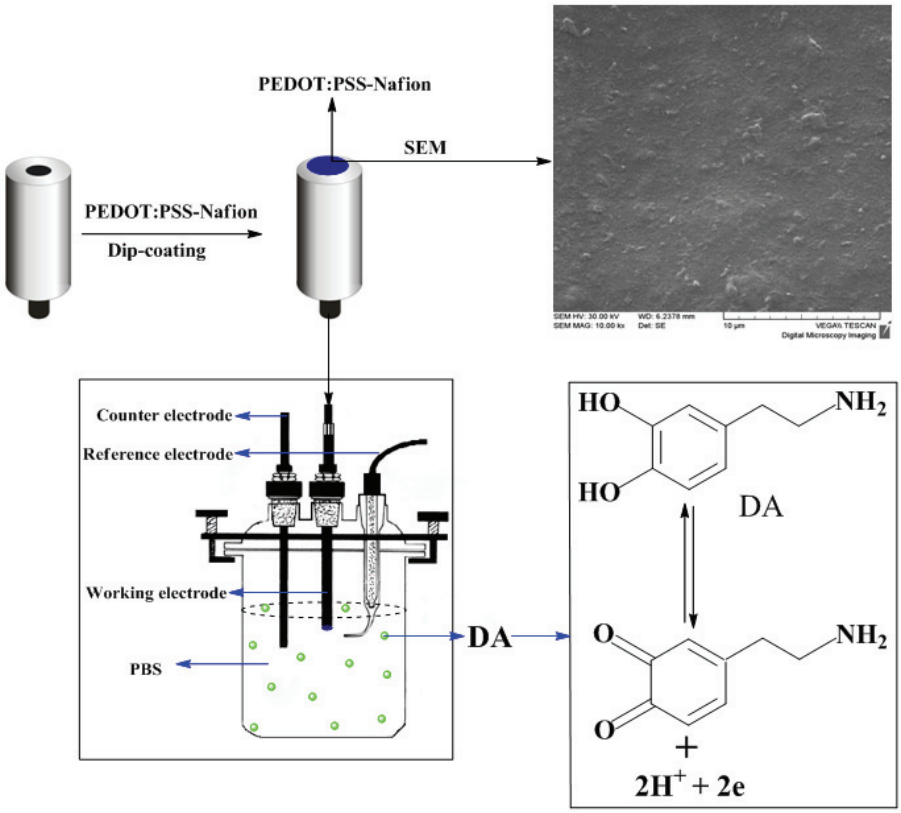

Fig. 1. The procedure for the fabrication of PEDOT:PSS–Nafion®/GCE and an SEM image of a PEDOT:PSS–Nafion® composite film.

Electrochemical characterization of PEDOT:PSS–Nafion® films

The cyclic voltammograms (CVs) of different electrodes in 0.1 M KCl containing 10 mM $[Fe(CN)_6]^{4-/3-}$ as a redox couple are shown in Fig. 2A: a) bare GCE, b) PEDOT:PSS/GCE and c) PEDOT:PSS–Nafion®/GCE. All elec-

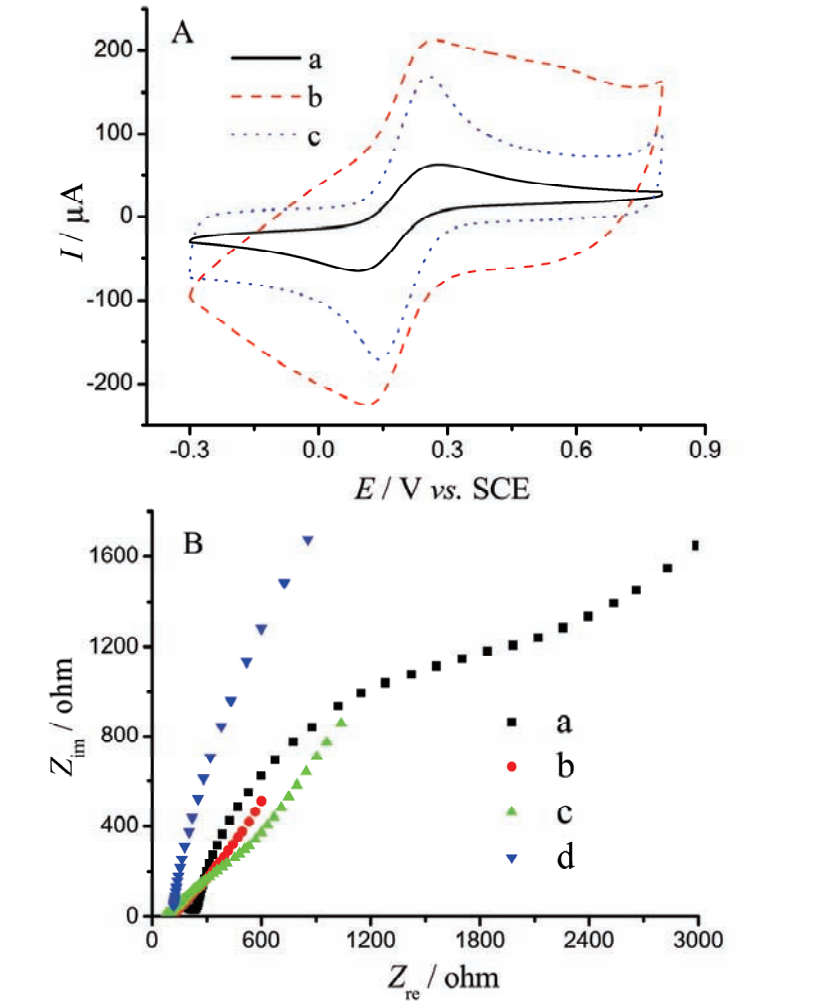

Fig. 2. A) CVs s of different electrodes in a 0.1 M KCl solution containing 10 mM $[Fe(CN)_6]^{4-/3-}$: a) bare GCE, b) PEDOT:PSS/GCE and c) PEDOT:PSS–Nafion®/GCE; Scan rate: 50 mV s^{-1}. B) Nyquist plots of a) bare GCE, b) PEDOT:PSS/GCE, c) PEDOT:PSS–Nafion®/GCE and d) Nafion®/GCE in the same solution.

trodes showed a pair of quasi-reversible redox peaks. Although the currents of the anodic and cathodic peaks at PEDOT:PSS/GCE were higher than at the other electrodes (the electrical conductivity of pure PEDOT:PSS films was 3.380 S cm^{-1}), pure PEDOT:PSS/GCE was extremely hygroscopic[10,31] and tended to swell or disintegrate in the aqueous media.[11] With the introduction of small amounts of Nafion® into PEDOT:PSS, the PEDOT:PSS–Nafion® displayed a decrease of electrical conductivity due to the increasing impedance of the com-

posite films (the electrical conductivity of the PEDOT:PSS–Nafion® composite film with a volume ratio of 1;1 was 0.246 S cm^{-1}), which is in accordance with previous reports,[23] a pair of well-defined quasi-reversible redox peaks appeared on the CV curve of PEDOT:PSS–Nafion®/GCE. Moreover, the potential difference (ΔE_p) between the anodic and cathodic peaks at PEDOT:PSS––Nafion®/GCE (107 mV) was smaller than that at the bare GCE (174 mV) and PEDOT:PSS/GCE (136 mV), indicating better reversibility of electrochemical reaction at the PEDOT:PSS–Nafion®/GCE.

EIS can be used as an efficient tool for describing the electron transfer properties of different composites electrodes. The results of EIS are illustrated in Fig. 2B on a) bare GCE, b) PEDOT:PSS/GCE, c), PEDOT:PSS–Nafion®/GCE and d) Nafion®/GCE using 10 mM $[Fe(CN)_6]^{3-/4-}$ redox couple as the indicator. The EIS was recorded at a potential of 0.17 V and the frequency range was 10 kHz to 100 mHz. The electron-transfer resistance (R_{ct}) value of PEDOT:PSS/ /GCE (almost like a straight line) was much lower than that of the bare GCE, which was attributed to the high conductivity of the PEDOT:PSS films that facilitated fast electron transfer between the solution and the electrode interface. For PEDOT:PSS–Nafion®/GCE, the R_{ct} value was between those of PEDOT:PSS/ /GCE and Nafion®/GCE, which is consistent with the results of CV. Therefore, these results demonstrated that the PEDOT:PSS–Nafion®/GCE had relatively better electrochemical ability and faster electron transfer, and that composite electrode could be utilized as the working electrode.

Electrochemical activity of DA at the PEDOT:PSS–Nafion®/GCE

To assess the performance of PEDOT:PSS–Nafion® composite electrodes, dopamine (DA) was selected for application of the fabricated electrochemical sensor. The CVs of different electrodes taken at a scan rate of 50 mV s^{-1} in 0.1 M PBS (pH 7.0) and 40 μM DA are shown in Fig. 3. Compared with the oxidation peak currents at a bare GCE and Nafion®/GCE, those at PEDOT:PSS/ /GCE and PEDOT:PSS–Nafion®/GCE were remarkably increased, which was attributed to the fact that PEDOT:PSS films have a moderate conductivity.[5,32] However, the PEDOT:PSS/GCE was not very stable and easily swelled or disintegrated in PBS, and the redox peak of DA was very weak. At bare GCE, a pair of redox peaks were observed for the detection of 40 μM DA. The oxidation and reduction peak potentials occurred at 0.404 and 0.058 V, respectively. At PEDOT:PSS–Nafion®/GCE, a well-defined redox wave of DA was observed with the anodic peak potential at 0.269 V and the corresponding cathodic peak potential at 0.098V. The oxidation and reduction peak currents were significantly increased and the electron transfer process to DA was more reversible. These results once again indicated that the determination of DA is feasible at a PEDOT:PSS–Nafion®/GCE.

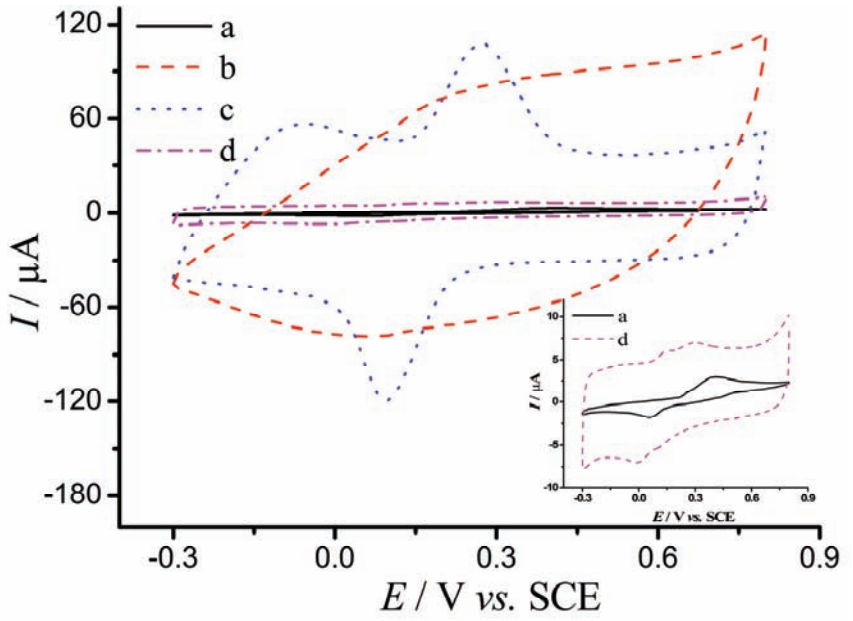

Fig. 3. CVs of different electrodes in 0.1 M PBS (pH 7.0) and 40 μM DA: a) bare GCE, b) PEDOT:PSS/GCE, c) PEDOT:PSS–Nafion®/GCE and d) Nafion®/GCE. Scan rate: 50 mV s^{-1}. Inset: CVs of bare GCE and Nafion®/GCE in 40 μM DA.

Effect of the scan rate towards DA

The effect of the scan rate on the electrochemical behavior of DA at PEDOT:PSS–Nafion®/GCE was studied by CV, and the result are shown in Fig. 4A. With increasing scan rate from 25 to 100 mV s^{-1}, the oxidation peak current (I_{pa}) and reduction peak current (I_{pc}) were in linear relationship to the scan rate (v). The regression equations were: I_{pa} (μA) = 1.78– 7.45v and I_{pc} (μA) = –2.06 – – 18.54v (v in mV s^{-1}), with correlation coefficients of 0.998 and 0.995, respectively. This indicates that the DA molecules can be adsorbed onto the electrode surface, and the electrochemical oxidation of DA at the PEDOT:PSS– –Nafion®/GCE was an adsorption-controlled process.[29]

Effect of pH values towards DA

The effect of pH value on the determination of DA at PEDOT:PSS–Nafion®/GCE in PBS within the range from 2.0 to 8.0 was investigated by CV and the results are shown in Fig. 5A. The pH value had a significant influence on both the redox peak potentials and peak currents. The relationship between the oxidation peak currents and pH value is presented in Fig. 5B. The results showed that the peak current of DA increased with increasing pH value until the highest peak current and the best peak shape were obtained at pH 7.0, while the peak current decreased dramatically when the pH value exceeded 7.0, which was pro-

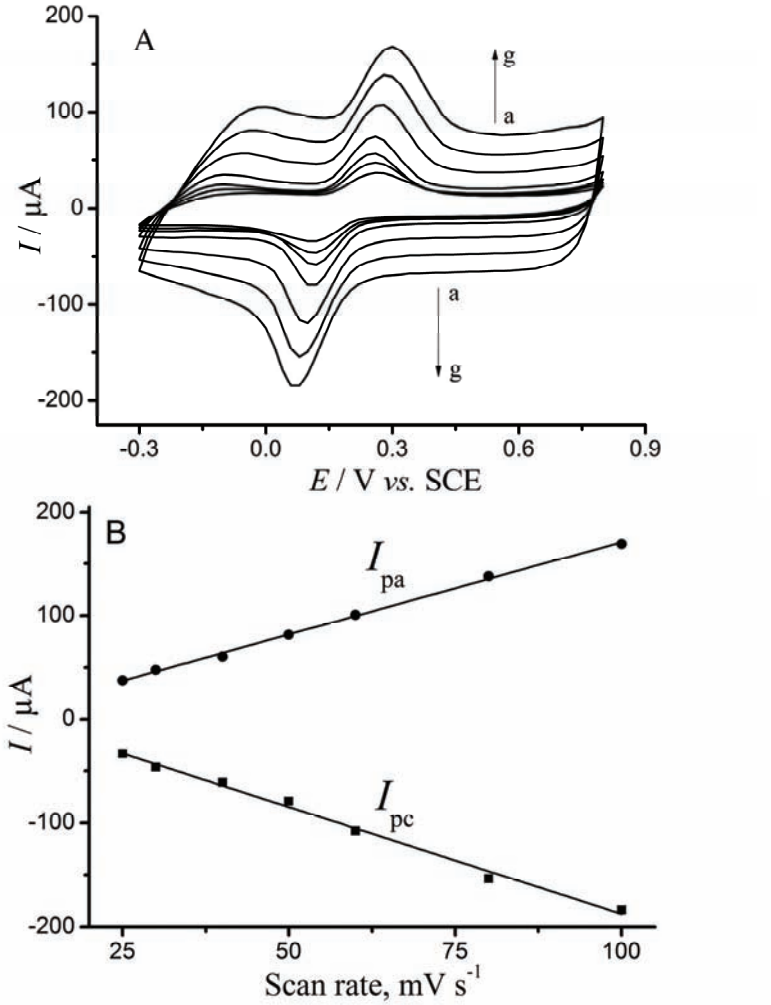

Fig. 4. A) CVs of 40 μM DA in 0.1 M PBS (pH 7.0) at scan rates of 25, 30, 40, 50, 60, 80 and 100 mV s^{-1} (from a to g) and B) the plots of redox peak currents *vs.* the scan rate.

bably due to the charge interactions between DA and electrode surface. In addition, the relationship between the oxidation peak potentials (E_{pa}) and pH values was also investigated and the results are shown in Fig. 5C. It can be observed that the E_{pa} shifted negatively as the pH value was increased, indicating that protons were involved in the electrode reaction. The curve presents two straight lines in the pH range 2.0–8.0. The regression equations were E_{pa} (V) = 0.4956 – 0.0156pH (R^2 = 0.9946) at the lower pH values 2.0–6.0 with a slope of 15.6 mV pH^{-1}, which is smaller than the theoretical value of –57.6 mV pH^{-1}. While the regression equations was E_{pa} (V) = 0.9901 – 0.995pH (R^2 = 0.9853) at the higher

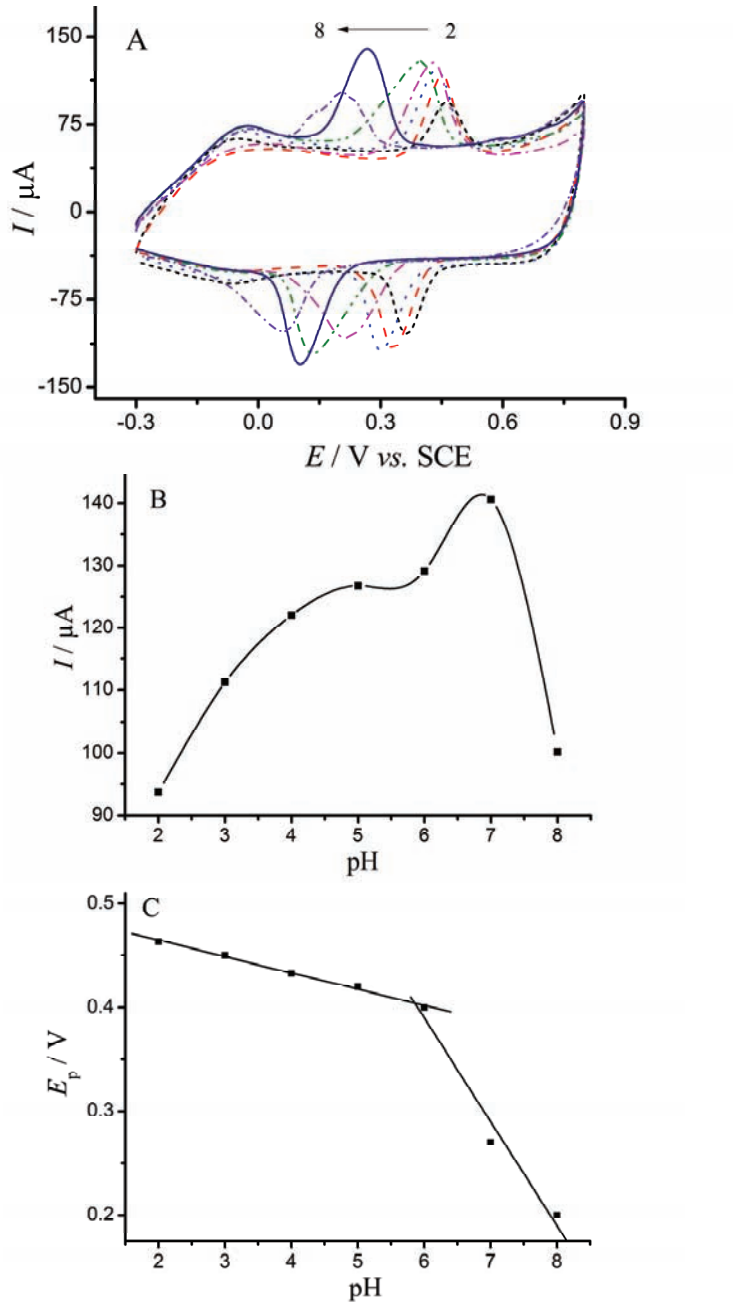

Fig. 5. A) CVs in 40 μM DA and 0.1 M PBS at different pH values: 2.0, 3.0, 4.0, 5.0, 6.0, 7.0 and 8.0. Effects of the pH value on: B) the oxidation peak currents and C) the oxidation peak potentials for the oxidation of 40 μM DA. Scan rate: 50 mV s^{-1}.

pH value between 6.0–8.0. The slope in this pH range was 99.5 mV pH^{-1}, which is high than the theoretical value. The reason for this is yet unclear. However, the pH value has an influence on both the peak potential and peak current, revealing that electron transfer and proton transfer participated in the reaction. Considering the physiological pH (7.4), pH 7.0 was chosen as optimal pH value of PBS.

Determination of DA

The determination of DA concentration at a PEDOT:PSS–Nafion®/GCE was performed by differential pulse voltammetry (DPV) in 0.1 M PBS (pH 7.0) and the results are shown in Fig. 6A. As can be seen in Fig. 6B, the oxidation peak current of DA was linearly proportional to its concentration in the range of 0.10 to 50 μM. The regression equation was I_{pa} (μA) = 9.04 + 0.41c (c in μM) (R^2 = = 0.996) with a detection limit of 0.03 μM (S/N = 3), where c is the concentration of DA. Compared with most of the modified electrodes reported in the literature (listed in Table I),[24,27,33–37] the fabricated PEDOT:PSS–Nafion®/GCE exhibited a good sensing performance.

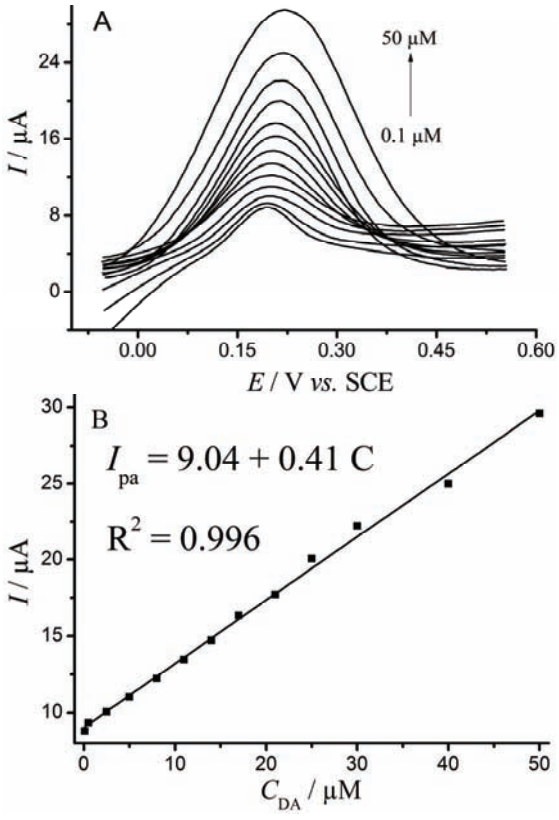

Fig. 6. A) DPVs in various concentrations of DA and 0.1 M PBS (pH 7.0) at a PEDOT:PSS–Nafion®/GCE. DA concentrations: 0.1, 0.5, 2.5, 5.5, 8, 11, 13, 17, 21, 25, 30, 40 and 50 μM. Scan rate: 50 mV s^{-1}. B) Linear relationship between peak current and the concentration of DA.

TABLE I. Comparison of different modified electrodes for the determination of DA; 6A2MBT: 6-amino-2-mercaptobenzothiazole; EPPGE: edge-plane pyrolytic graphite electrode; PEDOT–PANS: poly[3,4-ethylenedioxythiophene-*co*-(5-amino-2-naphthalenesulfonic acid)]; NBAR: *p*-nitrobenzenazo resorcinol; GCE: glassy carbon electrode; CNT: carbon nanotubes; IL: ionic liquid; RGO: reduced graphene oxide; CNOs: carbon nano-onions; PDDA: poly(diallyldimethylammonium chloride); AABA: 3-acrylamidophenylboronic acid; ACS: acetate buffer solution; *LCR*: linear concentration range; *LOD*: limit of detection

Electrode	Electrolyte	*LCR* / μM	*LOD* / μM	Reference
6A2MBT/Au	PBS (pH 7.2)	1–642	0.157	24
SWCNT–Fe_2O_3/EPPGE	PBS (pH 7.0)	3.2–31.8	0.36	27
PEDOT–PANS/GCE	ACS (pH 5.0)	2–8	0.5	33
polyNBAR/GCE	PBS (pH 4.0)	5–25	0.3	34
RGO/AuNPs/GCE	PBS (pH 7.4)	1–60	0.02	35
CNOs/PDDA /GCE	PBS (pH 5.0)	50–400	10	36
MWCNT/poly(AABA)/GCE	PBS (pH 7.4)	0.05–2	0.02	37
PEDOT:PSS–Nafion®/GCE	PBS (pH 7.0)	0.1–50	0.03	This work

Interference, stability and reproducibility studies

The reproducibility of PEDOT:PSS–Nafion®/GCE was studied by measurement the peak current response of 40 μM DA in 0.1 M PBS (pH 7.0) by CV. The relative standard deviation (*RSD*) of the oxidation peak currents during 20 successive measurements was 1.3 %, indicating good reproducibility (shown in Fig. 7). When the electrode was kept at 4 °C for two weeks, the peak currents remained at 96 % of their initial values. These results revealed that PEDOT:PSS––Nafion®/GCE had excellent water-stability, implying that Nafion® can improve the swelling and disintegration properties of PEDOT:PSS and lower the swelling of the modified electrode in aqueous media.[23,38]

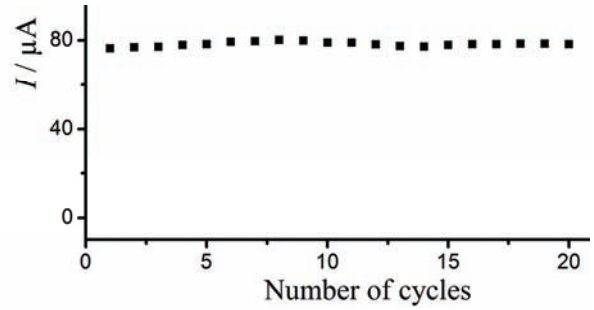

Fig. 7. The stability of a PEDOT:PSS–Nafion®/GCE in 0.1 M PBS (pH 7.0) containing 40 μM DA. Scan rate: 50 mV s^{-1}.

The possible interferences for DA determination were evaluated by the response current–time (*I–t*) curve and DPV. The *I–t* curve presented in Fig. 8A shows that addition of 10 μM DA caused a noticeable change in the current res-

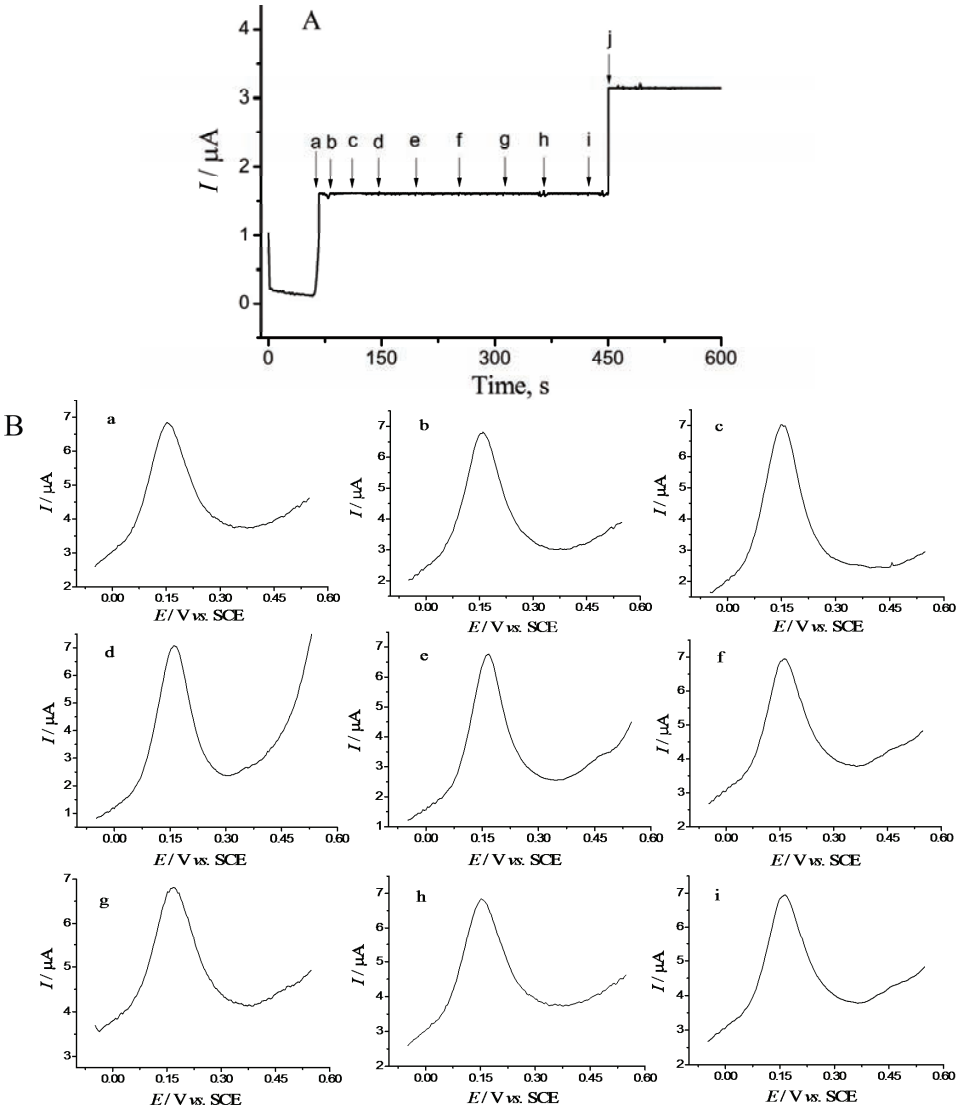

Fig. 8. A) The responses for interferents tested at a PEDOT:PSS–Nafion®/GCE by the amperometric method at an applied potential 0.3 V *vs.* SCE in 0.1 M PBS (pH 7.0). The injection of the potentially interfering compounds were a) 10 μM DA, b) 100 μM ascorbic acid, c) 100 μM uric acid, d) 100 μM cysteine, e) 1 mM glucose, f) 1 mM sodium citrate, g) 1 mM ethanol, h) 1 mM sodium chloride, i) 1 mM oxalic acid and j) 10 μM DA. B) The corresponding responses for interferents tested by DPV.

ponse. Then, addition of 10-fold amounts of ascorbic acid, uric acid and cysteine and 100-fold amounts of glucose, sodium citrate, ethanol, sodium chloride and oxalic acid were successively added, which had no obvious influence on the

electrode response, with deviations below 5 %. Then, 10 μM DA was added again, which caused the current to change significantly. This implied that the fabricated PEDOT:PSS–Nafion®/GCE had good selectivity, which may be largely attributed to the strong anti-interferent ability of Nafion®.[39] Moreover, the interference experiments were repeated using the common DPV technique. From Fig. 8B, it can be seen that again no obvious influence for most of the interfering substance was evidenced by the DPV method, while added ascorbic acid, uric acid or cysteine had a slight influence. Once again, the good selectivity of the PEDOT:PSS–Nafion®/GCE was indicated.

CONCLUSIONS

In summary, the commercially available water-dispersible PEDOT:PSS and the ion-exchange polymer Nafion® were successfully used to fabricate a simple water-stable and conducting composite PEDOT:PSS–Nafion®/GCE for sensing applications. Due to the high conductivity of PEDOT:PSS and strong adsorptive ability of the binding agent Nafion®, the PEDOT:PSS–Nafion®/GCE showed good electrochemical activities, excellent reproducibility and water-stability, fast electrode transfer, and low swell and disintegration. This composite electrode was used for the detection of DA with a fast current response, good selectivity, and strong anti-interferent ability, which provided a promising method for modified electrode materials. This work also enlarges the application of PEDOT:PSS in chemo/bio-sensing.

Acknowledgements. The authors thank NSFC (51073074, 51272096), Jiangxi Provincial Department of Education (GJJ11590, GJJ10678) and the Natural Science Foundation of Jiangxi Province (2010GZH0041) for providing financial support for this study.

ИЗВОД

ПРИМЕНА КОМЕРЦИЈАЛНОГ ПОЛИ(3,4-ЕТИЛЕН-ДИОКСИТИОФЕН):ПОЛИСТИРЕН СУЛФОНАТА ЗА ЕЛЕКТРОХЕМИЈСКУ ДЕТЕКЦИЈУ ДОПАМИНА

YUANYUAN YAO[1], YANGPING WEN[2], JINGKUN XU[1], LONG ZHANG[3] и XUEMIN DUAN[3]

[1] *Jiangxi Key Laboratory of Organic Chemistry, Jiangxi Science and Technology Normal University, Nanchang 330013, China,* [2] *Key Laboratory of Crop Physiology, Ecology and Genetic Breeding, Ministry of Education, Jiangxi Agricultural University, Nanchang 330045, China and* [3] *School of Pharmacy, Jiangxi Science and Technology Normal University, Nanchang 330013, P. R. China*

У раду је успешно направљена једноставна и стабилна композитна електрода на бази проводног полимера поли(3,4-етилендиокситиофен):полистирен-сулфонат (PEDOT:PSS) и јоноизмењивачког полимера, Nafion®, тако што је на површину електроде од стакластог угљеника нанета кап смеше комерцијално доступне водене дисперзије PEDOT:PSS и раствора Nafion®. PEDOT:PSS је имао улогу матрице, док је Nafion® примењен у циљу повећања стабилности композитног филма и његове адхезије на површини електроде. За карактеризацију описане композитне електроде коришћене су методе цикличне волтаметрије, диференцијалне пулсне волтаметрије, спектроскопије електрохемијске импеданције и скенирајуће електронске микроскопије. Електрода је пока-

зала добру стабилност у води, а затим је примењена за електрохемијску детекцију допамина. Одређивање њених перформанси при детекцији овог једињења је показало да композитни филм PEDOT:PSS има потенцијалну примену у електрохемијским сензорима и електрокатализаторима.

(Примљено 24. септембра 2012, ревидирано 26. марта 2013)

REFERENCES

1. Y. H. Kim, C. Sachse, M. L. Machala, C. May, L. Müller-Meskamp, K. Leo, *Adv. Funct. Mater.* **21** (2011) 1076
2. M. C. Scharber, D. Wuhlbacher, M. Koppe, P. Denk, C. Waldauf, A. J. Heeger, C. L. Brabec, *Adv. Mater.* **18** (2006) 789
3. M. Döbbelin, R. Marcilla, C. Tollan, J. A. Pomposo, J. R. Sarasuab, D. Mecerreyes, *J. Mater. Chem.* **18** (2008) 5354
4. K. M. Coakley, M .D. McGehee, *Chem. Mater.* **16** (2004) 4533
5. J. J. Xu, R. Peng, Q. Ran, Y. Z. Xian, Y. Tian, L. T. Jin, *Talanta* **82** (2010) 1511
6. C. Sriprachuabwong, C. Karuwan, A. Wisitsorrat, D. Phokharatkul, T. Lomas, P. Sritongkham, A. Tuantranont, *J. Mater. Chem.* **22** (2012) 5478
7. C. Bartic, A. Campitelli, S. Borghs, *Appl. Phys. Lett.* **82** (2003) 475
8. J. Liu, M. Agarwal, K. Varahramyan, *Sensors Actuators, B* **135** (2008) 195
9. M. Vázquez1, P. Danielsson, J. Bobacka, A. Lewenstam, A. Ivaska, *Sensors Actuators, B* **97** (2004) 182
10. A. M. Nardes, M. Kemerink, R. A. J. Janssen, J. A. M. Bastiaansen, N. M. M. Kiggen, B. M. W. Langeveld, A. J. J. M. Breemen, M. M. Kok, *Adv. Mater.* **19** (2007) 1196
11. T. Y. Dai, X. J. Jiang, S. H. Hua, X. S. Wang, Y. Lu, *Chem. Commun.* **36** (2008) 4280
12. G. Winroth, G. Latini, D. Credgington, L. Y. Wong, L. L. Chua, P. K. H. Ho, F. Cacialli, *Appl. Phys. Lett.* **92** (2008) 103308
13. W. G. Grot, *Macromol. Symp.* **82** (1994) 161
14. H. G. Haubold, T. Vad, H. Jungbluth, P. Hiller, *Electrochim. Acta* **46** (2001) 1559
15. Z. Y. Lin, J. H. Chen, G. N. Chen, *Electrochim. Acta* **53** (2007) 2396
16. P. B. Desai, A. K. Srivastava, *Sensors Actuators, B* **169** (2012) 341
17. S. Yang, R. Yang, G. Li, L. Qu, J. Li, L. Yu, *J. Electron. Mater.* **639** (2010) 77
18. X. Xie, T. Gan, D. Sun, K. Wu, *Fullr. Nanotub. Carbon* **16** (2008) 103
19. K. J. Huang, X. Liu, W. Z. Xie, H. X. Yuan, *Colloids Surfaces, B* **64** (2008) 269
20. M. Pan, H. L. Tang, S. P. Jiang, Z. Liu, *Electrochem. Commun.* **7** (2005) 119
21. L. Zhang, Z. Fang, Y. H. Ni, G. C. Zhao, *Int. J. Electrochem. Sci.* **4** (2009) 407
22. Z. G. Di, H. B. Li, M. Li, D. L. Mao, X. J. Chen, M. Xiao, J. Gu, *J. Power Sources* **207** (2012) 86
23. Y. P. Wen, J. K. Xu, D. Li, M. Liu, F. F. Kong, H. H. He, *Synth. Met.* **162** (2012) 1309
24. R. K. Shervedani, S. M. Siadat-Barzoki, M. Bagherzadeh, *Electroanalysis* **22** (2010) 969
25. M. P. D. Santos, A. Rahim, N. Fattori, L. T. Kubota, Y. Gushikem, *Sensors Actuators, B* **171**–**172** (2012) 712
26. A. Nagano-Saito, J. Q. Liu, J. Doyon, A. Dagher, *Neurosci. Lett.* **458** (2009) 1
27. A. S. Adekunle, B. O. Agboola, J. Pillay, K. I. Ozoemena, *Sensors Actuators, B* **148** (2010) 93
28. R. E. Sabzi, K. Rezapour, N. Samadi, *J. Serb. Chem. Soc.* **75** (2010) 537
29. P. Wang, Y. X. Li, X. Huang, L. Wang, *Talanta* **73** (2007) 431
30. C. C. Liu, J. K. Xu, B. Y. Lu, R. R. Yue, F. F Kong, *J. Electron. Mater.* **41** (2012) 639

31. J. Huang, P. F. Miller, J. S. Wilson, A. J. de Mello, J. C. de Mello, D. D. C. Bradley. *Adv. Funct. Mater.* **15** (2005) 291
32. J. Ou-yang, C. W. Chu, F. C. Chen, Q. Xu, Y. Yang, *Adv. Funct. Mater*. **15** (2005) 203
33. A. Balamurugan, S. M. Chen, *Anal. Chim. Acta* **596** (2007) 92
34. X. H. Lin, Y. F. Zhang, W. Chen, P. Wu, *Sensors Actuators, B* **122** (2007) 309
35. S. Liu, J. Yan, G. W He, D. D Zhong, J. X. Chen, L. Y Shi, X. M. Zhou, H.J. Jiang, *J. Electron. Mater*. **672** (2012) 40
36. J. Breczko, M. E. Plonska-Brzezinska, L. Echegoyen, *Electrochim. Acta* **72** (2012) 61
37. S. J. Hong, L. Y. S. Lee, M. H. So, K. Y. Wong, *Electroanalysis* **25** (2013) 1
38. A. A. Karyakin, E. A. Kotelnikova, L. V. Lukachova, E. E. Karyakina, J. Wang, *Anal. Chem.* **74** (2002) 1597
39. M. Liu, Y. P. Wen, D. Li, R. R. Yue, J. K. Xu, H. H. He, *Sensors Actuators, B* **159** (2011) 278.

Journal of the Serbian Chemical Society
JSCS-info@shd.org.rs • www.shd.org.rs/JSCS
J. Serb. Chem. Soc. 78 (9) 1413–1423 (2013)
JSCS–4507
UDC 577.182.24:537.363:543.544
Original scientific paper

Development of a capillary electrophoresis method for the simultaneous determination of cephalosporins

GABRIEL HANCU*, HAJNAL KELEMEN, AURA RUSU and ÁRPÁD GYÉRESI

Faculty of Pharmacy, University of Medicine and Pharmacy Târgu Mureş, Gh. Marinescu street 32, 540131 Târgu Mureş, Romania

(Received 17 November 2012, revised 22 February 2013)

Abstract: A rapid and simple capillary electrophoresis method has been developed for the simultaneous determination of six extensively used cephalosporin antibiotics (cefaclor, cefadroxil, cefalexin, cefuroxim, ceftazidim and ceftriaxon). The determination of cephalosporins was performed at pH 6.8, using a 25 mM phosphate/25 mM borate mixed buffer, and a voltage of 25 kV at a temperature of 25 °C. A baseline separation was achieved in approximately 10 min. The separation resolution was increased by the addition of an anionic surfactant, 50 mM sodium dodecyl sulfate, to the buffer solution. The proposed separation was evaluated based on the detection and quantification limits, effective electrophoretic mobility and relative standard deviation for the migration times and peak areas.

Keywords: cephalosporins; capillary zone electrophoresis; micellar electrokinetic chromatography.

INTRODUCTION

Nowadays, cephalosporins are one of the most important and probably the most frequently used antibiotics in the world, both in terms of the number of compounds currently on the market and of their use for the treatment of infectious diseases.

Cephalosporins are semi-synthetic antibiotics, derived from cephalosporin C, found among the fermentation products of *Cephalosporium acremonium* over fifty years ago. These antibiotics, derived from 7-aminocephalosporanic acid, are composed of a *β*-lactam ring fused with a dihydrothiazine ring and differ in the nature of the substituents attached to the cephem ring.[1]

More than 60 cephalosporins in four generations are already available on the market, so it is important to develop new analysis methods for their quality control. The analysis of cephalosporins is not only limited to pharmaceutical

* Corresponding author. E-mail: g_hancu@yahoo.com
doi: 10.2298/JSC121117028H

analysis, but also extends to food safety and environmental protection; all these analytical tasks require the development of high performance separation methods.

In this study, we analyzed six frequently used cephalosporin derivatives: cefalexin (CFL), cefadroxil (CFD) and cefaclor (CFC) – first generation oral cephalosporins; cefuroxim (CFR) – a second generation parenteral cephalosporin; and ceftazidim (CZI) and ceftriaxon (CTR) – third generation parenteral cephalosporins. Substitution of the various R and R′ groups results in cephalosporins with different pharmacological and pharmacokinetic properties. The chemical structures of the studied cephalosporins are presented in Table I.

TABLE I. The chemical structure of the studied cephalosporins[1]

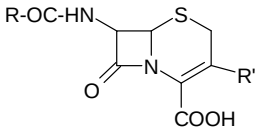

Cephalosporin derivative	R	R′
Cefalexin – CFL	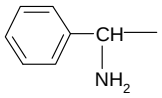	$-CH_3$
Cefadroxil – CFD	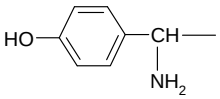	$-CH_3$
Cefaclor – CFC	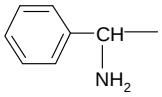	–Cl
Cefuroxim – CFR	‼ EMBED ISISServer	$-CH_2-O-CO-NH_2$
Ceftazidim – CZI	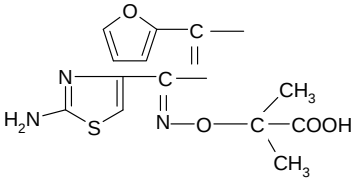	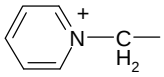
Ceftriaxon – CTR	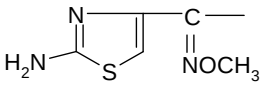	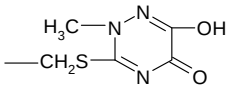

High performance liquid chromatography (HPLC) is usually the method of choice for the analysis of cephalosporins because of its specificity, rapidity and sensitivity. In recent years, capillary electrophoresis (CE), due to its short analysis time, high efficiency and low solvent and sample consumption; has proved to be a powerful analytical tool for the determination of pharmaceutical substances, being regarded as an alternative and also a complementary method to HPLC.[2,3]

In the last few years, some studies regarding the determination of cephalosporins by capillary zone electrophoresis (CZE),[4–9] micellar electrokinetic chromatography (MEKC)[10–12] and microemulsion electrokinetic capillary chromatography (MEEKC)[13] have been published.

CZE, also known as free solution capillary electrophoresis, is the simplest form of CE, the separation mechanism being based on differences in the charge-to-mass ratios of the analytes.[2]

MEKC is perhaps the most intriguing mode of CE, combining chromatographic and electrophoretic separation principles, the separation mechanism being based on the individual partition of the analytes between the micellar and aqueous phase.[2]

MEKC can separate both ionic and neutral substances, while CZE typically separates only ionic substances. Thus, MEKC has a great advantage over CZE for the separation of mixtures containing both ionic and neutral compounds.[2]

While MEKC proved itself to be especially useful for the determination of cephalosporins from biological samples (samples having high protein contents) as the disadvantageous matrix effects caused by organic materials are reduced, CZE proved itself to be a powerful analytical tool for determinations from pharmaceutical products.[6,7,8,14]

Structurally cephalosporins are a rather heterogeneous group; consequently, a large number of electrophoretic procedures using different analytical parameters could be used for their separation. Regarding previously published methods, several exemplify the fact that the simultaneous determination of structurally related cephalosporins is challenging because of their similar electrophoretic mobilities. For this reason, both structurally related cephalosporins from the same generation and cephalosporins from different generations and different structural characteristics were chosen as the subjects of the present study.[5,8,9,13]

The aim was to develop a rapid, simple and efficient method for the simultaneous separation of the studied cephalosporins and the optimization of the analytical conditions in order to obtain good separation resolution and a short analysis time.

EXPERIMENTAL

Cefalexin monohydrate, cefadroxil monohydrate, cefaclor monohydrate were obtained from Sandoz (Târgu Mureş, Romania); cefuroxim sodium from Medochemie (Cyprus), while ceftazidim pentahydrate, ceftriaxon sodium from Antibiotice (Iaşi, România). All the studied cephalosporins were of pharmaceutical grade.

Disodium hydrogen phosphate, methanol, phosphoric acid, sodium dodecyl sulfate (SDS), sodium tetraborate were purchased from Merck (Darmstadt, Germany). Sodium hydroxide 0.1 M was purchased from Agilent (Waldbronn, Germany). The water used in the study was purified with a Milli-Q water purification system (Millipore, Bedford, USA).

Capillary electrophoresis measurements were performed on an Agilent 6100 CE system with diode array detection. The electropherograms were recorded and processed by Chem-

station 7.01 (Agilent). The pH of the buffer solutions was determined with the Terminal 740 pH-meter (Inolab). The detection wavelengths were set at 210 and 270 nm. For the identification of the individual peaks, the UV spectrum of each cephaloasporin was recorded previously. Cephalosporins showed high UV absorption, and relatively similar spectra but small differences could be observed in the case of all components, which led to reliable and unambiguous identification.

The temperature was kept at 25 °C and a separation voltage of 25 kV was used. The samples were introduced into the system at the anodic end of the capillary by hydrodynamic injection applying a pressure of 50 mbar for 3 seconds. The separations were performed using polyimide-coated fused silica-capillaries of 56 cm (effective length: 48 cm)×50 μm I.D. (Agilent).

Stock solutions of 1 mg mL^{-1} for all cephalosporins were prepared in water and later diluted to the appropriate concentration. All the samples and buffers were degassed by ultrasound for 5 min before use and filtered through a 0.45 μm syringe membrane filter. The capillaries were preconditioned by washing with 0.1 M NaOH (2 min) and distilled water (3 min).

RESULTS

Preliminary study

The electrophoretic mobilities of cephalosporins depends not only on the number of ionizable carboxyl and amino groups of the analyte, but also on the pH of the buffer electrolyte because the dissociation of these groups is influenced by pH.[7,15]

In order to find suitable conditions for the separation of the studied cephalosporins, a series of preliminary experiments were conducted at different pH values and different compositions of the buffer (borate, citrate, phosphate) background electrolytes. In these preliminary experiments, satisfactory electrophoretic signals were obtained within the pH range 5–8, as the electrophoretic signals for some of the studied cephalosporins disappeared at pH values below 5. It was established that for a given type of background electrolyte, the magnitude of the total mobility of the analytes (electro-osmotic mobility plus electrophoretic mobility) depended mainly on the zeta potential, which decreased with decreasing buffer pH and/or increasing buffer concentration.[5] The migration behavior of the studied cephalosporins in different background electrolyte was significantly different, due to the different basicity on the side chain functional groups, but trends in the variation of the electrophoretic mobility were rather similar.

Comparing the different systems, the best results were obtained using 100 mM phosphate buffer at a pH around 7. However, the current generated in the electrophoretic system exceeded 100 μA; therefore, experimental difficulties appeared due to excessive Joule heating. Moreover, the use of a simple phosphate buffer led to rather long migration times and low resolution for the separation of CFD, CFL and CFC.

In order to improve the separation resolution, a mixed buffer electrolyte containing both disodium hydrogen phosphate (3.55 g L^{-1}) and sodium tetraborate

(5.03 g L^{-1}) was chosen and the pH of the buffer solution was adjusted by the addition of sodium hydroxide, respectively phosphoric acid.

Although the stability of cephalosporins antibiotics in the solid state is usually satisfactory, they are slowly hydrolyzed on dissolution in water to different degradation products. Preliminary studies using an internal standard (ciprofloxacin hydrochloride) as reference showed that degradation (hydrolysis) was insignificant within 4 h of dissolution.[6,7] Electrophoretic runs were performed as quickly as possible, but no later than 4 h after solution preparation, in order to avoid sample decomposition due to the instability of the *β*-lactam ring.

Optimization of the separation conditions

Optimization of the separation was achieved by manipulation of several analytical parameters, such as buffer pH and concentration, applied voltage and system temperature, and by the addition different additives to the buffer solution.

The buffer pH plays an essential role in the separation of ionizable analytes as it determines the extent of ionization of the analytes. The influence of pH on the migration times of a mixture of the six cephalosporins in electrolyte solutions adjusted to pH 5–8. This pH range was chosen in order to minimize any possible degradation of the cephalosporins due to hydrolysis of the *β*-lactam ring. The migration times of all the studied cephalosporins increased with decreasing buffer pH, but in the pH range 6 to 7, the migration times did not change significantly and peak overlapping between CFL with CFC was avoided (Fig. 1).

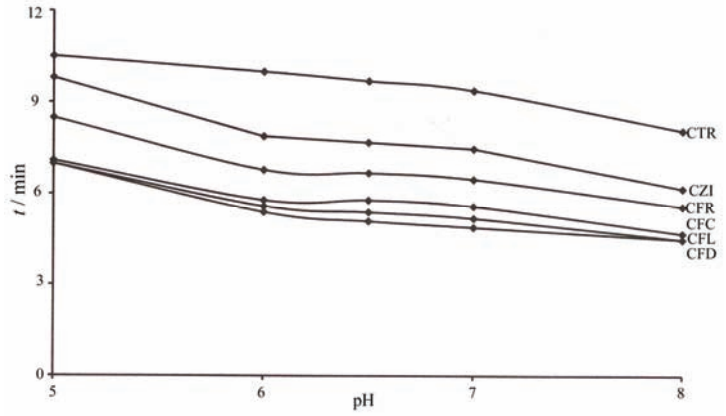

Fig. 1. Influence of pH on the separation of cephalosporins (separation conditions: capillary 56 cm×50 μm I.D., buffer electrolyte 25 mM phosphate – 25 mM borate, applied voltage: 25 kV, temperature: 25 C, detection: UV absorption at 270 nm).

At a given pH, increasing the buffer concentration resulted in a decrease in the electro-osmotic flow (EOF) and electrophoretic mobility and, consequently, an increase in the migration times of the analytes.

The separation of the six studied cephalosporins using the selected CZE parameters was achieved in approximately 10 min. The migration order was: CFD, CFL, CFC, CFR, CZI, CTR (Fig. 2).

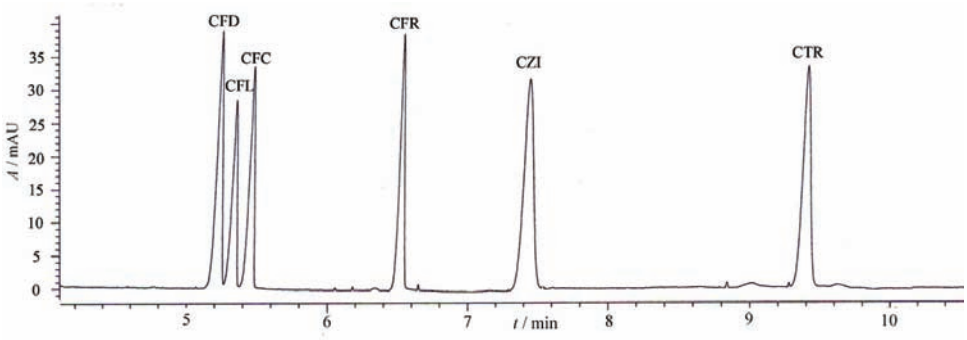

Fig. 2. Electropherogram of the separation of a mixture of the six cephalosporins (separation conditions: capillary 56 cm×50 μm I.D., buffer electrolyte 25 mM phosphate – 25 mM borate, pH – 6.8, applied voltage: 25 kV, temperature: 25 C, detection: UV absorption at 270 nm, concentration of each cephalosporin: 25 μg mL^{-1}).

Difficulties appeared in the separation of the three first generation oral cephalosporins (CFC, CFD and CFL), substances with very similar structural characteristics and, consequently, similar electrophoretic mobilities.

Cephalosporins are hydrophobic drugs that have similar polar groups but exhibit different partition behaviors between two phases (micellar and aqueous phase); consequently, MEKC is a well-suited method for their separation. Depending on the chemical structure of the cephalosporins, in addition to the hydrophobic interactions, various chemical interactions, such as dipolar interactions, may occur between them in the partitioning mechanism. Moreover, these analytes have carboxyl groups, and possible electrostatic repulsion between the analytes and the anionic SDS micelles might decrease, even if just partially, the micellar solubilization of the cephalosporins.[12,15]

Addition of SDS to the buffer solution led to a gradual increase in the migration times of the analytes, but improved resolution between the three structurally related cephalosporins (CFD, CFL and CFC). At neutral pH, a strong EOF moved in the direction of the cathode; SDS is an anionic surfactant consequently the electrophoretic migration of the anionic micelle was in the direction of the anode. As a result, the overall micellar migration velocity was slowed compared to the bulk flow of solvent. The separation was based on the differential partitioning of the analytes between the two-phase-system: the mobile aqueous phase and the pseudo-stationary micellar phase.

The migration times of the analytes increased with increasing SDS concentration as higher SDS concentration result in greater ionic strength and conse-

quently smaller EOF (Fig. 3). In MEKC, the migration times of the cephalosporins also increased with decreasing buffer pH.

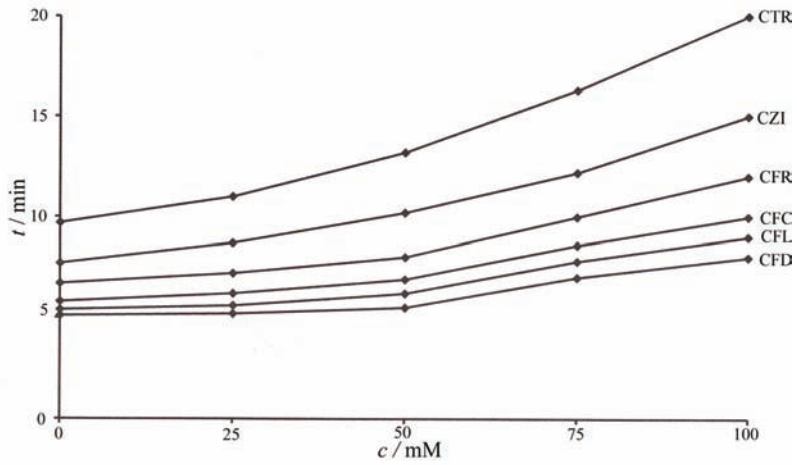

Fig. 3. Influence of SDS concentration on the separation of cephalosporins (separation conditions: capillary 56 cm×50 μm I.D., buffer electrolyte 25 mM phosphate – 25 mM borate, pH – 6.8, applied voltage: 25 kV, temperature: 25 °C, detection: UV absorption at 270 nm).

The optimum SDS concentration was set at 50 mM (14.42 g L^{-1}), as higher concentrations generated high currents (above 100 μA) and instability of the electrophoretic system.

The separation of the six studied cephalosporins using the selected MEKC parameters was achieved in approximately 15 min. The migration order was: CFD, CFL, CFC, CFR, CZI and CTR (Fig. 4).

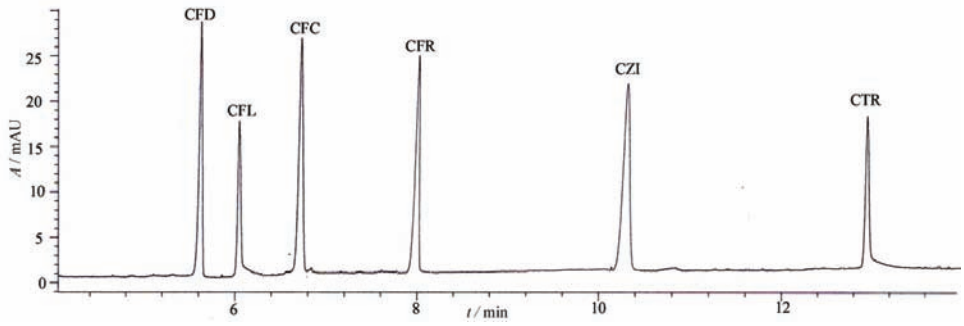

Fig. 4. Electropherogram of the separation of a mixture of the six cephalosporins (separation conditions: capillary 56 cm×50 μm I.D., buffer electrolyte 25 mM phosphate – 25 mM borate – 50 mM SDS, pH – 6.8, applied voltage: 25 kV, temperature: 25 °C, detection: UV absorption at 270 nm, concentration of each cephalosporin 25 μg mL^{-1}).

DISCUSSION

The migration order in CZE could be explained in terms of the electric charge and size of the analytes. In the CZE method, analytes with smaller molecular sizes migrate faster than the more bulky ones. At a pH above 5, the carboxylic group of the cephalosporins was fully dissociated, and the variation in the electrophoretic mobility of the analytes could be attributed to the deprotonation of either an amino group or a pyridinium group. There is also a possibility for the deprotonation of the benzyl position near to amino and pyridinium groups. It is also worth mentioning that at a pH between 5 and 7, CFL, CFD and CFC existed predominantly as zwitterions.[5]

In MEKC, analytes that have a greater affinity for the micelles have slower migration velocities compared to analytes that spend most of their time in the bulk phase. An analyte with charge opposite to that of the micelles will strongly interact with the micelle through electrostatic forces, while an analyte with the same charge as that of the micelle will interact weakly, due to electrostatic repulsion. The studied cephalosporins exhibited different hydrophobic–hydrophilic properties and contain various ring heteroatom, such as nitrogen, oxygen and sulfur, that form strong hydrogen bonds with water and micelles.[11]

Cephalosporins with more complex structures, *i.e.*, contain aromatic rings or long aliphatic side chains as substituents, are more strongly incorporated into the micelles and will migrate slower. CFD, CFL and CFC with simpler structures and obvious similarities will migrate first and the resolution between them will be poorer. CTR migrates much slower then the other cephalosporins, probably because of the characteristic highly acid heterocyclic system on the 3-thiomethyl group attached to the C-3 position of the cephem structure. The migration order of the three parenteral cephalosporins is in concordance with their pK_a values corresponding to the carboxylic group: CFR (pK_a 2.5), CZI (pK_a 1.9) and CTR (pK_a 1.7).[5,16]

Analytical performance

The analytical performance of the method was evaluated by measuring the detection (*LOD*) and quantification (*LOQ*) limits and relative standard deviations (*RSD*) for the migration times and peak areas. The optimized MEKC separation parameters were used for all these measurements.

All the cephalosporins exhibited negative electrophoretic mobilities and moved with the electrophoretic flow (Table II).

To evaluate repeatability of the peak areas and migration times, ten injections of mixture of cephalosporins were made and relative standard deviation was calculated (Table II).

The *LOD* and *LOQ* values were calculated within the concentration corresponding to signal-noise relation equal to 3 and 10, respectively (Table II).

TABLE II. Analytical parameters for the MEKC separation of the cephalosporin

Analyte	Migration time min	Electrophoretic mobility $cm^2\ kV^{-1}\ min^{-1}$	RSD migration time, %	RSD peak area, %	*LOD* $\mu g\ mL^{-1}$	*LOQ* $\mu g\ mL^{-1}$
CFD	5.52	–10.75	0.12	0.51	0.99	3.28
CFL	6.28	–12.98	0.15	0.75	2.59	8.63
CFC	6.87	–14.45	0.13	0.75	1.42	4.75
CFR	8.06	–16.76	0.09	0.42	1.96	6.55
CZI	10.16	–19.52	0.16	0.90	1.88	6.27
CTR	13.22	–21.97	0.16	1.03	2.73	9.09

To determine the linearity of the plots peak areas *vs.* concentration, six concentrations in a specific range and three replicates per concentration were used. The regression equations and correlation coefficients are presented in Table III. The correlation coefficients were higher than 0.99, which could be considered as evidence of good data fitting to a line regression.

TABLE III. Linearity regression data for the MEKC separation of the cephalosporin (concentration range: 5–100 $\mu g\ mL^{-1}$)

Analyte	Regression equation	Correlation coefficient
CFD	$y = 2.3594x + 4.5439$	0.999
CFL	$y = 1.6935x + 1.8458$	0.998
CFC	$y = 2.1355x + 3.0514$	0.999
CFR	$y = 2.0458x + 2.8607$	0.998
CZI	$y = 1.7939x + 5.0322$	0.992
CTR	$y = 1.668x + 3.4163$	0.997

CONCLUSIONS

This technique represents a suitable method for cephalosporin analysis, as it is easy to handle and exhibits good repeatability. It also increases knowledge about the electrophoretic behavior of cephalosporins, which could be advantageous in the qualitative and quantitative analysis of these frequently used β-lactam antibiotics.

The combined effects of buffer pH and buffer composition and concentration were taken into consideration to optimize separation of the examined cephalosporins. Correlations between the structural characteristics of the studied cephalosporins and their electrophoretic behavior were made in order to understand and explain the separation. Complete separation of the six studied cephalosporins was achievable under the optimized conditions. The use of a mixed borate–phosphate buffer proved to be superior to a simple phosphate or borate buffer in the CE separation of cephalosporins.

The method developed in this study, in comparison with others previously described in the literature, uses a mixed borate–phosphate buffer, which stabi-

lizes the electrophoretic system and presents a relatively short analysis time and a simple electrophoretic procedure.

Although in therapeutics, β-lactam antibiotics are not usually administered together, in this study, a mixture of six cephalosporins was analyzed in the same run to prove the suitability of the method for the determination of all six compounds in particular and for cephalosporins in general.

Using the described optimized procedures for CZE and MEKC, these techniques could be employed for the identification and determination of cephalosporins in formulated pharmaceutical products and for separations from complex mixtures.

И З В О Д

РАЗВОЈ МЕТОДЕ КАПИЛАРНЕ ЕЛЕКТРОФОРЕЗЕ ЗА ИСТОВРЕМЕНО ОДРЕЂИВАЊЕ ЦЕФАЛОСПОРИНА

GABRIEL HANCU, HAJNAL KELEMEN, AURA RUSU и ÁRPÁD GYÉRESI

Faculty of Pharmacy, University of Medicine and Pharmacy Târgu Mureş, Gh Marinescu street 32, 540131 Târgu Mureş, Romania

Развијена је брза и једноставна метода капиларне електрофорезе за истовремено одређивање шест широко коришћених цефалоспоринских антибиотика (цефаклор, цефадроксил, цефалексин, цефуроксим, цефтазидим и цефтриаксон). Одређивање цефалоспорина је изведено на pH 6,8, у пуферу 25 mM фосфат/25 mM борат, при напону од 25 kV и на температури од 25 °C. Постигнуто је раздвајање за око 10 min. Резолуција је побољшана додатком анјонског сурфактанта, 50 mM натријум-додецил-сулфата, у пуферски раствор. Предложена метода је евалуирана на основу граница детекције и квантификације, ефективне електрофоретске покретљивости и релативне стандардне девијације миграционих времена и површина пикова.

(Примљено 17. новембра 2012, ревидирано 22. фебруара 2013)

REFERENCES

1. J. M. Beale, in *Wilson and Gisvold's Textbook of Organic Medicinal and Pharmaceutical Chemistry*, 11th ed., J. H. Block, J. M. Beale, Jr., Eds., Lippincot Williams & Wilkins, Philadelphia, PA, 2004, p. 318
2. M. I. Jimidar, P. Van Nyen, W. Van Aen, M. De Smet, in *Capillary electrophoresis methods for pharmaceutical analysis*, S. Ahuja, M. I. Jimidar, Eds., Academic Press, London, 2008, p. 63
3. S. R. El-Shaboury, G. A. Saleh, F. A. Mohamed, A. H. Rageh, *J. Pharm. Biomed. Anal.* **45** (2007) 1
4. Y. Mrestani, R. H. Neubert, A. Hartl, J. Wohlrab, *Anal. Chim. Acta* **349** (1997) 207
5. C. E. Lin, H. W. Chen, E. C. Lin, K. S. Lin, H. C. Huang, *J. Chromatogr., A* **879** (2000) 197
6. A. Gáspár, M. Ándrasi, S. Kardos, *J. Chromatogr., B* **775** (2002) 239
7. A. Gáspár, S. Kardos, M. Ándrasi, Á. Klekner, *Chromatographia* **56** (2002) 109
8. A. R. Solangi, S. Q. Memon, M. Y. Khuhawar, M. I. Bhanger, *Acta Chromatogr.* **19** (2007) 81
9. P. Puig, F. Borrull, C. Aguilar, M. Calull, *Chromatographia* **65** (2007) 501

10. G. Pajchel, S. Tyski, *J. Chromatogr., A* **895** (2000) 27
11. Y. Mrestani, J. Martin, H. Ruttinger, R. H. Neubert, *J. Chromatogr., A* **873** (2000) 237
12. Y. Mrestani, Z. Marestani, R. H. Neubert, *Electrophoresis* **22** (2001) 3573
13. P. Puig, F. Borrull, M. Calull, C. Aguilar, *Chromatographia* **62** (2005) 603
14. M. Ándrasi, A. Gáspár, Á. Klekner, *J. Chromatogr., B* **846** (2007) 355
15. M. Ándrasi, P. Buglyo, L. Zekany, A. Gáspár, *J. Pharm. Biomed. Anal.* **44** (2007) 1040
16. V. G. Alekseev, *Pharm. Chem J.* **44** (2010) 14.

Journal of the Serbian Chemical Society
JSCS-info@shd.org.rs • www.shd.org.rs/JSCS
J. Serb. Chem. Soc. 78 (9) 1425–1441 (2013)
JSCS–4508
UDC 678.746–13+664.2:542.92.000.57:
547.391.3:628.113(282)
Original scientific paper

Biodegradation of starch–graft–polystyrene and starch–graft––poly(methacrylic acid) copolymers in model river water

VLADIMIR NIKOLIĆ[1]*, SAVA VELIČKOVIĆ[2#], DUŠAN ANTONOVIĆ[2#] and ALEKSANDAR POPOVIĆ[3]

[1]Innovation Center, Faculty of Chemistry, University of Belgrade, Studentski trg 12–16, 11000 Belgrade, Serbia, [2]Faculty of Technology and Metallurgy, University of Belgrade, Karnegijeva 4, 11000 Belgrade, Serbia and [3]Faculty of Chemistry, University of Belgrade, Studentski trg 12–16, 11000 Belgrade, Serbia

(Received 16 December 2012, revised 8 May 2013)

Abstract: In this paper, a biodegradation study of grafted copolymers of cornstarch and polystyrene (PS) and cornstarch and poly(methacrylic acid) in model river water is described. These copolymers were obtained in the presence of different amine activators. The synthesized copolymers and products of degradation were characterized by Fourier transform infrared (FTIR) spectroscopy and scanning electron microscopy (SEM). Biodegradation was monitored by mass decrease and the number of microorganisms by the Koch method. Biodegradation of both copolymers advanced with time, the starch––*graft*–poly(methacrylic acid) copolymers had completely degraded after 21 day, and the starch–*graft*–polystyrene had partially degraded (45.8–93.1 % mass loss) after 27 days. The differences in the degree of biodegradation are the consequences of the different structures of the samples, and there was a significant negative correlation between the share of polystyrene in the copolymer and the degree of biodegradation. The grafting degree of PS necessary to prevent biodegradation was 54 %. Based on experimental evidence, the mechanisms of both biodegradation processes are proposed, and influence of degree of starch and synthetic component of copolymers on the degradation of the samples were established.

Keywords: graft copolymers; model river water; degradation study; statistical analysis.

INTRODUCTION

The problem of the accumulation of synthetic polymeric materials in the environment is not only attracting growing attention worldwide, but also indi-

* Corresponding author. E-mail: nikolicv@chem.bg.ac.rs
# Serbian Chemical Society member.
doi: 10.2298/JSC121216051N

cates the requirement for producing new, alternative, biodegradable materials with high levels of biodegradability that could, in the future, replace the bulk polymers of today. Conventional polymeric materials are usually not degradable or biodegradable at measurable or significant rates under environmental conditions. For this reason, the search for polymers that could be biodegradable under environmental conditions, such as copolymers containing biodegradable component and conventional, non-biodegradable component, has become the focus of academic and industrial communities.[1]

Polystyrene (PS) and poly(methacrylic acid) (PMAA) represent two of the major "targets" for preparation of their biodegradable derivatives. Polystyrene has excellent physical properties, low price and is easy to process, while PMAA is an adaptable macromolecule that offers many benefits in the development of new materials for a host of applications. Modification/functionalization of these polymers to the extent where they will become submissive to microbial attack is one of the alternatives to overcome environmental problems. Modifications with natural polymers, such as carbohydrates, represent major techniques in the creation of more biodegradable polymers.[2–6] Gelatin,[7] natural rubber,[8] lignin[9] and other reactants can also be used for such a purpose. One of the ways biodegradable derivates of polymers can be obtained is through grafting reactions. Grafted copolymers of polystyrene and poly(methacrylic acid) with starch (starch–graft––PS and starch–graft–PMAA) can be obtained in different ways: by suspension[10] and emulsion polymerization,[11] or by ^{60}Co-radiation.[8,12] In all the mentioned grafting reactions, different initiating system can be used.[13–21] In investigation of degradation and biodegradation processes, different methods such as UV degradation, degradation in soil, degradation by different types of microorganisms, biodegradation in natural and waste water, *etc*. are being used.[22–27]

Degradation in river water was used for the study of biodegradation of surfactants,[28] such as linear alkyl benzene sulfonates (LAS),[29] bisphenol A[30,31] and various glycols.[32] Moreover, great attention has been paid to the degradation processes of chlorinated aliphatic hydrocarbons, such as 1,2-dichlorethane,[33] in three European rivers (the Ebro, Elbe and Danube) and polycyclic aromatic hydrocarbons (PAH) in simulated nuclear wastewater.[34] Biodegradations of synthetic polymers, such as fibers for drift net from poly(3-hydroxyalkanoic acids) in a reactor with different types of nature waters (river, sea and lake waters),[35] vinyl polymers, such as polyethylene in river water,[36] its blend and copolymers with natural polymers (in activated sludge),[37] poly(ethylene glycols) (PEGs)[38] and different polyurethanes[39] (both in sea water) were also studied.

Polystyrene is used for housings for TVs, refrigerators, air conditioners, microwaves, blenders, protect boxes for DVDs and all kinds of IT equipment where the criteria for use are combinations of function, form and esthetics and high performance/cost ratio. Starch–graft–PS copolymers were synthesized in order to

obtain new plastics with similar or better characteristic than pure polystyrene and to reduce environmental pollution caused by polystyrene. Potential applications for starch–graft–PS copolymers are in the textile industry (this copolymer increases the tensile strength of cotton yarn),[40] as superabsorbent[41] and as surface-sizing agents.[42] Potential applications for starch–graft–PMAA copolymers are in the textile industry (as a sizing agent that increases abrasion resistance compared to starch),[20] in waste water treatment for removal of dyes,[43,44] and hydrogels of this copolymer can be used as a matrix for drug delivery.[45,46]

In the present study, the biodegradation of starch–graft–polystyrene and starch–graft–poly(methacrylic acid) copolymers synthesized in aqueous medium with potassium persulfate (PPS) as an initiator and different amines as polymerization activators were investigated. To the best of our knowledge, no previous literature references describe the biodegradation of these graft copolymers in a river water system. A continuous flow system with recirculation, enabling the simulation of environmental conditions in the laboratory, was applied in the biodegradation study, while the biodegradation medium was model water of Sava River, an international river and one of the main tributaries of the Danube.

EXPERIMENTAL

Materials

The cornstarch (Centrohem, Serbia) used in the grafting experiments was dried for 3 days under vacuum at 50 °C, before use. Styrene (Aldrich Chemicals) was purified by distillation under reduced pressure prior to polymerization, while methacrylic acid (Fluka) was used as obtained. Potassium persulfate (PPS) (Aldrich Chemicals), sodium dodecyl sulfate (SDS) (Aldrich Chemicals), methanol (Fluka), chloroform (J. T. Baker), and amines – *N*,*N*-dimethylethanolamine, *N*,*N*-diethylethanolamine, triethylamine, *n*-propylamine, isobutylamine, *n*-pentylamine *n*-hexylamine, 1-(2-hydroxyethyl) piperazine and 4-(2-hydroxyethyl) morpholine (all Fluka) were used as obtained.

Water from the Sava River was taken from a location near the riverbank, 2 km before the confluence of the Sava and Danube Rivers. 2 L of this water were mixed with artificial wastewater, containing 800 mg of peptone, 550 mg of meat extract, 150 mg of urea, 35 mg of NaCl, 20 mg of $CaCl_2 \cdot 2H_2O$, 10 mg of $MgSO_4 \cdot 7H_2O$ and 140 mg K_2HPO_4 in 3 L of distilled water, thus making total of 5 L of model river water of pH 7.5.

Methods

Starch–graft–PS samples and starch–graft–PMAA samples used in biodegradation experiments were prepared in the laboratory prior to the experiments. Synthesis of starch–graft––PMAA copolymers and the obtained results were previously described.[47] The starch–graft–PS copolymers were prepared by emulsion polymerization in the presence of potassium persulfate/amine initiation redox system and sodium dodecyl sulfate (SDS) as the emulsifier. Water (80 mL), cornstarch (10 g), styrene (10 g) and SDS (0.23 g, 8.0×10^{-4} mol) were first added in the reaction vessel. The components were homogenized and heated to the reaction temperature of 75 °C. After reaching the reaction temperature, the initiator potassium persulfate (0.40 g, 0.0015 mol) in 20 ml of distilled water was added followed by the amine activator. Samples with different percentages of grafting were obtained using different amines

(*N*,*N*-dimethylethanolamine, *N*,*N*-diethylethanolamine, triethylamine, *n*-propylamine, isobutylamine, *n*-pentylamine *n*-hexylamine, 1-(2-hydroxyethyl) piperazine and 4-(2-hydroxyethyl) morpholine) or different amounts of the same amine (*N*,*N*-dimethylethanolamine in amount of 0.001, 0.002 and 0.004 mol). In all syntheses, the reaction mixture was stirred at 275 rpm, while the reaction time was 15 min, to prevent starch gelation. One reaction was performed under the same reaction conditions but without an amine activator. This reaction was used to evaluate the influence of the amine activator on percentage of grafting. Non-polymerized styrene monomer was removed by extraction in methanol for 24 h. In order to remove unbound polystyrene homopolymer, extraction in chloroform was performed, and the unbound polystyrene was then precipitated with methanol. In order to determine the amount of bound polystyrene and the percentage of grafted polystyrene (*G* / %) in the starch–graft–PS copolymer, the samples were hydrolyzed using 100 mL of 1 M HCl for 5 g of copolymer. The hydrolysis was performed for 2 h at 200 °C. After hydrolysis, non-hydrolyzed polystyrene remained (confirmed by FTIR spectroscopy) in the form of a solid residue which was filtered, rinsed with distilled water and dried at 50 °C to constant mass. Percentage of grafting was calculated by the following formula:

$$G = 100 \frac{m \text{ of PS after hydrolysis}}{m \text{ of copolymer before hydrolysis}} \quad (1)$$

In this investigation, graft copolymers of polystyrene and poly(methacrylic acid) with starch with maximal percentage of grafting were obtained. The targeted values for the percentage of grafting were 30 % (which is one of the highest values in the literature to date) or higher. For both types of copolymers, this value was achieved (32.5 % for starch–graft–PS and 40.9 % for starch–graft–PMAA copolymer).

From the sum of the mass of polystyrene that was extracted in chloroform, the mass of polystyrene after hydrolysis and mass of the styrene monomer, the yield of polystyrene (*Y)* could be calculated in the grafting reaction from the following formula:

$$Y / \% = 100 \frac{m \text{ of PS}}{m \text{ of styrene monomer}} \quad (2)$$

Each synthesis was performed three times in order to monitor the reproducibility of the results. Deviations in the grafting percent were very small, amounting to less than 2 %. The obtained grafting percent of the starch–graft–PS copolymers was one of the highest ever registered in the literature.

Eleven samples of starch–graft–PS copolymers, ten samples of starch–graft–PMAA copolymers synthesized with or without amine activator, and three control samples (pure starch, polystyrene and poly(methacrylic acid)) were subjected to the biodegradation process. All the copolymer samples contained different percentages of grafting. Copolymers with similar percentages of grafting were synthesized using different amine activators, and they were studied as different samples. Hence, samples obtained using different amine activators had different structures which affected the biodegradation results. Before biodegradation, the samples were milled and pressed in the form of discs with a diameter of 1 cm and thickness of 0.2 cm. Biodegradation of starch–graft–PS copolymers was performed separately from the biodegradation of the starch–graft–PMAA copolymers.

Different types of microorganisms were isolated in the water from the Sava River, such as *Escherichia coli*, *Proteus* sp., *Serratia marcescens*, *Klebsiella* sp., *Pseudomonas aeruginosa* and *Enterococcus faecalis*. The number of microorganisms was monitored by the Koch

method. This method determines the number of living cells indirectly, usually after cultivation. After incubation on a solid medium (agar) in Petri dishes, the colonies were counted with the assumption that each cell created one colony. This method provides a realistic number of cells, but its duration is long (at least 24 h). The number of microorganisms was expressed as log (*CFU* / mL^{-1}), where *CFU* stands for colony forming units and is expressed per mL of the model river water.

Characterization of the copolymers before and after biodegradation

Fourier transform infrared spectroscopy (FTIR) and scanning electron microscopy (SEM) were used before (to prove successful grafting) and after biodegradation (to confirm changes caused due to biodegradation) as methods for characterization of graft copolymers. The FTIR spectra were recorded from KBr discs on a MB-100 Bomem FTIR spectrophotometer. For SEM, the samples were mounted on copper and metallized with gold–palladium using a Polaron SC 502 sputter coater and recorded on a Jeol JSM 5800 scanning electron microscope with the filament operating at 20 keV.

Laboratory model of systems for biodegradation

Biodegradation of the starch–graft–PS and starch–graft–PMAA copolymers by natural microorganisms in model river water was performed at room temperature by fractional elution during 21 days (for starch–graft–PMAA copolymers) and 27 days (for starch–graft–PS copolymers). The employed apparatus, consisting of a reservoir for river water (A), a dosing pump (B), an aeration vessel (C), a sample storage vessel (D), a recirculation pump (E), an effluent collection vessel (F), an aeration pump (G) and flow meter (H), is shown schematically in Fig. 1.

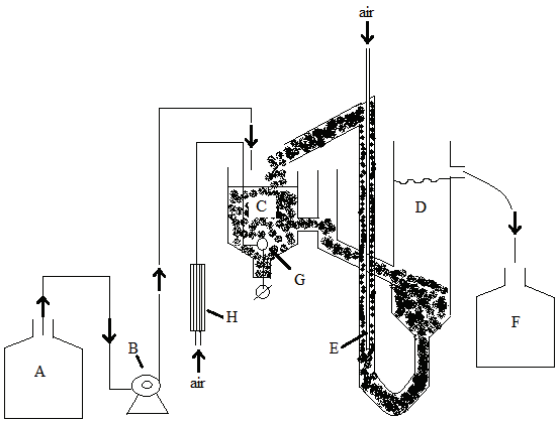

Fig. 1. Apparatus for the determination of the degree of biodegradation.

Biodegradation procedure

Five liters of model wastewater were added in vessel (A). Aeration vessel (C) and then sample storage vessel (D) were filled with water from vessel (A) using the dosing pump (B). When vessel D had been filled, the aeration pump (G) and the recirculation pump (E) were turned on. The aeration lasted for 48 h, until the microorganisms had adapted to the new conditions. The dosing pump (B) was set to minimum flow, conditions that could be considered as stationary. From time to time, it was necessary to empty the effluent collection vessel (F) by transfer of the effluent to vessel (A). After 48 h of recirculation, samples of copolymers

were added to the system, in column (D). All the 24 samples were put in a mesh, water permeable bag and after that, all samples of the same type of copolymer were put in a big, water permeable sack and sunk to the middle of column (D). The biodegradation experiments were performed separately. The biodegradation of the starch–graft–PS copolymers was the first to be monitored. After this experiment, the system was emptied, then cleaned and dried. A new amount of model wastewater (5 L) was made and the whole process was repeated using the starch–graft–PMAA copolymers.

The water flow was kept constant at 2 L day^{-1}. The samples were removed every 9 days when the starch–graft–PS copolymers were used and every 7 days for the starch–graft–PMAA copolymers. After removal, the samples were rinsed with distilled water and dried to constant weight under vacuum at 50 °C for 24 h. During drying of the samples under vacuum, the biodegradation test was not interrupted. After drying, the samples were returned to the aqueous system and the same samples were again exposed to the microorganisms. The percentage of biodegradation was calculated based on the following formula:

$$\text{Biodegradation} = 100\frac{(m_0 - m_x)}{m_0} \quad (3)$$

where m_0 is the sample mass before biodegradation and m_x is the sample mass after removal from model wastewater.

RESULTS AND DISCUSSION

Characterization of starch–graft–*PS and starch*–graft–*PMAA copolymers*

FTIR spectroscopy was used to verify that grafting had occurred. For starch––graft–PS copolymers, the characteristic peaks were: 3020–3080 (C–H vibrations of the aromatic ring), 2000–1660 (C–C vibrations in the benzene ring), 1490, 760 and 700 cm^{-1} (C–H stretching of the aromatic ring), originating from the polystyrene moieties, and 3000–3600 (O–H stretching), 2880–2920 (C–H stretching), 1645 (O–H first overtone) and 1190–950 cm^{-1} (C–O stretching), originating from the starch. The presence of these peaks indicated that the grafting was successful (Fig. 2).

The FTIR spectrum of the starch–graft–PMAA copolymer and its characteristic peaks were previously shown and described.[48]

The FTIR spectra of starch–graft–PS copolymers were also recorded after the biodegradation test. The FTIR spectrum of the copolymer with a grafting percentage of 12.9 % (sample 2) is shown in Fig. 3a together with the FTIR spectrum of pure polystyrene (Fig. 3b). It can be seen that these spectrums are identical and all the characteristic peaks of pure polystyrene are present in the spectrum of the copolymer after biodegradation. During biodegradation test, only starch was subjected to biodegradation, while no degradation of polystyrene occurred. At the end of the biodegradation process, only polystyrene remained and in case of sample 2, it can be concluded that the starch initially present was completely biodegraded.

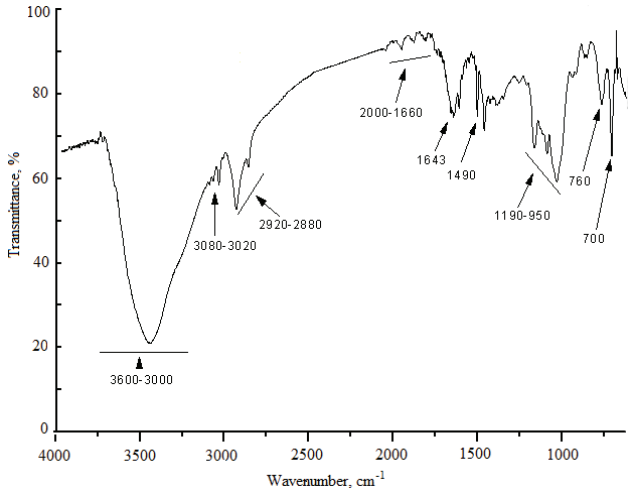

Fig. 2. FTIR Spectrum of starch–graft–PS with a grafting percentage of 20.9 %.

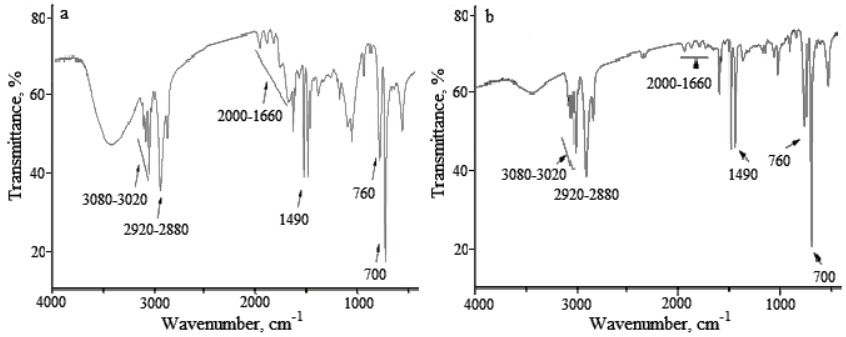

Fig. 3. FTIR Spectra of a) starch–graft–PS copolymer with a grafting percentage of 12.9 % after 27 days of the biodegradation test and b) pure polystyrene.

The FTIR spectra of the starch–graft–PMAA copolymers were not recorded after the biodegradation test because in all samples, as well as complete degradation of starch, complete dissolution of PMAA occurred.

SEM micrographs of grafted copolymers starch–graft–PS with different *G* are shown in Fig. 4. The structure of the starch–graft–PS copolymer in which the polystyrene links to starch granules (Sample 3, lower percentage of grafting) is depicted in Fig. 4a. This network structure does not cover the whole surface, thus the granules of starch are easily visible. Figure 4b (Sample 6) shows the sample of starch–graft–PS with a higher percentage of grafting, where polystyrene adheres to almost all the starch granules. Fig. 4c represents the SEM micrograph of pure cornstarch (starch used in grafting reaction). On comparing the SEM micrographs, it could be stated that there was a change in the granular shape of starch before and after copolymerization. When cornstarch granules are heated in the

presence of water, they undergo changes in size and shape. The granules initially swell and take the shape of a flattened disk. As the heating continues, the granules take on a puckered appearance.[48]

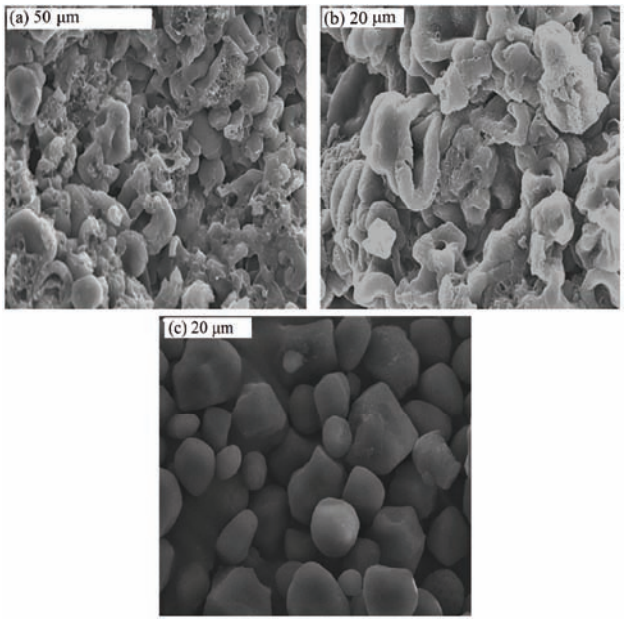

Fig. 4. SEM Micrographs of starch–graft–PS copolymers with percentages of grafting of a) 16.2, b) 25.3 % and c) of pure corn starch.

SEM Micrographs of starch–graft–PS copolymers (samples 3 and 6) after biodegradation test in model wastewater are shown in Fig. 5, which reveals that only polystyrene particles were present, while no starch granules can be seen. The remaining granules of starch are probably located in the interior and they are completely covered with polystyrene. Based on these micrographs, it could be concluded that biodegradation in the model wastewater truly occurred and that a portion of starch in the copolymer had been degraded.

The SEM microphotographs of starch–graft–PMAA copolymers with different percentage of grafting are shown in Fig. 6. The surface layer of copolymer with a grafting percentage of 22.0 % is shown in Fig 6a, while Fig. 6b presents an intersection of a copolymer with grafting percentage of 40.9 %.

The PMAA in the copolymer was not only present at the sample surface, but also in its interior. In Fig. 6a, it can be seen that starch granules are coming out from plate structure of PMAA and that a large amount of poly(methacrylic acid) can be found inside the sample (Fig. 6b). PMAA nearly completely covers the starch granules, probably in the form of a thin layer, as uncovered parts of the starch granules could be observed in some parts of the microphotograph.

Influence of amine on the initiation reaction

Amines have different abilities to facilitate the decomposition of the initiator. The main reason for using amines lies in decreasing the activation energy required for decomposition of the initiator. The mechanisms of the initiation reactions are different and depend on the type of the amine. If the primary and secondary amines are used, persulfate radical and radical on N-atom of amine molecule initiate grafting reaction, while with the tertiary amines radical center is on the C-atom of the amine component. Steric factors have great influence on the initiation and therefore on the percentage of grafting. During the initiation reaction, one type of complex between potassium persulfate and amine is formed and the size of the group and the alkyl chain lengths that are present on the N-atom of the amine have a great influence on the grafting reaction.

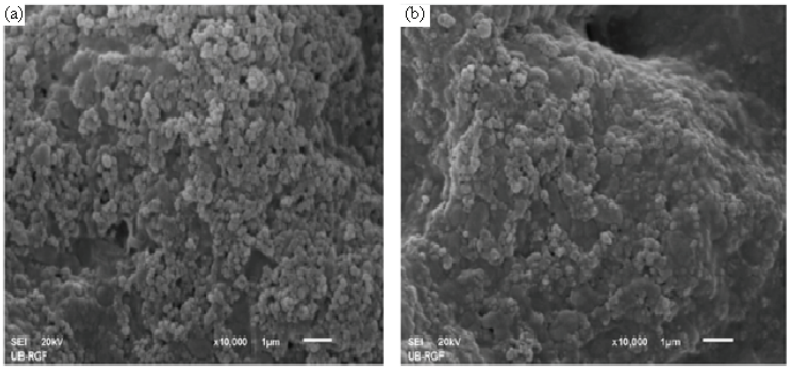

Fig. 5. SEM Micrographs of starch–graft–PS copolymers with percentages of grafting of a) 16.2 and b) 25.3 % after 27 days of biodegradation.

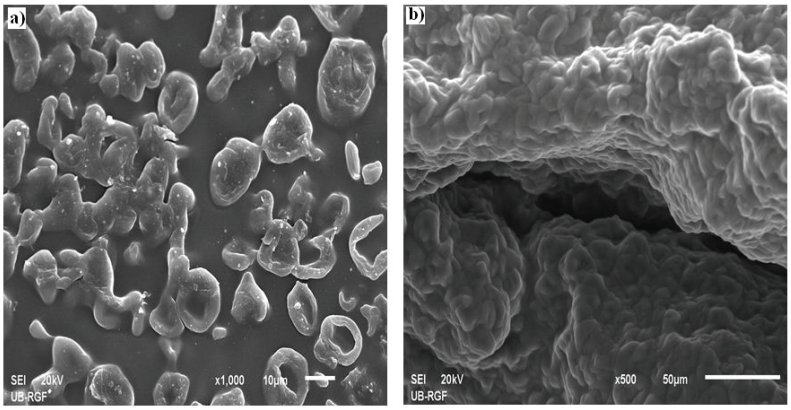

Fig. 6. SEM Micrographs of starch–graft–PMAA copolymers with percentages of grafting of a) 22.0 and b) 40.9 %.

Biodegradation studies

The results of monitoring the degradation of starch–graft–polystyrene and starch–graft–poly(methacrylic acid) copolymers in model river water are given in Tables I and II, which include the results for the negative control (distilled water adjusted to the same pH as the model river water). For starch–graft–PS copolymers in the negative control, the mass loss depended on the amount of starch in the copolymer (the mass loss increased with increasing amount of starch) and varied between 1.7 and 6 %. In the negative control for the starch–graft–PMAA copolymers, the mass loss of starch from the samples was between 1.2 and 4.6 %. These mass losses originated from the solubility of starch and degradation of starch by microorganisms that developed in the water during the experiment.

TABLE I. Monitoring of the degradation of copolymers of starch and polystyrene in model river water compared to the degradation of pure polystyrene and starch

Sample designation	G / %	Y / %	Mass loss after 9 days, %	Mass loss after 18 days, %	Mass loss after 27 days, %	Starch degradation in the samples, %
1	6.9	7.4	62.8	84.3	93.1	100
2	12.9	13.8	51.3	75.6	87.1	100
3	16.2	18.5	35.2	59.3	73.5	87.8
4	18.4	18.3	35.2	52.4	65.1	79.8
5	20.9	23.8	35.8	53.7	66.0	83.5
6	25.3	25.8	22.9	39.2	49.7	66.6
7	25.7	35.3	33.8	51.9	60.9	82.0
8	25.9	36.0	35.3	52.3	61.9	83.5
9	27.3	33.2	22.6	40.0	52.0	71.5
10	28.4	33.3	20.9	36.0	49.1	68.6
11	32.5	43.7	20.5	35.0	45.8	67.9
PS	–	–	0	0	0	–
Starch	–	–	66.8	94.3	100	100

As expected, the degradation processes of both copolymers in model river water advanced with time (Tables I and II). Due to the presence of non-degradable polystyrene, the starch–graft–polystyrene copolymers were not fully degraded after 27 days of the biodegradation process. The final level of degradation (from 45.8 to 93.1 % of total mass or from 66.6 to 100 % of starch mass present in the copolymers) depended on the percentage of grafting and increased with increasing amount of biodegradable starch in the copolymer. This is logical, since polystyrene is non-biodegradable and only the degradation of starch part of the copolymer affected the total biodegradation process. The highest percentages of biodegradation were 93.1 (sample 1) and 87.1 % of the total mass (sample 2) for the two samples with the highest amount of starch in the copolymers. These two samples were the only samples where complete degradation of the starch in the

copolymer occurred (Table I). With decreasing amount of starch in the copolymer, the biodegradation of the starch became incomplete, and this phenomenon could be explained by the different morphologies of the samples. With decreasing amount of starch (increasing of amount of PS) in the copolymer, larger amounts of the starch granules were trapped within the PS chains and thus inaccessible for the microorganisms. Hence, the percentage of biodegradation was smaller than theoretically possible. In addition, the influence of different morphologies could be seen on the example of three copolymers with similar percentages of grafting (samples 6–8). Although the percentages of starch in these samples were approximately the same, the biodegradation results for sample 6 were very different compared to the other two samples (66.6 % for sample 6 compared to 82.0 % for sample 7 and 83.5 % for sample 8), which could be explained by the different structure of the sample 6 compared to those of samples 7 and 8.

TABLE II. Monitoring of the degradation of copolymers of starch and poly(methacrylic acid) in model river water compared to the degradation of pure starch and pure poly(methacrylic acid)

Sample designation	*G* / %	Mass loss after 7 days, %	Mass loss after 14 days, %	Mass loss after 21 days, %
1	8.6	81.04	100	100
2	10.8	48.41	84.2	100
3	13.2	80.89	100	100
4	16.0	59.93	100	100
5	18.5	70.52	100	100
6	21.1	60.82	100	100
7	22.0	67.16	100	100
8	27.0	62.99	96.6	100
9	34.7	42.02	84.7	100
10	40.9	56.65	96.4	100
PMAA	–	100	100	100
Starch	–	39.90	71.0	100

If the percentage of grafting and the percentage of biodegraded copolymer (expressed as percentage mass loss during biodegradation) are correlated, it becomes obvious that there are significant correlations (significance of correlation $p < 0.05$) between these values after 9, 18 and 27 days of degradation (Table III, Fig. 7).

TABLE III. Correlation parameters between the percentage of grafting and the mass loss of starch–graft–polystyrene copolymer samples after 9, 18 and 27 days; number of samples: 11

Correlation parameter	After 9 days	After 18 days	After 27 days
R^a	–0.9210	–0.9419	–0.9596
p^b	0.000	0.000	0.000

[a]coefficient of correlation; [b]significance of correlation

Clearly, the fact that there are significant correlations between the degree of grafting and the degree of biodegradation proves that the level of biodegradation depends on the level of starch in the copolymer, and that, in the present system, the available starch in the starch–graft–PS copolymer degrades completely.

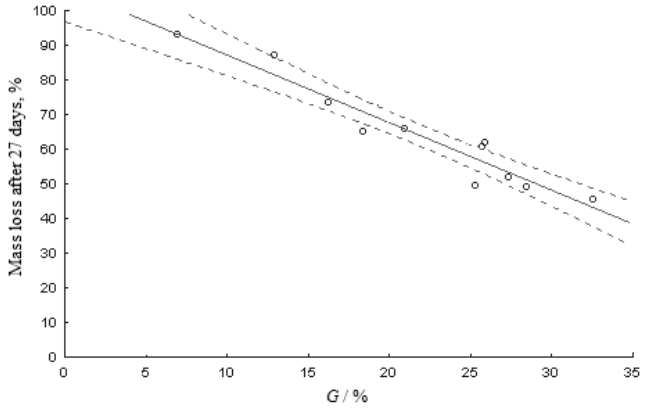

Fig. 7. Linear correlation between the percentage of grafting and mass loss of starch–graft–polystyrene samples after 27 days of biodegradation in model wastewater ($y = 106.70 – 1.952x$).

When the correlation equation is analyzed, it becomes obvious that the grafting degree necessary to prevent biodegradation (the value of percentage of grafting that would result in 0 % biodegradation) was approximately 54 %. Obviously, the biodegradation of the starch–graft–polystyrene copolymer in model river water would be completely suppressed because of the unavailability of microorganisms to degrade starch covered by polystyrene at levels of polystyrene of around 54 % or higher. Since in the examined copolymers, polystyrene was present to much smaller extent (6.9–32.5 %), biodegradation in the model wastewater occurred.

The degradation of starch–graft–PMAA copolymers (Table II) was much simpler than that of the previously discussed starch–graft–PS copolymers, because PMAA is soluble in water. Most of the samples of copolymer completely degraded after 14 days of biodegradation in the model river water, while all of them fully degraded after 21 days. Pure poly(methacrylic acid) completely dissolved after one week, while starch fully degraded after three weeks of the process.

The fact that degradation of starch–graft–poly(methacrylic acid) copolymer is slower than the solubility of pure poly(methacrylic acid) (Table II) probably indicates that the degradation mechanism of copolymer involves two steps: attack of microorganisms on the available starch and, after degradation of available

starch, release of chains of poly(methacrylic acid) that become free and soluble in water.

If the degradation results before completion of degradation, expressed as the percentage of mass loss after 7 days, are correlated with the degree of grafting, there is no dependence. This was expected, hearing in mind not only the fact that one of components is degradable, but also the mechanism of biodegradation proposed above. The rate of biodegradation depended not only on the percentage of grafting, but also on the distribution of starch and poly(methacrylic acid) in the copolymers.

It is also noteworthy that the biodegradation of these copolymers in model wastewater (21 and 27 days) was much faster than their biodegradation in soil samples.[8]

During the biodegradation test in model river water, the number of microorganisms was monitored for both types of copolymers. In case of starch–graft––PS copolymers (Fig. 8), the number of microorganisms increased during the first three days, which is associated with the addition of nutrients that were added before the addition of the samples. After the first three days, the number of microorganisms decreased with decreasing amount of starch in the copolymer to its minimum on the 19th day, when log (CFU / ml^{-1}) = 0. It could be concluded that the amount of pure starch and starch available to microorganisms that remains in copolymers was very small, so the number of formed colonies was zero at a dilution of 10^{-5}. To ensure full degradation after the 19th day, new amount of nutrients was added to the system, which increased the number of formed colonies on the 23th and 27th day. Hence, it could be assumed that the decrease in the number of colonies to zero occurred due to lack of nutrients.

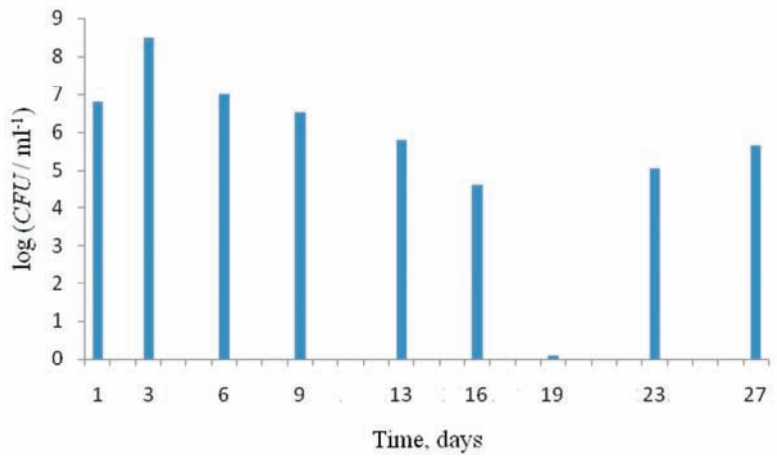

Fig. 8. The change in the number of microorganisms during the biodegradation of starch–graft–PS copolymers.

The number of formed colonies in the system with starch–graft–PMAA copolymers increased during first four days, which is associated with the addition of nutrients (Fig. 9). From the 7th to the 16th day, number of microorganisms was approximately constant (log (*CFU* / ml^{-1}) ≈ 8.5), which indicates sufficient amount of starch in the water. After 16 days, the number of microorganisms decreased and reached a minimum on the 18th day, which indicated the amount of starch in the copolymer had been reduced. To ensure complete degradation, new amounts of nutrients were added to the system, as in case of the starch–graft–PS copolymers.

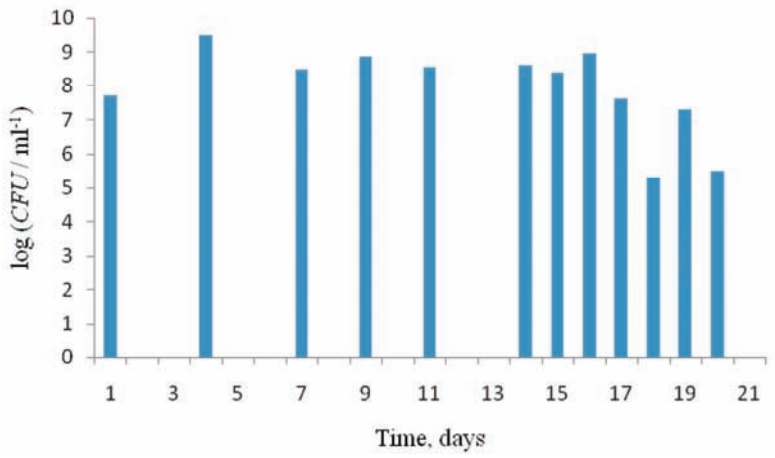

Fig. 9. The change in the number of microorganisms during the biodegradation of starch–graft–PMAA copolymers.

CONCLUSIONS

Graft copolymers of polystyrene and starch and poly(methacrylic acid) and starch, obtained by radical polymerization in the presence of different amine activators, were subjected to biodegradation in model river water. The biodegradation was monitored by the mass decrease of copolymers, FTIR spectroscopy and SEM. The biodegradation of both types of copolymers advanced with time. Starch–graft–poly(methacrylic acid) copolymers were completely degraded after 21 days and the starch–graft–polystyrene copolymers were partially degraded (45.8–93.1 % mass loss) after 27 days. The level of the biodegradation of the starch–graft–PS was significantly negatively correlated with the degree of grafting, *i.e.*, the higher the percentage of polystyrene in copolymer, the lower was the final degree of biodegradation. Only at relatively low levels of polystyrene in the copolymer (above 12.9, but certainly lower than 16.2 %), did all the starch in the copolymer degrade under the investigated conditions. With increasing content of non-degradable polystyrene in the copolymer, some of the starch remained

protected from biodegradation, up to a percentage of polystyrene of around 54 %, when, under the given conditions, practically no biodegradation should occur, and all the biodegradable part of the copolymer was effectively hindered by the polystyrene. Degradation of starch–graft–PMAA copolymers was faster because the copolymer consisted of a biodegradable part and one that was soluble in water. Most of the samples of copolymer had completely disappeared after 14 days of biodegradation in the model river water, while the rest had fully disappeared after 21 days. The degradation mechanism of this copolymer probably included two steps: the attack of microorganisms on the available starch, and, after the degradation of the available starch, the release of chains of poly(methacrylic acid) that were released and soluble in the river water.

Acknowledgment. This investigation was supported by the Ministry of Education, Science and Technological Development of the Republic of Serbia, through Project Nos. 172001 and 172062.

И З В О Д

БИОДЕГРАДАЦИЈА КАЛЕМЉЕНИХ КОПОЛИМЕРА СКРОБА И ПОЛИСТИРЕНА И СКРОБА И ПОЛИ(МЕТАКРИЛНЕ КИСЕЛИНЕ) У РЕЧНОЈ ВОДИ

ВЛАДИМИР НИКОЛИЋ[1], САВА ВЕЛИЧКОВИЋ[2], ДУШАН АНТОНОВИЋ[2] и АЛЕКСАНДАР ПОПОВИЋ[3]

[1]Иновациони центар Хемијског факултета, Универзитет у Београду, Студентски трг 12–16, 11000 Београд, [2]Технолошко–металуршки факултет, Универзитет у Београду, Карнегијева 4, 11000 Београд и [3]Хемијски факултет, Универзитет у Београду, Студентски трг 12–16, 11000 Београд

У овом раду проучавана је биодеградација калемљених кополимера кукурузног скроба и полистирена и кукурузног скроба и поли(метакрилне киселине) у речној води. Ови кополимери су синтетисани у присуству различитих аминоактиватора. Синтетисани кополимери и продукти биодеградације су карактерисани ФТИР спектроскопијом и СЕМ микроскопијом. Биодеградација је праћена губитком масе узорака, а број микроорганизама Коховом методом. Степен биодеградације обе врсте кополимера расте са временом. Калемљени полимери скроба и поли(метакрилне киселине) потпуно се разграђују за 21 дан, док се полимери на бази скроба и полистирена делимично разграђују након 27 дана (45,8–93,1 % од укупне масе). Разлике у степену биодеградације су последица различите структуре узорака, а постоји и значајна негативна корелација између удела полистирена у кополимеру и степена биодеградације. Степен калемљења полистирена (удео полистирена у кополимеру) који спречава биодеградацију износио је 54 %. На основу експерименталних доказа, предложени су механизми оба биодеградациона процеса и установљени су утицаји количине скроба и синтетске компоненте кополимера на биодеградацију.

(Примљено 16 децембра 2012, ревидирано 8. маја 2013)

REFERENCES

1. P. Galgali, U. S. Puntambekar, D. V. Gokhale, A. J. Varma, *Carbohydr. Polym.* **55** (2004) 393
2. A. Nagaty, F. Abd-Et-Mouti, O. Y. Mansour, *Eur. Polym. J.* **16** (1980) 343
3. M. M. Fares, A. S. El-Faqeeh, M. E. Osman, *J. Polym. Res.* **10** (2003) 119

4. P. Matzinos, V. Tserki, C. Gianikouris, E. Pavlidou, C. Panayiotou, *Eur. Polym. J.* **38** (2002) 1713
5. J. Zhou, Y. Ma, L. Ren, J. Tong, Z. Liu, L. Xie, *Carbohydr. Polym.* **76** (2009) 632
6. B. Y. Shin, S. H. Jang, B. S. Kim, *Polym. Eng. Sci.* **51** (2011) 826
7. R. P. Wool, D. Raghavan, G. C. Wagner, S. Billieux, *J. Appl. Polym. Sci.* **77** (2000) 1643
8. S. Kiatkamjornwong, M. Sonsuk, S. Wittayapichet, P. Prasassarakich, P. Vejjanukroh, *Polym. Degrad. Stabil.* **66** (1999) 323
9. O. Milstein, R. Gersonde, A. Huttermann, M. J. Chen, J. J. Meister, *Appl. Environ. Microbiol*. **58** (1992) 3225
10. K. Kaewtatip, V. Tanrattanakul, *Carbohydr. Polym.* **73** (2008) 647
11. C. G. Cho, K. Lee, *Carbohydr. Polym.* **48** (2002) 125
12. G. F. Fanta, R. C. Burr, W. M. Doane, C. R. Russell, *J. Appl. Polym. Sci.* **21** (1977) 425
13. P. Janarthanan, W. M. Z. W. Yunus, M. B. Ahmad, *J. Appl. Polym. Sci.* **90** (2003) 2053
14. R. A. D. Graaf, L. P. B. M. Janssen, *Polym. Eng. Sci.* **40** (2000) 2086
15. B. Singh, N. Sharma, *Polym. Degrad. Stabil.* **92** (2007) 876
16. M. I. Khalil, K. M. Mostafa, A. Hebeish, *Angew. Makromol. Chem.* **213** (1993) 43
17. M. H. Abo-Shosha, N. A. Ibrahim, *Starch/Starke* **44** (1992) 296
18. Kh. M. Mostafa, *Polym. Degrad. Stabil.* **50** (1995) 189
19. V. D. Athawale, S. C. Rathi, *J. Appl. Polym. Sci.* **66** (1997) 1399
20. M. K. Beliakova, A. A. Aly, F. A. Abdel-Mohdy, *Starch/Starke* **56** (2004) 407
21. M. Li, Z. Zhu, E. Jin, *Fiber. Polym.* **11** (2010) 683
22. H. Kaczmarek, A. Felczak, A. Szalla, *Polym. Degrad. Stabil.* **93** (2008) 1259
23. W. R. Waldan, M. A. De Paoli, *Polym. Degrad. Stabil.* **93** (2008) 273
24. E. Rudnik, D. Briassoulis, *J. Polym. Environ.* **19** (2011) 18
25. O. Motta, A. Proto, F. Carlo, F. Caro, E. Santoro, L. Brunetti, M. Capunzo, *Int. J. Hyg. Environ. Health* **212** (2009) 61
26. K. Ohkawa, H. Kim, K. Lee, *J. Polym. Environ.* **12** (2004) 211
27. S. Cometa, I. Bartolozzi, A. Corti, F. Chiellini, E. D. Giglio, E. Chiellini, *Polym. Degrad. Stabil.* **95** (2010) 2013
28. A. Szymanski, J. Jaroszynski, P. Jeszka, Z. Lukaszewski, *Water Res.* **30** (1996) 2465
29. J. A. Perales, M. A. Manzano, D. Sales, J. A. Quiroga, *Int. Biodeterior. Biodegrad.* **43** (1999) 155
30. J. H. Kang, F. Kondo, *Chemosphere* **49** (2002) 493
31. J. H. Kang, F. Kondo, *Chemosphere* **60** (2005) 1288
32. A. Zgola-Grzeskowiak, T. Grzeskowiak, J. Zembrzuska, Z. Lukaszewski, *Chemosphere* **64** (2006) 803
33. B. van der Zaan, J. de Weert, H. Rijnaarts, W. M. de Vos, H. Smidt, J. Gerritse, *Water Res.* **43** (2009) 3207
34. P. V. Tikilili, E. M. Nkhalambayausi-Chirwa, *J. Hazard. Mater.* **192** (2011) 1589
35. T. Ohura, Y. Aoyagi, K. Takagi, Y. Yoshida, K. Kasuya, Y Doi, *Polym. Degrad. Stabil.* **63** (1999) 23
36. E. Chiellini, A. Corti, S. D'Antone, *Polym. Degrad. Stabil.* **92** (2007) 1378
37. D. Bikiaris, C. Panayiotou, *J. Appl. Polym. Sci.* **70** (1998) 1503
38. M. Bernhard, J. P. Eubeler, S. Zok, T. P. Knepper, *Water Res.* **42** (2008) 4791
39. M. Rutkowska, K. Krasowska, A. Heimowska, I. Steinka, H. Janik, *Polym. Degrad. Stabil.* **76** (2002) 233
40. M. W. Meshram, V. V. Patil, S. T. Mhaske, B. N. Thorat, *Carbohydr. Polym.* **75** (2009) 71

41. H. Ismail, M. Irani, Z. Ahmad, *J. Appl. Polym. Sci.* **127** (2013) 4195
42. C. Wang, X. Li, J. Chen, G. Fei, H. Wang, Q. Liu, *J. Appl. Polym Sci.* **122** (2011) 2630
43. K. M. Mostafa, A. R. Samarkandy, A. A. El-Sanabary, *J. Appl. Polym. Sci.* **112** (2009) 2838
44. K. M. Mostafa, A. R. Samarkandy, A. A. El-Sanabary, *J. Appl. Polym. Sci.* **118** (2010) 2728
45. M. R. Saboktakin, A. Maharramov, M. A. Ramazanov, *Carbohydr. Polym.* **77** (2009) 634
46. M. M. Shaikh, S. V. Lonikar, *J. Appl. Polym. Sci.* **114** (2009) 2893
47. V. Nikolic, S. Velickovic, A. Popovic, *Carbohydr. Polym.* **88** (2012) 1407
48. P. Bowler, M. R. Wiliams, R. E. Angold, *Starch/Starke* **32** (1980) 186.

Journal of the Serbian Chemical Society
JSCS-info@shd.org.rs • www.shd.org.rs/JSCS
J. Serb. Chem. Soc. 78 (9) 1443–1460 (2013)
JSCS–4509
UDC 547.534:536.5.004.12:547.372:
541.25:532.13
Original scientific paper

Thermophysical properties of binary mixtures of *N*,*N*-dimethylformamide with three cyclic ethers

BISWAJIT SINHA[1]*, RAJENDRA PRADHAN[2], SANJOY SAHA[3], DHIRAJ BRAHMAN[1] and ABHIJIT SARKAR[1]

[1]*Department of Chemistry, University of North Bengal, Darjeeling-734013, India,* [2]*St. Joseph's College, Darjeeling-734101, India and* [3] *Department of Chemistry, Kalimpong College, Kalimpong-734301, India*

(Received 10 December 2012, revised 7 March 2013)

Abstract: Densities and viscosities of binary mixtures consisting of tetrahydrofuran (THF), 1,3-dioxolane (1,3-DO) and 1,4-dioxane (1,4-DO) with *N*,*N*-dimethylformamide (DMF) over the entire range of composition were measured at the temperatures 298.15, 308.15 and 318.15 K and at atmospheric pressure. The ultrasonic speeds of sound of these binary mixtures were measured at ambient temperature and atmospheric pressure (T = 298.15 K and p = = 1.01×10^5 Pa). The various experimental data were utilized to derive the excess molar volumes (V_m^E), excess viscosities (η^E) and excess isentropic compressibilities (κ_s^E). Using the excess molar volumes (V_m^E), the excess partial molar volumes ($\bar{V}_{m,1}^E$ and $\bar{V}_{m,2}^E$) and excess partial molar volumes at infinite dilution ($\bar{V}_{m,1}^{0,E}$ and $\bar{V}_{m,2}^{0,E}$) of each liquid component in the mixtures were derived and are discussed. The excess molar volumes (V_m^E) as a function of composition at ambient temperature and atmospheric pressure were used to test further the applicability of the Prigogine–Flory–Patterson (PFP) theory to the experimental binaries. The excess properties were found to be either negative or positive depending on the nature of molecular interactions and structural effects of the liquid mixtures.

Keywords: *N*,*N*-dimethylformamide; cyclic ethers; excess molar volumes; excess viscosities; excess isentropic compressibilities; Prigogine–Flory––Patterson theory.

INTRODUCTION

The volumetric, viscometric and acoustic properties of mixed solvent systems and their dependence on composition find applications in many important chemical, industrial and biological processes. The study of functions, such as excess molar volume and excess viscosity, *etc*., of binary mixtures are useful for

* Corresponding author. E-mail: biswachem@gmail.com
doi: 10.2298/JSC121210031S

the understanding of the nature and strength of molecular interactions between the component molecules.[1,2] This is primarily because of the close connection between the liquid state[3] and macroscopic properties. Excess molar volumes (V_m^E) and excess viscosities (η^E), *etc.* are often used to describe the intermolecular forces in mixtures, leading to an understanding of their behavior and enabling the development of theoretical models for their description and the simulation of processes. Hence, in recent years, there has been renewed interest in theoretical and experimental investigations of the excess thermodynamic properties of binary mixtures.[4–6,8–14]

DMF is a polar, non-associative aprotic solvent with a dipole moment, μ, of 3.86 Debye[15] and dielectric constant, ε, of 36.71[15,16] at 298.15 K. In the liquid state, it is self-associated due to dipole–dipole interactions;[17] while THF, 1,3-DO and 1,4-DO are non-polar, aprotic cyclic ethers differing in the number and position of the oxygen atom and carbon atoms; thus, these liquids differ in quadrupolar and dipolar order.[7] It is well known that DMF, THF, 1,3-DO and 1,4-DO are versatile solvents used in the separation of saturated and unsaturated hydrocarbons and in pharmaceutical synthesis and serve as solvents for many polymers. Therefore, the increasing employment of the liquids under investigation in many industries has greatly stimulated the need for extensive information on the acoustic, transport and thermodynamic properties of these liquids and their mixtures.

Therefore, in continuation of systematic studies[8–14] of the physicochemical properties of non-aqueous liquid mixtures, the present study attempts to unravel the nature of the molecular interactions in the binary mixtures of DMF with the cyclic ethers THF, 1,3-DO and 1,4-DO by measuring the densities, viscosities and ultrasonic speeds of sound of the mixtures over the entire composition range at different temperatures and at ambient pressure.

The calculated excess functions, such as excess molar volumes (V_m^E), excess viscosities (η^E) and excess isentropic compressibilities (κ_m^E) from the experimental data, were interpreted in terms of molecular interactions and structural effects. The partial molar volumes ($\bar{V}_{m,1}^0$ and $\bar{V}_{m,2}^0$) and excess partial molar volumes ($\bar{V}_{m,1}^{0,E}$ and $\bar{V}_{m,2}^{0,E}$) of each component at infinite dilution were also derived using the excess molar volumes (V_m^E) and interpreted in terms of the molecular interactions and the nature of the liquid mixtures. To the best of our knowledge, no comparable literature data for the systems studied in this work are available and treated in terms of the PFP theory; hence, a quantitative estimation of different contributions to the excess molar volumes (V_m^E) of the experimental binary systems at ambient temperature and pressure was attempted in terms of the PFP theory. Moreover, ultrasonic speeds of sound in all the binary mixtures were theoretically predicted based on some theories and empirical relations, such as the collision factor theory, the Nomoto relation, the impedance dependence relation and the ideal mixture relation, and the Flory theory.

EXPERIMENTAL

Materials

DMF (S. D. Fine Chemicals, India, AR, purity > 99 %) was purified by the method described by Y. Zhao *et al.*[18] 1, 4-DO and THF (Merck, India, purity > 99 %) were purified as described earlier.[19] 1,3-DO (S. D. Fine Chemicals, India, AR, purity > 99 %) was refluxed with PbO_2 and fractionally distilled after the addition of xylene.[16] After purification, all the purified chemicals were found to be better than 99.5 % pure as ascertained by GLC and also by comparing their experimental densities and viscosities at the experimental temperatures with their literature values[20-31] (given in Table I).

TABLE I. Physical properties of pure liquids at 298.15, 308.15 and 318.15 K

Pure liquid	T / K	$\rho\times10^{-3}$ / kg m^{-3}		η /mPa s		u / m s^{-1}	
		Exp.	Lit.	Exp.	Lit.	Exp.	Lit.
DMF	298.15	0.9442	0.9442[18]	0.803	0.802[20]	1464.8	1465.0[20]
			0.9445[19]		0.803[21]		1462.0[20]
	308.15	0.9350	0.9344[20]	0.709	0.706[22]	–	–
			0.9347[21]				
	318.15	0.9258	0.9251[20]	0.617	0.633[22]	–	–
			0.9252[21]				
THF	298.15	0.8807	0.8807[22]	0.463	0.4630[24]	1277.8	1292.2[24]
							1277.8[25]
	308.15	0.8712	0.8712[22]	0.428	0.4277[24]	–	–
	318.15	0.8614	0.8614[22]	0.390	0.3902[24]	–	–
1,3-DO	298.15	1.0571	1.0577[22]	0.588	0.5878[24]	1338.2	1338.2[26]
			1.0572[24]		0.588[26]		1340.2[27]
	308.15	1.0459	1.0463[22]	0.513	0.5128[24]	–	–
			1.0462[26]				
	318.15	1.0334	1.03364[26]	0.458	0.4580[24]	–	–
1,4-DO	298.15	1.0265	1.0278[27]	1.196	1.196[29]	1343.4	1344.4[24]
			1.0282[28]		1.178[30]		1344.8[27]
					1.1779[24]		
	308.15	1.0166	1.0168[22]	1.013	0.9985[24]	–	–
					0.999[30]		
	318.15	1.0052	1.00526[26]	0.887	0.901[31]	–	–

Methods

The binary mixtures were prepared by mass in a dry box and each thus prepared solution was distributed into three recipients (in airtight bottles) to perform all the measurements in triplicate with the aim of determining possible dispersions in the obtained results. The mass measurements, made on a digital electronic analytical balance (Mettler, AG 285, Switzerland), accurate to ±0.01 mg. The reproducibility in mole fraction was within ±0.0002. The densities were measured with a vibrating-tube density meter (Anton Paar, DMA 4500M), maintained at ±0.01 K of the desired temperatures and calibrated at the experimental temperatures with doubly distilled water and dry air. The uncertainty in the density was estimated to be ±0.0001 g cm^{-3} and that of the temperature was ±0.01 K. The viscosity was measured by means of a suspended Ubbelohde type viscometer, thoroughly cleaned, dried and calibrated at the experimental temperatures with triply distilled water and purified methanol.[15,32,33] It was

filled with experimental liquid and placed vertically in a glass sided thermostatted maintained constant to ±0.01 K. After attainment of thermal equilibrium, the efflux times of flow of the liquids were recorded with a digital stopwatch correct to ±0.01 s. In all determinations, an average of three measurements was taken into account and adequate precautions were taken to minimize evaporation loses during the actual measurements. The uncertainty in viscosity measurements was within ±0.003 mPa s. The ultrasonic speeds of sound (u) were measured with an accuracy of 0.3 % using a single crystal variable-path ultrasonic interferometer (Mittal Enterprise, New Delhi, M-81) working at 2 MHz. It was calibrated with doubly distilled water, purified methanol and benzene at 298.15 K. During the measurements, the temperature was maintained within ±0.01 K of 298.15 K by circulating thermostatted water around the jacketed cell (of 2 MHz) containing the experimental solutions with the aid of a circulating pump. The uncertainty of the ultrasonic speed measurements was around ±0.2 m s^{-1}. Adequate precautions were taken to minimize evaporation loses during all the measurements. The details of the methods and measurement techniques had been described elsewhere.[14,34,35]

RESULTS AND DISCUSSION

The experimental densities (ρ), viscosities (η), excess molar volumes (V_m^E) and excess viscosities (η^E) for the binary mixtures studied at different temperatures are listed in Table S-I of the Supplementary material. The excess molar volumes (V_m^E) were calculated using the following equation:

$$V_m^E = \sum_{i=1}^{2} x_i M_i (1/\rho - 1/\rho_i) \quad (1)$$

where ρ is the density of the mixture and x_i, M_i and ρ_i are the mole fraction, molar mass and density of the i^{th} component in the mixture, respectively. The estimated uncertainty in the excess molar volumes, V_m^E, was ±0.005 cm^3 mol^{-1}. Excess molar volumes (V_m^E) of the binary mixtures as a function of mole fraction (x_i) of DMF at the experimental temperatures are shown graphically in Fig 1. The excess molar volumes (V_m^E) for all the binary systems, except for the DMF + 1,4--DO system at 298.15 and 308.15 K, were negative over the entire range of compositions at all the experimental temperatures. The values of excess molar volumes (V_m^E) for the three systems were observed to follow the order: DMF + 1,4-DO > DMF + 1,3-DO > DMF + THF. According to Treszczanowicz *et al.*[36] V_m^E is a function of several opposing effects generally categorized into three types *viz*., physical, chemical, and structural. While physical effects offer a positive contribution to V_m^E, the chemical or specific intermolecular interactions (such as hydrogen bond interaction, dipole–dipole/dipole-induced–dipole interaction, formation of charge transfer complexes, *etc.*) result in a net volume decrease, and thus offer negative contributions to V_m^E. The structural effects such as interstitial accommodation (due to differences in size and shape of the components) and changes in the free volume also offer negative contributions to V_m^E. Therefore, the actual volume change would depend on the relative strength of these effects.

The molar volumes of DMF are 77.42, 78.18 and 78.96 cm^3 mol^{-1}, and those of THF, 1,3-DO and 1,4-DO are 81.87, 82.77 and 83.71 cm^3 mol^{-1}; (70.07, 70.83 and 71.68) cm^3 mol^{-1}; and 85.83, 86.67, and 87.65 cm^3 mol^{-1} at 298.15, 308.15 and 318.15 K, respectively. Evidently, the molar volumes of the components in the studied mixtures differ appreciably and, depending on the differences in the molar volumes of the components, it is to be expected that the mutual or geometrical fitting of the component liquids may follow the order: DMF + 1,4--DO > DMF + 1,3-DO > DMF + THF; but a reversed trend in the V_m^E values was observed for the studied binary mixtures. A perusal of Fig. 1 shows that the V_m^E values increase in the order: DMF + THF < DMF + 1,3-DO < DMF + 1,4-DO. It is satisfying to observe that the values of the dielectric constant of the cyclic ethers follow the reverse order: THF (ε = 7.58[37]) > 1,3-DO (ε = 7.13[38]) > 1,4-DO (ε = 2.21[37]). This indicates that a cyclic ether with a larger value of dielectric constant than another has greater specific interactions with DMF and that the negative V_m^E values for all the studied systems can primarily be attributed to dipole–dipole or dipole-induced–dipole interactions between the component liquids in the mixtures. Moreover, the V_m^E values decrease with increasing temperatures of the mixtures, indicating an increase in intermolecular interactions between the component molecules with increasing temperature, which is probably due the greater thermal agitation that ultimately increases the mutual fitting of the mixing components to some extent at higher temperatures.

The partial molar volumes, $\bar{V}_{m,i}$ of the i^{th} component in the binaries over the entire composition range at the experimental temperatures were calculated using the relation:

$$\bar{V}_{m,i} = V_{m,i}^E + V_{m,i}^* + (1 - x_i)(dV_{m,i}^E / dx_i)_{T,p} \quad (2)$$

where $V_{m,i}^*$ is the molar volume of the i^{th} component in the binaries. The derivatives, $(dV_{m,i}^E / dx_i)_{T,p}$, used in Eq. (2) were obtained by following the procedure[12] of fitting the excess molar volumes (V_m^E) of the binary mixtures to the Redlich–Kister polynomial,[39] with standard deviations (*SD*) in the range 0.000––0.002. Redlich–Kister polynomial is expressed as follows:

$$V_{m,i}^E = x_1 x_2 \sum_{i=1}^{2} a_i (1 - 2x_2)^i \quad (3)$$

where x_1 and x_2 are the mole fractions of the liquid 1 and 2, respectively, and a_i represent the multiple-regression coefficients. The standard deviations (*SD*) were calculated using the relation:

$$SD = \left[\sum_{i=1}^{n} (V_{m,Calc}^E - V_{m,Expt}^E)^2 / (n - j) \right]^{1/2} \quad (4)$$

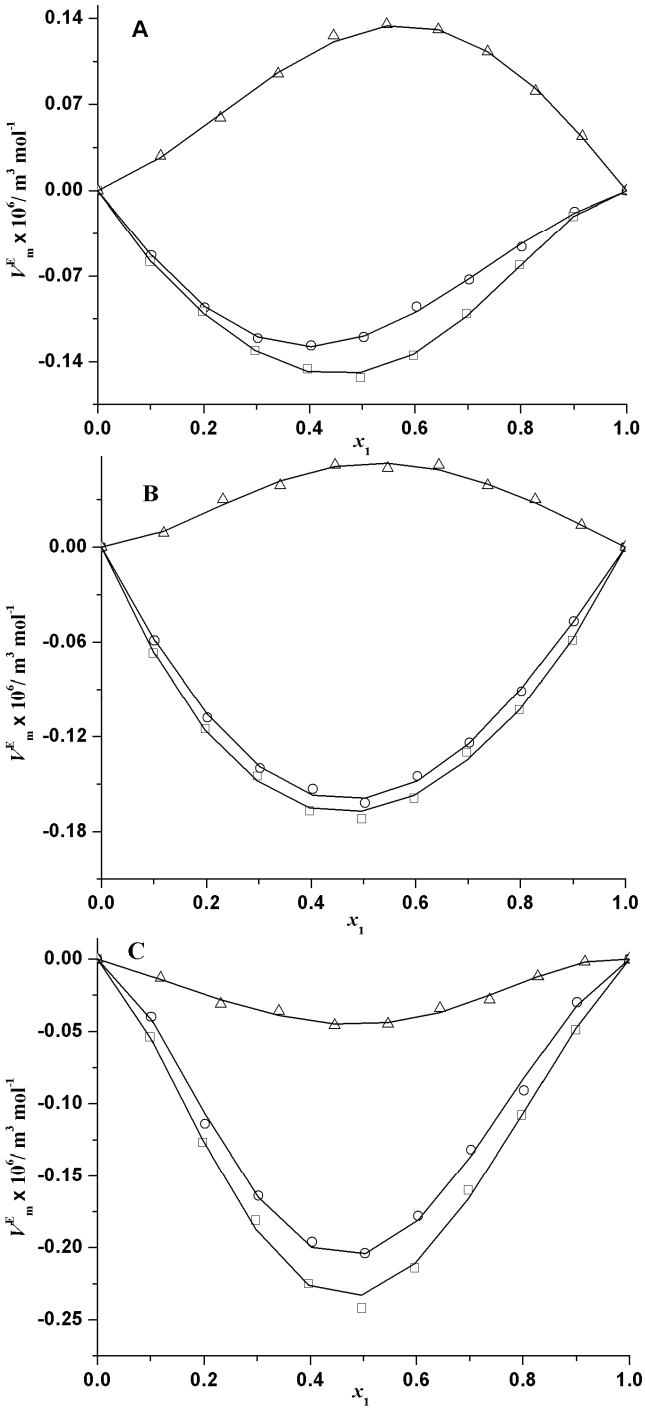

Fig. 1. Excess molar volume (V_m^E) *vs.* mole fraction of DMF (x_1) for binary mixtures of DMF + cyclic ethers: A, at T = 298.15 K; B, at T = 308.15 K; C, at T = 318.15 K. The graphical points represent the excess molar volumes (V_m^E): □, THF; ○, 1,3-DO; Δ, 1,4-DO. Lines represent the V_m^E values obtained from the Redlich–Kister polynomial.

where n is the number of experimental data points and j is the number of a_i coefficients. For the excess molar volumes (V_m^E) fitted to the Redlich–Kister polynomial, the standard deviations (SD) were in the range 0.002–0.006. The values of the partial molar volumes, $\bar{V}_{m,i}$ allow the calculation of the excess partial molar volumes ($\bar{V}_{m,1}^E$) by using the following relation:

$$\bar{V}_{m,i}^E = \bar{V}_{m,i} - V_{m,i}^* \quad (5)$$

The excess partial molar volume at infinite dilution ($\bar{V}_{m,i}^{0,E}$) can be determined from the following relation:

$$\bar{V}_{m,i}^{0,E} = (dV_{m,i}^E / dx_i)_{x_i=0,T,p} \quad (6)$$

The excess partial molar volumes ($\bar{V}_{m,1}^{0,E}$ and $\bar{V}_{m,2}^{0,E}$) at infinite dilution for the three binaries at the experimental temperatures are listed in Table S-II of the Supplementary material.

The excess partial molar volumes ($\bar{V}_{m,1}^E$ and $\bar{V}_{m,2}^E$) of each component in the studied binaries are graphically shown in Fig. 2 as a function of x_1. The $\bar{V}_{m,1}^E$ and $\bar{V}_{m,2}^E$ values were found to be negative for all the studied binary systems, except that containing 1,4-DO over the entire composition range at the experimental temperatures. Moreover, the excess partial molar volumes at infinite dilution ($\bar{V}_{m,1}^{0,E}$ and $\bar{V}_{m,2}^{0,E}$) were negative for both components in all the binary systems except for that containing 1,4-DO (however, $\bar{V}_{m,1}^{0,E}$ and $\bar{V}_{m,2}^{0,E}$ values were negative at 318.15 K for this system). These results suggest that while the 1,4-DO system is characterized by volume expansion on mixing with DMF at 298.15 and 308.15 K, the other systems are characterized by volume contraction on mixing with DMF.

In recent years, Flory's statistical theory[40–43] and its modified version known as the Prigogine–Flory–Patterson theory,[44,45] have been successfully used to estimate and analyze theoretically the excess thermodynamic functions of binary liquid mixtures; the PFP theory is applicable to both non-polar and polar molecules present in a binary mixture. The reduced equation of state in Flory's notation[42] is given by:

$$\frac{\tilde{P}\tilde{V}}{\tilde{T}} = \frac{\tilde{v}^{1/3}}{\tilde{v}^{1/3}-1} - \frac{1}{\tilde{v}\tilde{T}} \quad (7)$$

$$\tilde{v} = \frac{V}{V^*} \quad (8)$$

$$\tilde{T} = \frac{T}{T^*} \quad (9)$$

$$\tilde{p} = \frac{p}{p^*} \quad (10)$$

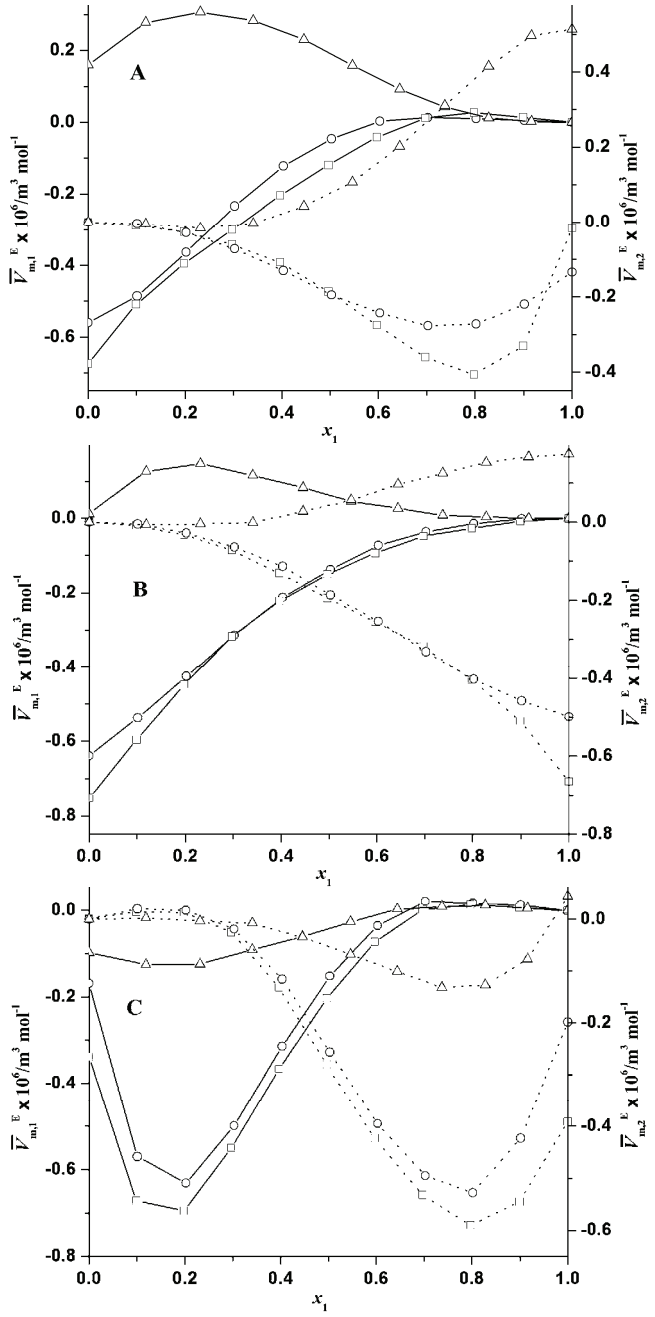

Fig. 2. Excess partial molar volume ($\overline{V}_{m,i}^{E}$) for the i^{th} component against mole fraction of DMF (x_1) for binary mixtures of DMF + + cyclic ethers: A, at T = = 298.15 K; B, at T = 308.15 K; C, at T = 318.15 K. The graphical points represent the $\overline{V}_{m,i}^{E}$ values for the mixtures of DMF with THF, □; 1,3-DO, ○; 1,4-DO, Δ. Lines represent the $\overline{V}_{m,i}^{E}$ values for DMF and the dotted curves represent the $\overline{V}_{m,i}^{E}$ values for cyclic ethers.

where are $\tilde{v}$, $\tilde{T}$ and $\tilde{p}$ are the reduced volume, reduced temperature and reduced pressure, respectively, and V^*, T^* and p^* are the characteristic volume, charac-

teristic temperature and characteristic pressure, respectively, of each pure liquid component. In the Flory treatment, the reduced equation of state in the limit of zero pressure (or without appreciable error at 1 atmospheric pressure[43]) takes the following forms:

$$\tilde{T} = \frac{\tilde{v}^{1/3} - 1}{\tilde{v}^{4/3}} \tag{11}$$

$$\tilde{v} = \left[\frac{1 + (4/3)\alpha T}{1 + \alpha T}\right]^3 \tag{12}$$

$$T^* = \frac{T}{\tilde{T}} = \frac{T\tilde{v}^{4/3}}{\tilde{v}^{1/3} - 1} \tag{13}$$

$$p^* = \gamma T \tilde{v}^2 \tag{14}$$

where the thermal expansion coefficient (α) and thermal pressure coefficient (γ) are given by the following relations:

$$\alpha = V^{-1}(\mathrm{d}V / \mathrm{d}T)_P = -\rho^{-1}(\mathrm{d}\rho / \mathrm{d}T)_p \tag{15}$$

$$\gamma = (\mathrm{d}P / \mathrm{d}V)_V = \alpha\kappa_T^{-1} \tag{16}$$

where κ_T is the isothermal compressibility, which can be determined using the relation:

$$\kappa_T = \kappa_S + \frac{T\alpha^2 V}{C_p} \tag{17}$$

The Flory parameters for each liquid component are given in Table II. Isobaric enthalpies (C_p) for the different component liquids required for the calculation of isothermal compressibilities (κ_T) were taken from literature.[46,47]

Using the well-known Prigogine–Flory–Patterson theory,[48,49] a quantitative estimation of the different contributions to V_m^E can be obtained. In terms of three contributions, the approximate expression for V_m^E is:

$$\frac{V_m^E}{x_1V_1^* < + x_2V_2^*} = \underbrace{\frac{(\tilde{v}^{1/3} - 1)\tilde{v}^{2/3}\psi_1\theta_2}{[(4/3)\tilde{v}^{-1/3} - 1]P_1^*}\chi_{1,2}}_{\chi_{1,2}\text{ contribution}} - \underbrace{\frac{(\tilde{v}_1 - \tilde{v}_2)^2[(14/9)\tilde{v}^{-1/3} - 1]\psi_1\psi_2}{[(4/3)\tilde{v}^{-1/3} - 1]\tilde{v}}}_{\tilde{v}\text{ contribution}} + \underbrace{\frac{(\tilde{v}_1 - \tilde{v}_2)(p_1^* - p_2^*)\psi_1\psi_2}{(p_1^*\psi_2 + p_2^*\psi_1)}}_{p^*\text{contribution}} \tag{18}$$

where p_i^*, V_i^* and ψ_i are characteristic pressure, volume and the molecular contact energy fraction of i^{th} pure component, respectively, and θ_2 is the molecular site fraction of the second component in a binary liquid mixture. The molecular

contact energy fraction and the molecular site fractions are defined by the relations:

$$\psi_1 = 1 - \psi_2 = \frac{\varphi_1 P_1^*}{\varphi_1 P_1^* + \varphi_2 P_2^*} \quad (19)$$

$$\theta_1 = 1 - \theta_2 = \frac{\varphi_1}{\varphi_1 + (V_1^* / V_2^*)^{1/3}} \quad (20)$$

$$\varphi_1 = 1 - \varphi_2 = \frac{x_1 V_1^*}{x_1 V_1^* + x_2 V_2^*} \quad (21)$$

TABLE II. The Flory parameters for pure liquids at 298.15 K

Liquid	$\tilde{v}$	$\tilde{T}\times10^2$	$V^*\times10^6$ / m^3 mol^{-1}	p^* / Pa	T^* / K	$\alpha\times10^4$ / K^{-1}	$K_T\times10^{10}$ / Pa^{-1}
DMF	1.2424	5.618	62.31	701.85	5307	9.744	6.389
THF	1.2670	5.987	64.62	562.13	4980	10.96	9.329
1,3-DO	1.2720	6.067	55.09	726.60	4921	11.21	7.442
1,4-DO	1.2553	5.815	68.37	674.51	5127	10.38	7.227

Actually, in deriving the interaction parameter ($\chi_{1,2}$), the V_m^E values of each composition (of each system) were fitted to Eq. (18) using Eqs. (11)–(17) using a computer program that finally provided an optimized value of the interaction parameter ($\chi_{1,2}$) with least error and values of different contributions to the V_m^E values embodied in Eq. (18). Table III contains the optimized $\chi_{1,2}$ values, the calculated and experimental V_m^E values, their deviation and values of different contributions to the V_m^E values for equimolar ($x_1 \approx 0.5$) composition at 298.15 K. It is clear from Table III that the calculated values of excess molar volumes $V_{m,PFP}^E$ reasonably agree with the experimental excess molar volumes $V_{m,exp}^E$ values for all the studied systems. A comparison between the $V_{m,exp}^E$ values and the $V_{m,PFP}^E$ values as a function of mole fraction (x_1) of DMF at 298.15 K is depicted in Fig. S-1 of the Supplementary material.

TABLE III. The values of the interaction parameter ($\chi_{1,2}$), the calculated and experimental values of the excess molar volumes ($V_{m,PFP}^E$ and $V_{m,exp}^E$), their deviations (ΔV_m^E) and the different PFP contributions at 298.15 K

DMF (1) +	$\chi_{1,2}$ J m^{-3}	$V_{m,exp}^E\times10^6$ m^3 mol^{-1}	$V_{m,PFP}^E\times10^6$ m^3 mol^{-1}	$\Delta V_m^E\times10^6$ m^3 mol^{-1}	PFP contributions$\times10^3$		
					int[a]	fv[b]	ip[c]
THF (2)	–4.588	–0.1531	–0.1427	–0.0104	–0.826	–0.224	–1.362
1,3-DO (2)	–15.08	–0.1204	–0.1204	0	–1.979	–0.326	0.255
1,4-DO (2)	18.01	0.1353	0.1243	0.0110	2.270	–0.063	–0.128

[a]interaction contribution; [b]free volume contribution; [c]internal pressure contribution

According to the PFP theory, the interaction contribution is proportional to the interaction parameter $\chi_{1,2}$, the free volume contribution arises from the

dependence of the reduced volume on the reduced temperature due to the differences between the degree of expansion of the two mixing components (always negative as $\mathrm{d}V^2/\mathrm{d}T^2$ is positive) and the internal pressure contribution depends on the product of the differences between the reduced volumes and characteristic pressures of the mixing components. Table III shows that the interaction contributions are negative for the systems with THF and 1,3-DO but positive for the system with 1,4-DO; the internal pressure contributions, except for 1,3-DO system, are negative for all the systems. From Table III, it is evident that while the interaction contribution ($\chi_{1,2}$) plays a dominant role in deciding the sign and magnitude of the $V^{\mathrm{E}}_{\mathrm{m,PFP}}$ values for the systems containing 1,3-DO and 1,4-DO, the internal pressure contribution (p^*) plays a major role in deciding the nature of $V^{\mathrm{E}}_{\mathrm{m,exp}}$ for the remaining system with THF.

The excess viscosity (η^{E}) can be defined as the difference between the measured viscosity (η) and the ideal viscosity (η_{id}) of a solution and is expressed by Eq. (20):[50]

$$\eta^{\mathrm{E}} = \eta - \eta_{\mathrm{id}} \tag{22}$$

Using the Eyring approach of viscosity as a rate process,[51] η_{id} can be defined by Eq. (23):

$$\eta_{\mathrm{id}} = \exp\left(\sum_{\mathrm{i}=1}^{2} x_{\mathrm{i}} \ln \eta_{\mathrm{id}}\right) \tag{23}$$

where η_i is the viscosity of the i^{th} component in the mixture and the additivity law in a logarithm form is considered for ideal mixtures. The estimated uncertainty for the excess viscosities (η^{E}) was within ±0.004 mPa s. Plots of the excess viscosity (η^{E}) *versus* the mole fraction (x_1) of DMF for the different binary mixtures at the experimental temperatures are depicted in Fig. 3. The η^{E} values of the binary mixtures were fitted to Redlich–Kister polynomial (shown as curves in Fig. 3) with standard deviations (*SD*) lying in the range 0.001–0.002.

Figure 3 shows that the η^{E} values, except for the system with THF at 318.15 K, are negative for all the mixtures over the entire composition range at all the experimental temperatures. The negative values indicate the presence of dispersion forces in these mixtures, while positive values may be attributed to the presence of specific interactions. As expected, the values of η^{E} become less negative or increase as the temperature increases but decrease as the dielectric constant of the ethers decrease from THF to 1,4-DO (Fig. 3). This suggests that the strength of molecular interactions in the mixture follows the order: DMF + THF > DMF + + 1,3-DO > DMF + 1,4-DO and increase with increasing temperature. Thus, the functions $V^{\mathrm{E}}_{\mathrm{m}}$ and η^{E} compliment each other in describing the behavior of the studied binary mixtures.

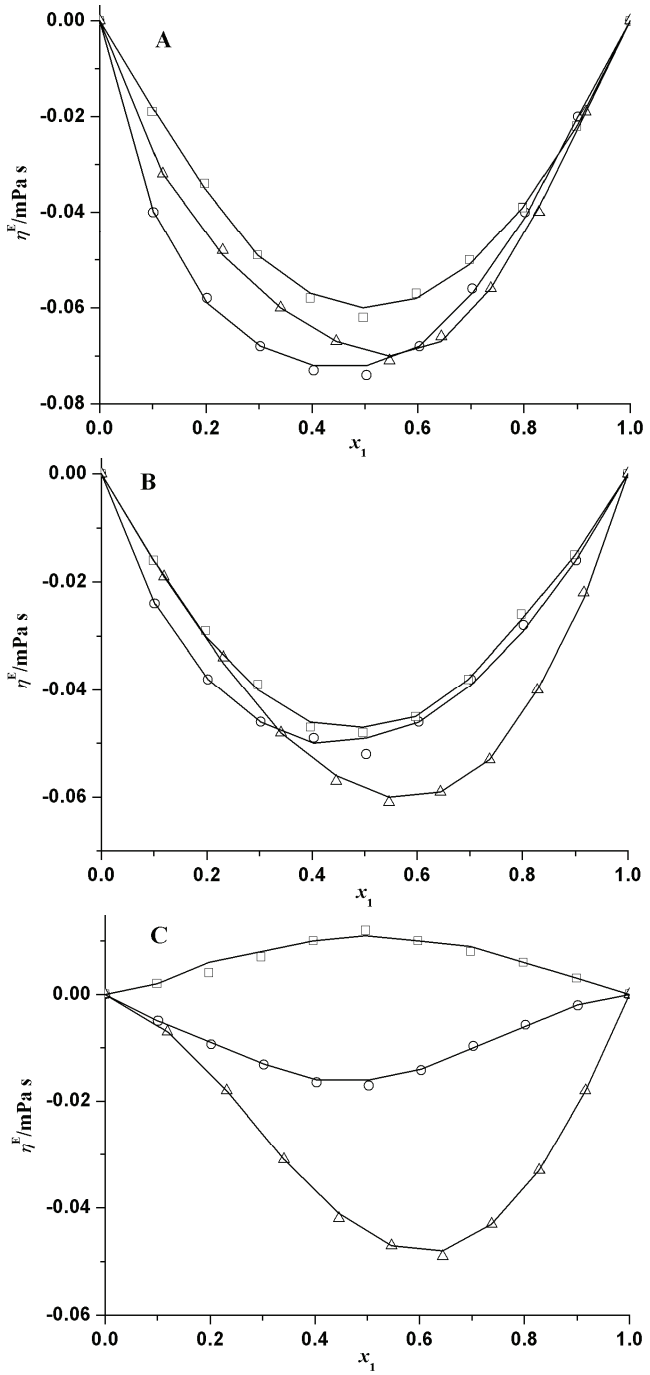

Fig. 3. Excess viscosities (η^E) *vs.* mole fraction of DMF (x_1) for binary mixtures of DMF with cyclic ethers: A, at T = 298.15 K; B, at T = = 308.15 K; C, at T = 318.15 K. The graphical points represent the experimental η^E values: □, THF; ○, 1,3-DO; Δ, 1,4-DO and lines represent the η^E values obtained from the Redlich–Kister polynomial.

The Eyring viscosity relation[51] yields the following equation for the free energy of viscous flow (ΔG^*):

$$\eta = (hN / V)\exp(\Delta G^* / RT) \tag{24}$$

where h is Planck's constant, N is Avogadro's number and the other symbols have their usual meanings. Rearranging Eq. (24) and putting $\Delta G^* = \Delta H^* - T\Delta S^*$, one obtains the relation:

$$R\ln(\eta V / hN) = \Delta H^* / T - \Delta S^* \tag{25}$$

Thus, the linear regressions of $R\ln(\eta V/hN)$ against $(1/T)$ could give the values of enthalpy (ΔH^*) and entropy (ΔS^*) of activation of viscous flow from the slope and negative intercept, respectively. The values of ΔH^*, ΔS^* and the linear regression coefficient (R^2) values as given in Table S-III of the Supplementary material show that while the ΔH^* values are positive, the ΔS^*values are negative for all the studied binary mixtures throughout the entire composition range. According to Corradini *et al.*[52] the enthalpy of activation of viscous flow may be regarded as a measure of the degree of cooperation between the species participating in the viscous flow. In a highly structured liquid, there will be a considerable degree of order; hence, for cooperative movement of the entities, a large heat of activation is required for the flow process. Thus the ΔH^* values indicate that the ease of formation of activated species necessary for viscous flow follow the order: DMF + THF > DMF + 1,3-DO > DMF + 1,4 DO. This order is also supported by negative values of ΔS^* for the mixtures.

A combination of the ultrasonic speed (u) and density data enabled the determination of the isentropic compressibilities (κ_S) and the excess isentropic compressibility (κ_S^E)[53] of the binary mixtures using the following equations:

$$\kappa_S = 1/u^2\rho \tag{26}$$

$$\kappa_S^E = \kappa_S - \kappa_S^{id} \tag{27}$$

$$\kappa_S^{id} = \sum_{i=1}^{2}\varphi_i\left[\kappa_{S,i} + \frac{TV_i\alpha_i^2}{C_{p,i}}\right] - \left\{\frac{T\sum_{i=1}^{2}(x_iV_i)\sum_{i=1}^{2}(\varphi_i\alpha_i)^2}{\sum_{i=1}^{2}(x_iC_{p,i})}\right\} \tag{28}$$

where φ_i, $\kappa_{S,i}$, V_i, α_i and $C_{p,i}$ are the volume fraction, isentropic compressibility, molar volume, thermal expansion coefficient and isobaric enthalpy of the i^{th} pure component in the binary mixtures, respectively, at 298.15 K. The experimental values of the speeds of sound, the isentropic compressibilities (κ_S) and the excess isentropic compressibilities (κ_S^E) at 298.15 K are given in Table S-IV of the

Supplementary material. The estimated uncertainty of the isentropic compressibility (κ_S) was within $\pm 1.0\times10^{10}$ Pa^{-1}.

For all the investigated binary mixtures, the excess isentropic compressibilities (κ_S^E) were negative, except for that containing 1,4-DO in the 1,4-DO-rich region, as shown in Table S-IV of the Supplementary material. The κ_S^E values of the binary mixtures were also fitted to the Redlich–Kister polynomial (shown as curves in Fig. 4) with standard deviations (*SD*) lying in the range 0.003–0.007.

Figure 4 depicts the composition dependence of the excess isentropic compressibilities κ_S^E for the investigated binary mixtures at 298.15 K are depicted in Fig. 4. It shows that the values of excess isentropic compressibility (κ_S^E) decrease in the order: DMF + 1,4-DO > DMF + 1,3-DO > DMF + THF, thereby supporting the observations obtained from the V_m^E and η^E values.

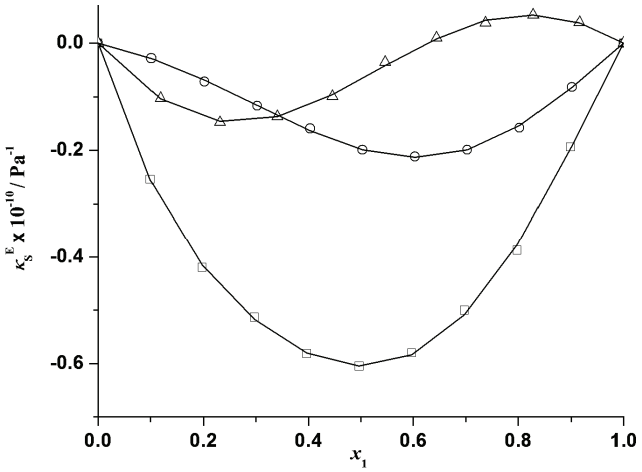

Fig. 4. The excess isentropic compressibility (κ_S^E) *vs.* mole fraction of DMF (x_1) for binary mixtures of DMF with cyclic ethers at T = 298.15 K. The graphical points represent experimental κ_S^E values: □, THF; ○, 1,3-DO; Δ, 1,4-DO and lines represent κ_S^E values obtained from the Redlich–Kister polynomial.

Ultrasonic speeds of sound of all the three binary mixtures were theoretically predicted using the following theories and empirical relations:

The Flory theory[40] yields:

$$u_{FLO} = \left(\frac{10^4\sigma}{6.3\rho}\right) \tag{29}$$

where σ is the surface tension of a liquid or liquid mixture calculated following the Pandey approach[54] through an extension of the work of Patterson and Rastogi.[55]

The collision factor theory (CFT)[56] yields:

$$u_{\mathrm{CFT}} = u_{\infty} \frac{\sum_{i=1}^{2}(x_i S_i)\sum_{i=1}^{2}(x_i B_i)}{V_{\mathrm{mix}}} \tag{30}$$

where u_{∞} = 1600 m s^{-1}, S_i and B_i represent the collision factor and actual volume of a molecule per mole for the i$^{\mathrm{th}}$ pure component in the mixtures, respectively.

The Nomoto relation (NOM)[57] yields:

$$u_{\mathrm{NOM}} = \left(\frac{\sum_{\mathrm{i}=1}^{2}(x_{\mathrm{i}} R_{\mathrm{i}})}{\sum_{\mathrm{i}=1}^{2}(x_{\mathrm{i}} V_{\mathrm{i}})} \right)^3 \tag{31}$$

where R_i stands for the molar speed of sound for the i^{th} pure component in the mixtures.

The impedance dependence relation (IDR)[58] yields:

$$u_{\mathrm{IDR}} = \frac{\sum_{i=1}^{2}(x_i Z_i)}{\sum_{i=1}^{2}(x_i \rho_i)} \tag{32}$$

where Z_i stands for specific acoustic impedance for the i^{th} pure component in the mixtures.

The ideal mixture relation (IMR)[59] yields:

$$u_{\mathrm{IMR}} = \left[\sum_{i=1}^{2}(x_i M_i)\sum_{i=1}^{2}(x_i / M_i u_i^2) \right]^{-\frac{1}{2}} \tag{33}$$

where u_i is the ultrasonic speed of sound for the i^{th} pure component in the mixtures. It was observed that the values obtained from all the theories and empirical relations show some deviations from the experimental speeds of sound and based on the *MRSD* % values, listed in Table S-V and shown graphically in Fig S-2 of the supplementary material, the relative predictive capability for the different equations follows the orders: for the DMF + THF system: FLORY > IDR > CFT > NOM >> IMR; for the DMF + 1,3-DO system: CFT ≈ NOM > IDR > IMR >> >> FLORY and for the DMF + 1,3-DO system: CFT > IDR > NOM ≈ IMR >> >> FLORY.

CONCLUSIONS

Based on the nature and magnitude of various excess functions (V_m^E, η^E and κ_S^E) and other derived parameters ($\bar{V}_{m,1}^E$, $\bar{V}_{m,2}^E$, $\bar{V}_{m,1}^{0,E}$, $\bar{V}_{m,2}^{2,E}$, *etc.*), evidently the molecular interactions in the studied binary systems can primarily be attributed to dipole–dipole or dipole-induced–dipole interactions. The PFP theory provided satisfactory quantitative estimations of the different contributions to the excess molar volumes (V_m^E) of the systems at ambient temperature and pressure.

SUPPLEMENTARY MATERIAL

Comparisons of the experimental results with literature data, and some derived parameters (Tables S-I, S-II, S-III, S-IV and S-V, and Figs. S-1 and S-2) are available electronically from http://www.shd.org.rs/JSCS/ or from the corresponding author on request.

Acknowledgement. The authors are grateful to the Departmental Special Assistance Scheme under the University Grants Commission, New Delhi (No. F 540/27/DRS/2007, SAP-1) for financial support.

И З В О Д

ТЕРМОФИЗИЧКА СВОЈСТВА БИНАРНИХ СМЕША *N,N*-ДИМЕТИЛФОРМАМИДА СА ТРИ ЦИКЛИЧНА ЕТРА

BISWAJIT SINHA[1], RAJENDRA PRADHAN[2], SANJOY SAHA[3], DHIRAJ BRAHMAN[1] и ABHIJIT SARKAR[1]

[1]*Department of Chemistry, University of North Bengal, Darjeeling-734013, India,* [2]*St. Joseph's College, Darjeeling-734101, India и* [3] *Department of Chemistry, Kalimpong College, Kalimpong-734301, India*

Густине и вискозности бинарних система тетрахидрофурана (THF), 1,3-диоксолана (1,3-DO) и 1,4-диоксана (1,4-DO) са *N,N*-диметилформамидом (DMF) измерене су на температурама од 298,15, 308,15 и 318,15 K и атмосферском притиску у целом опсегу удела компоненти. Измерена је и брзина звука кроз ове системе на собној температури и атмосферском притиску (T = 298,15 K и p = 1,01×10^5 Pa). На бази измерених вредности израчуната је допунска моларна запремина (V_m^E), допунска вискозност (η^E) и допунска изентропска компресибилност (κ_S^E). Коришћењем допунских моларних запремина, израчунате су и анализиране допунске парцијалне моларне запремине ($\bar{V}_{m,1}^E$ и $\bar{V}_{m,2}^E$) и ове при бесконачном разблажењу ($\bar{V}_{m,1}^{0,E}$ и $\bar{V}_{m,2}^{0,E}$) свих течних компонената у смеши. Зависност V_m^E од састава смеше на атмосферским условима коришћена је за проверу применљивости Prigogine–Flory–Patterson (PFP) теорије. Утврђено је да су вредности допунских величина или негативне или позитивне у зависности од природе молекулских интеракција и структуре компонената у течним смешама.

(Примљено 10. децембра 2012, ревидирано 7. марта 2013)

REFERENCES

1. B. Garcia, R. Alcalde, J. M. Leal, J. S. Mantos, *J. Chem. Soc., Faraday Trans.* **93** (1997) 1115
2. Y. Mahan, C. N. Liew, A. E. Mather, *J. Solution Chem.* **31** (2002) 743
3. C. R. Reid, B. E. Poling, *The properties of Gases and Liquids*, McGraw Hill, New York, 1998, Ch. 1

4. A. Villares, S. Rodriguez, C. Lafuente, F. M. Royo, M. C. Lopez, *J. Solution Chem.* **33** (2004) 1119
5. A. Ali, J. D. Pandey, N. K. Soni, A. K. Nain, B. Lal, D. Chand, *Chin. J. Chem.* **23** (2005) 377
6. A. K. Nain, *J. Solution Chem.* **35** (2006) 1417
7. P. Brocos, E. Calvo, A. Pineiro, R. Bravo, A. Amigo, *J. Chem. Eng. Data* **44** (1999) 1341
8. M. N. Roy, A. Sinha, B. Sinha, *J. Solution Chem.* **34** (2005) 1311
9. M. N. Roy, B. Sinha, *J. Mol. Liq.* **136** (2006) 128
10. M. N. Roy, B. Sinha, *J. Mol. Liq.* **133** (2007) 89
11. M. N. Roy, B. K. Sarkar, B. Sinha, *J. Chem. Eng. Data* **54** (2009) 1076
12. B. Sinha, *Phys. Chem. Liq.* **48** (2010) 183
13. R. S. Sah, B. Sinha, M. N. Roy. *J. Chem. Eng. Data* **55** (2010) 4536
14. B. K. Sarkar, A. Choudhury, B. Sinha, *J. Solution Chem.* **41** (2012) 53
15. J. A. Dean, *Lange's Handbook of Chemistry*, 11th ed., McGraw Hill, New York, 1973
16. J. A. Riddick, W. B. Bunge, T. K. Sakano, *Organic solvents. Techniques of Chemistry*, Vol. 2, 4th ed., Wiley Interscience, New York, 1986
17. R. Gopal, S. Agarwal, D. K. Agarwal, *J. Chem. Thermodyn.* **8** (1976) 1205
18. Y. Zhao, J. Wang, X. Xuan, J. Lu, *J. Chem. Eng. Data* **45** (2000) 440
19. M. N. Roy, R. Dey, A. Jha, *J. Chem. Eng. Data* **46** (2001) 1327
20. I. Johnson, M. Kalidoss, R. Srinivasamoorthy, *J. Chem. Eng. Data* **47** (2002) 1388
21. P. S. Nikam, S. J. Kharat, *J. Chem. Eng. Data* **50** (2005) 455
22. S. Akhtar, A. N. Qmar Faruk, M. A. Saleh, *Phys. Chem. Liq.* **39** (2001) 383
23. P. Pacak, *J. Solution Chem.* **16** (1987) 71
24. M. Das, M. N. Roy, *J. Chem. Eng. Data* **51** (2006) 2225
25. A. Valen, I. Gascon, C. Lafuente, J. S. Urieta, F. M. Royo, M. Postigo, *Int. J. Thermophys.* **23** (2002) 1587
26. L. Sarkar, M. N. Roy, *J. Chem. Eng. Data* **54** (2009) 3307
27. A. Villares, S. Martin, M. Haro, B. Giner, H. Artigas, *J. Chem. Thermodyn.* **36** (2004) 1027
28. A. Inglese, J.-P. E. Groller, E. Wilhelm, *J. Chem. Eng. Data* **28** (1983) 124
29. S. M. Contreras, *J. Chem. Eng. Data* **46** (2001) 1149
30. T. M. Aminabhavi, V. B. Patil, *J. Chem. Eng. Data* **43**, 497(1998)
31. K. P. Rao, K. S. Reddy, *J. Chem. Eng. Data* **33** (1988) 130
32. K. N. Marsh, *Recommended Reference Materials for the Realisation of Physicochemical Properties*, Blackwell Scientific Publications, Oxford, UK, 1987
33. A. Chatterjee, B. Das, *J. Chem. Eng. Data* **51** (2006) 1352
34. M. N. Roy, D. K. Hazra, *Indian J. Chem. Technol.* **1** (1994) 93
35. P. S. Nikam, M. Hosan, *J. Chem. Eng. Data* **33** (1988) 165
36. A. J. Treszczanowicz, O. Kiyohora, G. C. Benson, *J. Chem. Thermodyn.* **13** (1981) 253
37. J. F. Coetzee, T.-H. Chang, *Pure. Appl. Chem.* **57** (1985) 633.
38. A. Sinha, M. N. Roy, *J. Mol. Liq.* 1**40** (2008) 39
39. O. Redlich, A. T. Kister, *Ind. Eng. Chem.* **40** (1948) 345
40. P. J. Flory, R. A. Orwell, A. Vriji, *J. Am. Chem. Soc.* **86**, (1964) 3507
41. P. J. Flory, R. A. Orwell, A. Vriji, *J. Am. Chem. Soc.* **86** (1964) 3515
42. P. J. Flory, *J. Am. Chem. Soc.* **87** (1965) 1833
43. A. Abe, P. J. Flory, *J. Am. Chem. Soc.* **87** (1965) 1838
44. D. Patterson, G. Delmas, *J. Polym. Sci., C* **30** (1970) 1
45. D. Patterson, *Pure. Appl. Chem.* **47** (1976) 305

46. C. de Visser, G. Perron, J. E. Desnoyers, *J. Chem. Eng. Data* **22** (1977) 74
47. P. Brocos, E. Calvo, R. Bravo, M. Pintos, A. Amigo, *J. Chem. Eng. Data* **44** (1999) 67
48. I. Prigogine, R. Defay, *Chemical Thermodynamics*, 5th ed., Longman, London, 1694, p. 8
49. P. Tancrede, P. Bothorel, P. St. Romain, D. Patterson. *J. Chem. Soc., Faraday Trans. II* **73** (1977) 15
50. M. A. Saleh, S. Akhtar, M. S. Ahmed, *Phys. Chem. Liq.* **44** (2006) 551
51. S. Glasstone, K. J. Laidler, H. Eyring, *The Theory of Rate Processes*, McGraw-Hill, New York, 1941
52. F. Corradini, L. Marcheselli, A. Marchetti, M. Tagliazucchi, L. Tassi, G. Tosi, *Bull. Chem. Soc. Jpn.* **65** (1992) 503
53. D. Kiyohora. G. C. Benson, *J. Chem. Thermodyn.* **11** (1979) 861
54. J. D. Pandey, *J. Chem. Soc., Faraday Trans. I* **75** (1979) 2160
55. D. Patterson, A. K. Rastogi, *J. Phys. Chem.* **74** (1970) 1067
56. B. Jacobson, *J. Chem. Phys.* **20** (1952) 927
57. O. Nomoto, *J. Phys. Soc. Jpn.* **13** (1958) 1528
58. M. Kalidoss, R. Srinivasamoorthy, *J. Pure. Appl. Ultrason.* **19** (1997) 9
59. W. Van Dael, E. Vangael, in *Proceedings of 1st International Conference on Calorimetry and Thermodynamics*, Warsaw, Poland, 1969, p. 555.

Journal of the Serbian Chemical Society
JSCS@tmf.bg.ac.rs • www.shd.org.rs/JSCS
J. Serb. Chem. Soc. 78 (9) S110–S116 (2013) *Supplementary material*

SUPPLEMENTARY MATERIAL TO

Thermophysical properties of binary mixtures of *N*,*N*-dimethylformamide with three cyclic ethers

BISWAJIT SINHA[1]*, RAJENDRA PRADHAN[2], SANJOY SAHA[3], DHIRAJ BRAHMAN[1] and ABHIJIT SARKAR[1]

[1]*Department of Chemistry, University of North Bengal, Darjeeling-734013, India,* [2]*St. Joseph's College, Darjeeling-734101, India and* [3]*Department of Chemistry, Kalimpong College, Kalimpong-734301, India*

J. Serb. Chem. Soc. 78 (9) (2013) 1443–1460

TABLE S-I. Densities (ρ), viscosities (η), excess molar volumes (V_m^E), excess viscosities (η^E) for the binary mixtures of DMF (1) with the three cyclic ethers (2) at 298.15, 308.15 and 318.15 K; x_1 – mole fraction of DMF

x_1	$\rho\times10^{-3}$ / kg m^{-3}	η / mPa s	$V_m^E\times10^6$ / m^3 mol^{-1}	η^E / mPa s
DMF (1) + THF (2)				
		T = 298.15 K		
0	0.8807	0.463	0	0
0.0988	0.8873	0.470	–0.058	–0.019
0.1978	0.8938	0.482	–0.099	–0.034
0.2971	0.9003	0.496	–0.131	–0.049
0.3967	0.9067	0.518	–0.146	–0.058
0.4966	0.9131	0.547	–0.153	–0.062
0.5967	0.9193	0.586	–0.135	–0.057
0.6971	0.9254	0.630	–0.101	–0.050
0.7978	0.9315	0.679	–0.061	–0.039
0.8988	0.9377	0.737	–0.021	–0.022
1	0.9442	0.803	0	0
		T = 308.15 K		
0	0.8712	0.428	0	0
0.0988	0.8779	0.434	–0.067	–0.016
0.1978	0.8845	0.444	–0.115	–0.029
0.2971	0.8910	0.458	–0.145	–0.039
0.3967	0.8975	0.476	–0.167	–0.047
0.4966	0.9039	0.502	–0.172	–0.048
0.5967	0.9102	0.533	–0.159	–0.045

* Corresponding author. E-mail: biswachem@gmail.com

TABLE S-I. Continued

x_1	$\rho\times10^{-3}$ / kg m^{-3}	η / mPa s	$V_m^E\times10^6$ / m^3 mol^{-1}	η^E / mPa s
DMF (1) + THF (2)				
T = 308.15 K				
0.6971	0.9164	0.570	–0.130	–0.038
0.7978	0.9227	0.614	–0.103	–0.026
0.8988	0.9289	0.659	–0.059	–0.015
1	0.9350	0.709	0	0
T = 318.15 K				
0	0.8614	0.390	0	0
0.0988	0.8680	0.410	–0.054	0.002
0.1978	0.8749	0.431	–0.127	0.004
0.2971	0.8817	0.454	–0.181	0.007
0.3967	0.8885	0.478	–0.225	0.010
0.4966	0.8951	0.502	–0.242	0.012
0.5967	0.9013	0.523	–0.214	0.010
0.6971	0.9073	0.545	–0.160	0.008
0.7978	0.9134	0.568	–0.108	0.006
0.8988	0.9195	0.592	–0.049	0.003
1	0.9258	0.617	0	0
DMF (1) + 1,3-DO (2)				
T = 298.15 K				
0	1.0571	0.588	0	0
0.1012	1.0454	0.567	–0.053	–0.040
0.2021	1.0338	0.568	–0.096	–0.058
0.3028	1.0222	0.578	–0.121	–0.068
0.4032	1.0106	0.594	–0.127	–0.073
0.5033	0.9991	0.614	–0.120	–0.074
0.6032	0.9876	0.642	–0.095	–0.068
0.7028	0.9764	0.676	–0.073	–0.056
0.8021	0.9654	0.715	–0.046	–0.040
0.9012	0.9546	0.759	–0.017	–0.020
1	0.9442	0.803	0	0.
T = 308.15 K				
0	1.0459	0.513	0	0
0.1012	1.0345	0.506	–0.059	–0.024
0.2021	1.0232	0.510	–0.108	–0.038
0.3028	1.0119	0.520	–0.140	–0.046
0.4032	1.0006	0.535	–0.153	–0.049
0.5033	0.9895	0.552	–0.162	–0.052
0.6032	0.9783	0.578	–0.145	–0.046
0.7028	0.9673	0.606	–0.124	–0.038
0.8021	0.9564	0.637	–0.091	–0.028
0.9012	0.9456	0.671	–0.047	–0.016
1	0.9350	0.709	0	0

TABLE S-I. Continued

x_1	$\rho\times10^{-3}$ / kg m^{-3}	η / mPa s	$V_m^E\times10^6$ / m^3 mol^{-1}	η^E / mPa s
DMF (1) + 1,3-DO (2)				
T = 318.15 K				
0	1.0334	0.458	0	0
0.1012	1.0221	0.467	–0.040	–0.005
0.2021	1.0115	0.477	–0.114	–0.009
0.3028	1.0008	0.488	–0.164	–0.013
0.4032	0.9901	0.500	–0.196	–0.016
0.5033	0.9793	0.515	–0.204	–0.017
0.6032	0.9683	0.534	–0.178	–0.014
0.7028	0.9573	0.555	–0.132	–0.010
0.8021	0.9466	0.576	–0.091	–0.006
0.9012	0.9359	0.597	–0.030	–0.002
1	0.9258	0.617	0	0
DMF (1) + 1,4-DO (2)				
T = 298.15 K				
0	1.0265	1.196	0	0
0.1181	1.0173	1.109	0.028	–0.032
0.2316	1.0082	1.043	0.059	–0.048
0.3406	0.9992	0.984	0.095	–0.060
0.4455	0.9904	0.934	0.126	–0.067
0.5465	0.9820	0.891	0.135	–0.071
0.6439	0.9739	0.859	0.131	–0.066
0.7377	0.9661	0.835	0.113	–0.056
0.8282	0.9586	0.820	0.081	–0.040
0.9156	0.9513	0.811	0.044	–0.019
1	0.9442	0.803	0	0
T = 308.15 K				
0	1.0166	1.013	0	0
0.1181	1.0077	0.952	0.009	–0.019
0.2316	0.9988	0.899	0.030	–0.034
0.3406	0.9902	0.849	0.039	–0.048
0.4455	0.9817	0.807	0.052	–0.057
0.5465	0.9735	0.772	0.050	–0.061
0.6439	0.9654	0.746	0.052	–0.059
0.7377	0.9576	0.726	0.039	–0.053
0.8282	0.9499	0.714	0.030	–0.040
0.9156	0.9424	0.708	0.014	–0.023
1	0.9350	0.709	0	0
T = 318.15 K				
0	1.0052	0.887	0	0
0.1181	0.9968	0.843	–0.013	–0.007
0.2316	0.9886	0.797	–0.031	–0.018
0.3406	0.9804	0.753	–0.036	–0.031

TABLE S-I. Continued

x_1	$\rho\times10^{-3}$ / kg m^{-3}	η / mPa s	$V_m^E\times10^6$ / m^3 mol^{-1}	η^E / mPa s
DMF (1) + 1,4-DO (2)				
		T = 318.15 K		
0.4455	0.9724	0.713	–0.046	–0.042
0.5465	0.9644	0.680	–0.045	–0.047
0.6439	0.9564	0.653	–0.034	–0.049
0.7377	0.9486	0.636	–0.028	–0.043
0.8282	0.9408	0.624	–0.012	–0.033
0.9156	0.9332	0.618	–0.002	–0.018
1	0.9258	0.617	0	0

TABLE S-II. Redlich–Kister coefficients (a_k), standard deviations (SD) for the least squares fitting of the excess molar volumes (V_m^E), excess partial molar volumes ($\bar{V}_{m,1}^E$ and $\bar{V}_{m,2}^E$) and these ($\bar{V}_{m,1}^{0,E}$ and $\bar{V}_{m,2}^{0,E}$) at infinite dilution ($\bar{V}_{m,1}^{0,E}$ and $\bar{V}_{m,2}^{0,E}$) of each component in the studied binary mixtures at T = (298.15, 308.15 and 318.15) K; molar volumes are given in cm^3 mol^{-1}

Parameter	DMF (1) +		
	THF (2)	1,3-DO (2)	1,4-DO (2)
	T = 298.15 K		
a_0	–0.596	–0.480	0.520
a_1	0.145	0.290	0.238
a_2	0.251	0.133	–0.180
a_3	0.184	–0.077	–0.058
SD	0.002	0.002	0.003
$\bar{V}_{m.1}^E$	76.75	76.86	77.58
$\bar{V}_{m.2}^E$	81.86	69.94	86.35
$\bar{V}_{m.1}^{0,E}$	–0.674	–0.560	0.160
$\bar{V}_{m,2}^{0,E}$	–0.016	–0.134	0.520
	T = 308.15 K		
a_0	–0.669	–0.637	0.212
a_1	0.097	0.086	0.041
a_2	–0.040	0.068	–0.119
a_3	–0.053	–0.016	0.040
SD	0.004	0.003	0.003
$\bar{V}_{m.1}^E$	77.43	77.54	78.19
$\bar{V}_{m.2}^E$	82.11	70.33	86.84
$\bar{V}_{m.1}^{0,E}$	–0.753	–0.639	0.012
$\bar{V}_{m,2}^{0,E}$	–0.665	–0.499	0.174
	T = 318.15 K		
a_0	–0.933	–0.819	–0.182
a_1	0.177	0.190	0.023
a_2	0.568	0.635	0.155
a_3	–0.203	–0.205	0.048
SD	0.006	0.006	0.003
$\bar{V}_{m,1}^E$	78.62	78.79	78.86

TABLE S-II. Continued

Parameter	DMF (1) +		
	THF (2)	1,3-DO (2)	1,4-DO (2)
	T = 318.15 K		
$\bar{V}^{E}_{m,2}$	83.32	71.49	87.70
$\bar{V}^{0,E}_{m,1}$	–0.339	–0.169	–0.098
$\bar{V}^{0,E}_{m,2}$	–0.391	–0.199	0.044

TABLE S-III. Values of enthalpy (ΔH^*) and entropy (ΔS^*) of activation of viscous flow for the binary mixtures; x_1 – mole fraction of DMF

x_1	ΔH^* / kJ mol^{-1}	ΔS^* / J K^{-1} mol^{-1}	R^2
	DMF (1) + THF (2)		
0	5.884	–18.150	0.9948
0.0988	4.527	–22.725	0.9902
0.1978	3.588	–25.992	0.9089
0.2971	2.695	–29.152	0.7474
0.3967	2.406	–30.410	0.5981
0.4966	2.636	–30.051	0.6587
0.5967	3.736	–26.902	0.8361
0.6971	4.958	–23.390	0.9473
0.7978	6.273	–19.605	0.9956
0.8988	7.865	–14.926	0.9999
1	9.604	–9.790	0.9972
	DMF (1) + 1,3-DO (2)		
0	8.965	–8.460	0.9981
0.1012	6.775	–15.570	0.9902
0.2021	6.041	–18.118	0.9809
0.3028	5.856	–18.963	0.9783
0.4032	5.999	–18.804	0.9849
0.5033	6.158	–18.629	0.9856
0.6032	6.494	–17.973	0.9944
0.7028	7.005	–16.778	0.9971
0.8021	7.753	–16.830	0.9992
0.9012	8.687	–12.288	1.0000
1	9.604	–9.790	0.9972
	DMF (1) + 1,4-DO (2)		
0	10.970	–9.314	0.9971
0.1181	10.022	–11.775	0.9970
0.2316	9.842	–11.781	0.9977
0.3406	9.810	–11.317	0.9978
0.4455	9.929	–10.405	0.9988
0.5465	9.947	–9.876	0.9996
0.6439	10.097	–8.997	1.0000
0.7377	10.014	–8.957	1.0000
0.8282	10.030	–8.673	0.9999

TABLE S-III. Continued

x_1	ΔH^* / kJ mol^{-1}	ΔS^* / J K^{-1} mol^{-1}	R^2
DMF (1) + 1,4-DO (2)			
0.9156	9.956	–8.754	0.9997
1	9.604	–9.790	0.9972

TABLE S-IV. Ultrasonic speeds (u), isentropic compressibilities (κ_S) and excess isentropic compressibilities (κ_S^E) of binary mixtures of DMF (1) + the cyclic ethers (2) at 298.15 K; x_1 – mole fraction of DMF; x_1 – mole fraction of DMF

x_1	u / m s^{-1}	$\kappa_S \times 10^{10}$ / Pa^{-1}	$\kappa_S^E \times 10^{10}$ / Pa^{-1}
DMF (1) + THF (2)			
0	1277.8	6.954	0
0.0988	1313.2	6.535	–0.254
0.1978	1343.8	5.196	–0.420
0.2971	1369.6	5.921	–0.513
0.3967	1395.5	5.663	–0.581
0.4966	1418.8	5.441	–0.605
0.5967	1438.1	5.260	–0.580
0.6971	1452.1	5.125	–0.500
0.7978	1462.9	5.016	–0.387
0.8988	1463.5	4.979	–0.194
1	1464.8	4.936	0
DMF (1) + 1,3-DO (2)			
0	1338.2	5.283	0
0.1012	1352.6	5.229	–0.028
0.2021	1369.8	5.155	–0.072
0.3028	1387.8	5.079	–0.117
0.4032	1406.2	5.004	–0.159
0.5033	1424.9	4.930	–0.199
0.6032	1440.4	4.880	–0.212
0.7028	1452.3	4.856	–0.199
0.8021	1460.2	4.858	–0.158
0.9012	1462.8	4.896	–0.082
1	1464.8	4.936	0
DMF (1) + 1,4-DO (2)			
0	1343.4	5.398	0
0.1181	1368.4	5.250	–0.103
0.2316	1386.5	5.160	–0.148
0.3406	1397.5	5.124	–0.137
0.4455	1404.8	5.116	–0.099
0.5465	1408.6	5.132	–0.036
0.6439	1414.5	5.122	0.010
0.7377	1422.7	5.076	0.038
0.8282	1432.7	5.029	0.053
0.9156	1446.9	4.983	0.039
1	1464.8	4.936	0

TABLE S-V. Relative predictive capabilities of various theories and empirical relations for ultrasonic speeds of the binary mixtures at 298.15 K

DMF (1) +	*MRSD*[a] / %				
	FLORY	CFT	NOM	IMR	IDR
THF (2)	1.96	2.50	2.86	3.15	2.43
1,3-DO (2)	1.48	1.10	1.10	1.40	1.39
1,4-DO (2)	1.74	0.70	0.76	0.76	0.72

[a] $MRSD = 100\left[\frac{1}{N}\sum\{(u_{\exp} - u_{\text{cal}})/u_{\exp}\}^2\right]^{1/2}$; N is number of data points

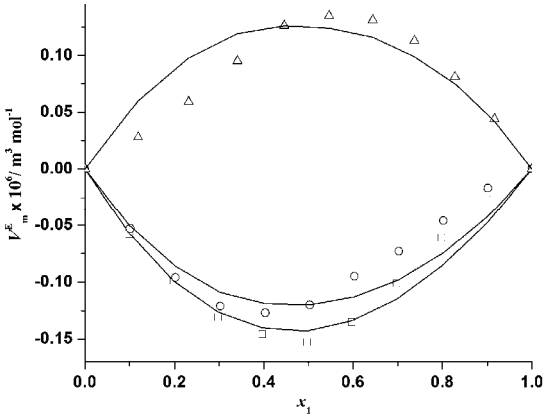

Fig. S-1. Comparison between the experimental excess molar volumes and the excess molar volumes obtained from the Prigogine–Flory–Patterson theory as a function of the mole fraction of DMF (x_1) for binary mixtures of DMF with cyclic ethers at T = 298.15 K. The graphical points represent the experimental excess molar volumes ($V^{\text{E}}_{\text{m,exp}}$): □, THF; ○, 1,3-DO; Δ, 1,4-DO and the smooth curves represent the $V^{\text{E}}_{\text{m,PFP}}$ values obtained from the Prigogine–Flory–Patterson theory.

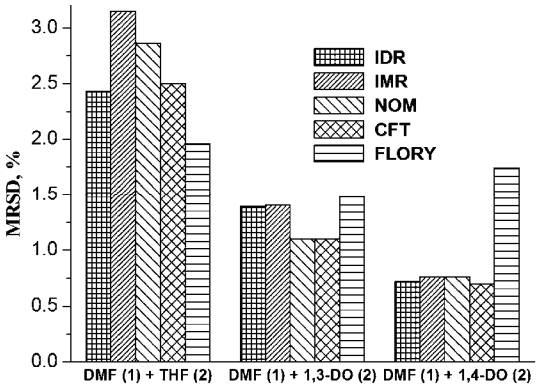

Fig. S-2. MRSD values for the theoretical prediction of the ultrasonic speeds by different theories and empirical relations for the binary mixtures of DMF + cyclic ethers at T = 298.15 K.